HIGH PRESSURE PHASE EQUILIBRIA: EXPERIMENTAL AND MONTE CARLO SIMULATION STUDIES

Vol. 1

by

ATHANASSIOS Z. PANAGIOTOPOULOS

Dipl. Chem. Eng., National Technical University of Athens
(1982)

SUBMITTED TO THE DEPARTMENT OF CHEMICAL ENGINEERING
IN PARTIAL FULFILLMENT OF THE REQUIREMENTS
FOR THE DEGREE OF

DOCTOR OF PHILOSOPHY

at the

MASSACHUSETTS INSTITUTE OF TECHNOLOGY
(September 1986)

Signature of author _____
Department of Chemical Engineering
August 25, 1986

Certified by _____
Professor Robert C. Reid
Thesis Supervisor

_____
Professor Ulrich W. Suter
Thesis Supervisor

Accepted by _____
Professor William M. Deen, Chairman
Departmental Committe on Graduate Students

Στη μνημη του πατερα μου

HIGH PRESSURE PHASE EQUILIBRIA: EXPERIMENTAL AND MONTE CARLO SIMULATION STUDIES

by

ATHANASSIOS ZOIS PANAGIOTOPOULOS

Submitted to the Department of Chemical Engineering
on August 25, 1986 in partial fulfillment of the requirements
for the degree of Doctor of Philosophy in Chemical Engineering

ABSTRACT

High pressure phase equilibria in ternary mixtures consisting of water, supercritical carbon dioxide and polar organic compounds (acetone, *n*-butanol, acetic acid and *n*-butyric acid) were studied experimentally using a high pressure optical cell with external recirculation. The main features of the ternary phase diagrams include the presence of extensive multiphase (three- and four-phase) equilibrium regions and a dramatic change in system behavior as pressure was increased above the critical pressure of carbon dioxide. The observed phase equilibrium behavior can form the basis for practical separations between a polar organic compound and water. Selectivities of supercritical carbon dioxide for the organic compound over water were found to be higher for the less polar solutes.

A correlation technique based on the application of a novel density-dependent mixing rule for cubic equations of state was used for modelling the experimental results. The model describes quantitatively many features of the experimentally observed behavior. In most cases, the model parameters were obtained from binary data only, thus providing a means for prediction of the ternary behavior from limited experimental information.

A methodology was developed for the direct determination of phase equilibria in fluid mixtures from Monte Carlo simulation, based on fundamental information on intermolecular interactions. The Widom test-particle expression was used for the evaluation of the chemical potential. The novel features of the proposed methodology include use of fluctuation theory to allow one to "observe" the approach of the system to a stability limit, and the introduction of an interchange algorithm to facilitate the calculation of properties for highly non-ideal mixtures.

The Monte Carlo simulation methodology was applied for mixtures of simple, spherically symmetric Lennard-Jones molecules. It was shown that the interaction energies between unlike molecules are particularly important in determining the tendency of a system to phase-separate or to form an

azeotrope. Molecular size differences between components were found to be less important. Finally, by choosing potential parameters that reproduce the critical constants of carbon dioxide and acetone, a simulated phase diagram was obtained that captures all the essential elements of the phase equilibrium behavior of the real mixture.

Thesis supervisors:	Professor Robert C. Reid
	Professor Ulrich W. Suter
Titles:	Professor of Chemical Engineering (emeritus)
	Bayer Associate Professor of Chemical Engineering

ACKNOWLEDGEMENTS

It is a pleasure to acknowledge several organizations and individuals that were of significant help during the course of this work.

Primary financial support was provided by the National Science Foundation, under Grant CPE-8318494. The Office for Advanced Scientific Computing at NSF provided a grant of supercomputer time and the John von Neumann Computing Center at Princeton a supplementary grant, that made the Monte Carlo simulation part of this work possible. I would also like to acknowledge Halcon Inc. for a one-year graduate fellowship.

I am happy to have been able to work these past four years with Professor Bob Reid. He taught me a great many things, including but by no means limited to thermodynamics and the ways of research. He provided me with guidance and support, and opened up for me whole new areas of thinking. His teachings and friendship I truly honor.

Professor Ulrich Suter has greatly contributed, with his enthusiastic encouragement, innovative ideas and valuable criticism, to the enjoyment I derived from doing this work.

The members of my thesis committee, Professors Charlie Cooney, George Stephanopoulos and Preetinder Virk provided their knowledgeable input throughout this thesis. Special thanks go to Professor Stephanopoulos for initiating me in research, back in the National Technical University of Athens.

Pablo Debenedetti, Sanat Kumar and Richard Willson were always there, with lively ideas, practical help and constructive comments. Beyond and above that, I am happy that I can call them my friends.

Stavroula, my wife and companion of the past seven years, has given me all her love and asked for little in return. Without her, it would have been impossible to face all the difficulties and frustrations, or enjoy the many happy moments that she made possible.

TABLE OF CONTENTS

TABLE OF CONTENTS (Continued)

TABLE OF CONTENTS (Continued)

TABLE OF CONTENTS (Concluded)

LIST OF TABLES

LIST OF TABLES(continued)

LIST OF TABLES(concluded)

LIST OF FIGURES

LIST OF FIGURES (continued)

LIST OF FIGURES (continued)

LIST OF FIGURES (continued)

LIST OF FIGURES (concluded)

SUMMARY

0.1. Introduction and research objectives

0.1.1 Motivation

In the recent years, there has been considerable interest in the use of gases above their critical temperature and pressure (supercritical fluids) as novel solvents for separations. The main advantage in using such solvents, relative to conventional liquid extraction or distillation, is the ease of recovery of the dissolved material by pressure or temperature changes. Numerous studies of the solubilities of pure solids in supercritical solvents have appeared in the literature (Paulaitis et al., 1983), but there are relatively few studies for multicomponent solid mixtures. Phase equilibria in binary fluid systems, especially for hydrocarbons, have also been extensively studied. However, experimental results are not readily available for multicomponent systems that contain highly polar components (such as water) and a supercritical fluid.

A potentially important new area for the application of separation techniques using supercritical solvents is the recovery of organic compounds from dilute aqueous solutions. Such mixtures commonly arise as products of biochemical processes, and are often difficult to separate. This challenge provided the primary motivation for the experimental part of this work, in which we studied the phase behavior of low molecular weight polar organic compounds, such as alcohols and carboxylic acids, in ternary mixtures with water and supercritical carbon dioxide.

To realize the full potential of any separation process, accurate values are needed for the physical properties of the mixtures to be separated

over a wide range of conditions. The most common way to extend the experimental data outside the immediate range for which they were obtained is to extrapolate using semiempirical models, with adjustable parameters obtained from data regression. Substantial effort and activity has thus been centered on the development of new correlation techniques that can be used for polar, asymmetric mixtures at high pressures.

An alternative to semiempirical methods is the use of models with a firm theoretical basis that can extrapolate from limited experimental information and accurately predict the behavior of systems for which no data exist. Two sets of difficulties prevent such predictions of macroscopic properties of pure substances and mixtures from first principles: (i) the energies of interaction (repulsion and attraction) between molecules are rarely known quantitatively and (ii) the problem of utilizing knowledge about the molecular interactions to calculate properties of large collections of molecules is very difficult to solve. For the first problem, we now believe that the interaction energies are direct manifestations of the electromagnetic interactions between elementary charges but, until now, we have only a few a priori calculated potentials for simple atoms and molecules (Maitland et al., 1981). Addressing the second problem is one of the main objectives of this work.

A powerful approach for the investigation of the properties of fluids and fluid mixtures based on fundamental knowledge about the intermolecular interactions is direct computer simulation. Molecular dynamics (Alder and Wainwright, 1959) or Monte Carlo simulation methods (Metropolis et al., 1953) can, in principle, be used to obtain the thermodynamic properties of fluids. There have been, however, few studies that attempt to calculate phase equilibrium properties of mixtures, despite recent significant advances in the methods available for the evaluation of the chemical potential (Shing and Gubbins, 1983a).

The integration of the various approaches for the determination of physical properties and phase equilibria is schematically summarized in Figure 1.2 (page 59). Experimental methods play a central role by providing

data for the development of new separation techniques and for testing of models, theories and simulation results. Correlation methods draw on experiment for the determination of the model parameters, but they can be used to enhance the usefulness of experimental data and provide input for detailed process modelling and optimization. Computer simulation can be used both for the prediction of properties of real mixtures and for the testing of theoretical models by generating exact results for model systems. Finally, theoretical models are developed with input from both experiment and computer simulation.

0.1.2 Problem definition

The general area of interest of this work is the investigation of phase equilibria in fluid mixtures at high pressures. The term high pressure is used relative to the gas-liquid critical pressure of the components of a system. This would imply that pressures from above atmospheric to a few hundred bar are considered. We approached the problem from two directions, namely (i) from an experimental and correlation point of view and (ii) in terms of a purely predictive molecular simulation technique. The two approaches are complementary: experiment and correlation provide information directly usable for the development of practical separations and data for the testing of theoretical models; the parallel investigation of direct computer simulation techniques for determining phase equilibria in dense fluid mixtures may eventually extend the range of confidence of limited experimental information.

Our basic goals were as follows:

Experimental and correlation: The primary objective in this area was to evaluate the potential of high-pressure separations using supercritical solvents for the recovery of polar organic materials from aqueous solutions. The specific aspects of the problem that we addressed are summarized below:

a. We attempted to obtain a general picture of the relevant phase equilibria in ternary systems with a polar organic compound, water and a supercritical fluid. We selected to use carbon dioxide as the supercritical fluid and acetone, *n*-butanol, acetic acid and *n*-butyric acid as model polar organic compounds. Possible trends with different functional groups and molecular weight of the compounds were of interest.

b. We developed new correlation techniques, based on the use of density-dependent mixing rules for cubic equations of state, to represent the relevant phase equilibria.

c. Finally, the implications for the development of new separation processes were determined, based on the experimentally observed phase equilibrium behavior and the correlation results.

Molecular simulation: The basic objective in this area was the prediction of phase equilibrium behavior of dense fluid mixtures with assumed intermolecular interactions. Specifically:

a. We investigated techniques to predict the phase diagrams for nonideal fluid mixtures. The Lennard-Jones potential was employed to represent the interactions between like and unlike molecules. The Widom (1963) test particle method was used for the calculation of the chemical potential, augmented by two novel techniques: the use of fluctuation theory for the determination of stability limits and a particle interchange technique that facilitated the calculation of the properties of highly asymmetric systems.

b. We investigated the effect of primary microscopic parameters (size and attractive well depth) on the macroscopic phase equilibrium behavior and the local structure of a fluid.

c. Finally, we compared some of the results from direct molecular simulation to available experimental information.

0.2. Experimental and correlation

0.2.1 Background

Previous studies in the phase equilibrium behavior of fluid mixtures at high pressures have illustrated a wide range of possible phase diagrams for binary (Scott and van Konynenburg, 1970) and ternary systems (Elgin and Weinstock, 1959) that can serve as a guide to the selection of systems and conditions for separations.

Experimental studies for ternary systems with water, a polar organic compound and a supercritical fluid are relatively scarce. Todd (1952) and Snedeker (1956) investigated equilibria with carbon dioxide and ethylene in binary and ternary systems with liquid organic compounds. Francis (1954) presented a large number of ternary diagrams of near-critical (liquid) carbon dioxide. Elgin and Weinstock (1959) were the first to observe the "salting out" effect of a supercritical fluid on aqueous solutions of organic compounds. In the more recent years, Paulaitis et al. (1981), McHugh et al. (1981) and Gilbert and Paulaitis (1986) investigated phase equilibria relevant to the recovery of ethanol from water using a supercritical fluid. Radosz (1984) and Paulaitis et al. (1984) have determined phase equilibria for the system isopropanol - water - carbon dioxide. The results from these investigations suggest that supercritical solvents may possibly be used for the recovery of ethanol from aqueous solutions, but the distribution coefficients are low. Distribution coefficients for isopropanol are higher. No systematic study of the effect of changing the carbon chain length within a homologous series of compounds or comparisons for components with different functional groups has been reported.

The most successful approach to date for modelling high pressure phase equilibria has been the equation of state approach, in which the volumetric properties of a mixture are described by a pressure explicit expression. An important group is cubic equations of state (van der Waals, 1873;

Redlich and Kwong, 1949; Peng and Robinson, 1976). Some of the attractive features of this type of equations are their analyticity (because of their cubic form) and the small number of adjustable parameters. Their limitations and drawbacks stem primarily from their empirical character.

In the recent years, several attempts have been made to improve the performance of cubic equations of state, especially for highly nonideal mixtures. The basic factor determining the behavior of the equations is the mixing rules used. The quadratic mixing rules normally used are theoretically correct at low densities (Hirschfelder et al., 1954), but are not appropriate for asymmetric mixtures at high densities. An important trend in the efforts to model nonideal mixtures has been the use of *density-dependent* mixing rules that preserve the quadratic form at low densities but substitute a higher-order dependence at high densities. Examples of this approach are the works by Whiting and Prausnitz (1982) and Mathias and Copeman (1983). Simple equations of state with higher-order mixing rules appear to be successful in representing phase equilibria in asymmetric mixtures. This approach is the focus of the effort to develop new correlation methods for the data obtained in this work.

0.2.2 Development of new correlation techniques

Pure component parameter evaluation

Before using an equation of state, a method must be devised to obtain pure component parameters that give a reasonable representation of the pure component thermodynamic properties. The conventional approach (e.g., Peng and Robinson, 1976), using the critical point parameters, suffers from increasing inaccuracy away from the critical point. We have developed a new generalized technique (Panagiotopoulos and Kumar, 1985), based on dimensional analysis of two-parameter equations of state, that enables the direct calculation of pure component parameters that exactly reproduce vapor pressure and liquid volume of a pure component at a given temperature. We have utilized this technique for the determination of the pure component

parameters for all subcritical components of interest. For the supercritical components, however, the conventional critical-point correlations were used.

Higher order mixing rules for cubic equations of state

For the representation of the experimental information we selected the Peng-Robinson cubic equation of state as the starting point. This equation is a special case of the general cubic equation of state given by Eq. 2.7.

$$P = \frac{RT}{V - b_m} - \frac{a_m}{V^2 + 2Vb_m - b_m^2} \qquad [0.1]$$

The mixture parameters a_m and b_m are related to the pure component parameters and the mixture composition through a mixing rule. Eqs. 2.8 and 2.9 show a common choice for the mixing rules, the van der Waals 1-fluid mixing rule that we also use:

$$a_m = \sum_i \sum_j X_i X_j a_{ij} \qquad [2.8]$$

$$b_m = \sum_i X_i b_i \qquad [2.9]$$

The conventional combining rule for the interaction parameter a_{ij},

$$a_{ij} = \sqrt{a_i a_j} \ (1-k_{ij}) \qquad [2.10]$$

does not reproduce well the properties of highly polar and asymmetric systems. To improve the representation of the phase equilibrium behavior of such systems, we introduced a modification of the mixing rules that involves an additional parameter to be regressed from experimental data. The form of the new combining rule is given below:

$$a_{ij} = \sqrt{a_i a_j}\,(1-k_{ij}) + \frac{b_m}{VRT}\,(X_i \lambda_{ij} + X_j \lambda_{ji}) \qquad [3.6]$$

where $\lambda_{ij} = -\lambda_{ji}$ is <u>one</u> additional parameter per binary system.

Eq. 3.6 results in a *density dependent* mixing rule: at low, gas-like densities ($V \to \infty$), the theoretically correct quadratic dependence of the mixture second virial coefficient on mixture composition is recovered, whereas at high densities a higher-order dependence necessary for the representation of the properties of asymmetric mixtures is introduced.

The physical significance of the original interaction parameter in Eq. 2.10, k_{ij}, is that it provides corrections to the geometric-mean rule for unlike-pair attractive interactions. The physical basis of the proposed higher order dependence at high densities in Eq. 3.6 lies in the concept of local compositions: in non-ideal systems, the local environment around molecules of different types deviates from the global (average) composition. The interaction parameter λ_{ij} provides additional corrections to the geometric-mean rule that are due to differences in the local environment around each molecule. The corrections are assumed linear in the mole fractions of the two interacting components.

An example of the representation of the properties of highly non-ideal mixtures using Eq. 3.6 with Eqs. 0.1, 2.8 and 2.9, is given in Figure 3.6 for the binary system ethanol - water at four temperatures. As can be seen, a good description of the phase diagram of this system is obtained, including the location of the azeotrope. Representation of the properties of non-ideal liquid mixtures has, until now, only been possible using activity coefficient models. The equation of state approach has the advantage of being capable of providing a unified description of both the high- and low- pressure regions.

We have used this model (Eq. 3.6 with Eq. 0.1, 2.8 and 2.9) to represent the experimental results for all ternary systems studied.

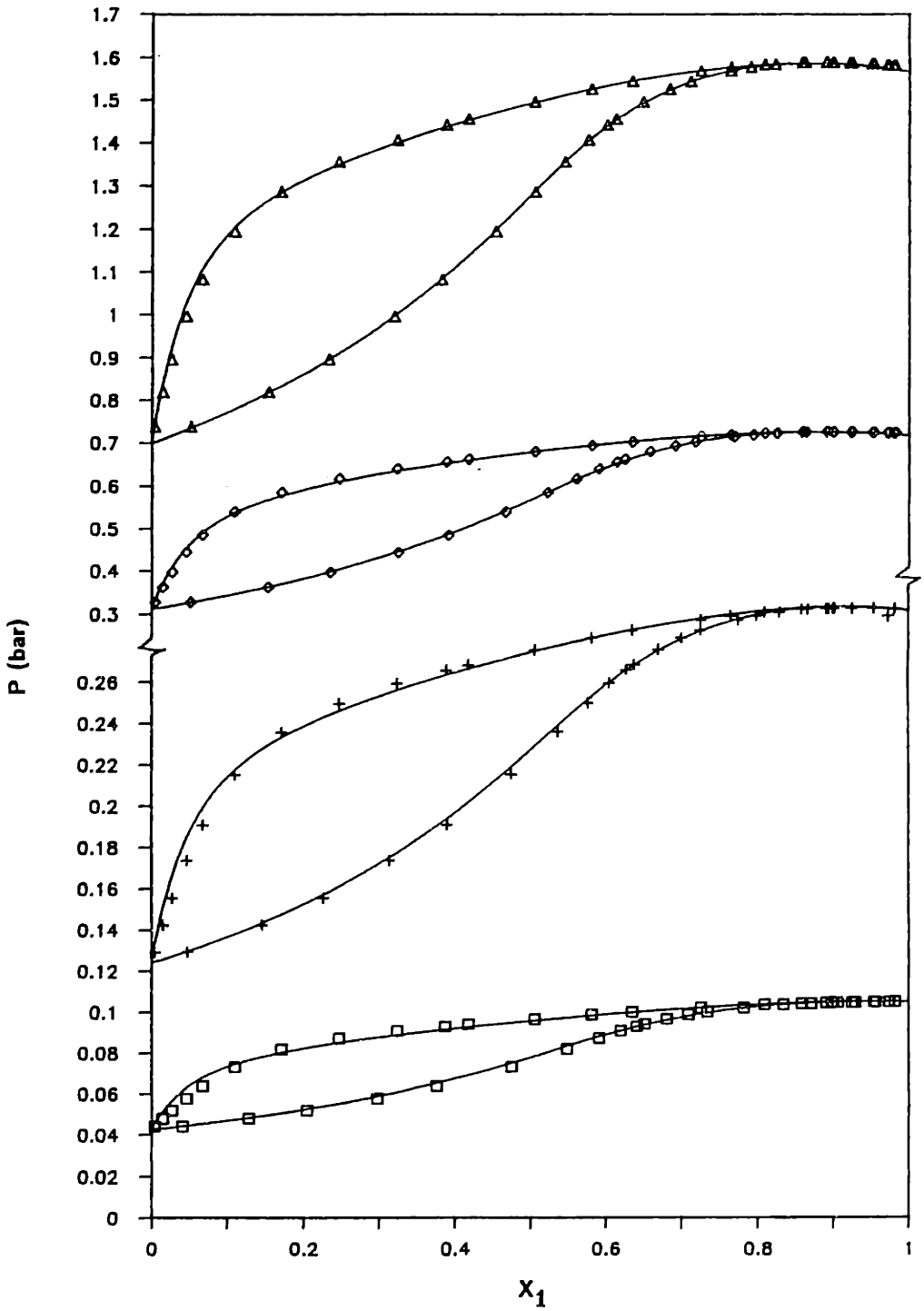

Figure 3.6 *Phase equilibrium behavior for the system ethanol - water at 303 - 363 K. Data are from Pemberton and Mash (1978): (□) 303 K; (+) 323 K; (◊) 343 K; (△) 363 K. Lines are calculated using the density-dependent model (Eq. 3.6).*

0.2.3 Summary of experimental and correlation results

Equipment and procedures

The experimental set-up used is shown in Figure 4.1. The basic element of the equipment was a high-pressure cell equipped with windows that enabled visual observation of all phases present. Direct chromatographic sampling with high-pressure switching valves was utilized for the determination of the composition of the phases, and a vibrating tube density meter was used for density measurements.

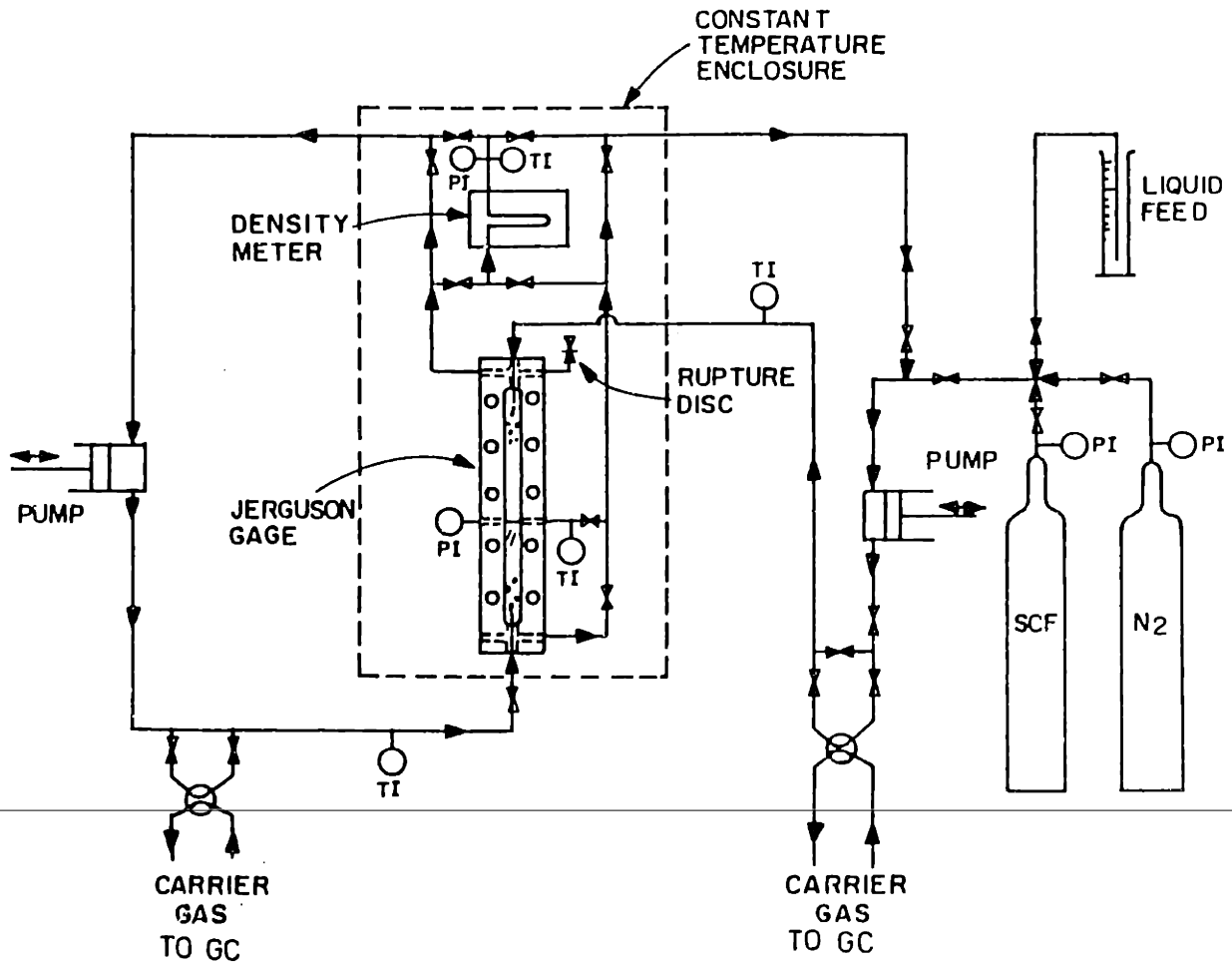

Figure 4.1 *Schematic diagram of the equipment.*

Acetone - water - carbon dioxide

The experimental results for this ternary system at 333 K are shown in Figure 4.3 for a series of pressures from 20 to 150 bar. The phase behavior for this system illustrates several of the general characteristics of the behavior of ternary systems with water and a supercritical fluids:

a. At low pressures, the phase diagram represents equilibrium between a liquid mixture of water and acetone with a carbon dioxide phase that contains small dissolved quantities of acetone and water. The solubility of CO_2 in water is small, but significant quantities of CO_2 dissolve in an acetone-rich liquid.
b. As pressure is increased, the presence of dissolved carbon dioxide results in a liquid-liquid phase split between acetone and water ("salting out with a gas"), and a three-phase region appears. This happens at pressures significantly lower than the carbon dioxide critical pressure (7.4 MPa).
c. At even higher pressures, the immiscibility gap between carbon dioxide and acetone narrows and eventually disappears at approximately 10.0 MPa. The three-phase equilibrium region also narrows and disappears at approximately the same pressure.
d. At high pressures, the phase diagram represents equilibrium between two phases, a phase rich in carbon dioxide that has dissolved substantial quantities of acetone and lesser amounts of water, and an aqueous phase with small quantities of acetone or carbon dioxide.

The results from the density-dependent model (Eq 3.6) are shown on the same figure. The interaction parameters were derived solely from binary data. As can be seen, the model represents the experimental behavior quite closely, including the evolution of the three-phase region with pressure.

n-Butanol - water - carbon dioxide

The experimentally observed behavior at 333 K is shown in Figure 4.8 (Panagiotopoulos and Reid, 1986b). The general pattern of behavior has similarities with the acetone system, but in this case, *n*-butanol and water are immiscible at all pressures studied. This results in a three-phase region that extends down to atmospheric pressure even in the absence of carbon dioxide.

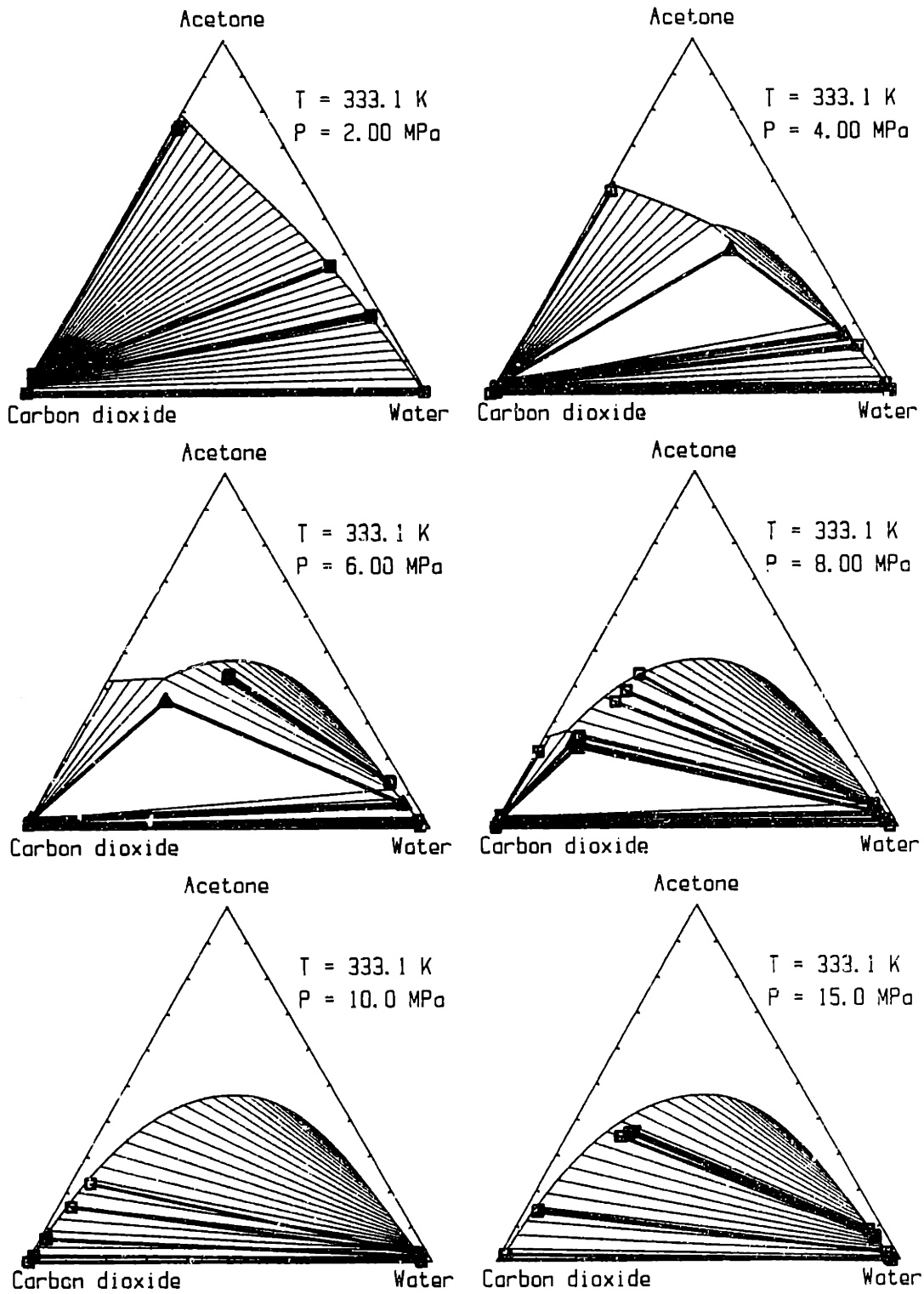

Figure 4.3 Phase equilibrium behavior for the system water - acetone-carbon dioxide at 333 K. (□) and (—) experimental phase compositions and tie-lines; (△) experimental three-phase equilibrium compositions; (—) predicted tie-lines using Eq. 3.6.

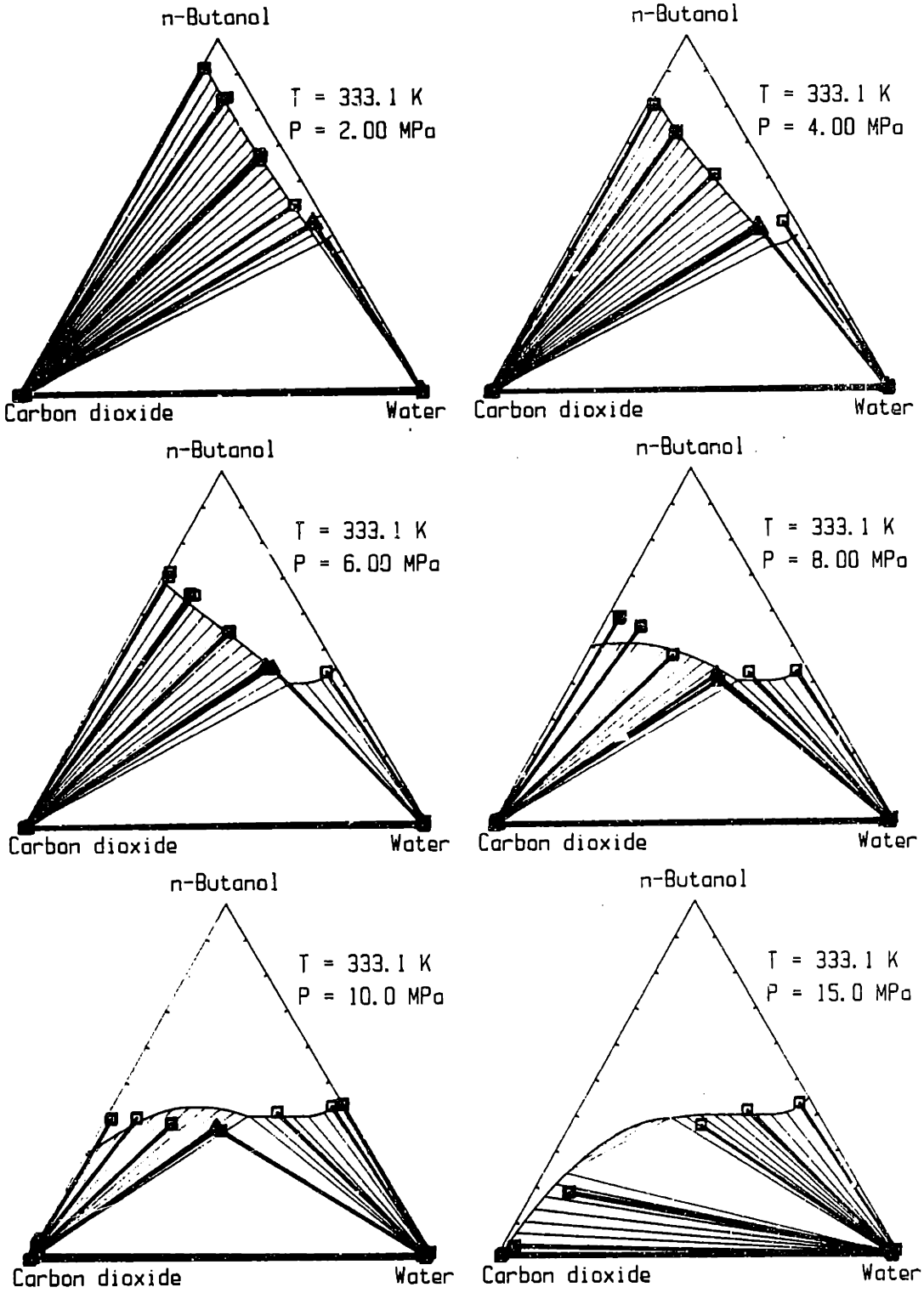

Figure 4.8 ***Phase equilibrium behavior for the system water - n-butanol-carbon dioxide at 333 K. Symbols are as in Figure 4.3.***

A unique characteristic of this system is the presence of a four phase LLLG equilibrium region at 313 K. The evolution of the phase behavior with pressure at the vicinity of the four-phase equilibrium point is shown in Figure 4.10, both from the experimental measurements and the predictions from the density-dependent model (Eq 3.6). As can be seen, the model correctly predicts the presence of a four-phase equilibrium region at 313 K, but at a slightly different pressure (7.86 MPa, as compared to the experimental value of 8.25 MPa). The predicted phase compositions differ from the measured ones, especially for the (less dense) phases rich in CO_2. It is important to note, however, that no information about the four-phase equilibrium region was incorporated into the model parameters.

The very presence of a four-phase equilibrium region implies the existence of more than one three-phase region in the immediate vicinity of the four-phase point (a point of fixed pressure at constant temperature, according to the phase rule). The evolution of two three-phase regions into a four-phase region and then again into two different three-phase regions, was originally proposed by Gibbs in 1876, based solely on thermodynamic arguments (no data were available). Figure 4.11 presents schematic three-dimensional diagrams of the topology of Gibbs space at the vicinity of the four-phase equilibrium point, for pressure slightly above and below the four-phase equilibrium pressure at constant temperature. The appearance of four equilibrium phases is necessarily related to the presence of four distinct local minima in the Gibbs energy space (the negative Gibbs energy is plotted in Figure 4.11). At exactly the four-phase equilibrium point, all four peaks must be coplanar.

Carboxylic acids - water - carbon dioxide

The phase equilibrium behavior for acetic acid and *n*-butyric acid in ternary systems with water and carbon dioxide was determined in this work. In addition, Willson (1987) studied the phase equilibrium behavior for propionic acid using the same equipment and experimental procedures. A comparison of the behavior of the three acid systems at T = 313 K and P = 15.0 MPa is given in Figure 4.15. The slope of the tie-lines, and therefore the distribution coefficient of the organic acid between the supercritical

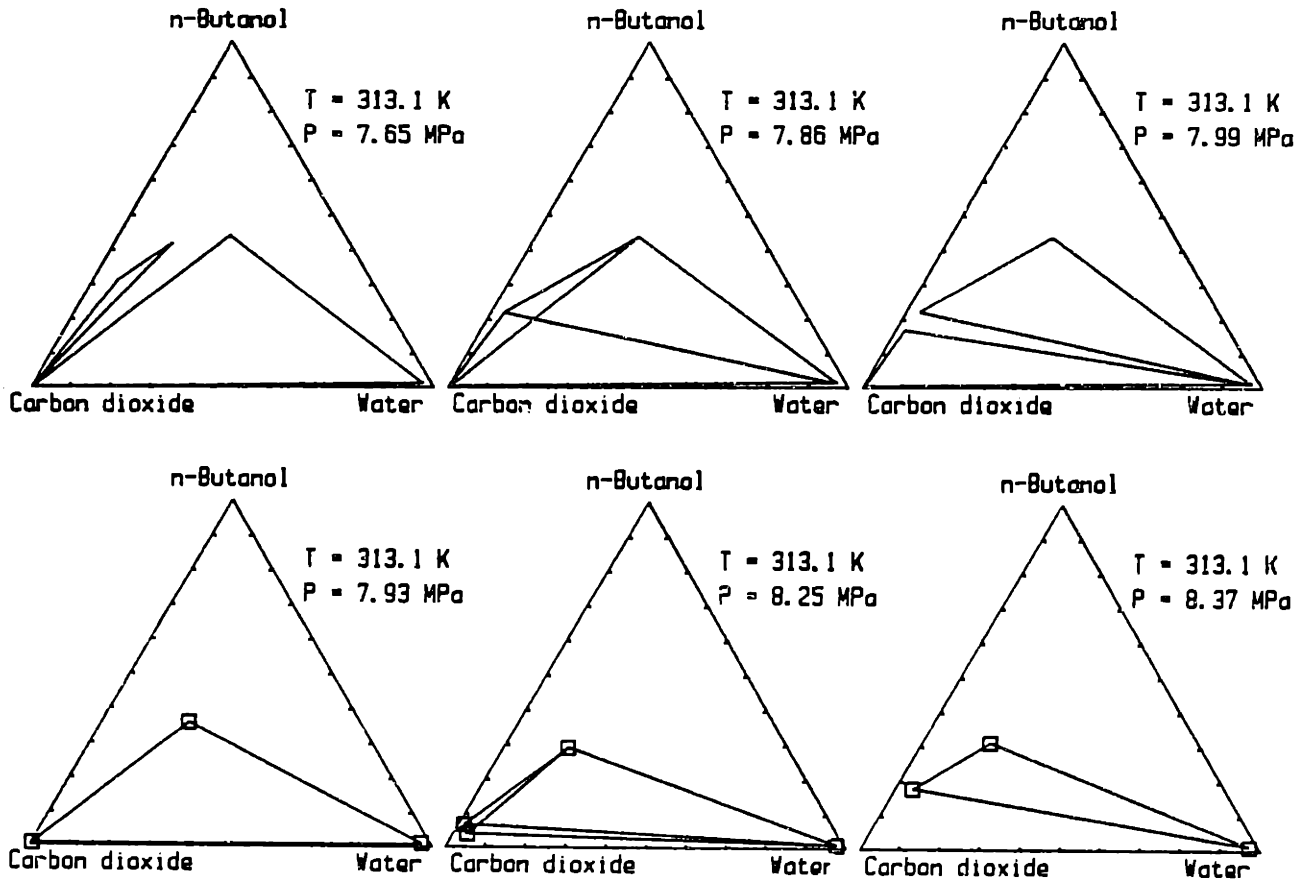

Figure 4.10 *Phase diagrams at the vicinity of the four-phase equilibrium pressure at 313 K. Lower row: experimental ; upper row: model prediction.*

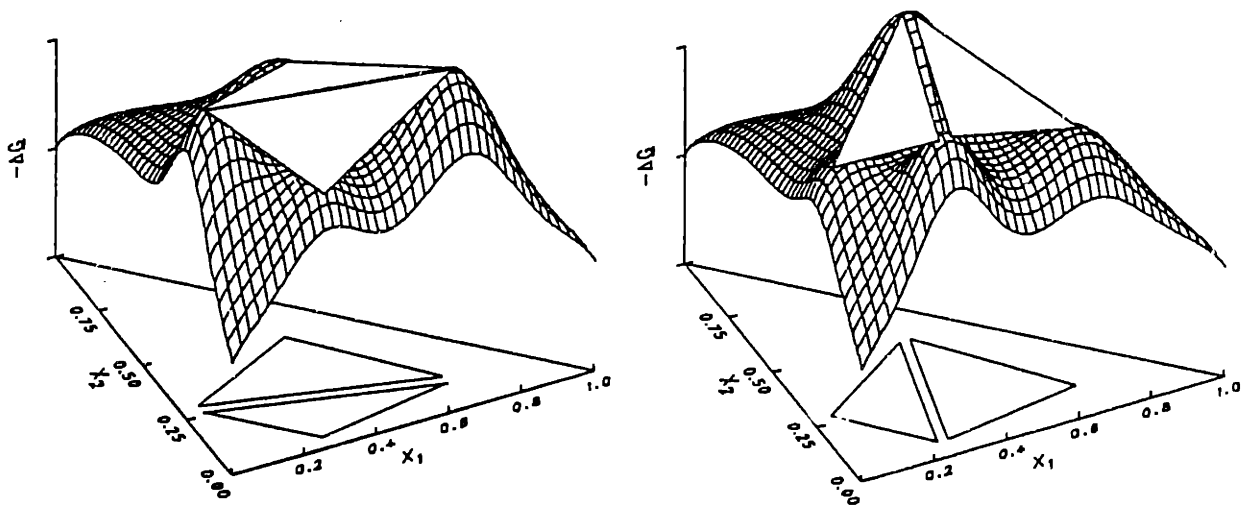

Figure 4.11 *Schematic diagram of the topology of Gibbs space at the vicinity of a four-phase equilibrium point.*

fluid and aqueous phases changes gradually from less than 1 (the acid prefers the aqueous phase) for acetic acid, to greater than 1 (the acid preferentially distributes itself to the supercritical phase) for *n*-butyric acid. In addition, the extent of the two-phase envelope (in a mole fraction basis) is less the higher the chain length of the acid.

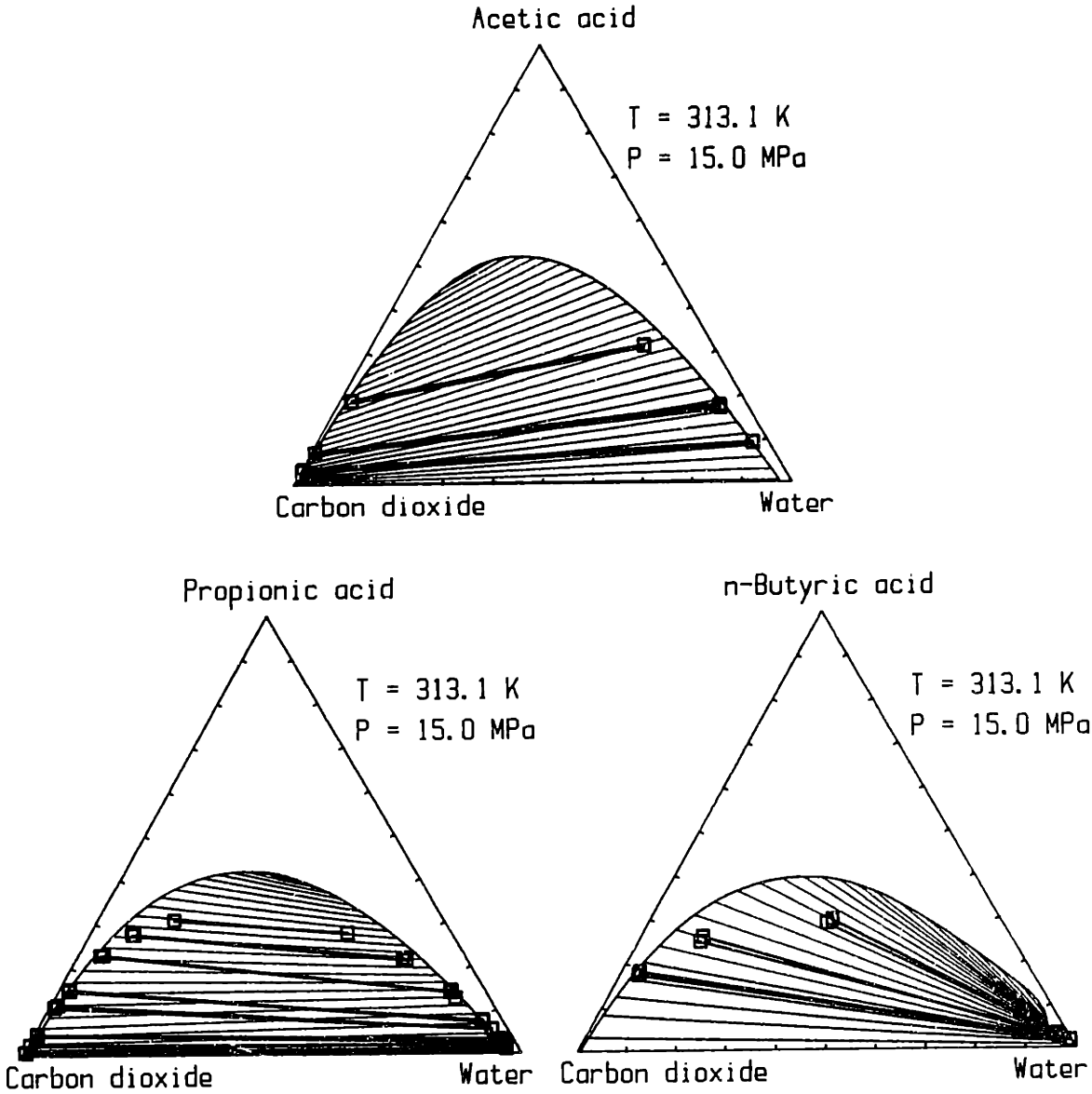

Figure 4.15 *Comparison of the ternary phase equilibrium behavior at 313 K and 150 bar for acetic, propionic and n-butyric acids. Data for propionic acid are from Willson (1987).*

Overview of experimental results

A summary of the experimentally observed behavior for the ternary systems measured is given in Table 0.1. The table also provides information for the three- and four-phase equilibrium regions we determined.

Table 0.1 Summary of experimental results

Ternary system	T K	Range[1] MPa	3 Phase[2] MPa	4 Phase[3] MPa	class[4]
acetone - water	313	1.0-26.3	2.9-8.0	–	2
- carbon dioxide	333	0.9-16.5	3.9-9.3	–	2
n-butanol - water	313	0.3-26.5	all	8.25	3
- carbon dioxide	333	0.1-20.0	all	–	3
acetic acid - water	313	1.9-15.0	7.7-8.2	–	2
- carbon dioxide	333	1.9-20.0	10.2	–	2
n-butyric acid - water carbon dioxide	313	1.9-20.0	4.0-8.0	–	2

[1] Pressure range of experimental measurements.
[2] Range of pressures over which three-phase equilibria were observed. Since no attempt was made to locate the critical end points, this would represent the minimum pressure range for three-phase coexistence.
[3] Measured four-phase coexistence pressure.
[4] Classification according to Elgin and Weinstock (1959).

0.2.4 Process implications

The phase equilibrium behavior observed for several organic compounds, can form the basis for recovery of a solute from a dilute aqueous solution. Such a process would operate between a high pressure, where the dissolving power of the supercritical fluid is high, and a low pressure where near-complete precipitation of the dissolved material would occur.

To illustrate the extent of separation possible using such a process, we present in Figure 4.6 a plot of the concentration of acetone in the supercritical phase as a function of the concentration of acetone in the liquid phase for a single step extraction with supercritical carbon dioxide at 150 bar and 333 K. Both concentrations are given as weight percent on

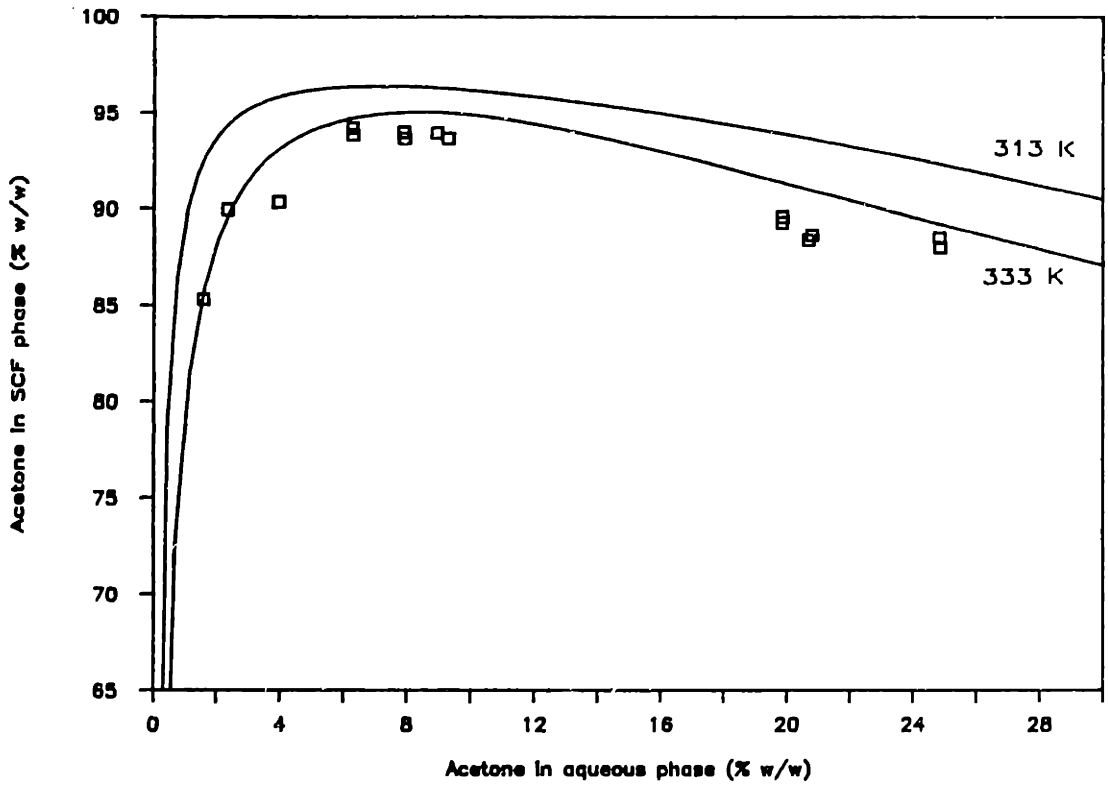

Figure 4.6 *Concentration of acetone in the supercritical fluid phase as a function of the concentration of acetone in the liquid phase at 150 bar. Concentration is given in % w/w on a CO_2-free basis. (□) experimental, 333 K; (—) predicted (Eq 3.6), 333 K and 313 K.*

a solvent-free basis. The physical significance of this representation is that after precipitation and complete removal of the solvent, the purity of the product acetone can be determined from the graph for any inlet stream composition. As can be seen, the curve has a broad maximum between 3% and 10% w/w concentration of acetone in the aqueous phase. The maximum possible purity of acetone is close to 95% w/w.

For a compound such as acetic acid, that has a low distribution coefficient between the supercritical and aqueous phase, the maximum possible purity after a single step extraction is again close to 95% w/w, but this is only possible with an inlet concentration of acid close to 65 % w/w and a high solvent to feed ratio. This implies that the selectivity of the solvent for acetic acid over water is still high, but the affinity of the acid for the highly polar aqueous versus the less polar supercritical environment is much lower.

0.3. Monte Carlo simulation

0.3.1 Methods

Metropolis importance sampling technique

The determination of the properties of a thermodynamic system using direct computer simulation originated in the 1950's, when the first electronic computing devices became available. The Metropolis (1953) Monte Carlo technique is based on the generation of a long sequence of configurations of a system. In its simplest form, the basic step is a random perturbation of a configuration $\underline{x}_\nu$, to generate a trial configuration $\underline{x}_\nu$,. The new configuration is accepted (becomes part of the sequence of configurations) or rejected (in which case the old configuration is counted once more), based on the following acceptance criterion:

$$\text{Probability of transition } (\underline{x}_\nu \rightarrow \underline{x}_\nu,) = \begin{cases} 1 & \text{if } \Delta H \leq 0 \\ e^{-\Delta H/k_B T} & \text{if } \Delta H > 0 \end{cases} \qquad [5.5]$$

where $\Delta H = H_\nu, - H_\nu$, the difference in energy between the old and new configurations. No constraint is placed upon the particular method used to generate configuration $\underline{x}_\nu'$ from configuration $\underline{x}_\nu$, other than the requirement of not biasing the Markov chain by favoring some particular types of configurations. The basic step is repeated using the generated configuration as the new starting point, and a large number of steps ($\sim 10^6$ in this study) are executed and used to calculate the ensemble average properties of the system.

The number of molecules of a system that can be investigated, even with the largest available computers, is limited to a few hundred or a few thousand, whereas our primary interest is in the calculation of properties of a macroscopic fluid, with $O(10^{23})$ molecules. One way to overcome this difficulty is the use of spatially periodic boundary conditions: the basic simulation cell is embedded in an infinite medium consisting of periodic

images of itself. This alleviates surface effects that would be dominant is an isolated cell but imposes an artificial periodicity not found in a true macroscopic system. The effect of the periodic boundary conditions on the calculated properties of the fluid is small, except near a critical point or phase stability limit.

In Figure 6.1 (Panagiotopoulos et al., 1986), we give an example of the calculated properties of the pure Lennard-Jones fluid at a subcritical and a supercritical temperature (the critical temperature of the Lennard-Jones fluid in the reduced units used is T^*_{cr}=1.30). As can be seen, the agreement between results from previous investigators and our calculated results is excellent, thus demonstrating the validity of our simulation procedures.

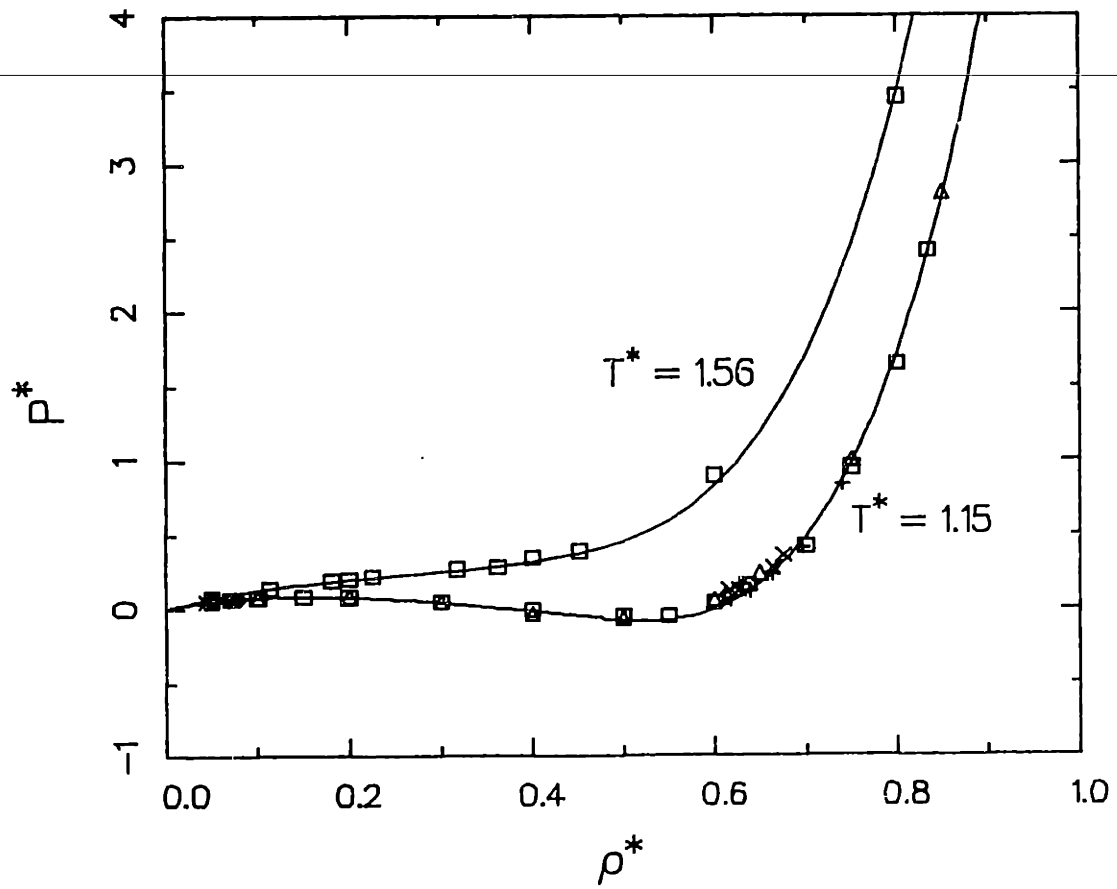

Figure 6.1 *Pressure-density relationship for the pure Lennard-Jones (6,12) fluid. (□) This study ; (△) Hansen and Verlet (1969) ; (+) Adams (1976) ; (×) Adams (1979); (◊) Yao et al. (1982); (—) Equation of state, Nicolas et al. (1979).*

Fluctuation theory and its applications

A canonical ensemble Monte Carlo simulation can directly provide information on the observable thermodynamic properties (e.g energy or pressure) for a homogeneous fluid. Our primary interest is, however, the determination of phase boundaries. Inside a phase separation region where a macroscopic fluid would completely separate into phases of different composition and density, a simulated system exhibits large local fluctuations in density and composition but cannot truly phase separate because of the system periodicity. An instantaneous configuration of the Lennard-Jones fluid at a set of conditions where a macroscopic fluid would phase-separate is given in Figure 6.2.

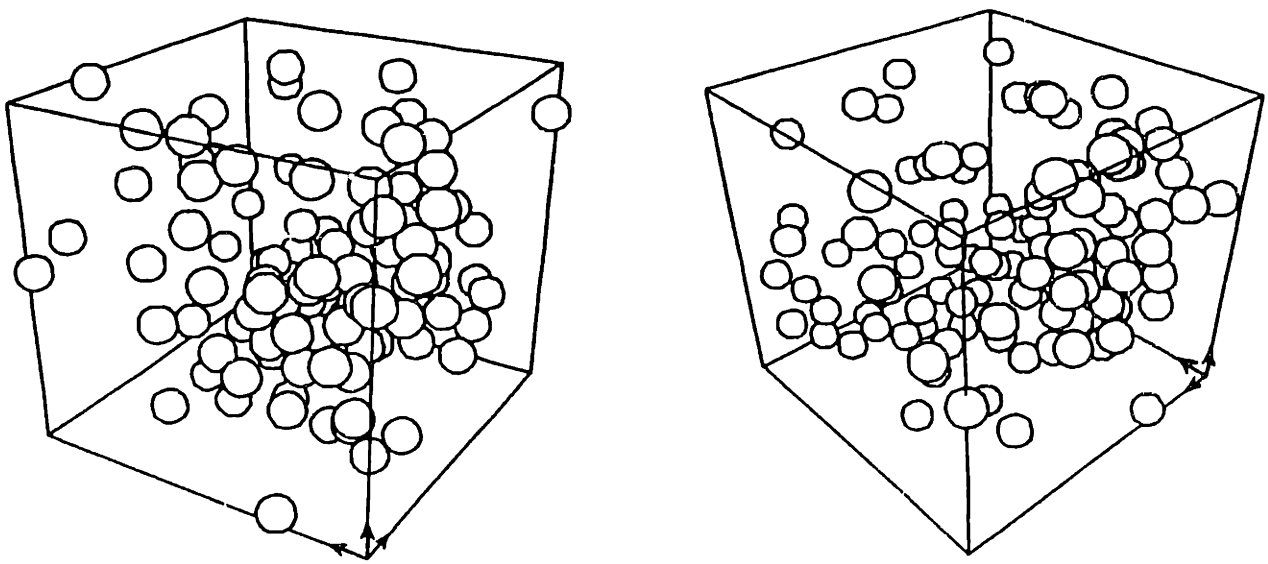

Figure 6.2 *Three dimensional representation of one instantaneous configuration for the pure Lennard-Jones fluid at $T^*=1.15$ and $\rho^*=0.20$, with N=108 molecules. The molecules are drawn at a distance equal to 0.8σ. The same configuration is represented in both halves with the origin of the coordinate system (indicated by the arrows) rotated by 90°.*

It can be shown using fluctuation theory (Landau and Lifshitz, 1980; Debenedetti, 1986; Panagiotopoulos and Reid, 1986a) that for a macroscopic fluid, at the point of phase instability, the fluctuations in local density would diverge. One method to obtain a quantitative estimate of the magnitude of the fluctuations is to follow the number of molecules in subcells of our basic simulation cell (the total number of molecules in the canonical ensemble we simulate is strictly constant). Using this technique, we were able to obtain qualitative information on the presence and approximate position of the phase transitions, thus preparing the ground for the precise determination of the phase coexistence curves by calculation of the chemical potential.

Determination of the chemical potential

The calculation of the observable thermodynamic properties of a system from a representative ensemble of configurations is relatively straight forward. This is not so, however, for the derived thermodynamic properties, such as the entropy and chemical potential. The Widom (1963) test particle method, provides a means of directly obtaining the chemical potential in a normal canonical ensemble simulation. The method has been recently extended (Shing and Gubbins, 1982) and used for the determination of the chemical potential in fluids (Romano and Singer, 1980; Powles et al., 1982; Shing and Gubbins, 1983a; Fincham et al., 1986). The essence of the method is the placement, at random positions in the fluid, of a "test" particle that does not affect in any way the course of the simulation. The chemical potential can then be calculated as an ensemble average of the interaction energies between the test particle and the rest of the fluid:

$$\beta\mu_{i,r} = - \ln \langle \exp(-\beta u_i^f) \rangle \qquad [5.7]$$

A corresponding expression can be written (Shing and Gubbins, 1982) for the calculation of the chemical potential using the properties of a "real" particle that normally takes part in the simulation:

$$\beta\mu_{i,r} = \ln \langle \exp(+\beta u_i^g) \rangle \qquad [5.9]$$

A combination of both expressions provides the means of more accurately calculating the chemical potential and testing the validity of a simulation run in terms of coverage of the relevant regions of configuration space:

$$\ell n \frac{f_i(u)}{g_i(u)} = \beta u - \beta \mu_{i,r} \qquad [5.12]$$

where $f_i(u)$ and $g_i(u)$ are the test- and real-particle distribution functions, that describe the frequency of occurrence of a given interaction energy during the simulation. An example of the application of this method is given in Figure 6.6, in which the right-hand side of Eq. 5.12 is plotted versus the dimensionless energy, u^* for the pure Lennard-Jones fluid.

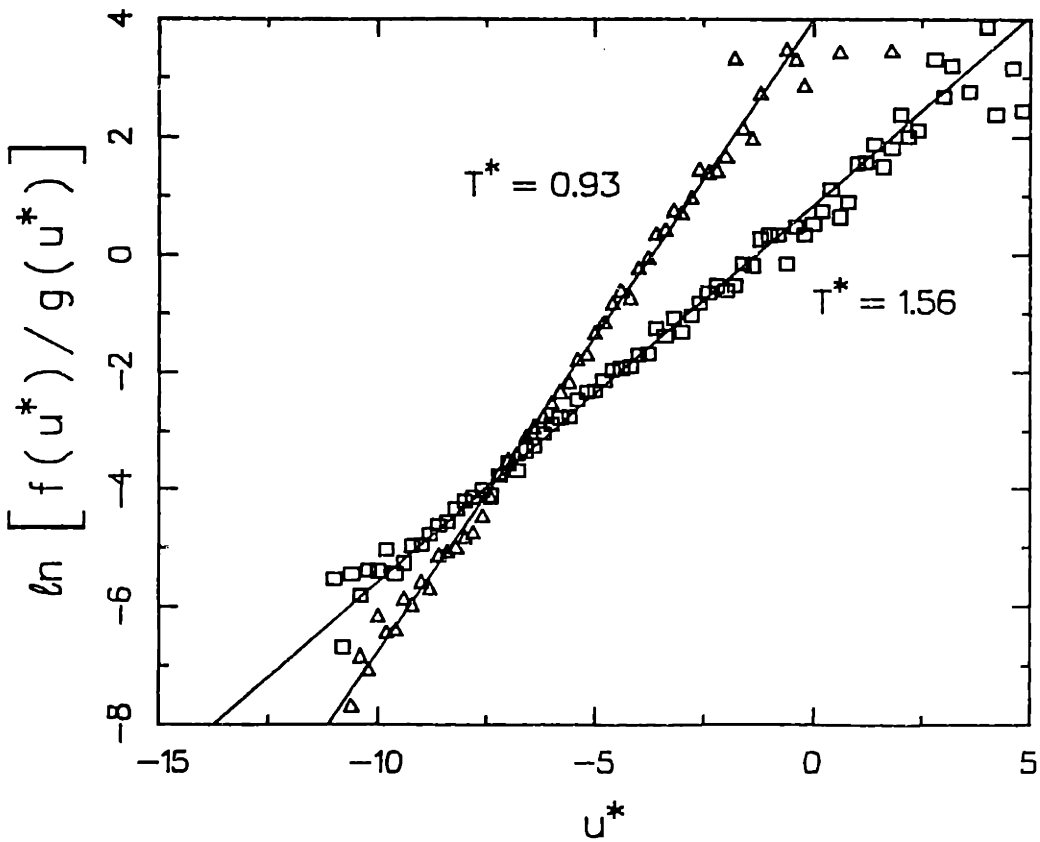

Figure 6.6. *The function* $\ell n[f(u^*)/g(u^*)]$ *vs. the energy* u^* *for the pure Lennard-Jones fluid at* $\rho^* = 0.60$. *The line has slope exactly equal to* $\beta = 1/k_B T$ *and intercept fitted to the points;* (△) $T^* = 0.93$; (□) $T^* = 1.56$.

Let us examine the energy-distribution functions and their behavior for the Lennard-Jones fluid. Figure 6.4 presents the results for the test-particle energy-distribution function for the pure Lennard-Jones fluid at $T^*=1.56$. Figure 6.5 presents the corresponding results for the real-particle distribution function. Comparable results, but at a lower reduced temperature, have been presented by Powles et al. (1982). Several observations can be made:

a. At low densities, both real- and test-particle energy-distribution functions show a sharp peak at $u^* = 0$, corresponding to an isolated molecule. A peak is also observed at a value of $u^* = -1$, corresponding to a pair of interacting molecules. The distribution functions drop off rapidly for positive and negative values of u^*, since interactions in the low density gas are uncommon.

b. As density is increased, the maximum value of the test-particle distribution function decreases significantly, the peak becomes less sharp and shifts towards lower energy values. This is explained by the fact that the probability of accommodating a test particle in a "hole" of suitable size, without overlap with any of the real particles, becomes smaller as the density increases. On the other hand, in any such configuration, the test particle is likely to be surrounded by several real particles, thus interacting with a large negative energy.

c. The real-particle distribution functions show similar trends towards less sharp peaks and lower energies as density increases, but the value of the distribution function at the maximum (and thus the relative probability of occurrence of favorable energy configurations) remains constant. In a macroscopic fluid, or during a simulation, a real molecule is not likely to find itself in a configuration of high positive energy.

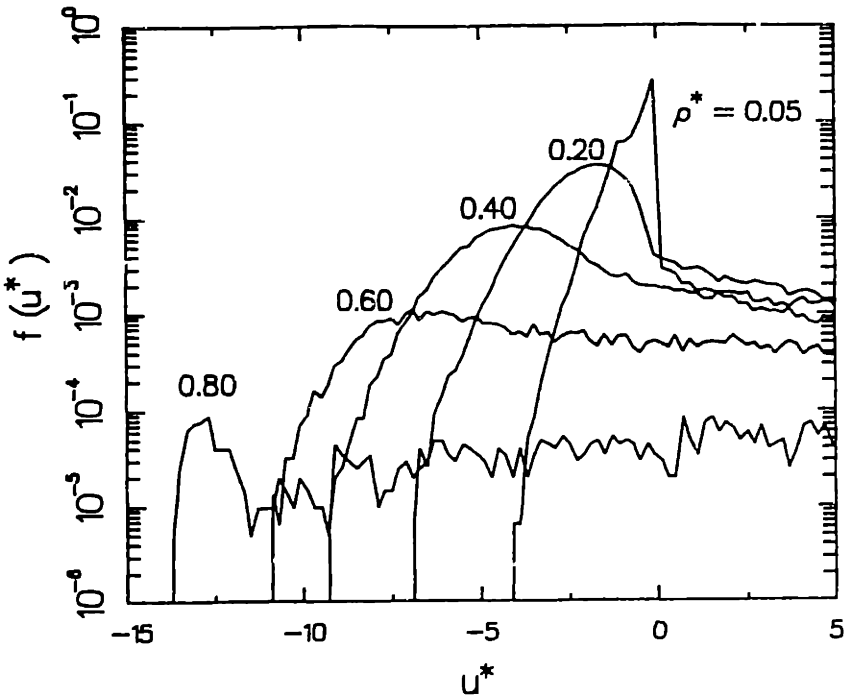

Figure 6.4 *Test-particle energy-distribution functions for the pure Lennard-Jones fluid at T^*=1.56 for a series of reduced densities.*

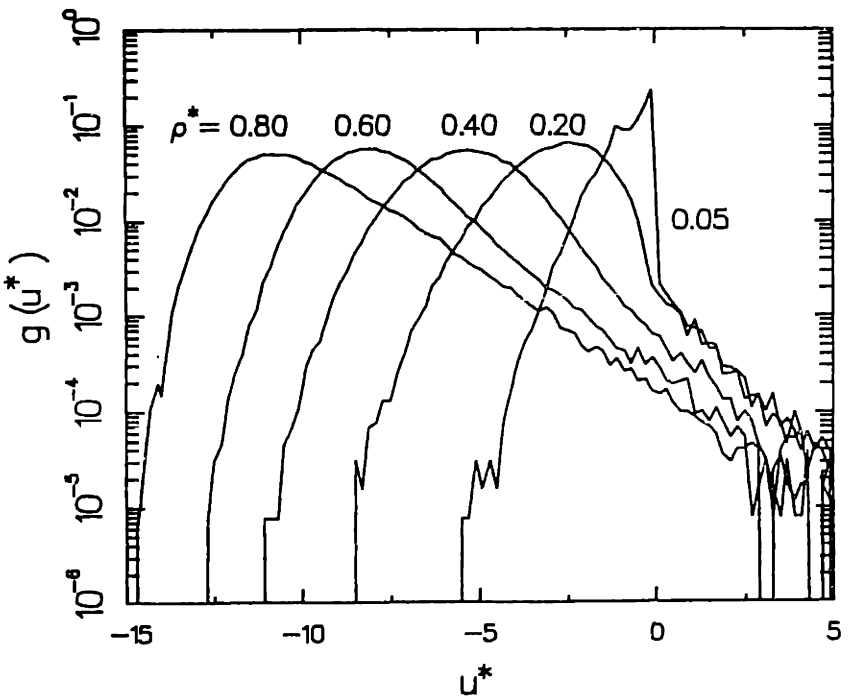

Figure 6.5 *Real-particle energy-distribution functions for the pure Lennard-Jones fluid at T^*=1.56 for a series of reduced densities.*

0.3.2 Determination of mixture phase diagrams

The study of the influence of the mixture parameters on the phase equilibrium behavior was performed in a series of model systems, using the Lennard-Jones (6,12) potential to describe the interactions between like and unlike molecules. The intermolecular potential parameters used for the three mixtures studied is given in Table 5.1. The analysis of the behavior of the mixtures follows.

Table 5.1 Lennard-Jones (6,12) potential parameters for the mixtures studied

Mixture	ϵ^*_{11}	ϵ^*_{12}	ϵ^*_{22}	σ^*_{11}	σ^*_{12}	σ^*_{22}	T^*
I	1	0.75	1	1	1	1	1.15
II	1	1	1	1	0.885	0.769	1.15
III	1	0.773	0.597	1	0.884	0.768	0.93-1.19

Mixture I. An interesting class of mixtures is one in which the components have similar sizes, but interact with specific forces that lead to unlike-pair energy interactions different from like-pair interactions. To investigate the effect of changing unlike-pair interactions, we calculated the properties of a mixture of molecules with unlike-pair parameters equal to 75% of the like-pair parameters. The molecules in their pure state are completely identical, so the mixture is symmetric. Because the unlike-pair interactions are less favorable than the like-pair interactions, we expect the mixture to show positive deviations from Raoult's law and, since the pure components have the same vapor pressures, positive azeotropy is suggested.

Figure 6.16 presents the calculated phase diagram for this mixture at $T^* = 1.15$. As expected, there is an azeotrope at equimolar composition. In addition, a liquid-liquid phase split at higher pressures is suggested by the dashed curve at the high-pressure range.

A set of energy distribution functions for this mixture at $T^* = 1.15$, $\rho^* = 0.50$, is shown in Figure 6.15. The functions $f(u^*)\exp(-\beta u)$ and $g(u^*)\exp(+\beta u)$ are plotted rather than $f(u^*)$ and $g(u^*)$, because the chemical potential of the corresponding species can be directly obtained from the integral under the curves. The peak of the functions as plotted in Figure

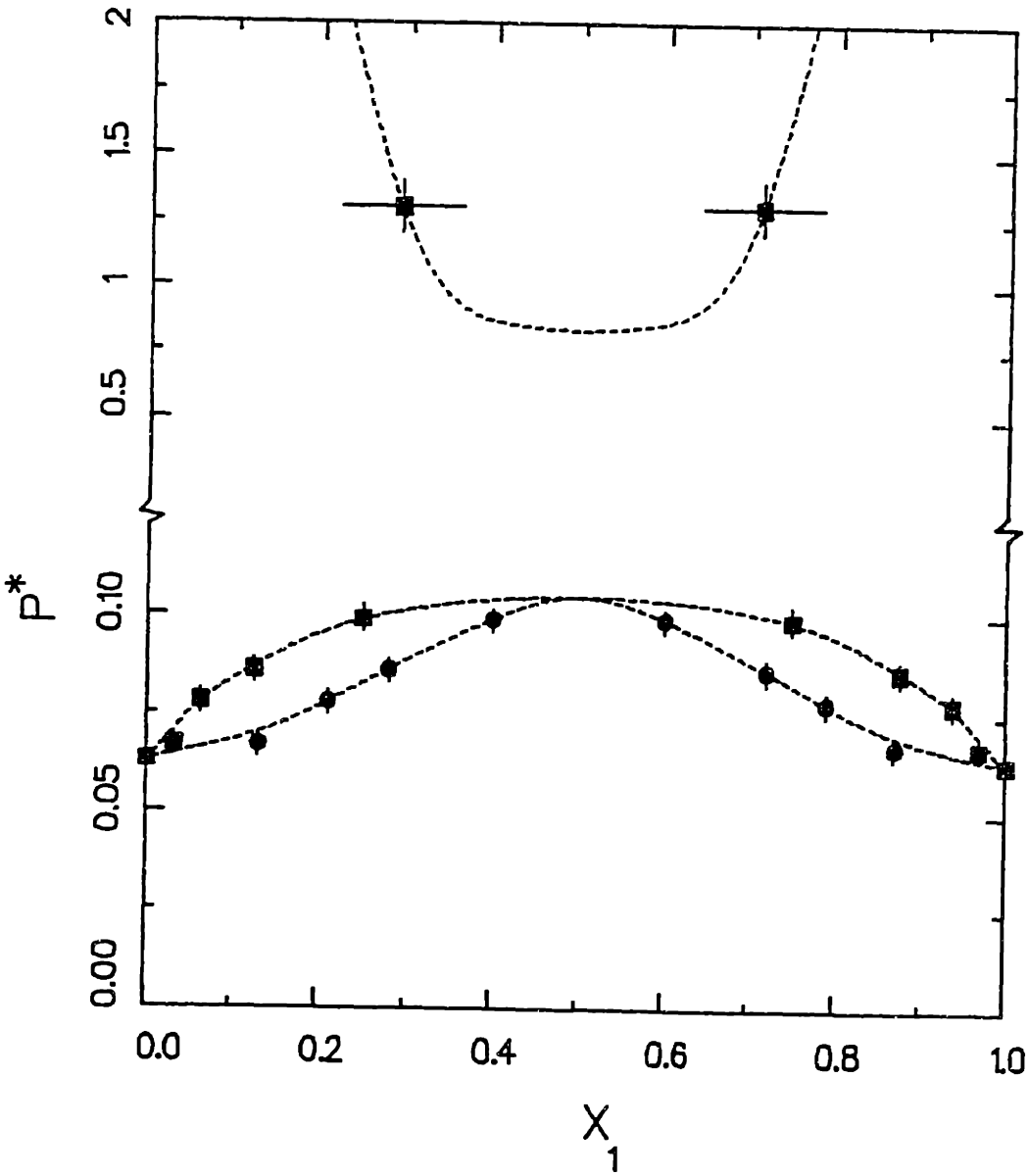

Figure 6.16 *Phase-coexistence curves for mixture I at $T^* = 1.15$. (▪) liquid phase compositions; (•) gas phase compositions. The dashed lines are drawn through the points for visual clarity. The solid lines at the points indicate estimated errors for the pressure and concentration.*

6.15 correspond to the interaction energy contributing most to the chemical potential of a component. At low concentrations of component 1, the peaks of the test and real particle energy distribution functions are shifted to positive values relative to component 2. This is a direct consequence of the unfavorable unlike-pair interactions.

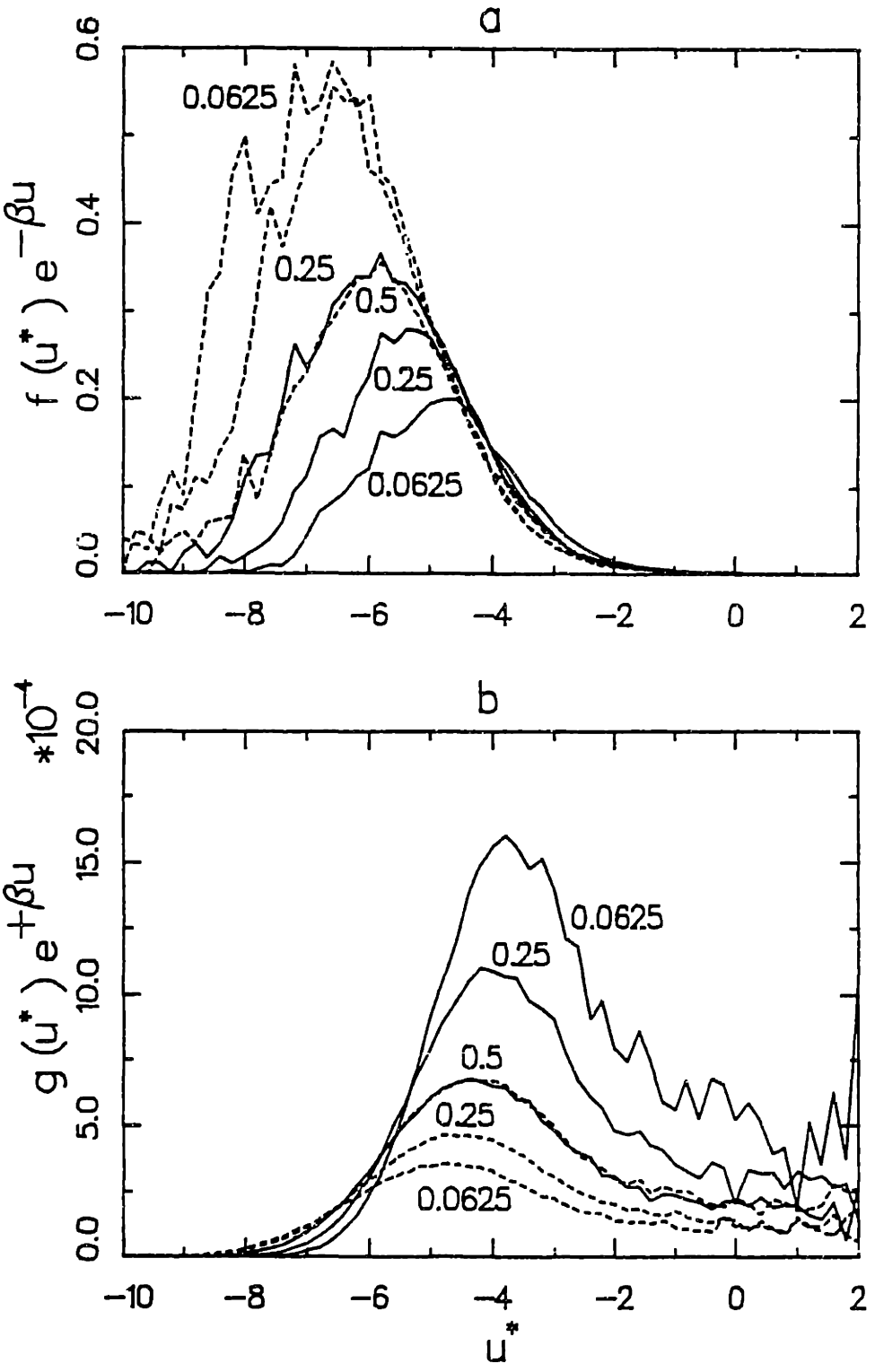

Figure 6.15. *Test- and real-particle energy-distribution functions for mixture I at T^*=1.15, ρ^*= 0.500. (——) component 1; (---) component 2. The parameter on the curves is the mole fraction of component 1, X_1.*

Mixture II. The case of mixtures of molecules of unequal sizes but similar potential well depths is not very common for real fluids since increasing size of a molecule usually results in a larger effective ϵ. Exceptions are fluorocarbon molecules that have low attractive well parameters. The ratio of volumes of the two components chosen for mixture II is equal to $(\sigma_{22}/\sigma_{11})^3 = 0.45$, so the two components have a significant size disparity. The unlike size parameter, σ_{12}, is taken as the average of the pure-component size parameters (Lorenz rule).

Figure 6.19 summarizes the phase coexistence properties of this mixture. Despite the large size difference, the phase behavior of the mixture is close to ideal. The calculation of the mixture phase diagram from Monte Carlo simulation was still possible, despite this relatively narrow coexistence region.

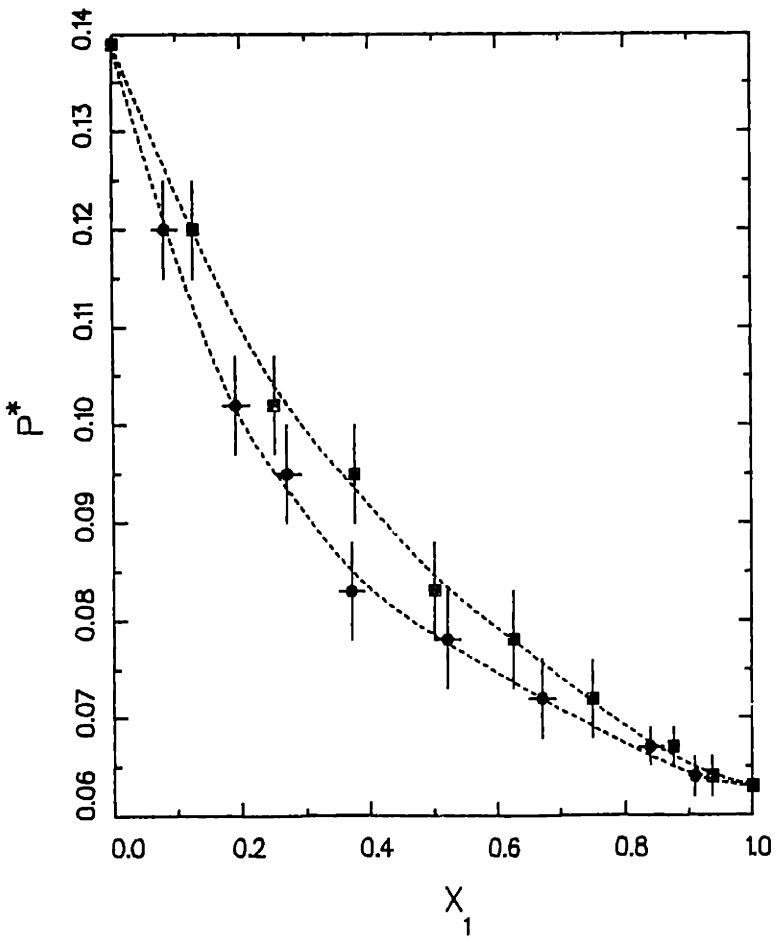

Figure 6.19 *Phase-coexistence curve for mixture II at T^*=1.15. For an explanation of the symbols used, see legend of Figure 6.16.*

Mixture III. As a test of the case where both size and energy interaction parameters are different, and also to test the ability of the simulation to reproduce phase diagrams of real mixtures, we performed a series of simulations for a mixture that is a simple model of a real asymmetric system, namely the acetone-carbon dioxide system at temperatures above the critical temperature of carbon dioxide. There is significant practical interest in the properties of mixtures of a supercritical fluid and a component of lower volatility. To obtain the potential parameters, we fitted the critical temperature and critical volume of the corresponding components using values from Reid et al. (1977). The Lorenz-Berthelot rules were used for the unlike-pair parameters (arithmetic mean of the pure component parameters for σ_{12} and geometric mean for ϵ_{12}).

The calculated phase diagram for this mixture at $T^* = 0.928$ ($T = 350$ K) is shown in Figure 6.26a, together with experimental data for the mixture carbon dioxide-acetone at three temperatures in Figure 6.26b. Only results from the cubic equation of state are available for the properties at 350 K. The mixture critical pressure is lower than the experimental value ($P_{cr} = 91$ bar from Monte Carlo; $P_{cr} = 115$ bar from the extrapolation of the experimental data) and the solubility of acetone in the supercritical phase is higher than what is experimentally observed, but the general shape of the coexistence curve is well reproduced. This agreement is all the more significant since this is a completely *a priori* prediction of the properties of the mixture with no adjustment of the potential parameters. The good representation of the properties of this mixture using the Lennard-Jones potential with no polar or quadrupolar interactions that are present in real acetone and carbon dioxide suggest that the properties of the mixture are primarily influenced by the difference in size and energy parameters and not by the detailed shape or multipolar moments of the molecules. The ability to obtain direct information on the factors responsible for a given type of macroscopic behavior is a distinct advantage of molecular simulation methods.

An important parameter characterizing fluid mixtures is the shape and location of the mixture critical curve. Close to critical points, the accurate calculation of properties of fluids from molecular simulation is impossible

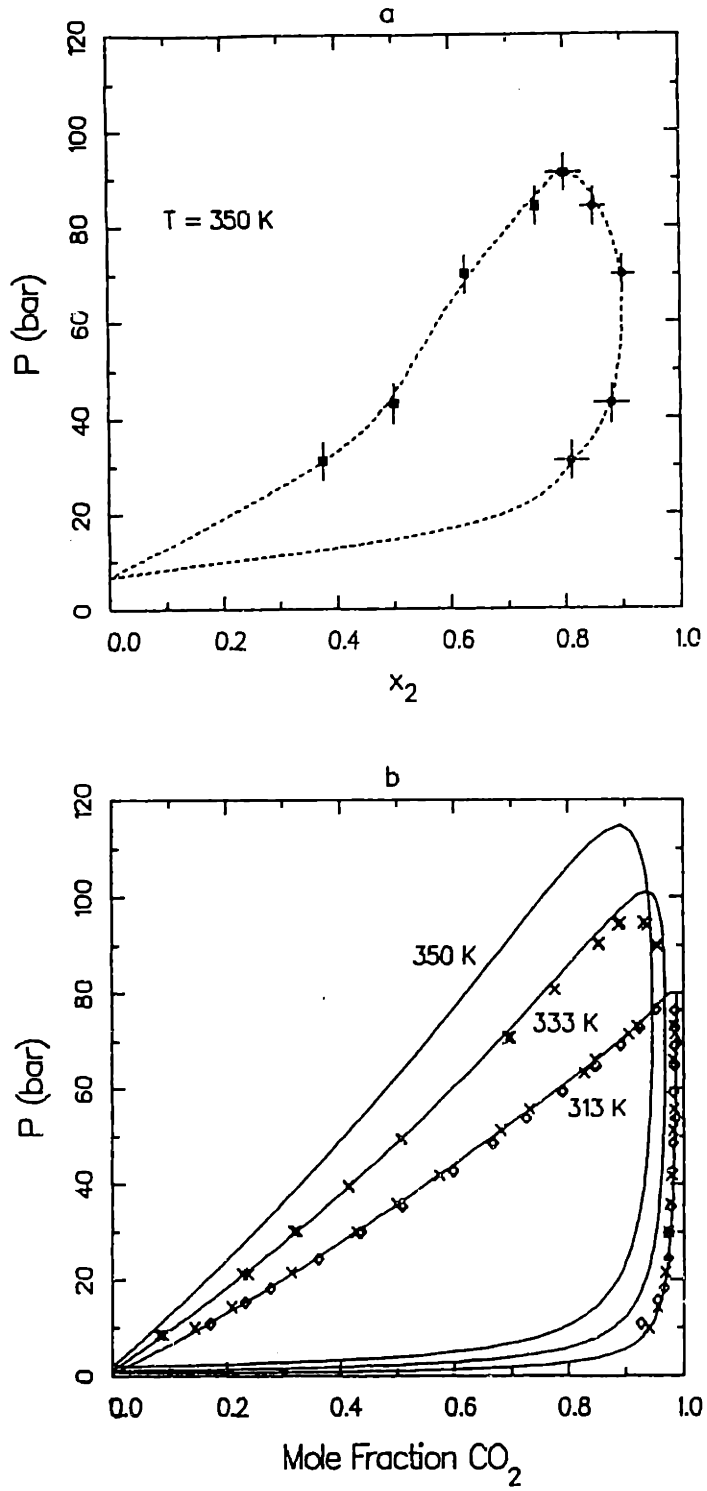

Figure 6.26 *Phase-coexistence curve for mixture III. a: Monte Carlo simulation results at T = 350 K (for an explanation of the symbols, see legend of Figure 6.16). b: (×,◊) experimental and (—) equation of state results for the mixture carbon dioxide - acetone at 313, 333 and 350 K (adapted from Panagiotopoulos and Reid, 1986b).*

because of the very large correlation lengths. We can, nevertheless, obtain the approximate location of the critical point (in the classical mean-field approximation for distances larger than the cut-off distance) by determining the point beyond which no solution to the two-phase equilibrium problem can be found. We performed a series of simulations for mixture III to obtain the mixture critical curve at several temperatures. Figure 6.27 presents the results of these calculations (no experimental data are available). The mixture critical curve is continuous from the critical point of one to the critical point of the other component; therefore, this is a type I mixture according to the classification by Scott and van Konynenburg (1970).

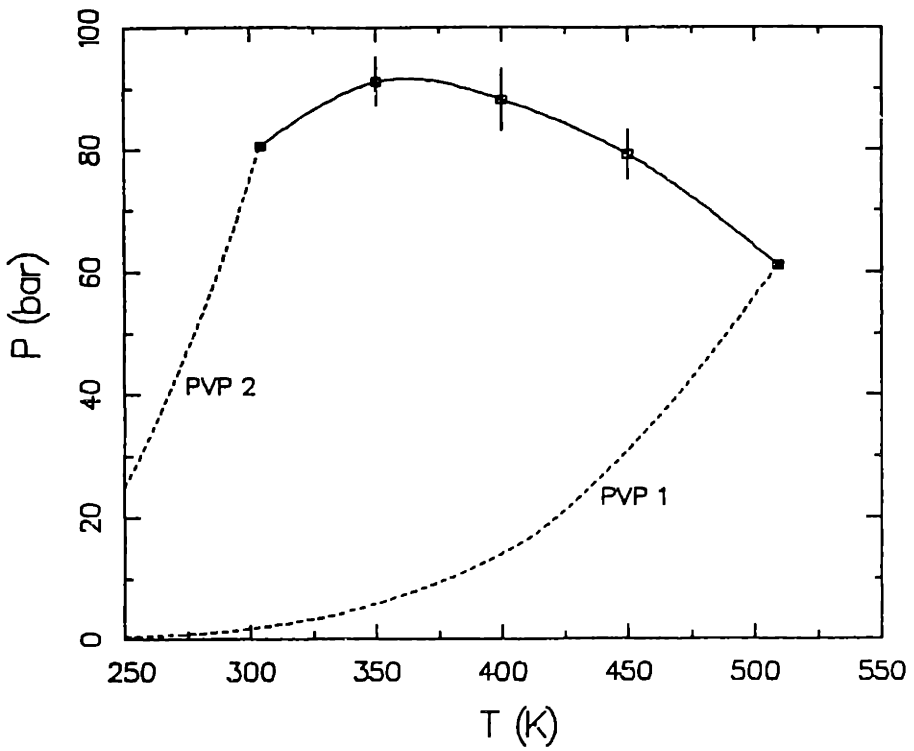

Figure 6.27 *Mixture critical curve for mixture III from Monte Carlo simulation.* (---) *pure component vapor pressures;* (□) *calculated mixture critical points;* (——) *interpolated mixture critical line.*

0.4. Conclusions and significance

Experimental and correlation

The experimental data obtained in this work demonstrate the basic characteristics of phase equilibrium behavior in ternary systems with water, a polar organic compound and a supercritical fluid. It was shown that a drastic change in phase equilibrium behavior occurs as pressure is increased above the supercritical component critical pressure. This change in behavior can be exploited for developing methods for separation of polar organic compounds from water.

A common feature of the phase equilibrium behavior in the systems studied is the presence of multiphase equilibrium regions. Three-phase equilibrium regions occur over a range of pressures comparable to the critical pressures of the supercritical fluid - organic compound binaries. The presence of a three-phase region at relatively low pressures is associated with a high selectivity of the supercritical fluid for organic compound over water. Equilibria between four fluid phases were observed for one of the systems studied (*n*-butanol - water - carbon dioxide). This type of multiphase equilibria has rarely been reported in the past.

A summary of the phase equilibrium results and their possible implications for the development of new separation methods is given below:

a. Organic compounds of moderate polarity can be extracted from dilute aqueous mixtures with high selectivity and favorable solvent capacities. For example, single-step extraction of a 4% w/w aqueous solution of acetone with carbon dioxide at 333 K and 15 MPa results in approximately 93% w/w acetone in the solvent phase (on a solvent-free basis).

b. Organic compounds, such as acetic acid, that strongly associate with water can still be selectively extracted, but the distribution coefficients between the solvent and the aqueous phase are significantly less than 1.

c. Increasing the hydrocarbon chain length in a homologous series of polar organic compounds results in improved separation efficiency, at least for the lower molecular weight compounds.

The development of new methods for recovery of fermentation products from aqueous solutions using supercritical fluids needs to take into account both the solvent ability to extract selectively the desired compound, and, in the case of in situ extraction, the solvent effect on the growing microorganisms. The results from this study suggest that the type of compounds best suited for consideration in supercritical fluid recovery processes would be low to moderately polar compounds of relatively low molecular weight.

A new density-dependent mixing rule for cubic equations of state was developed for modelling the experimental results. The model, in conjunction with a novel technique to obtain pure component parameters for equations of state, can quantitatively reproduce phase equilibrium data for highly non-ideal systems at both low and high pressures. Ternary data were predicted with parameters determined from binary data only. The methods developed can thus be used for the extension of limited experimental information and can greatly facilitate process design and optimization.

Monte Carlo simulation

The Monte Carlo simulation technique provides a direct means for predicting the macroscopic behavior of fluids and fluid mixtures when the intermolecular interactions are known. Phase envelopes, solubilities and mixture critical curves can be obtained with sufficient accuracy to permit practical use of the results. Since no empirical approximations are involved, this is a method for a priori calculation of the properties of mixtures. The technique is only limited by the lack of knowledge for the intermolecular potentials acting between real fluids, but it can still be used to elucidate the effect of the primary molecular parameters (size, shape, specific forces) on the macroscopic behavior of mixtures. Direct molecular simulation also

provides detailed information at the molecular level that cannot be obtained in any other way.

The Widom test particle expression provides a direct means for the calculation of the chemical potential from simulation. The method has limitations at high densities, but is adequate for fluids over a wide range of densities of practical importance. The energy distribution functions obtained with this approach provide useful information on the microscopic structure and energetic interactions in fluid mixtures.

Two specialized techniques developed in this work can facilitate the calculation of thermodynamic properties of non-ideal fluid mixtures. The first is based on the observation of microscopic fluctuations and enables a qualitative determination of the presence or absence of a phase transition. The second involves a particle interchange step that enables a faster and more accurate calculation of the properties of mixtures with dissimilar components.

Calculated phase diagrams for a range of mixtures using simple Lennard-Jones potential energy functions show significant variety, including azeotropes and liquid-liquid immiscibilities. Simulation of a model system of the mixture acetone-carbon dioxide demonstrates that a simple potential gives a good representation of the phase equilibrium behavior of this non-ideal mixture.

CHAPTER 1
INTRODUCTION

1.1 High pressure separations

The successful development and operation of manufacturing processes in the chemical and related industries is often determined by the ability to separate and recover desired products from a mixture. Conventional physical separations, such as distillation, have served successfully the needs of the petrochemical and oil industries, but appear to be less well suited for important new areas such as the field of biotechnology. Novel separation techniques that operate with non-traditional materials or conditions need to be explored and developed. One such new technique is the use of fluids near their critical point as solvents: the method has become known as supercritical fluid extraction.

The use of supercritical fluids has received wide attention in the recent years, and commercial applications have been proposed in such diverse areas as extraction of natural products and coal liquids, enhanced oil recovery, and supercritical fluid chromatography. For the successful development of such processes, an understanding of phase equilibria at high pressures must be achieved. In the past, only systems not involving highly polar or very dissimilar compounds, at conditions far removed from critical have been extensively studied. For such systems (e.g. hydrocarbon mixtures), reliable, although primarily empirical correlations have been developed. To the contrary, for systems such as those commonly encountered in supercritical fluid extraction, both reliable data as well as an adequate theoretical framework seem to be lacking. Because of this, the rational design of processes is difficult. The advantages associated with the use of supercritical fluids as solvents can be summarized as follows:

- High energy efficiency: The density of a supercritical fluid is the primary variable influencing its solvent power. The recovery of solute can often be achieved with relatively small changes in pressure or temperature, since close to the critical point, a small change in either of these conditions has a significant effect on the solvent density and its solvent power. In Figure 1.1, this strong effect of both temperature and pressure on the density of carbon dioxide near the critical point is illustrated.

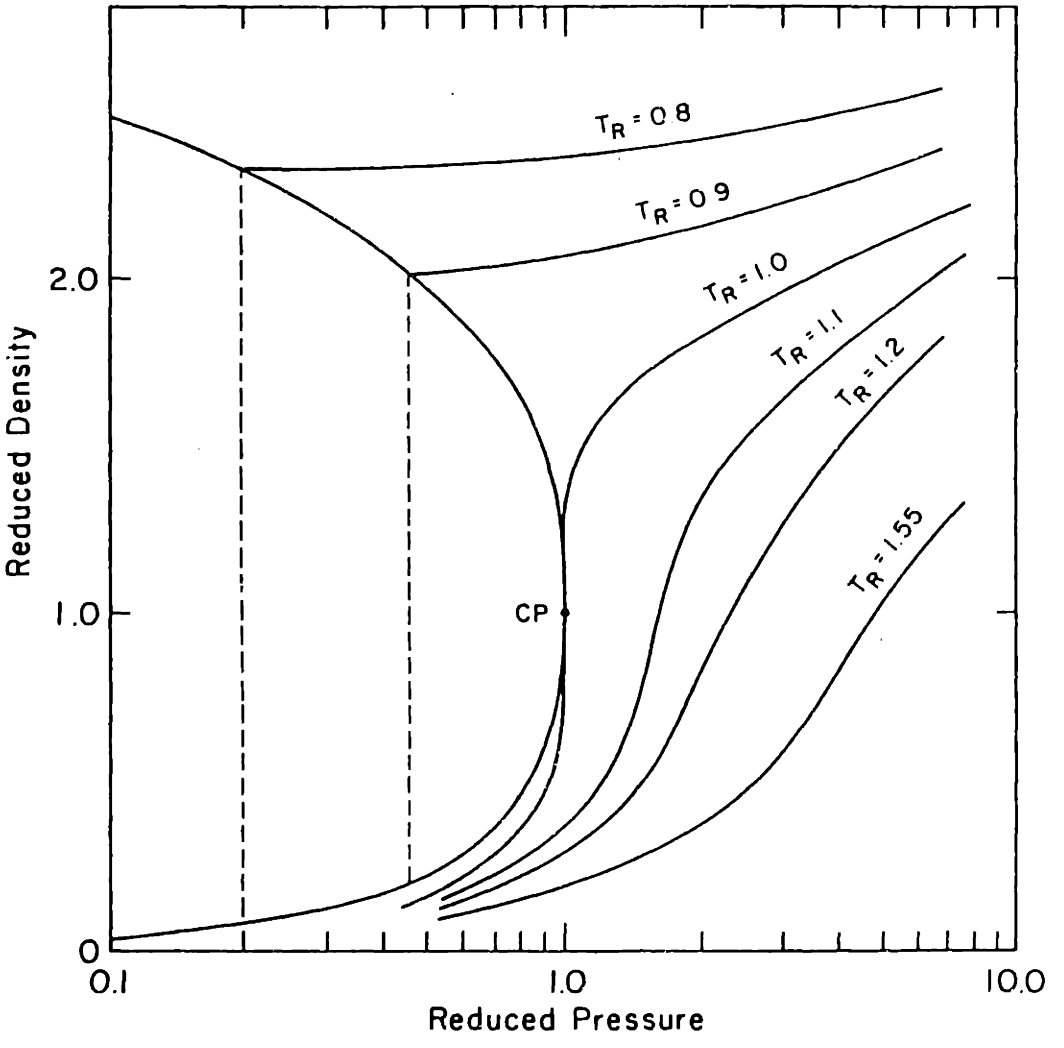

Figure 1.1 *Reduced density versus reduced pressure for carbon dioxide at the vicinity of the critical point (CP) for several isotherms (from Paulaitis et al., 1983).*

- Use of readily available and environmentally acceptable materials, such as CO_2 or light hydrocarbon gases. Other solvents, such as fluorocarbons, could also be used. They offer the advantage of lower operating pressures, although they are more expensive and questionable from an environmental-impact point of view.
- Highly favorable transport properties of the solvents. A typical comparison of the properties of a supercritical fluid to those of a liquid is given in Table 1.1 (Paulaitis et al., 1984). As can be seen, while having a density close to that of a liquid, supercritical fluids have viscosity and diffusion coefficients intermediate in value to those of a liquid and a low-pressure gas. The effective diffusion coefficients for supercritical fluids can be almost an order of magnitude higher than the values shown in Table 1.1, due to strong natural convection effects, as shown by Debenedetti (1984). Both these properties are desirable, since they lead to enhanced mass transfer characteristics for high pressure phase extraction processes.
- Supercritical fluids often show higher selectivities for some compounds than those expected from the compound's volatility. This may result in improved separation efficiencies relative to distillation.

Table 1.1 Order-of-magnitude comparison of the properties of typical low-density gases, liquids and supercritical fluids

Property	Gas	Supercritical fluid†	Liquid
Density (kg/m^3)	1	700	1000
Viscosity (Ns/m^2)	10^{-5}	10^{-4}	10^{-3}
Self diffusion coefficient (cm^2/s)	10^{-1}	10^{-4}	10^{-5}

†At $T_r \approx 1$ and $P_r \approx 2$

A promising potential application of high-pressure extractions is to recover organic chemicals from aqueous solutions in a more efficient way than conventional liquid-liquid extraction od distillation. The importance of this particular application becomes apparent if one considers the role that biotechnology has assumed in recent years. Biochemical processes

have provided new opportunities for the synthesis of a wide variety of chemical products which at present are mostly high-value, small-volume chemicals such as pharmaceuticals. High-volume, commodity chemicals traditionally manufactured by direct chemical synthesis can also be made. Biochemical conversions can utilize cheap, readily available raw materials such as lignocellulosic biomass or coal- or biomass- derived synthesis gas, and provide increased selectivity and the possibility of operation near room temperatures. A general problem, however, especially severe for the lower value products, may be product recovery from dilute aqueous solutions, containing cells, salts, and possibly insoluble substrates. For a chemical such as ethanol, the energy required for distillation of the product from the aqueous broth, is the limiting factor for the economic viability of the process. One can also hope to eliminate an additional restraint that often limits the productivity of biotechnological processes, namely the problem of product inhibition. A high pressure fluid may be used for the in situ recovery of one or more products from a fermentation broth.

1.2 Prediction of macroscopic properties

To realize the full potential of any separation process, accurate information on the physical properties of the mixtures to be separated are needed. Clearly, the range of process conditions that may be used in practice, especially for complex mixtures with many degrees of freedom, is much greater than the amount of direct experimental information that can be obtained. This is especially true for new separation methods, such as extraction with dense gases, that operate in a range of conditions where relatively little experimental information has been obtained in the past.

The most common way to extend the experimental data base outside the immediate range of conditions for which it was obtained, is to extrapolate using empirical or semiempirical models, with adjustable parameters obtained from regression of experimental data. Substantial effort and activity has been centered on the question of developing new correlation methods that can be used for polar, asymmetric mixtures at high pressures, but the

problem of obtaining methods that will be successful for a wide range of conditions outside the data range on which they are based remains open. An alternative for such methods is the use of models with a firm theoretical basis that can use very limited experimental information to predict the behavior of a system over a wide range of process conditions.

Two sets of difficulties prohibit the prediction of macroscopic properties of pure substances and mixtures from first principles: (i) the energies of interaction (repulsion and attraction) between molecules are rarely known quantitatively and (ii) the problem of utilizing knowledge about the molecular interactions to calculate properties of large collections of molecules is very difficult to solve. For the first problem, we now believe that the interaction energies are direct manifestations of the electromagnetic interactions between elementary charges but until now, we have only a few a priori calculated potentials for simple atoms and molecules (Maitland et al., 1981). The second problem is the basic theme of statistical thermodynamics.

One approach to the estimation of macroscopic properties when the intermolecular interactions are known is primarily analytical. The partition function or the Helmholtz energy of the system is expanded in a perturbation series around a fluid of known properties (Barker and Henderson, 1967; Weeks et al., 1971) or a closure of the integral equations describing the fluid is attempted (Yvon-Borg-Green hierarchy and Ornstein-Zernike equations). Detailed discussions of both types of methods are given by Hansen and McDonald (1976) and Gray and Gubbins (1984). The resulting expressions have the advantage of being analytical or semi-analytical in nature, but the theories are not generally applicable to complex or highly non-ideal mixtures differing substantially from the reference fluids. In the application of these methods, data are needed for the thermodynamic properties of a wide variety of mixtures with known intermolecular interactions. Such data are not normally available for complex fluids.

Another approach uses computer simulation techniques, namely molecular dynamics (Alder and Wainwright, 1959) or Monte Carlo simulation (Metropolis et al., 1953) to investigate fluids with specified intermolecular interactions. In principle, results can be obtained that closely approximate the exact

properties of a fluid model. The price for the higher flexibility and accuracy is the substantial computational effort associated with these methods, as well as the non-analytical form of the results. The calculations must be repeated for a wide range of conditions and molecular potential parameters to obtain a broad picture of the behavior of different classes of fluids. These techniques should therefore be regarded as complementing, rather than replacing, the theoretical methods mentioned above. Incorporation of results from molecular simulation of well defined mixtures can greatly facilitate the development of theories of the liquid state. The techniques can also help to obtain thermodynamic data for mixtures outside the practical limits for experimentation (high pressures, hazardous mixtures).

The integration of the various approaches for the determination of physical properties and phase equilibria is schematically summarized in Figure 1.2. Experimental methods play a central role by providing the data for the development of new separation methods and for the testing of models, theories and simulation results. Correlation methods draw on experimental data for the determination of parameters, but they extend the usefulness and provide input for detailed process modelling and optimization. Computer simulation can be used both for the prediction of properties of real mixtures and for the testing of theoretical models, by generating exact results for model systems. Finally, theoretical models are developed with input from both experiment and computer simulation. The distinction between "correlation" and "theory" is often not as clear-cut as represented in the schematic diagram, since many successful correlation techniques use theoretical expressions as their starting point, but make approximations to render the models more tractable.

1.3 Problem definition

The general area of interest of this work is the investigation of phase equilibria in fluid mixtures at high pressures for systems that have a potential for development of novel separation methods. The term high pressure means pressures comparable or greater than the critical pressures

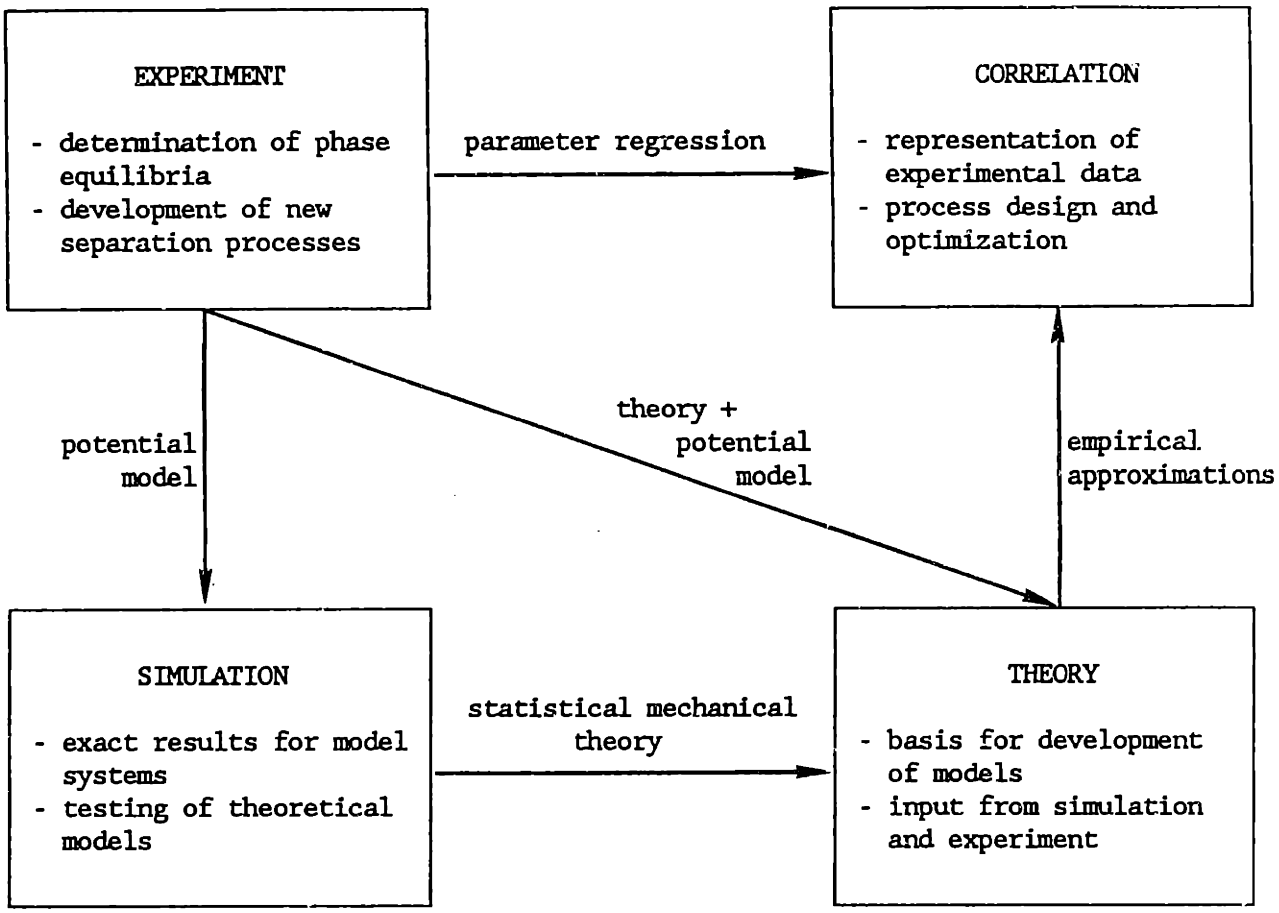

Figure 1.2 *Relationships between the various techniques for the investigation of phase equilibria.*

of the systems in question. In general, this would imply that pressures from above atmospheric to a few hundred bar are considered. We approached the problem from two directions, namely (i) from an experimental and correlation point of view and (ii) in terms of purely predictive molecular simulation techniques. The two approaches are complementary: the experimental and correlation parts of the work provide new experimental information for the range of conditions that may be useful for practical separations and data for the testing of theoretical models; the parallel investigation of the applicability of direct computer simulation techniques to the determination

of phase equilibria in dense fluid mixtures may eventually extend the range of validity of experimental information.

We can identify our basic objectives as follows:

Experimental and correlation: The basic goal in this area is to obtain experimental information to evaluate the potential of high pressure separations with supercritical solvents for the recovery of polar organic materials from aqueous solutions. The specific aspects of the problem that need to be addressed can be summarized below:

a. What are promising solutes and solvents with potential for efficient separations?
b. What kind of experimental information is needed to obtain an understanding of the basic phase equilibrium phenomena for the systems of interest?
c. Can we develop correlation techniques for the relevant experimental data valid for a wide range of process conditions?

Molecular simulation: The basic goal in this area, is the determination of the ability to predict the phase equilibrium behavior of dense fluid mixtures when the intermolecular interactions are known. Specifically, we are interested in the following questions:

a. Can we predict the phase diagram for mixtures with known intermolecular interactions?
b. How do microscopic properties (size, attractive well depth, dipole and quadrupole moment, cross potential parameters) affect the phase behavior?
c. How do the results from direct molecular simulation compare to the available experimental information?

A detailed presentation of the specific research objectives for the two parts of this work is given in the first sections of Chapters 2 and 4.

CHAPTER 2
EXPERIMENTAL AND CORRELATION: BACKGROUND

2.1 Research objectives

2.1.1 Systems of interest

The main focus of the proposed research, as stated in Section 1.2, is on systems that include a supercritical fluid and an aqueous solution of a low molecular weight organic compound. Phase equilibrium data are needed to evaluate the potential of supercritical fluid extraction for separations of products of biochemical syntheses. Moreover, we need to test theoretical and semi-empirical models for their applicability in the correlation and prediction of high-pressure phase behavior in systems that include polar compounds. The selection of the systems to be investigated, must take into account both objectives.

The criteria that were used for the selection of the compounds to be extracted (solutes) were as follows:

- The solutes were required to be representative of a class of organic compounds. This helps in generalizing the results, as most properties of organic compounds show a regular change in behavior within a homologous series.
- It was desirable that the compounds were either primary products of fermentations, substrates, or undesired by-products that inhibit the growth of microorganisms.
- The solutes were chosen to have simple chemical structures, so that the effect of various functional groups on the properties of the mixtures could be investigated.

Based on these criteria, the solutes selected, were:

n-Butanol: A product of synthesis by some anaerobic bacteria, one problem for its production by fermentation is the high toxicity to the producing microorganisms. Because of this, the maximum product concentration that can be achieved is only around 1% w/w. *n*-Butanol is representative of the higher alcohols, and preliminary evidence (Schultz and Randall, 1970) suggested that it may be considerably more extractable than ethanol. This was found indeed to be the case (Section 4.3).

Acetone: Acetone can also be produced by anaerobic fermentation, usually simultaneously with *n*-butanol (e.g. from *clostridium aceto-butilicum*). The reason this compound was included is that it has a fairly simple structure, and is representative of ketones, an industrially important class of organic compounds.

Acetic acid: A study of the effect of the carboxyl group and its strong acidic character on the phase equilibrium behavior is possible using this compound. In general, carboxylic acids form an important group of compounds for which data for the evaluation of supercritical fluid extractio processes are lacking.

n-Butyric acid: The inclusion of this compound in our base set enables us to form a complete 2 X 2 matrix of alcohols (together with literature results for ethanol) and monocarboxylic, straight-chain organic acids. In this way, both the effect of changing a functional group at a given carbon number, and the effect of changing chain length, can be evaluated.

For the selection of solvents, a different set of criteria applied. The most important among them were:

- They should be readily available industrial gases.
- Their critical temperature should be in the temperature region where common microorganisms show the maximum productivity (approx. 300-330 K).
- Favorable safety characteristics, namely non-flammability and low toxicity, were desirable.

The most favorable selection, that satisfies all of the above constraints, is carbon dioxide. This gas was used as the common solvent

for this work. With a critical temperature of 304 K, low cost, and non-toxic, non-flammable character, it appears to be an attractive potential solvent. It is for this reason, that CO_2 has been so extensively studied, and indeed, has sometimes been considered as a unique "supercritical solvent". For the purposes we are interested in, there are, nevertheless, some potential disadvantages. The most important is its acidic nature in an aqueous environment. This creates problems for the viability of the microorganisms if CO_2 is used for <u>in vivo</u> extraction (Willson *et al.*, 1986).

2.1.2 Objectives

The basic requirement from the experimental and correlation part of this work is to obtain sufficient information for the evaluation of the use of supercritical solvents for the recovery of polar organic compounds from aqueous solutions. Several specific subtasks can be identified:

- We need to obtain a general picture of the relevant phase equilibria in the ternary systems we selected for study, and identify possible trends with different functional groups or molecular weight of the compounds.
- To achieve such a general picture, we need to use existing correlation techniques or develop new ones to represent the phase equilibria in the range of conditions of interest.
- Finally, we need to investigate the possible implications for the development of new separation processes, based on the experimentally observed phase equilibrium behavior and the correlation results.

The range of conditions of interest should be sufficient to cover the potential useful range of operation of separation processes. We chose to operate at two temperatures, 313 and 333 K, both above the critical temperature of the solvent (T_c = 304 K for CO_2). Operation at higher temperatures seems less desirable because the favorable characteristics of the supercritical solvent are gradually reduced away from the critical point.

The pressure range for the experimental investigation is from 20 - 250 bar total pressure. The critical pressure of carbon dioxide is 74 bar, so the range of operating conditions covers both regions where the solvent is a low-density gas and the dense fluid region. The latter region is important for determining the maximum solvent power of the supercritical fluid. The low-pressure region is important for the investigation of solvent losses and solute recoveries after depressurization.

2.2 Literature review - Experimental

2.2.1 Historic development of supercritical extraction

Over 100 years ago, Hannay and Hogarth (1879) and Hannay (1880) noticed that gases above their critical points possess solvent power very similar to that of liquids, a fact which they used to argue for the fundamental continuity of the liquid and gas phases above the critical point. They worked primarily with solid solutes, and observed the peculiar dependence of the solubility on the temperature (retrograde solubility region, in which the solubility decreases with increasing temperature at constant pressure). Several decades passed before there was a renewed interest in supercritical fluids as solvents. Equilibria between solids and supercritical fluids were extensively investigated by Diepen and Scheffer (1948,1953), van Welie and Diepen (1961) and Tsekhanskaya et al. (1962,1964). Recent industrial efforts for the use of supercritical solvents have been stimulated primarily by work at the Max Planck Institute für Kolhenforschung in Germany (Zosel,1978), that concentrated on the extraction of various natural products.

In the area of equilibria between supercritical fluids and liquids early work at Princeton University (Todd, 1952; Snedeker, 1956) concentrated on the equilibria of supercritical carbon dioxide and ethylene in binary and ternary systems with liquid organic compounds. Francis (1954) investigated a large number of ternary systems of liquid carbon dioxide near its critical point and demonstrated that it can be useful as an extracting agent. Elgin and Weinstock (1959) were the first to investigate

extensively ternary systems of ethylene, water, and an organic liquid, and to propose possible applications for the separation of organics from water. One of their important observations, was that a supercritical gas can act as a "salting out" agent and induce a phase split of an aqueous solution.

The use of supercritical solvents for the energy-efficient recovery of alcohols from aqueous solutions has been recently been proposed by several investigators. Paulaitis et al. (1981) and McHugh et al. (1981) investigated the recovery of ethanol with carbon dioxide, ethylene and ethane. Kuk and Montagna (1983) presented results for the recovery of ethanol and isopropanol using supercritical carbon dioxide. Radosz (1984) and Paulaitis et al. (1984) have determined phase equilibria for the system isopropanol - water-carbon dioxide. The results from these investigations suggest that supercritical solvents can be used for the recovery of ethanol from aqueous solutions, but the distribution coefficients are low, with resulting large requirements for solvent. Distribution coefficients for isopropanol are more favorable.

The field of supercritical fluid extraction, has been reviewed in the past by several authors (Irani and Funk, 1977; Williams, 1981; Randall, 1982). The last author concentrates on the development of dense gas chromatography, but also provides an extensive review of experimental data. The review of Paulaitis et al. (1983) covers much of the literature up to 1982.

2.2.2 Phase equilibria at high pressures

In the following, we restrict our attention to equilibria between fluid (liquid, gas, or supercritical) phases. Equilibria involving solid phases are substantially more complex, because of the large number of possible solid phases for a component or a mixture. We also do not discuss the case of a single pure component.

Binary mixtures: The equilibria between fluid phases at high pressures has been the subject of several investigations in the past, especially for

binary systems. A useful generalization of the possible forms of binary phase diagrams was given by Scott and van Konynenburg (1970). The classification is based on the location of the mixture critical locus and the presence of liquid-liquid or fluid-fluid immiscibility regions. Figure 2.1 (Shing and Gubbins, 1983b) shows the six possible types of high

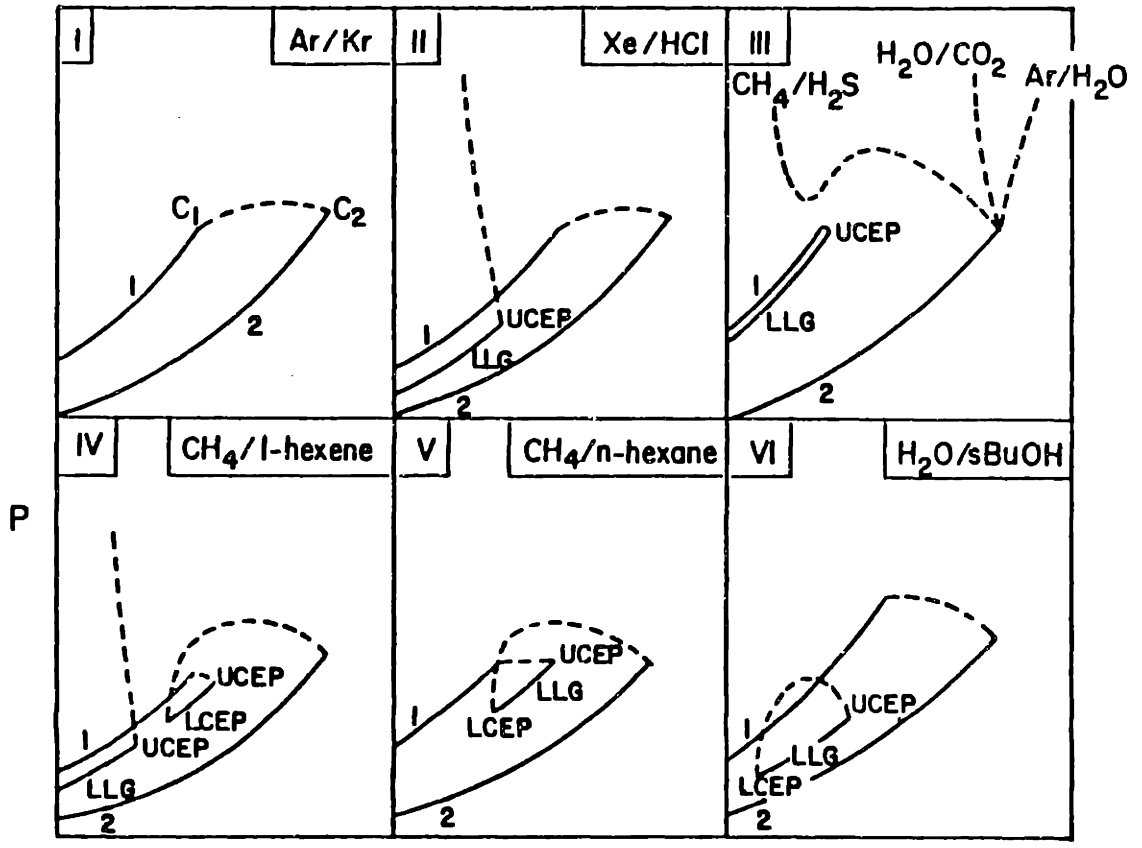

Figure 2.1 *Classification of phase diagrams in binary fluid mixtures. Curves 1 and 2 are pure component vapor pressures. Dashed lines are critical loci, LLG are liquid-liquid-gas equilibrium lines that terminate in upper (UCEP) and lower (LCEP) critical end-points (Shing and Gubbins, 1983b).*

pressure phase diagrams. A discussion of the relationship between molecular structure and the resulting type of phase equilibrium behavior is given by Rowlinson and Swinton (1982). In general, simple molecules with small differences in size and interaction energies give rise to a type I behavior. as the difference in molecular parameters of the two components becomes larger, liquid-liquid immiscibilities (type II behavior) or a critical curve that ends at a lower critical end point (type IV or V) become likely. An open critical locus (type III) or a liquid-liquid immiscibility with both an upper and a lower critical solution temperature is usually associated with strong specific forces (e.g. hydrogen bonding) between the components of a mixture.

Ternary systems: For the complete representation of phase equilibrium in a system that includes more than two components, even a three-dimensional construction is no longer sufficient. The usual practice is to keep one or more of the variables (often temperature and/or pressure) constant, and present the remaining variables using two- or three-dimensional projections. In several cases, the qualitative features of a ternary or higher-order system can be derived from the corresponding binary phase equilibrium behavior.

In the following, we will discuss only a few examples of the behavior that can be expected for systems that include a supercritical gas and a mixture of two relatively non-volatile liquids. According to the classification of Elgin and Weinstock (1959), three distinct patterns are possible:

Type 1 behavior: The isothermal pressure-composition diagrams for this type of mixtures is shown in Figure 2.2, together with the corresponding isobaric isothermal sections. It is assumed that temperature is slightly above the critical temperature of the solvent. At low pressures, the solubilities of both water and solute in the supercritical phase are small. As pressure increases, the miscibility gap between the supercitical fluid and the solute narrows, until they form a single phase. This behavior is typical of solutes that have a strong affinity for water, usually because of a strong tendency to form hydrogen bonds. Ethanol is an example of a compound that has been experimentally

shown to comply with this type of behavior in mixtures with a variety of supercritical solvents like CO_2, ethane and ethylene (see Section 2.2.4 for references).

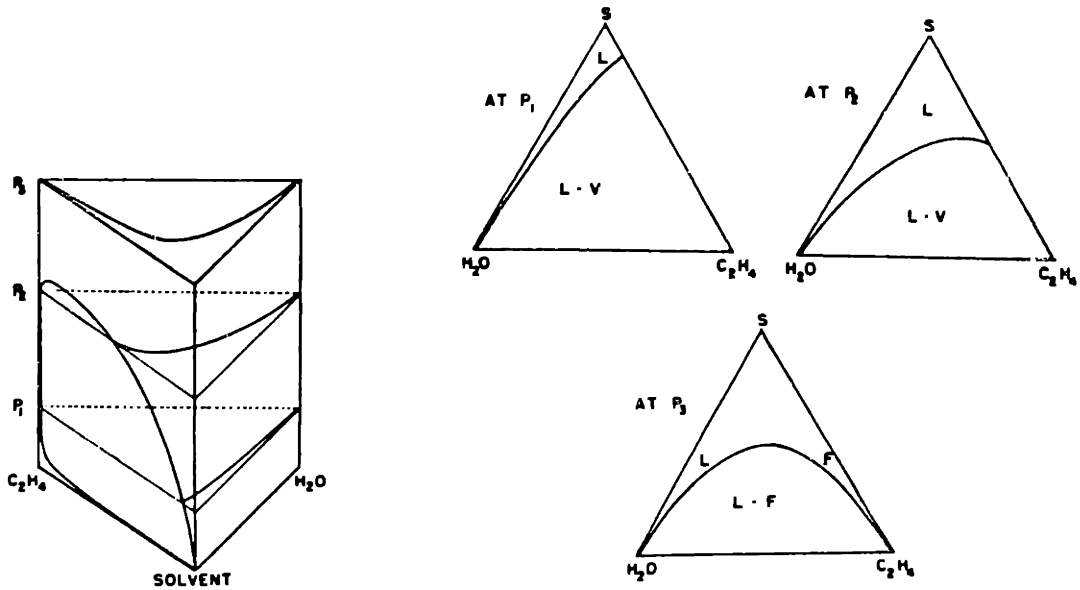

Figure 2.2 *Type 1 phase behavior in supercritical fluid - water-organic compound systems (Elgin and Weinstock, 1959). C_2H_4 was used as the supercritical fluid, and "solvent" or "S" denotes the organic compound.*

Type 2 behavior: Figure 2.3 shows the phase behavior in this case. The most important feature, is a solvent induced immiscibility between water and the solute for a range of pressures. This "salting out effect" may be advantageous for the recovery of the solute. This is a case in which the ternary behavior cannot be qualitatively predicted from the binary behavior. In this category belong systems that have a lesser tendency to form hydrogen bonds, but still have active hydrogen atoms and donor atoms in their structure. For example, Elgin and Weinstock

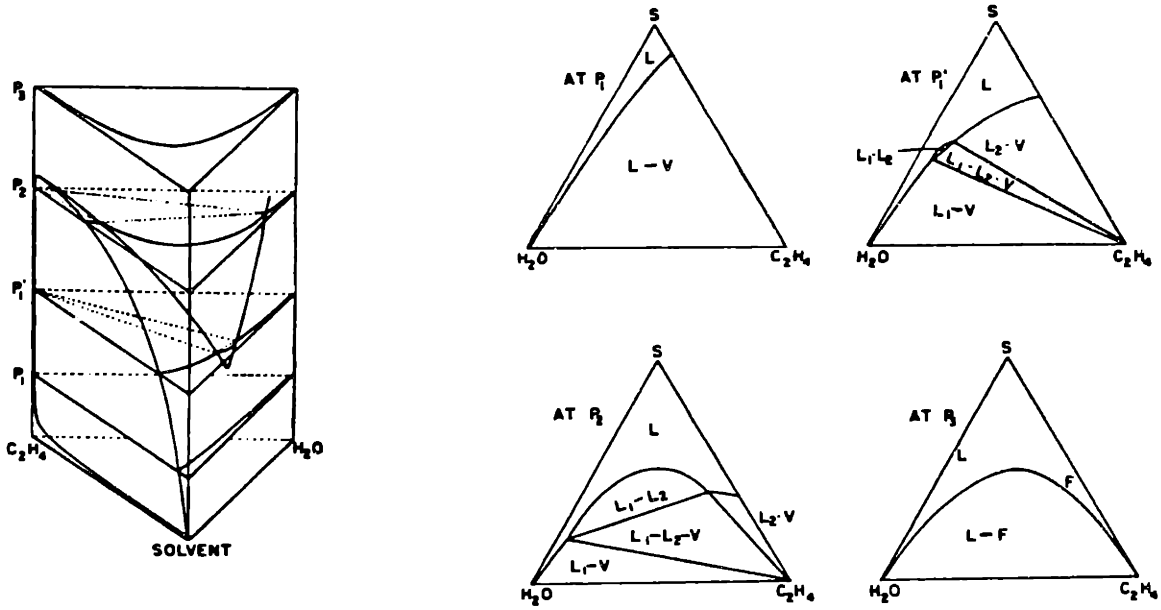

Figure 2.3 *Type 2 phase behavior in supercritical fluid - water-organic compound systems (Elgin and Weinstock, 1959). The notation is the same as for Figure 2.2.*

(1959) observed this type of behavior, among others, for acetone, *n*-propyl alcohol, acetic and propionic acids in ethylene at 278-288 K.

Type 3 behavior: For these systems, the solute-water immiscibility exists even when no supercritical solvent is present (Figure 2.4). As pressure is increased, the immiscibility gaps for both the water - solute and the solute - fluid pairs close up. Systems that belong to this category, are typically expected to include solutes with little or no hydrogen-bonding capacity, and, therefore, low affinity with water.

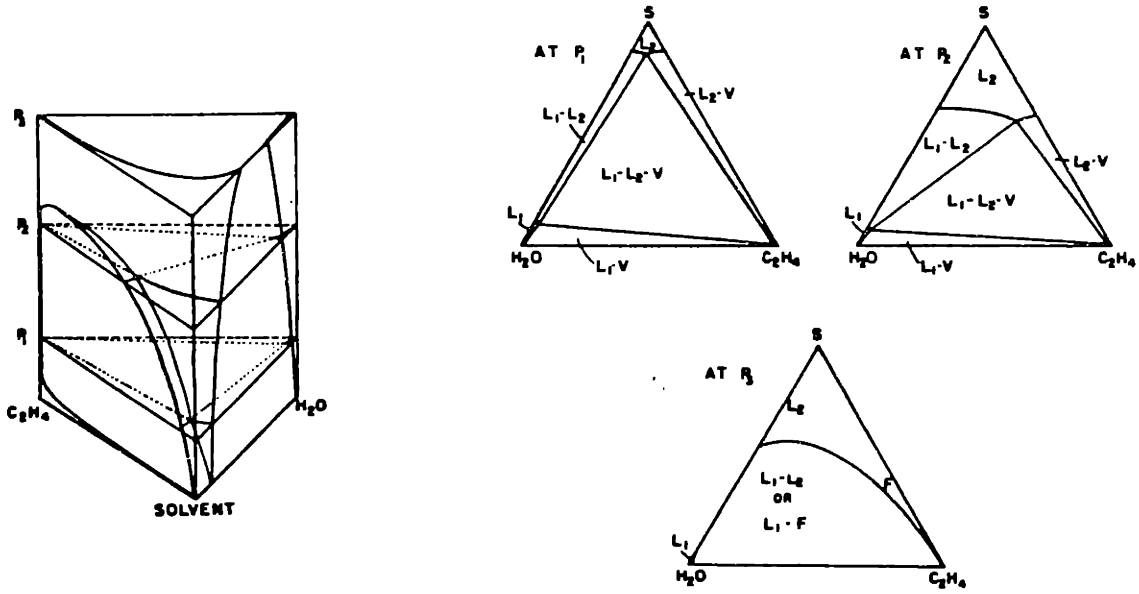

Figure 2.4 *Type 3 phase behavior in supercritical fluid - water-organic compound systems (Elgin and Weinstock, 1959). The notation is the same as for Figure 2.2.*

The classification of a system as belonging to one of the three categories is a function of the temperature of interest. It is possible that a system can pass from type 3 to type 2 to type 1 behavior, by only a modest increase in temperature. A system may show an even more complex behavior: the appearance of additional phases, four-phase equilibrium regions, or the formation of solids (hydrates) are a few such additional possibilities.

2.2.3 Experimental techniques

The experimental investigation of high pressure phase equilibria requires the use of specialized equipment. Among the variety of methods

proposed for the experimental investigation of equilibria between fluid phases at high pressure the following general methods can be identified:

Flow-through methods: In these designs, the more volatile component in the fluid state is passed through a liquid mixture at a specified temperature and pressure and the composition of the effluent gas determined. The technique is able to operate with very non-volatile components, since large quantities of sample can be obtained; the same technique has also been extensively applied for the determination of equilibria between solids and supercritical fluids (Kurnik et al., 1982). It is, however, less useful for multiphase systems, or for volatile components. A variation of the method that can operate even for volatile mixtures involves a continuous flow of both liquid mixture and solvent (Paulaitis et al., 1981). The major uncertainty is attainment of equilibrium in the relatively short contact time available.

Static analytical methods: These designs are based on preparing a mixture with the desired components and determining the number and composition of the coexisting phases after equilibration. Visual cells are often used to enable a direct observation of the presence of multiple phases. The major problem here is withdrawing representative samples of the phases without disturbing the equilibrium. Mercury displacement (Elgin and Weinstock, 1959) or chromatographic sampling (Kuk and Montagna, 1983; Richon and Renon, 1983; Radosz, 1984) are often used for the sampling. These techniques are not very suitable for low-solubility components because of the limited sample size, but can handle multiphase equilibria in many-component systems.

Static synthetic methods: At very high pressures, the only practical method is a static one in which a mixture with predetermined composition is confined in a sample chamber, often equipped with windows for visual observation, and the conditions for appearance or disappearance of the various phases are determined. A variation of the technique for the determination of multiphase equilibria was used by DiAndreth (1985). Since no sampling is involved, the technique avoids disturbing the equilibrium, but application to many-component systems is tedious.

For the experimental part of this work, we have adopted the static analytical method with external recirculation of all coexisting phases. The equipment used is similar in many aspects with the designs of Kuk and Montagna (1981) and Radosz (1984). A detailed description of the experimental apparatus and operating procedures is given in Section 3.1.

2.2.4 Available experimental data for ternary aqueous systems

A summary of the available experimental data for phase equilibria in ternary systems with water, a supercritical fluid and an organic compound is given in Table 2.1.

2.3 Literature review - methods for phase equilibrium calculations

2.3.1 Overview

The problem of calculating the equilibrium mole fractions in different phases for a multicomponent mixture can be solved if a way can be found to relate the fugacities of all components of the mixture to temperature, pressure and composition (generally different for each phase at equilibrium). The general problem of phase equilibrium between phases I,II, ...,M that contain components 1,2,...,n can be expressed thermodynamically with the relationships:

$$\begin{aligned} P^{I} &= P^{II} = \ldots = P^{M} \\ T^{I} &= T^{II} = \ldots = T^{M} \\ \mu_i^{I} &= \mu_i^{II} = \ldots = \mu_i^{M} \end{aligned} \qquad [2.1]$$

where P is the pressure, T is the temperature and μ_i is the chemical potential (partial molar Gibbs energy) of component i. In addition to Eqs. 2.1, there is a requirement for *stability*: all phases must be stable

Table 2.1 Available equilibrium data for water - organic compound - supercritical fluid ternary systems

Reference	Solvent	Solute	P(MPa)	T(K)
Snedeker (1956)	CO_2	acetone	2.2-4.3	305
		acetic acid	6.1-7.0	305
Baker and Anderson (1957)	CO_2	ethanol	6-20	283-323
Elgin and Weinstock (1959)	C_2H_4	acetone	2.8-4.9	288
		methyl ethyl ketone	3.6	288
		n-propyl alcohol	4.9	288
		tert-butyl alcohol	3.6	288
		acetic acid	5.4	288
		propionic acid	5.4	288
		acetonitrile	3.6	288
Tsiklis (1960)	C_2H_4	ethanol	3-17	470-570
Fleck (1967)	C_2H_4	*n*-propyl alcohol	4-6.4	308
	C_2H_6		3.4	308
	CO_2		5.8-7.9	308
	$CClF_3$		2.8	308
	CHF_3		3.7	308
Shvarts and Efremova (1970)	CO_2	ethanol	8.1-9.1	310-320
Paulaitis et al. (1981)	CO_2	ethanol	7.2-14	308
	C_2H_4	ethanol	14	308
McHugh et al. (1981)	C_2H_6	ethanol	5-8	313-323
Kuk and Montagna (1983)	CO_2	ethanol	7.5-21	313-323
	CO_2	isopropanol	10	313
Radosz (1984)	CO_2	isopropanol	10-12	335
DiAndreth (1985)	CO_2	isopropanol	10-13	313-333
Gilbert and Paulaitis (1986)	CO_2	ethanol	10-17	308-338

with respect to arbitrary small perturbations. The conditions for stability for a multicomponent system are (Modell and Reid, 1983):

$$y^{(n)}_{(n+1)(n+1)} > 0 \qquad [2.2]$$

where $y^{(n)}$ is the n-order Legendre transform of energy.

There are numerous approaches to this fundamental problem. In the sections that follow, we will discuss practical approaches for the correlation and prediction of phase equilibrium data in fluid mixtures.

2.3.2 Excess Gibbs energy models

In this approach, an equation, usually with a few adjustable parameters, is proposed to represent the mixture excess Gibbs energy, that is, the difference between the total Gibbs energy at the state of interest and at a reference state denoted by $^+$:

$$\Delta \underline{G}^{EX} = \underline{G}(T,P,N1,N_2,\ldots,N_n) - \underline{G}(T,P^+,N_1^+,N_2^+,\ldots,N_n^+) \qquad [2.3]$$

The activities and fugacities of the components can then be directly calculated. Representative models of this type include the Wilson (Wilson,1964), NRTL (Renon and Prausnitz, 1968), and UNIQUAC (Abrams and Prausnitz, 1975) equations, which, in conjunction with group-contribution methods, have been quite successful in correlating and predicting from limited experimental information VLE data at low pressures. However, the need to use reference states, and the use of different models for the different phases at equilibrium prevent the successful application of this approach for systems at pressures comparable to the critical pressure of one or more of the major components of the mixture.

2.3.3 Helmholtz energy models

This is a more general method, in which the properties of all phases at equilibrium are described by the same equation. In this approach, the starting point is an expression for the residual Helmholtz energy in terms of the state variables:

$$\underline{A}_r(T,\underline{V},N_1,N_2,\ldots,N_n) = \underline{A}(T,\underline{V},N_1,N_2,\ldots,N_n) - \underline{A}^0(T,\underline{V},N_1,N_2,\ldots,Nn) \quad [2.4]$$

The equations for the pressure and chemical potentials are then obtained from the thermodynamic identities:

$$P = -(\partial\underline{A}/\partial\underline{V})_{T,N_i} \quad [2.5]$$

$$\mu_k = (\partial\underline{A}/\partial N_k)_{T,\underline{V},N_{i[k]}} \quad [2.6]$$

A recent promising development for the generation of theoretically-founded expressions for the mixture Helmholtz energy is based on perturbation theories. In this approach, the thermodynamic properties of a mixture are expanded in terms of the known properties of a model system (such as the hard sphere mixture), and a number of perturbation variables to describe the difference between the model and the real mixture. Examples in this category, include the work of Gubbins and Twu (1977a,1977b) using a Lennard-Jones reference fluid and Barker and Henderson (1967) using a hard sphere reference fluid. A recent effort to incorporate different expansions for the Helmholtz energy in different density regions is the work by Cotterman et al. (1985) and Cotterman and Prausnitz (1985). A common difficulty in this approach is the increasing complexity of the resulting expressions, and the large number of unknown parameters that must be determined for each component and combination of components. The area has been reviewed by Henderson (1974,1979), Gubbins (1983) and Shing and Gubbins (1983b).

2.3.4 Equation of state approach

In this method, the volumetric properties of the system of interest are described by an equation, usually explicit in pressure. This is essentially a subcase of the previous case, since an equation of state (EOS) can be obtained from a Helmholtz energy model using Eq. 2.5. The reason this method is treated separately is that there exists a very large number of such equations, mostly of a semi-empirical nature. A very successful group is one that originates from the cubic EOS proposed by van der Waals in 1873. Modern versions of this equation have found extensive practical use for the correlation and prediction of volumetric and phase equilibrium properties of mixtures, especially at high pressures. Among the more common of the currently used cubic EOS are the Soave (1972) modification of the Redlich-Kwong (1949) and the Peng-Robinson EOS (1976). The functional form of both equations, as well as several other proposed cubic forms, can be represented in a general manner as shown in Eq. 2.7 (Schmidt and Wenzel, 1980):

$$P = \frac{RT}{V - b_m} - \frac{a_m}{V^2 + uVb_m + wb_m^2} \qquad [2.7]$$

where u and w are numerical constants. Table 2.2 lists the values of u and w for some common EOS.

For a mixture, parameters a_m and b_m are related to the pure component parameters and the mixture composition through a mixing rule. Eqs. 2.8 and 2.9 show one common choice for the mixing rules, the van der Waals 1-fluid mixing rule:

$$a_m = \sum_i \sum_j x_i x_j a_{ij} \qquad [2.8]$$

$$b_m = \sum_i x_i b_i \qquad [2.9]$$

Table 2.2 Parameters for some common cubic Equations of State

Equation of State	u	w
van der Walls (1873)	0	0
Redlich-Kwong (1949)	1	0
Peng-Robinson (1976)	2	-1

The cross-parameters a_{ij} are related in turn to the pure-component parameters by a "combining rule". Eq. 2.10 shows a common form of the combining rule for a_{ij} :

$$a_{ij} = \sqrt{a_i\ a_j}\ \ (1-k_{ij}) \qquad [2.10]$$

In Equation 2.10, k_{ij} is called a binary interaction parameter, and was originally introduced so that the equation could better reproduce experimental composition data in systems that contained components other than the light hydrocarbons.

Some of the attractive features of this type of equations are their analyticity (because of their cubic form) and the small number of adjustable parameters. The limitations and drawbacks stem primarily from their empirical character.

In the recent years, several attempts have been made to improve the performance of cubic equations of state, especially for highly asymmetric and non-ideal mixtures. The basic factor determining the behavior of the equations for mixtures is the mixing rules used. The quadratic mixing rule represented by Eq. 2.8 is theoretically correct at low densities, but is not appropriate for highly asymmetric mixtures at high densities, where a higher-order mixing rule is required. Huron and Vidal (1979) proposed a modification of Eq. 2.8 that results in an infinite-pressure excess Gibbs energy similar to the one predicted by the NRTL equation; the low-pressure quadratic behavior is not preserved. An important trend in the efforts to incorporate such dependence has been the use of *density-dependent* mixing

rules that preserve the quadratic form at low densities (as dictated by the theoretical requirement for the dependence of the mixture second virial coefficient on composition) but substitute a higher-order dependence at high densities. Examples of this approach are the works by Whiting and and Prausnitz (1982) and Mathias and Copeman (1983). The use of simple equations of state with higher-order mixing rules appears to successfully represent phase equilibria in asymmetric mixtures similar to the ones used in this work. This approach was the focus of the effort to develop correlation methods for the data obtained in this work.

CHAPTER 3
DEVELOPMENT OF NEW CORRELATION TECHNIQUES

3.1 Methods

3.1.1 Computational techniques

For the correlation of experimental data, we elected to use as a starting point a simple cubic equation of state, as described in Section 2.3.4. Little difference among the various cubic equations of state presented in Table 2.2 exists when the same mixing rule and appropriate pure component parameters are used (Goral et al., 1981), but the Peng and Robinson (1976) form was selected based on its slightly better representation of the volumetric and phase equilibrium properties of simple mixtures. As will be demonstrated in the sections that follow, the conventional mixing rules with these equations of state cannot adequately represent phase equilibria in the highly asymmetric systems of interest, and modifications of the mixing rules were required. The development of the new mixing rules was performed using the general form of a cubic equation of state given in Eq. 2.7, but only the Peng-Robinson form (Eq. 0.1) was utilized.

To use the equation of state approach, we first need to have an algorithm for the calculation of phase equilibria in multicomponent systems. The basic elements of the algorithm we implemented for this purpose are as follows: We start by assuming that the component and interaction parameters are known at a given temperature and postulate the existence of a given number of phases (normally 2 or 3). Newton's method is applied for the solution of the system of non-linear equations given by Eq. 2.1. The implementation of the Newton's method requires the determination of the derivatives of the functions to be solved; these derivatives were obtained by numerical differentiation. Also, a transformation of the solution

domain for the unknown mole fractions from [0,1] to the interval $[-\infty,+\infty]$, using a trigonometric tangent function, was required to avoid excursions of the solution vector into physically unrealistic regions. Without the transformation, the problem is especially severe when one or more of the unknown mole fractions is small.

In addition to the conditions of phase equilibria, we performed a thermodynamic stability analysis, based on Eq. 2.2, for all the calculated phase equilibrium points. This provided a means of deciding when a multiphase equilibrium calculation was necessary: if the initial guess as to the number of phases in a system at given conditions were wrong, the phase stability criteria would be violated and a calculation with an increased number of coexisting phases became necessary.

The values of the binary interaction parameters were regressed from experimental binary phase equilibrium data using a simple optimization algorithm. Normally, the sum of the absolute deviations in the calculated mole fractions was utilized as the objective function for the optimizations. In the case where one or more of the coexisting phases had very small concentrations of one component (as is the case for highly asymmetric systems), the deviations were multiplied by the inverse of the smaller mole fraction.

A description of the computer programs used for the phase equilibrium calculations is given in Appendix B.

3.1.2 Pure component parameter estimation

For the modelling of phase equilibria using the equation of state approach, the determination of pure component parameters is the first step for the use of an equation of state. Generalized correlations are available employing the principle of corresponding states: for example, Peng and Robinson (1976) give such a generalized expression for use with the equation of state they propose. Such generalized correlations are based on application of the criticality conditions to determine the values of the parameters at

the critical point, followed by regression of experimental data for vapor pressures and liquid densities of a series of substances. They give the desired pure-component parameters in terms of the critical properties and the reduced temperature. The accuracy of the correlations is variable, and the errors can be more that 10%, especially at low reduced temperatures. For subcritical components, the pure component vapor pressures must be reproduced to a much higher degree of accuracy for a reasonable modelling of the corresponding low-pressure phase equilibria. Modelling of the low-pressure equilibria for subcritical components is important for the determination of the corresponding interaction parameters.

One way to overcome this difficulty, is to use pure component parameters in an equation of state that directly reproduce the measured vapor pressure and one additional property (usually liquid density) at the temperature of interest. This would normally require the solution of a non-linear system of equations for every component at each temperature. By using the general properties of a cubic equation of state (Eq. 2.7), analytical expressions can be obtained (Panagiotopoulos and Kumar, 1985) for the values of the pure component parameters for an equation of state that exactly reproduce vapor pressure and liquid density of a subcritical component. Appendix A gives a detailed exposition of the method developed and provides analytical expressions for the determination of pure component parameters of subcritical components. For the supercritical components, we employed the conventional generalized correlations (Peng and Robinson, 1976).

In Appendix D, tables are presented with the pure component parameters thus obtained, together with the necessary data (vapor pressure and liquid densities for the subcritical components) used in the calculation of the parameters.

3.2 New mixing rules for cubic equations of state

3.2.1 Density-independent mixing rules

The conventional quadratic mixing rules given by Eq. 2.8-2.10 do not give a good representation of the properties of asymmetric mixtures. An illustration of this deficiency is given in Figure 3.1 for the binary system CO_2 - water, a binary that appears in all the ternary systems studied in this work. This binary system has a large immiscibility gap up to very high pressures for temperatures close to the critical point of carbon dioxide: two phases, one mostly aqueous and one with high concentration of carbon dioxide coexist. The prediction of the conventional mixing rule using the Peng and Robinson (1976) equation of state for this system at 323 K is given in Figure 3.1 by the continuous lines marked $k_{12}=k_{21}=+0.160$. The parameters were fitted to the experimental phase equilibrium data for the solubility of water in the supercritical carbon dioxide phase (Y_2). As can be seen, while the representation of the data in the aqueous phase is good, the solubility of carbon dioxide in the aqueous phase is underpredicted by more than two orders of magnitude.

The physical reason behind this failure lies most likely in the large difference in local environment around the solution molecules in an water-rich and a carbon dioxide-rich phase. This observation provides the physical basis for several proposed local composition models (e.g. Renon and Prausnitz, 1968; Abrams and Prausnitz, 1975). The conventional quadratic mixing rule for the attractive parameter in cubic equations of state is not appropriate when significant asymmetries in local environment exist, as verified by the inability to reproduce experimental results for asymmetric mixtures.

In order to correct this deficiency, it has been proposed (Robinson et al., 1984) to utilize <u>different</u> values of the interaction parameters for coexisting highly asymmetric phases. The approach gives good results for aqueous systems with hydrocarbon gases. However, since, in essence, different equations of state are applied to the different phases, the approach cannot be used to model cases where the compositions of the two phases would approach each other, for example, close to vapor-liquid critical point or a plait point.

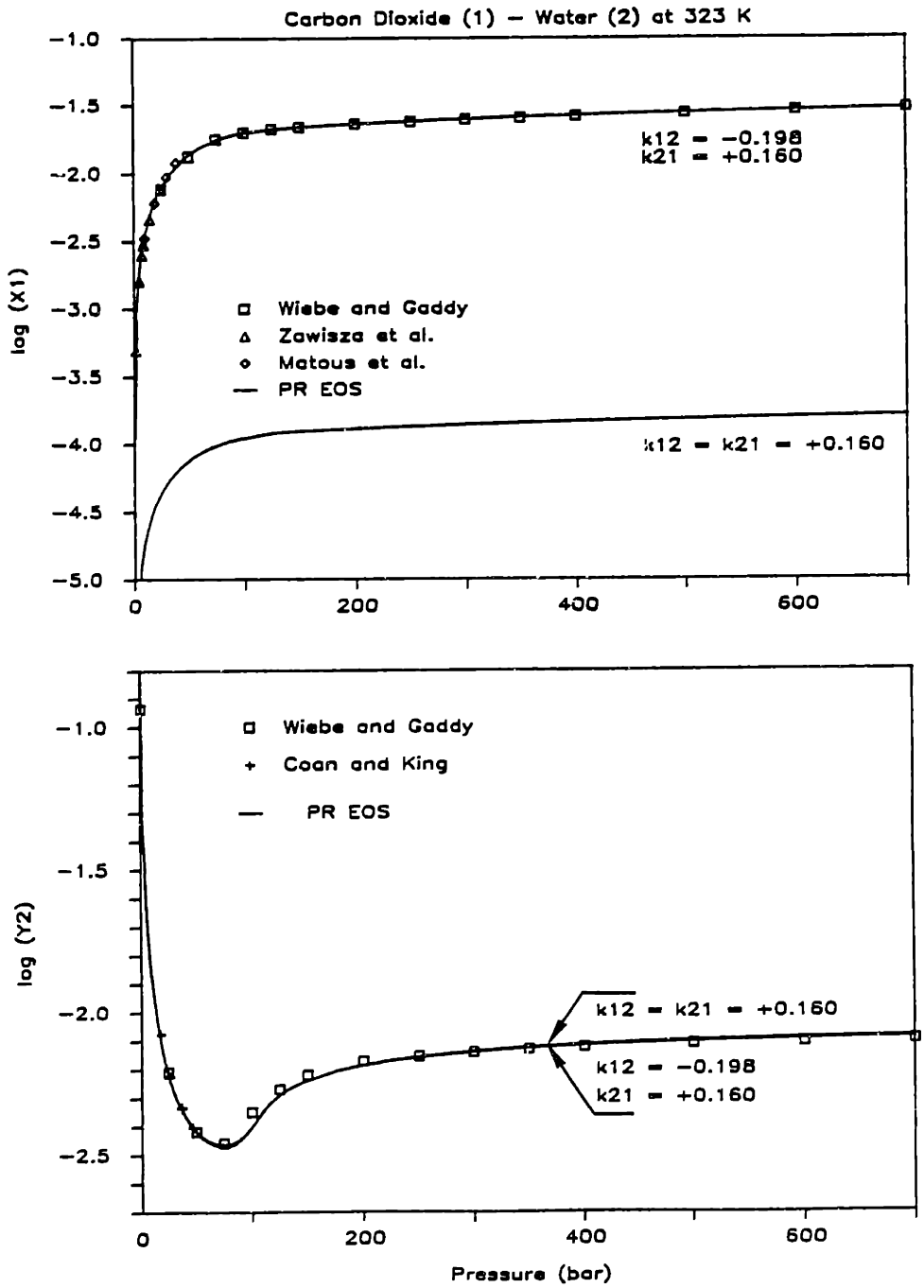

Figure 3.1 *Experimental and predicted phase equilibrium behavior for the system CO_2-water at 323 K. X1 is the mole fraction of CO_2 in the liquid phase and Y2 the mole fraction of water in the fluid phase. Experimental data: (□) Wiebe and Gaddy (1941); (△) Zawisza et al. (1981); (◊) Matous et al. (1969). Predicted using Eq. 3.1 (—).*

In order to improve the representation of the phase behavior in non-ideal mixtures, an empirical modification of the quadratic combining rule given by Eq. 2.10 was developed (Panagiotopoulos and Reid, 1986c). In our approach, we relax the assumption $k_{ij} = k_{ji}$ thus introducing a second interaction parameter per binary:

$$a_{ij} = \sqrt{a_i a_j}\,[1-k_{ij}+(k_{ij}-k_{ji})X_i] \qquad [3.1]$$

Eq. 3.1 has the following characteristics:

- If $k_{ij} = k_{ji}$, the original mixing rule given by Eq. 2.10] is recovered.

- The "effective" interaction parameter between components i and j approaches k_{ij} as X_i, the mole fraction of component i, approaches zero. It also approaches k_{ji} if X_i approaches unity. The apparent asymmetry under an interchange of i and j is corrected by the fact that both a_{ij} and a_{ij} enter in the calculation of the mixture parameter a_m symmetrically.

- Application of the rule given by Eq. 3.1 for the calculation of the mixture parameter a_m results in a cubic expression for the mole fraction dependence of the mixture parameter a_m. This is different from the case of the conventional mixing rule which leads to a quadratic expression for a_m.

The physical significance of the interaction parameters k_{ij} and k_{ji} is that they provide a measure for the deviations of the attractive part of the molecular interactions from the geometric-mean rule. The two parameters give two different limits at the two ends of the concentration spectrum.

An important feature of the new method is that the two parameters are essentially uncorrelated in many cases, as shown in the previous example, in which the parameters were determined from data in different phases. This is generally true only for systems in which the compositions of the coexisting phases are very different.

Using this mixing rule with Eq. 2.7, we can obtain the fugacity coefficient of a component in a mixture as:

$$\ln\phi_k = \ln\frac{f_k}{X_k P} = \frac{b_k}{b_m}\left(\frac{PV}{RT} - 1\right) - \ln\frac{P(V-b_m)}{RT} +$$

$$+ \left[\frac{\sum_i X_i(a_{ik}+a_{ki}) - \sum_i\sum_j X_i X_j (k_{ij}-k_{ji})\sqrt{a_i a_j} + X_k\sum_i X_i (k_{ki}-k_{ik})\sqrt{a_k a_i}}{a_m} - \frac{b_k}{b_m}\right] \times$$

$$\times \frac{a_m}{\sqrt{u^2 - 4w}\, b_m RT} \ln\frac{2V + b_m(u-\sqrt{u^2-4w})}{2V + b_m(u+\sqrt{u^2-4w})} \qquad [3.2]$$

Using the mixing rule given by Eq. 3.1 results in excellent agreement with the experimental data for both phases for the system CO_2-water, as demonstrated in Figure 3.1 (lines marked $k_{12} = -0.198$, $k_{21} = 0.160$).

In comparing the results of the conventional (one-parameter) mixing rule and the proposed correlation (two-parameter), we should keep in mind that the introduction of one additional adjustable parameter necessarily results in at least some improvement of the representation of the experimental data. To investigate if the proposed method has any real advantages over previously proposed two-parameter correlations, we used a two-parameter correlation proposed by Heidemann and his co-workers (Evelein et al., 1976) that uses a quadratic mixing rule for b_m analogous to Eq. 2.10]. In Figure 3.2, the data of Figure 3.1 are replotted on a different scale and the results of the proposed correlation are compared to the results of the Heidemann model. The proposed correlation is seen to be in significantly better agreement with the experimental data, especially for the high pressure range.

It has also been shown (Panagiotopoulos and Reid, 1986c) that the mixing rule can represent a wide variety of phase equilibrium data for highly non-ideal mixtures, that include low-pressure VLE data and high-pressure ternary data predicted using only binary parameters. A similar mixing rule was proposed independently by Stryjek and Vera (1986a, 1986b). It was found to represent phase equilibrium data for a variety of low-pressure, highly nonideal mixtures with the same or better accuracy as the conventional activity coefficient models discussed in Section 2.3.2. The

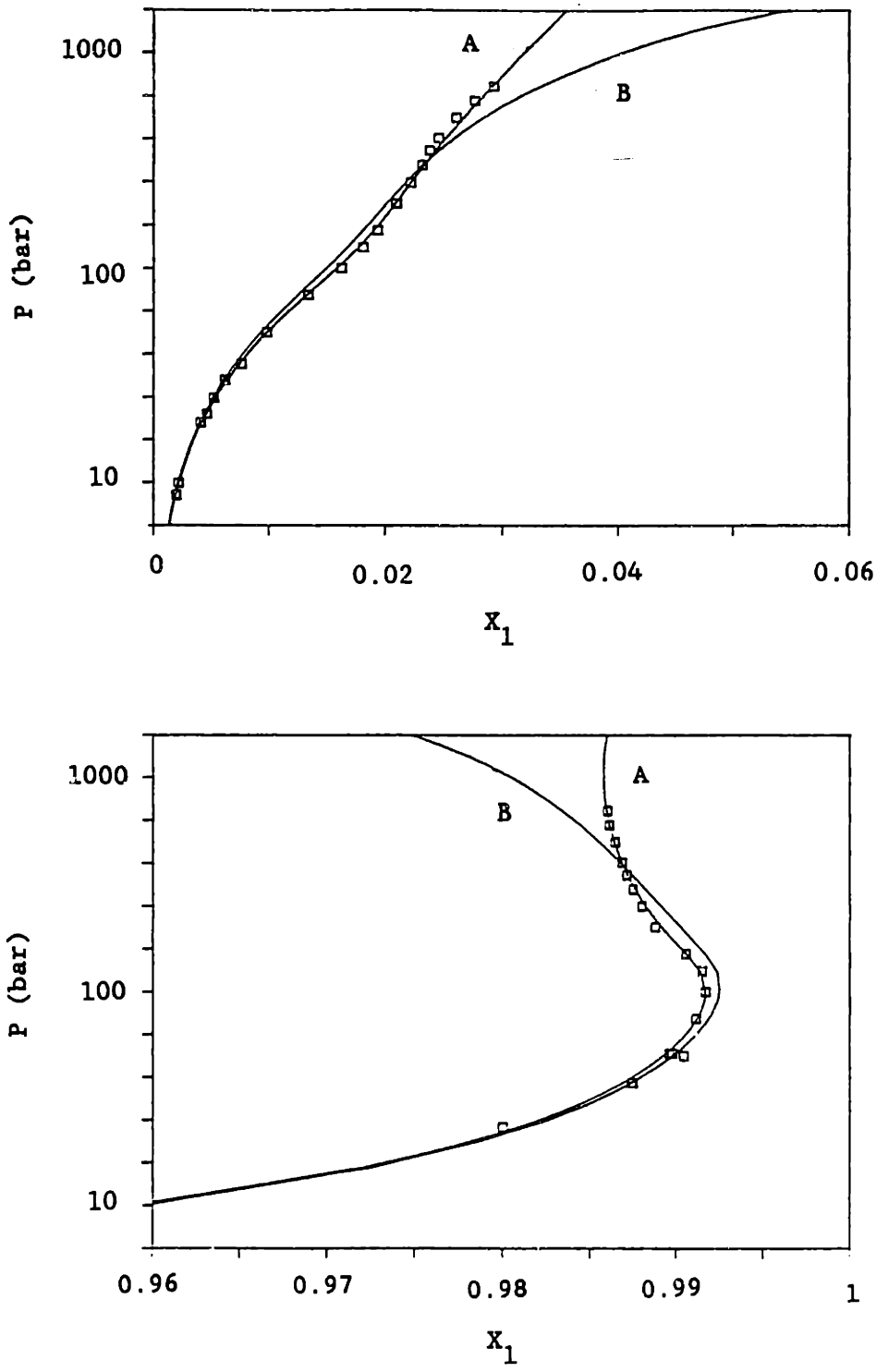

Figure 3.2 *Comparison of the prediction of the proposed density-independent mixing rule (curves A) with the results of the two-parameter correlation by Evelein et al., 1976 (curves B) for the system carbon dioxide-water at 323 K (data sources as for Figure 3.1).*

same number of adjustable parameters (two per binary) was used for all models compared.

A significant deficiency, however, of the combining rule given in Eq. 3.1 is that the dependence of the mixture second virial coefficient,

$$B_m = b_m - a_m/RT \qquad [3.3]$$

is now a cubic function of mole fraction. This result is contrary to the theoretical requirement for a quadratic dependence on the mixture mole fraction at low densities (Hirschfelder et al., 1954, pp. 153). The problem is that, while the quadratic dependence of a_m on mixture composition is exact at the limit of low, gas-like densities, a higher-order dependence is required for a reasonable representation of the properties of non-ideal mixtures at high densities. The solution to this problem, as suggested by several authors in the recent years (e.g. Mollerup, 1981.; Whiting and Prausnitz, 1982; Mathias and Copeman, 1983) is to introduce density dependence in the combining rules,such that they may reproduce the required limits for both density ranges. The modification of Eq. 3.1 for this purpose is presented in the following section.

3.2.2 Density-dependent mixing rules

First, we rewrite the combining rule given by Eq. 3.1 in the form:

$$a_{ij} = \sqrt{a_i\ a_j}\left(1 - \frac{k_{ij}+k_{ji}}{2} + \left[\frac{k_{ij}-k_{ji}}{2}\right](X_i - X_j)\right) \qquad [3.4]$$

In Eq. 3.4, the term $(k_{ij}+k_{ji})/2$ corresponds closely to k_{ij} in Eq. 2.8. The term that multiplies $(X_i - X_j)$ leads to the cubic dependence of a_m on mixture composition at high densities. In order to introduce density dependence in Eq. 3.4, we need to multiply this term by a function that will reduce to zero at low densities, while being approximately constant

at high densities. Several "interpolation functions" have been proposed (e.g. Topliss et al., 1982; Lüdecke and Prausnitz, 1985), but no theoretical guidelines exist for the rational development of such functions. Since we would like to avoid introducing additional adjustable parameters into the equations, a simple, parameter-free function of density appears appropriate. We have selected to use the function b_m/VRT, in which case the combining rule analogous to Eq. 3.4 is

$$a_{ij} = X_i X_j \sqrt{a_i a_j}\,(1-k_{ij}) + \frac{b_m}{VRT} X_i X_j (X_i \lambda_{ij} + X_j \lambda_{ji}) \qquad [3.6]$$

where $k_{ij} = k_{ji}$, $\lambda_{ij} = -\lambda_{ji}$, are binary interaction parameters (again two per binary).

The mixing rule given by Eq. 3.6 is similar to the density dependent form proposed by Lüdecke and Prausnitz (1985), with the important difference that b_m, the mixture volume parameter is introduced in the numerator. At high, liquid-like densities, the mixture volume parameter b_m is roughly proportional to the mixture molar volume V, so the density-dependent function, b_m/VRT, in Eq. 3.6 is insensitive to composition and density.

The physical significance of k_{ij} and λ_{ij} in the proposed mixing rule, is now different for the two parameters. The term k_{ij} represents an deviations from the geometric mean rule for the attractive parameter, whereas λ_{ij} measures the composition-dependent deviations (assumed symmetric in mole fraction). It would be physically appealing to identify k_{ij}, as obtained from the regression of high-pressure data, with the limiting behavior at low densities given by the second virial coefficient, but unfortunately this is not possible.

The expressions for the parameters of a general cubic equation of state using Eq. 3.6 and the resulting expressions for the fugacity coefficient of a component in a mixture are given below.

$$a_m^0 = \sum_i \sum_j X_i X_j \sqrt{a_i a_j}\,(1-k_{ij}) \qquad [3.7]$$

$$a_m = a_m^0 + \frac{b_m}{VRT} \sum_i \sum_j X_i X_j (X_i \lambda_{ij} + X_j \lambda_{ji}) \quad ; \quad \lambda_{ij} = -\lambda_{ji} \qquad [3.8]$$

$$b_m = \sum_i x_i b_i \qquad [3.9]$$

$$\ell n \phi_k = \ell n \frac{\hat{f}_k}{X_k P} - \frac{b_k}{b_m} \left(\frac{PV}{RT} - 1 \right) - \ell n \frac{P(V-b_m)}{RT} +$$

$$- + \frac{-a_m^0 b_k + 2b_m \Sigma_0 + u/2w \left[2b_k/b_m \, \Sigma\Sigma - 2 \Sigma_1^k - \Sigma_2^k \right]}{\sqrt{u^2 - 4w}\, b_m^2 RT} \ell n \frac{2V + b_m (u - \sqrt{u^2 - 4w})}{2V + b_m (u + \sqrt{u^2 - 4w})}$$

$$- \frac{2b_k/b_m \, \Sigma\Sigma - 2\Sigma_1^k - \Sigma_2^k}{2w \, b_m^2 RT} \ell n \frac{V^2}{V^2 + u b_m V + w b_m^2} \qquad [3.10]$$

where $\Sigma\Sigma = \sum_i \sum_j \lambda_{ij} X_i^2 X_j$

$$\Sigma_0^k = \sum_i X_i (1 - k_{ik}) \sqrt{a_i a_k}$$

$$\Sigma_1^k = \sum_i X_i X_k \lambda_{ki}$$

$$\Sigma_2^k = \sum_i X_i^2 \lambda_{ik}$$

It was found that Eqs. 3.1 and 3.6 are approximately equivalent in correlating phase equilibria at high and low pressures, the basic difference being the dependence of the mixture second virial on composition at low density. A test of the proposed mixing rules with literature data for a variety of systems is given in the sections that follow.

3.3 Testing of proposed mixing rules

3.3.1 Polar - supercritical fluid systems

An example of the application of the proposed density-dependent mixing rules for the case of highly asymmetric systems, is given in Figure 3.3 for the binary system carbon dioxide - water for a series of temperatures. A good representation of the properties of this highly non-ideal system is obtained for all temperatures studied. The regressed parameters as a function of temperature for this system, as well as for the other systems studied are given in Appendix D in tabular form. As can be seen from table D.2, the absolute magnitude of λ_{12} for this system is high relative to most of the other systems studied. This reflects the asymmetric character of the system, and is consistent with the large difference between the parameters k_{12} and k_{21} for the density-independent model (Figure 3.1). This binary system illustrates one possible type of behavior (type III, according to the classification discussed in Section 2.2.2) with an immiscibility gap that persists up to very high pressures. This type of behavior is typical for systems with water and several light hydrocarbon gases (e.g. ethane) that may also be used for supercritical extraction of organic compounds.

One additional example for another class of systems is provided in Figure 3.4 for the system ethanol - carbon dioxide. The binary data were obtained during calibration of the equipment described in Section 4.1, and are presented in tabular form in Appendix C. The system illustrates a typical phase equilibrium behavior between carbon dioxide and a low molecular weight organic compound above the CO_2 critical temperature. For the temperature range studied, the solubility of carbon dioxide in the liquid phase is considerable even at low reduced pressures. The solubility of the organic compound in the supercritical fluid phase is much lower. Binary critical points occur at pressures comparable to the pure carbon dioxide critical pressure. The mixture critical pressure

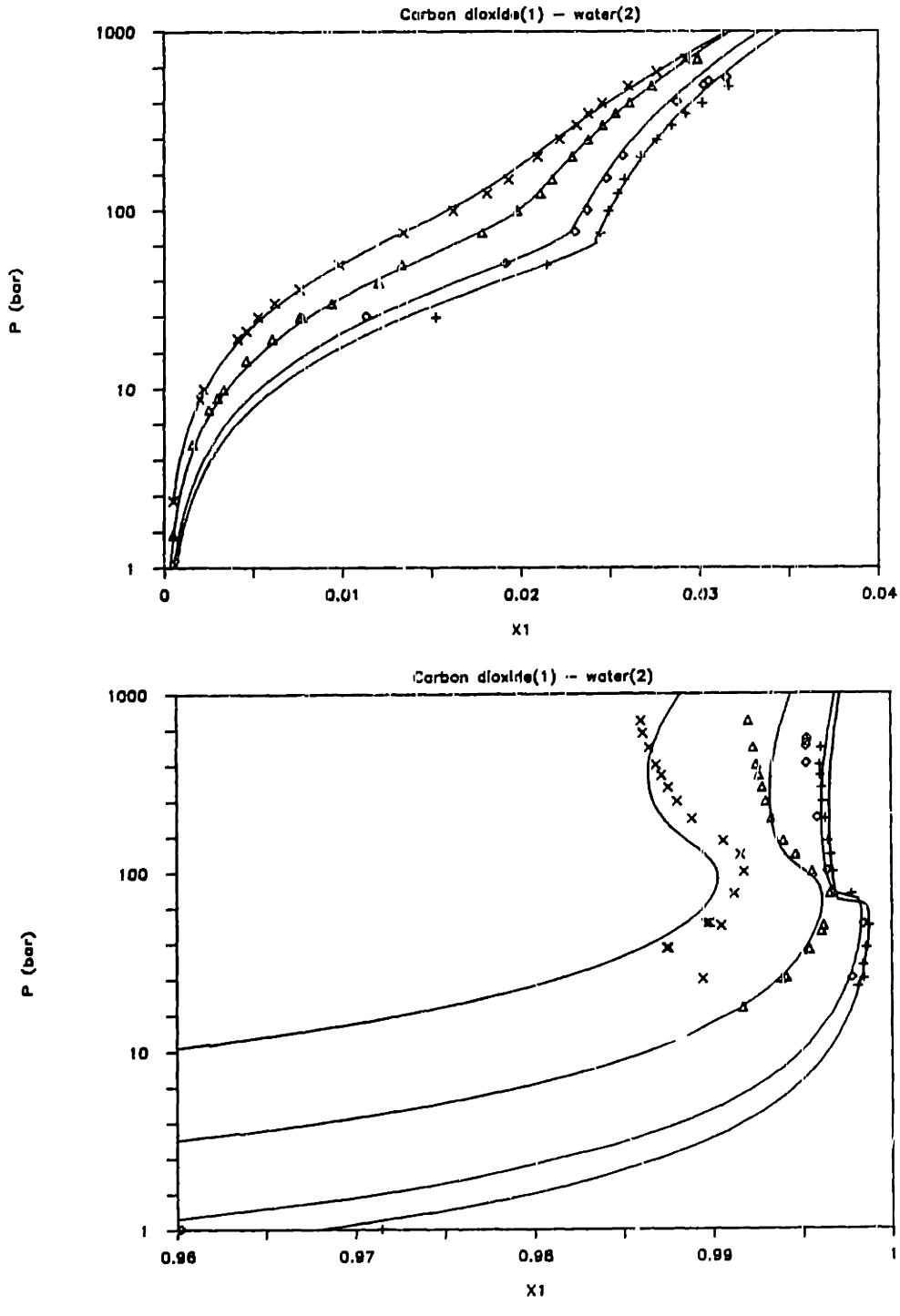

Figure 3.3 *Phase equilibrium behavior for the system carbon dioxide-water at a series of temperatures. Data are from Wiebe (1941) and Wiebe and Gaddy (1941): (+) 298 K; (◊) 304 K; (△) 323 K; (×) 348 K. Lines are calculated with the density-dependent mixing rule given by Eq. 3.6.*

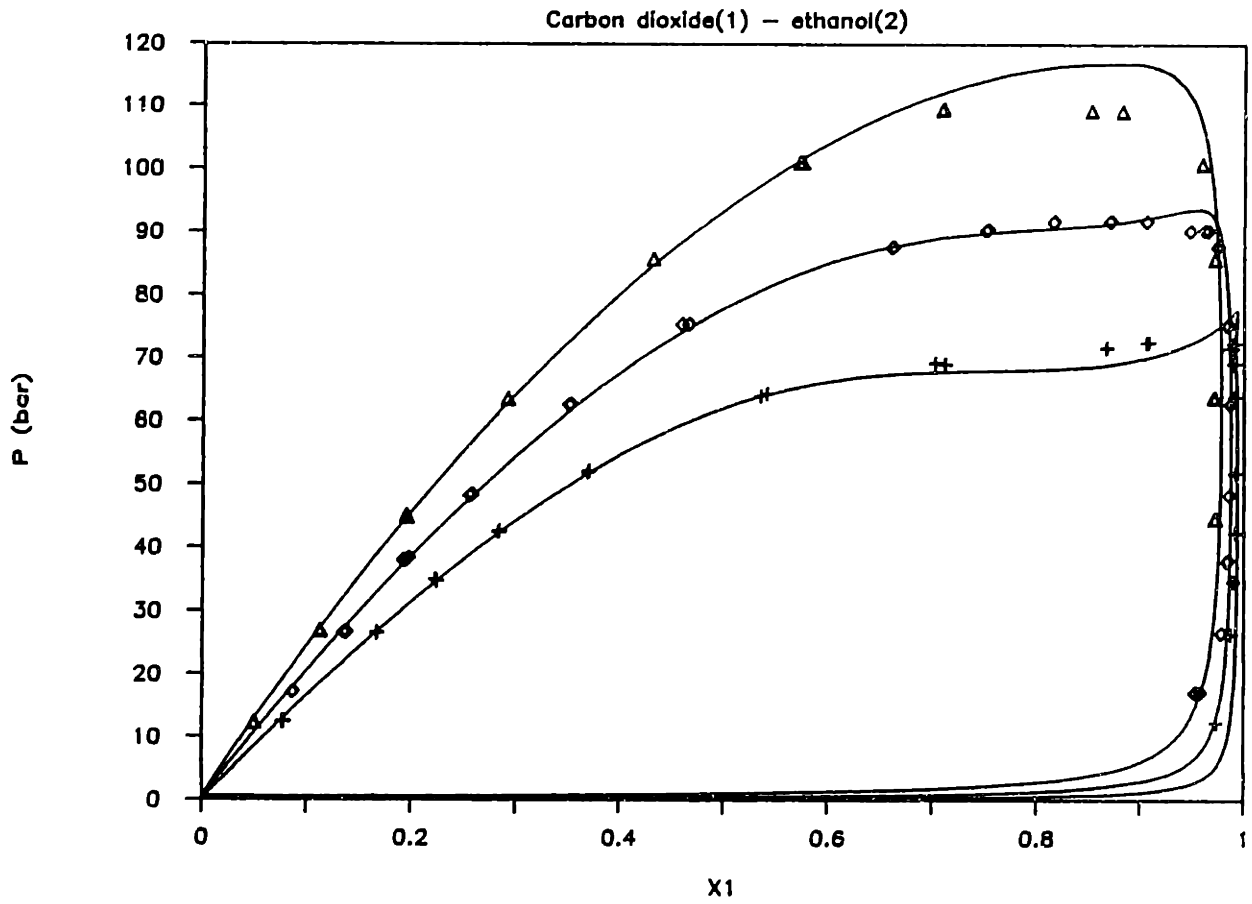

Figure 3.4 Phase equilibrium behavior for the system carbon dioxide - ethanol at a series of temperatures. Experimental data are from this work (Appendix C.6): (+) 308 K; (◊) 323 K; (Δ) 338 K. Lines are calculated with the density-dependent mixing rule given by Eq. 3.6.

increases with temperature for the temperature range studied. Above that pressure, the two components are completely miscible at all proportions. This behavior is consistent with the fact that liquid carbon dioxide and ethanol are also completely miscible (Francis, 1954). The same behavior is also common for several other low molecular weight organic compounds. The model reproduces the experimental behavior well, except near the critical pressure.

One additional example for this type of behavior is given in Figure 3.5, where the phase equilibrium behavior for the system acetone-carbon dioxide at T = 313 K is presented. For this system, the regressed value for λ_{12} is very close to zero, and the mixing rule essentially reduces to the conventional one-parameter mixing rule given by Eq. 2.8. The ability to directly use regressed parameters for the widely used conventional cubic equations of state for systems that can be adequately represented by the conventional approach is a distinct advantage of the proposed correlation method.

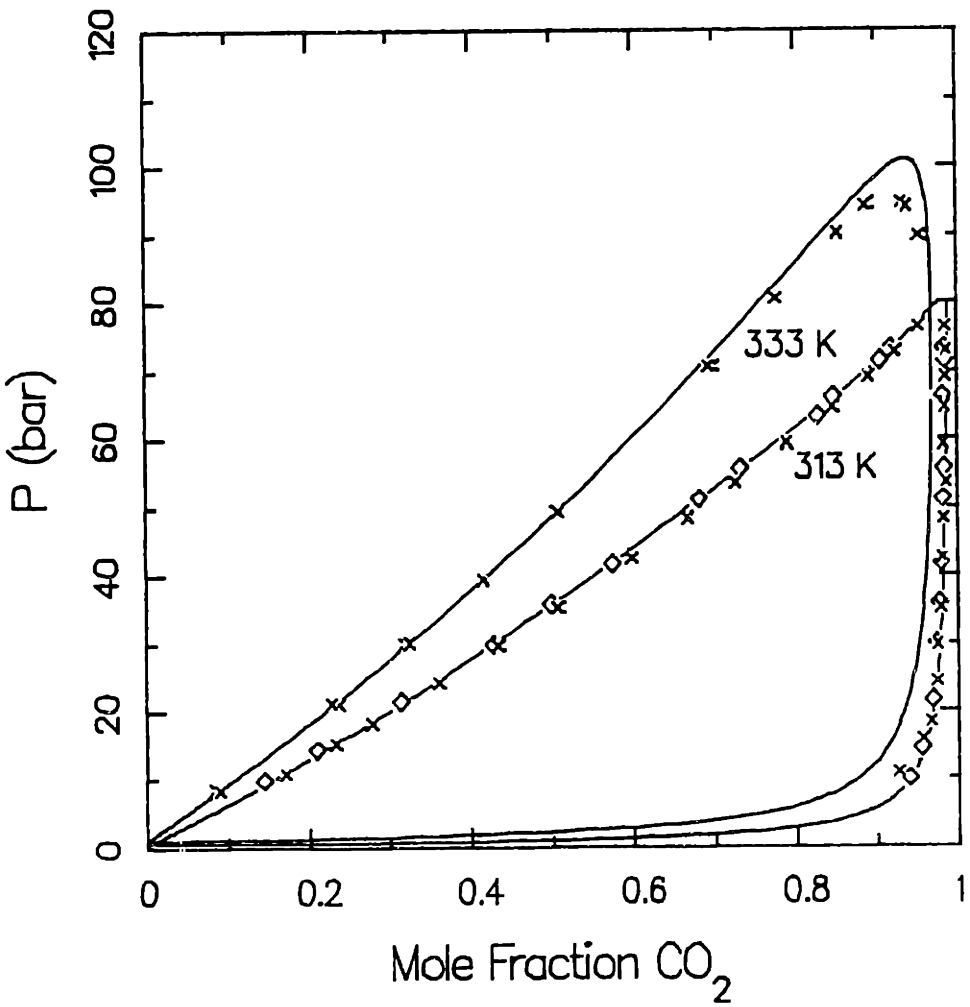

Figure 3.5 *Phase equilibrium behavior for the system acetone - carbon dioxide at 313 and 333 K. Data are from: (□) Katayama et al. (1975); (×) this work. Lines are calculated with the density-dependent mixing rule given by Eq. 3.6.*

3.3.2 Low pressure vapor-liquid equilibria

A desirable property of any equation-of-state model is the ability to predict low-pressure phase equilibrium data. Such data have been traditionally modelled using the excess Gibbs energy approach (Section 2.3.2). It has been repeatedly demonstrated (Goral et al., 1981; Stryjek and Vera, 1986a, 1986b), however, that an equation-state model that reproduces properly the pure component vapor pressures can represent experimental data for VLE at low pressures with an accuracy equal to or exceeding that of excess Gibbs energy models with the same number of adjustable parameters.

For our purposes of modelling ternary phase equilibrium data at high pressures, it is also important that we obtain a reasonable representation of all binaries between the components. The binary system between water and the polar organic compound is normally completely miscible at high pressures, and the determination of the interaction parameters must be based on low pressure data.

In Figure 3.6, we present results from the density-dependent model for the system ethanol-water, a highly non-ideal system that includes an azeotropic point at all temperatures indicated in Figure 3.6. As can be seen, the model reproduces the experimental phase compositions to a good accuracy, including the location of the azeotropic point. Similar good agreement is obtained for the system acetone - water, as demonstrated in Figure 3.7. This system has a wide phase coexistence envelope.

3.3.3. Ternary systems

One of the most important tests for a proposed correlation is the ability to predict ternary behavior when only the binary behavior is known. In Figure 3.8, the model predictions for the ternary system carbon dioxide - ethanol - water are presented. The model predictions are based solely on values of the interaction parameters regressed from binary data, as shown on Figures 3.3, 3.4 and 3.6.

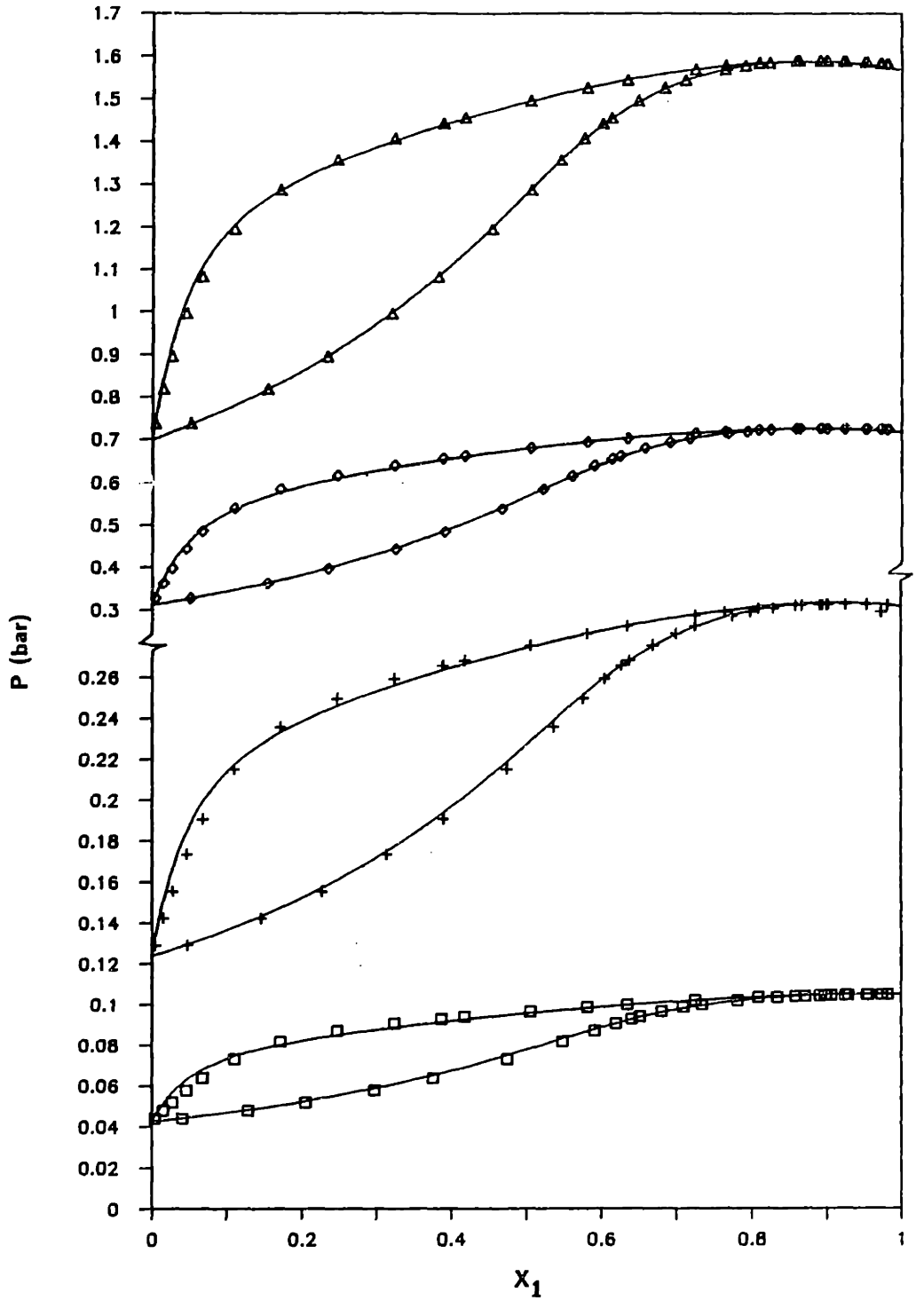

Figure 3.6 *Phase equilibrium behavior for the system ethanol - water at 303 - 363 K. Data are from Pemberton and Mash (1978): (□) 303 K; (+) 323 K; (◊) 343 K; (Δ) 363 K. Lines are calculated using the density-dependent mixing rule given by Eq. 3.6.*

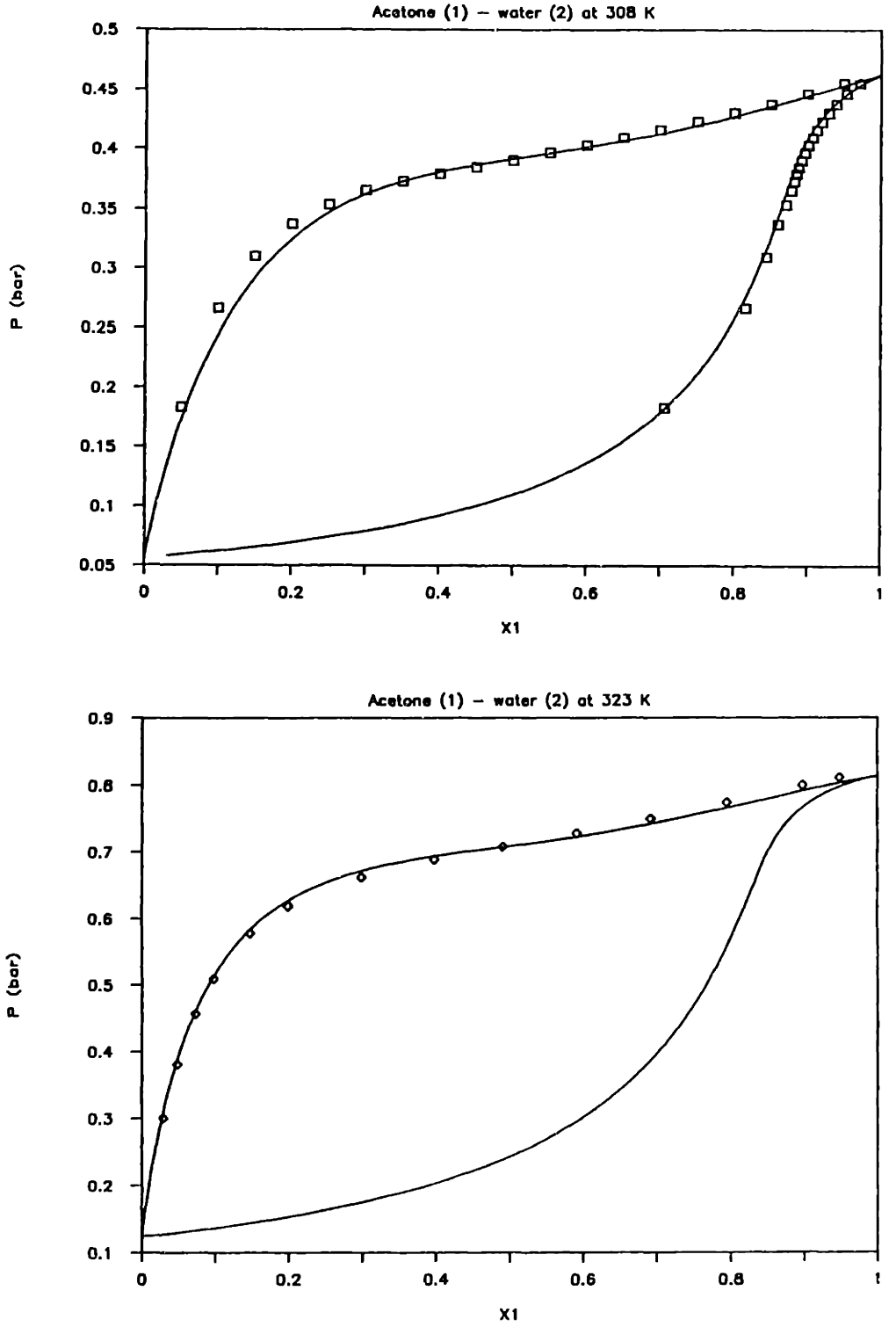

Figure 3.7 *Phase equilibrium behavior for the system acetone - water at 308 and 323 K. Data are from: (□) Lieberwirth and Schuberth (1979) and (◊) Chaudhry et al. (1980). Lines are calculated using Eq. 3.6.*

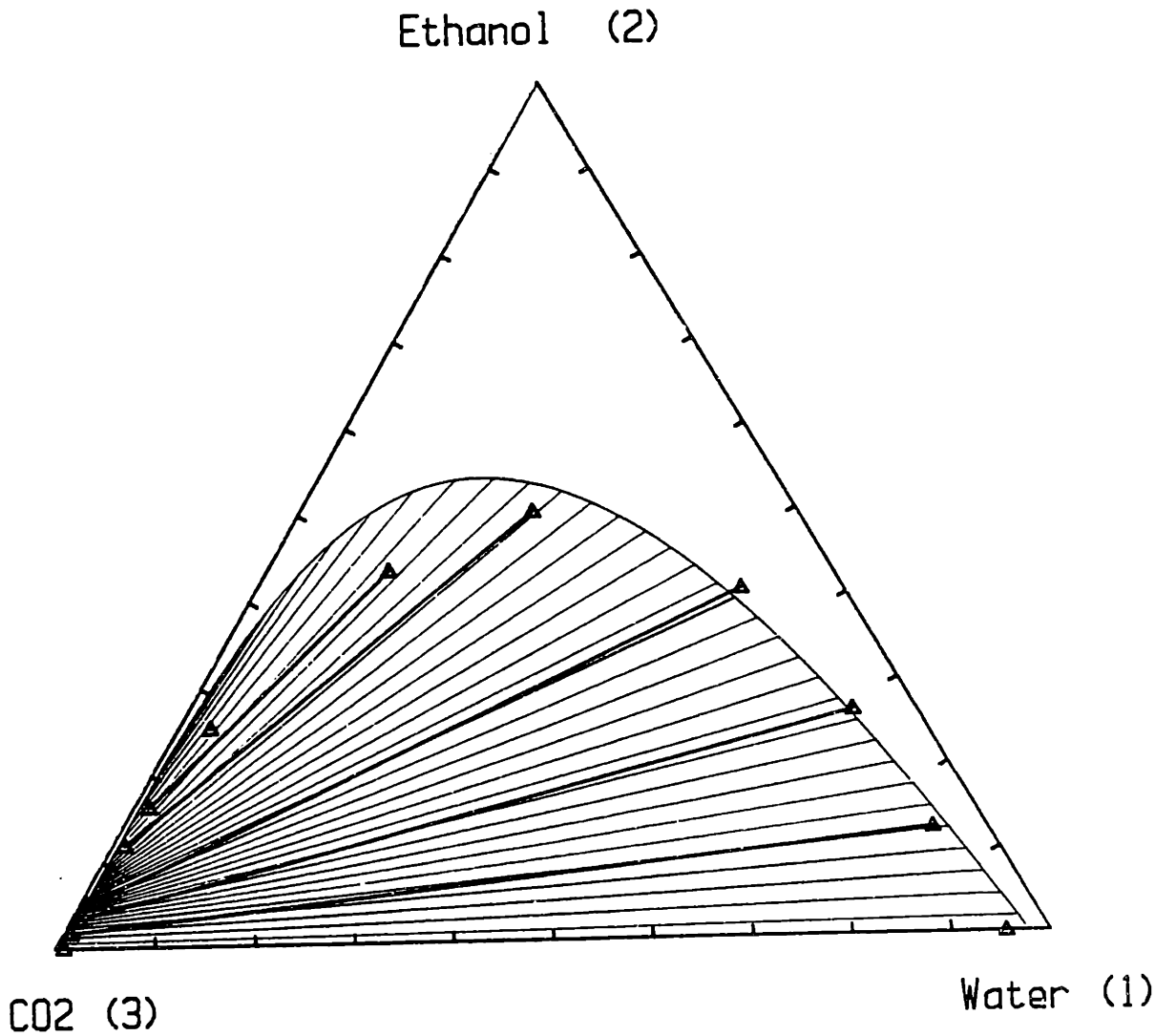

Figure 3.8 *Phase equilibrium behavior for the system water - ethanol - carbon dioxide at T=313 K and P=10.2 MPa. (Δ) Experimental data (Kuk and Montagna, 1983). Lines are calculated using Eq. 3.6.*

As can be seen from Figure 3.8, the accuracy of the model predictions for the shape and extent of the two-phase region at this temperature is reasonable, but the shape of the coexistence envelope deviates somewhat from the experimental measurements as the plait point is approach, and the overall agreement is reasonable. A comparison of the model predictions with the experimentally observed values for the distribution coefficients of the components in the two coexisting phases, however, indicates that the model gives values for the distribution coefficients of water that are systematically too low by as much as 50%. Similar deviations for the same system using different sets of density-dependent mixing rules were obtained by other investigators (Mathias, 1986).

It is significant, however, that no ternary parameters are used to fit the data and the results for the ternary mixture are essentially predictions. Several previously proposed models for equilibria in non-ideal mixtures lack this attribute (a correlation of the ternary system discussed above that required ternary parameters was presented by Topliss et al., 1982). The ability of the model to predict correctly phase coexistence envelopes for ternary mixtures at a range of pressures will be valuable for the systems that we discuss in Chapter 4.

3.4 Overall evaluation of proposed mixing rules

The new two-parameter mixing rule (Eq. 3.6) proposed for use in cubic equations of state was shown to be useful in correlating the phase equilibrium behavior in highly polar systems that cannot be correctly represented by a conventional one-parameter mixing rule. The introduction of Eq. 3.6, is at this point an empirical modification of the original form of the mixing rule. The modification is related, but is not directly derived from, the idea of local compositions, that has been shown in the past to result in improved representation of the phase equilibrium behavior in highly polar and asymmetric mixtures.

Among the advantages of the proposed mixing rule, are the relative simplicity of the resulting expressions for the derived thermodynamic properties, together with the fact that the model can be easily reduced to

the conventional one-parameter mixing rule for which a substantial amount of regressed interaction parameters exists. The model is shown to reproduce accurately data for both high pressure polar - supercritical fluid, and low pressure polar - polar binary phase equilibrium. In addition, predictions for ternary systems based on coefficients regressed from binary data only, are qualitatively correct for the systems studied.

CHAPTER 4
EXPERIMENTAL AND CORRELATION: RESULTS

4.1 Equipment and procedures

4.1.1 Equipment design

The experimental setup used is shown in Figure 4.1. The main elements of the equipment are described below.

Equilibrium cell: The equilibrium cell was a high pressure optical cell (Jerguson gage model 19-TCH-40). The internal space of the cell consisted of a long rectangular vertical channel of approximate dimensions 32cm × 1.3cm × 1.3cm (internal volume approximately 50 cm^3), confined between two high-strength borosilicate glass plates and a 316 stainless steel enclosure. A full view of the contents of the cell was possible. The cell served as a mixing and separating vessel, and for the visual observation of the number and degree of separation of the coexisting phases.

Recirculation system: Connections at the bottom, top and side of the vessel permit withdrawal of the lower, upper and middle phases, any two of which can be recirculated externally with a dual high-pressure Milton-Roy Mini Pump. An on-line Mettler-Paar vibrating tube density meter (DMA 60 with a DMA 512 cell) was used to measure the density of one of the recirculating phases. The density meter could be switched to sample any of recirculating streams.

Temperature control: The equilibrium cell was immersed in a constant temperature bath with silicon fluid (Dow-Corning DC 200) as the heat-transfer medium, that also thermostated the density meter. The bath temperature was

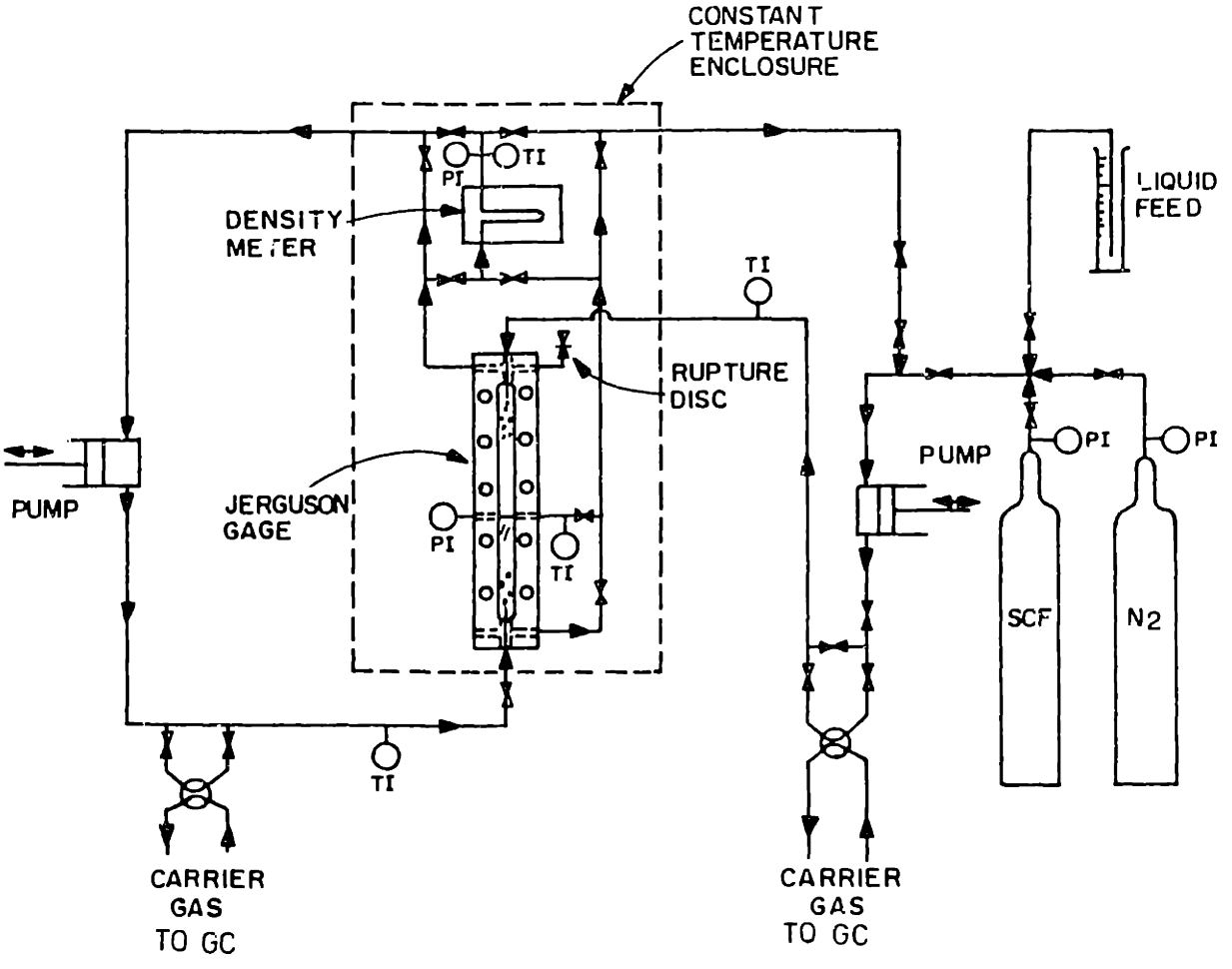

Figure 4.1 *Schematic diagram of the equipment.*

controlled to ± 0.01 K with a Thermomix 1460 temperature regulator. The lines external to the bath were maintained at the bath temperature with the help of heating tapes. The supercritical fluid sampling valve was placed in a heated enclosure with an independent temperature controller.

Other measurements: Temperature was measured with a calibrated mercury-in-glass thermometer to within 0.01 K. Temperatures at several

points along the external recirculation and sampling loops were monitored with thermocouples. Pressure was measured with two calibrated Heise pressure indicators to within ±.16 bar for pressures up to 160 bar and to within ±.4 bar for pressures up to 350 bar. A vibrating tube density meter (Mettler-Paar DMA 60 with a DMA 512 high-pressure cell) was used to measure the density of the recirculating phases. The density meter could be manually switched to sample any of the recirculating streams. The density meter directly measures the frequency of oscillation of a U-shaped tube filled with the fluid being sampled. The calculation of density from the measured frequency involves calibration with fluids of known density. Nitrogen gas and water were used for the calibrations. The observed accuracy and reproducibility of the density measurements was $\pm 10^{-4}$ g/cm^3.

Sampling: Sampling was performed with two high pressure switching valves with internal volume .5 μl (for the upper phase) and .2 μl for the lower or middle phases. The samples were directly depressurized into a He carrier gas stream and analyzed with a Perkin Elmer Sigma 2 Gas Chromatograph, using a Porapak Q column supplied by Supelco. The response factors for the materials used were found to be close to the values reported by Dietz (1967). Typical reproducibility of the analysis was ±.003 in mole fraction, with somewhat larger deviations for the gas-phase compositions at low pressures. Because only a small fraction of the material in the cell was withdrawn during sampling, no measurable pressure drop could be observed. Repeated sampling was possible using a single loading of the equilibrium cell. The small quantity of the sample also facilitated rapid evaporation into the carrier gas stream. For the supercritical fluid sampling loop, it was determined that irreproducible results with an erroneously high concentration of water were obtained if the temperature of the sampling valve was not equal or slightly above the temperature of the cell. The problem was especially severe at low pressures (≤8.0 MPa).

Safety aspects: The use of high pressures in the experimental apparatus warranted the careful examination of the safety issues associated with the operation of the equipment. The main component of the experimental setup (the Jerguson gage), had an internal volume of approximately 50 cm^3. The

additional volume in the system (piping, valves) added less than 10% to the total internal volume. The potential for damage by rapid depressurization of the CO_2 in the system was, therefore, small. For protection against overpressure, a safety head with a rupture pressure of 35 MPa was installed. This pressure is equal to the pressure rating of the cell and well below that of the other equipment components. The line that was connected to the safety head, as well as all other purge lines, led to a hood for the safe removal of the purged gases. For added protection of the operator, in case of a failure of the sides of the Jerguson gage or the bath (made of Pyrex glass), a 1/2 inch thick Lexan enclosure surrounded the equilibrium bath. The liquid chemicals used are flammable and some (acetic acid, butyric acid) are corrosive. Since only small quantities (max 25 g) are used for every set of runs, the standard laboratory precautions, such as use of rubber gloves, safety goggles and adequate ventilation were found to be adequate.

4.1.2 Operating procedures

After purging and evacuation of the equipment, the cell was charged with a liquid mixture of known composition and the supercritical component up to the desired pressure. The recirculation pumps were started, and approach to equilibrium monitored by the stability of pressure, density and composition measurements with time. For the mixtures studied, a typical equilibration time is 15 min, but at least 30 min are allowed before the final sampling. At least two samples were taken from each phase at equilibrium. A new pressure point could then be immediately established by introducing or removing supercritical fluid or liquid, so that the level of the interfaces in the cell at the new desired pressure was appropriate for sampling through the available ports. Entrainment of the phases was not normally a problem, except near a critical point. Selective flashing and adsorption on the switching valves was sometimes a difficulty for the upper (gas) phase sampling loop at low pressures.

4.2. Acetone - water - carbon dioxide

The first of our series of model systems, is the ternary system carbon dioxide - acetone - water. The experimentally determined phase equilibrium behavior of this system at 313 K and 333 K is shown in Figures 4.2 and 4.3 as a series of triangular diagrams at various pressures. Tables with the experimental values for the composition of the coexisting phases are presented in Appendix C.2. On Figures 4.2 and 4.3, the results from the density-dependent model (Eq. 3.6 with the Peng-Robinson form of Eq. 2.7) are presented; the values of the pure component and interaction parameters used for the generation of the modelling results are given in Appendix D. The interaction parameters were determined solely from regression of binary phase-equilibrium data for the constituent binaries.

The most distinctive feature of the system behavior is an extensive three-phase region at both temperatures. The three-phase region is first observed at a pressure of less than 3.0 MPa at 313 K and approximately 3.5 MPa at 333 K and extends up to approximately the critical pressure of the binary carbon dioxide - acetone system. Table 4.1 summarizes our experimental results for the composition of the three phases at equilibrium as a function of pressure and temperature.

The physical picture that underlies this behavior, as pointed out first by Elgin and Weinstock (1959), is the "salting out" effect by a supercritical fluid on an aqueous solution of an organic compound. As pressure is increased, the tendency of the supercritical fluid to solubilize in the liquid results in a phase split in the aqueous phase at a lower critical solution pressure (which varies with temperature). As pressure is further increased, the second liquid phase and the supercritical phase become more similar to each other and merge at an upper critical solution pressure. Above this pressure only two phases can coexist at equilibrium. This pattern of behavior was also observed by Elgin and Weinstock for the system ethylene - acetone - water at 288 K. In addition, the same type of behavior, but at quite different pressures relative to the pure solvent critical pressure was reported by Paulaitis et al. (1984) and Radosz (1984) for the system carbon dioxide - isopropanol - water, by McHugh et al.

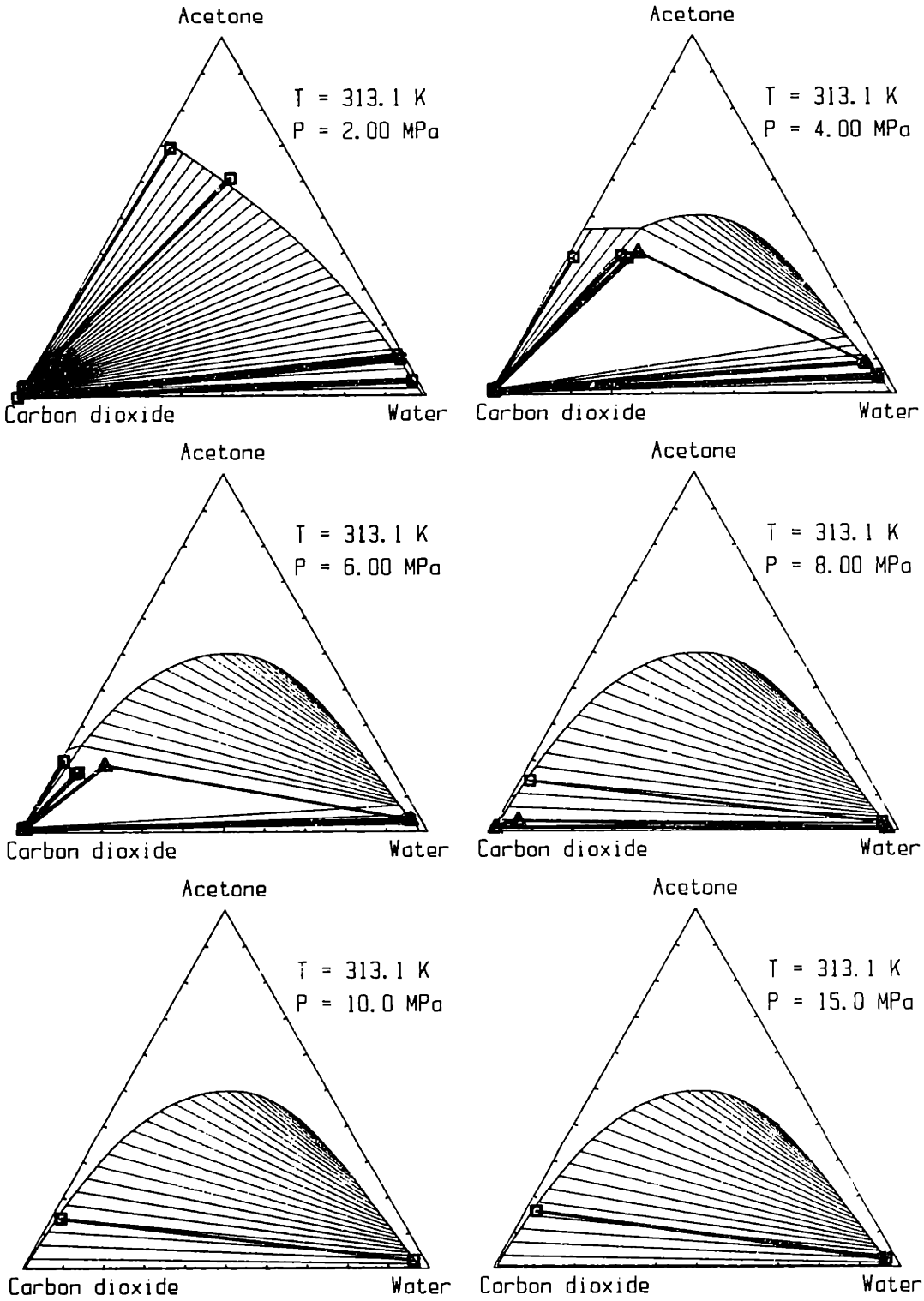

Figure 4.2 ***Phase equilibrium behavior for the system water - acetone-carbon dioxide at 313 K. (□) and (—) measured tie-lines; (△) measured three-phase equilibrium compositions; (—) predicted tie-lines (Eq. 3.6).***

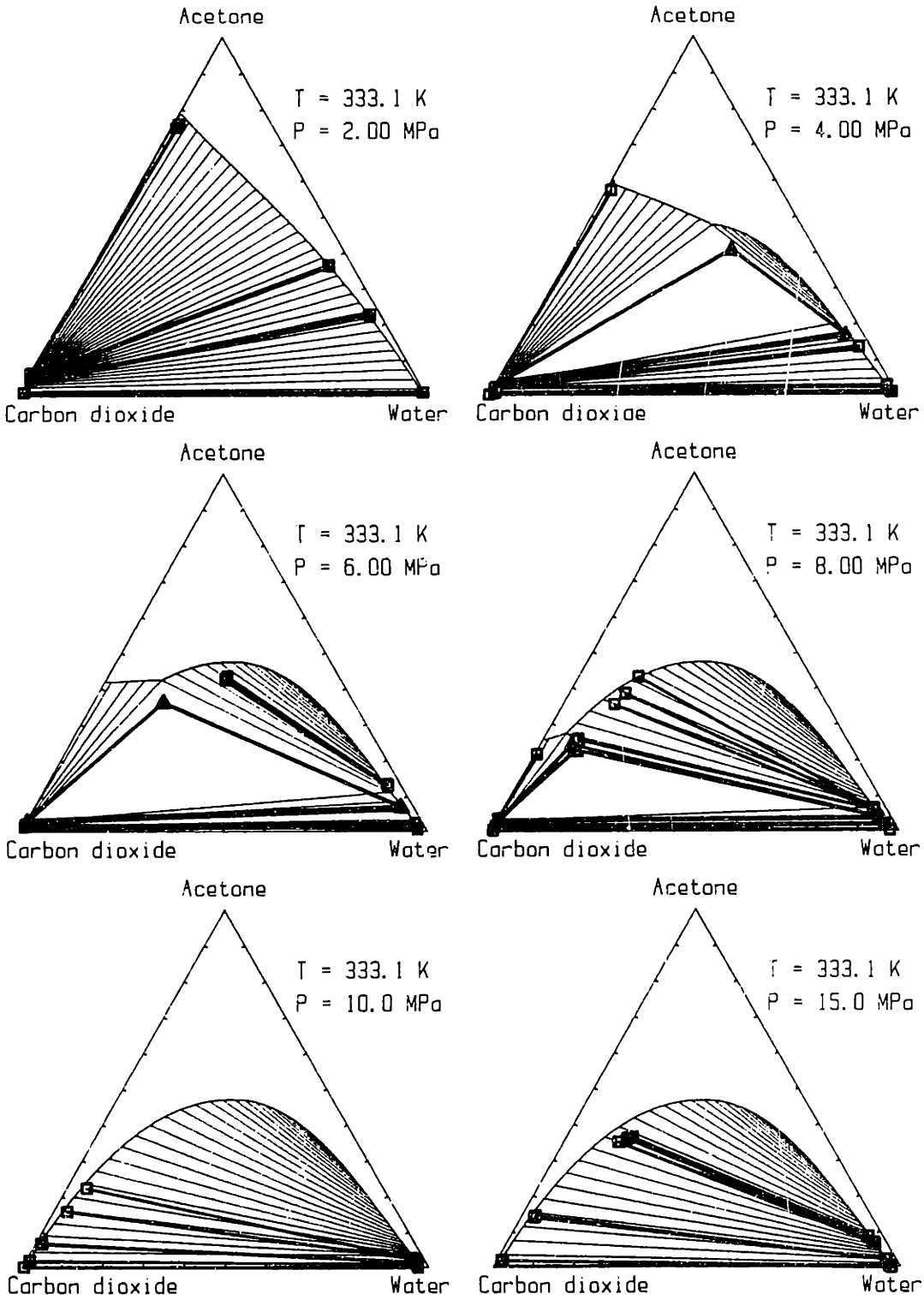

Figure 4.3 *Phase equilibrium behavior for the system water-acetone-carbon dioxide at 333 K. Symbols as in Figure 4.2.*

Table 4.1 Three phase equilibrium compositions for the system water(1) - acetone(2) - carbon dioxide(3) at 313 and 333 K

P(bar)	lower phase			upper phase			middle phase		
	x_1	x_2	x_3	y_1	y_2	y_3	z_1	z_2	z_3
				T = 313 K					
29.3	0.810	0.153	0.037	0.005	0.025	0.970	0.294	0.454	0.252
35.9	0.864	0.106	0.030	0.006	0.019	0.975	0.197	0.427	0.376
43.2	0.904	0.075	0.021	0.003	0.017	0.980	0.153	0.360	0.487
55.9	0.920	0.052	0.028	0.002	0.015	0.983	0.119	0.230	0.651
61.1	0.942	0.037	0.021	0.004	0.015	0.981	0.114	0.191	0.695
65.8	0.944	0.032	0.024	0.002	0.015	0.983	0.130	0.148	0.722
75.2	0.959	0.017	0.024	0.002	0.014	0.984	0.020	0.069	0.911
79.6	0.966	0.011	0.023	0.002	0.015	0.983	0.049	0.035	0.916
				T = 333 K					
39.4	0.795	0.163	0.042	[1]			0.400	0.398	0.202
51.1	0.880	0.091	0.029	[1]			0.182	0.418	0.400
59.4	0.906	0.068	0.026	0.006	0.030	0.964	0.173	0.359	0.468
70.3	0.925	0.049	0.026	0.008	0.035	0.957	0.117	0.300	0.583
79.2	0.939	0.039	0.022	0.006	0.032	0.962	0.089	0.234	0.677
92.6	0.946	0.029	0.025	0.010	0.046	0.944	0.084	0.127	0.789

[1] We were not able to obtain results for these state conditions.

(1981) for the system ethane - ethanol - water and by Paulaitis et al. (1981) for the system carbon dioxide - ethanol - water. This behavior appears then to be quite common. The phase equilibrium behavior for this system, can be classified as type 2, according to the system proposed by Elgin and Weinstock (1959), as discussed in Section 2.2.2.

The changes in the system behavior as pressure is increased result in a dramatic change in the slope of the tie-lines between the low-pressure and high-pressure diagrams. This reflects the change in the behavior of the solvent (carbon dioxide) from a low-pressure gas with relative little solvent power to a high-density efficacious solvent at pressures higher

than the critical pressure for the binary acetone-carbon dioxide. This change in behavior can be exploited for the development of separation processes.

It is interesting to note that the intervening three-phase region at intermediate pressures in effect "generates" the tie-lines for the high pressure side. This is evidenced by the fact that the plait-point and the position of the tie lines on the liquid-liquid immiscibility region change little with pressure. A further verification of this insensitivity is obtained by comparison of the diagrams at 100 and 150 bar in Figures 4.2 and 4.3. This suggests that similar separations can be achieved by operation at a range of pressures above the upper critical solution pressure of approximately 95 bar.

From an engineering point of view, the most important quantities in the evaluation of a separation scheme based on a phase behavior pattern such as the ones shown, are the selectivity of the separation with respect to the desired component, as well as the loading of the desired component in the extractant phase. It is well known that those two factors usually increase in different directions. In Figures 4.4 and 4.5, we present experimental data and model predictions for the distribution coefficient of acetone, and the selectivity ratio α of acetone over water (defined as the ratio of distribution coefficients of acetone and water in the liquid and fluid phases). The distribution factor shows a sharp maximum at both temperatures, with a higher value at the higher temperature, whereas the selectivity decreases smoothly from the limiting value of ~300 at low acetone concentrations to 1 as the plait point is approached. The experimental data show the same trends, although there is some scatter due to the fact that small absolute errors in the low supercritical phase concentrations of acetone and water result in large relative errors for the distribution coefficient and selectivity factors. Selectivities are generally higher for the lower temperature, but loadings are lower.

In Figure 4.6, we present the weight fraction of acetone in the supercritical phase on a CO_2-free basis versus the corresponding concentration of acetone in the liquid phase. The physical significance of this representation is that, for practical applications, the supercritical phase

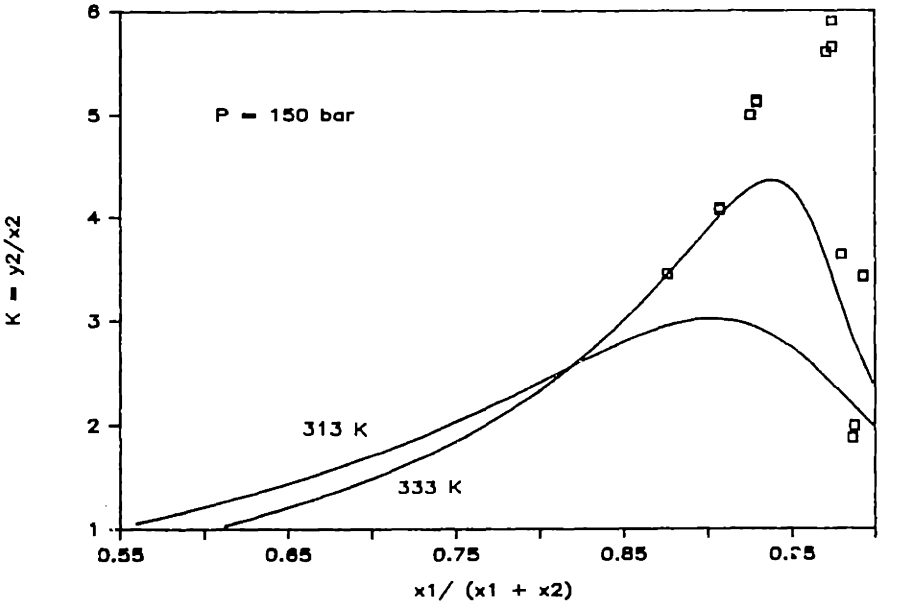

Figure 4.4 *Distribution coefficient of acetone for the system water (1) - acetone (2) - carbon dioxide (3) at P = 15.0 MPa, as a function of the water concentration in the lower phase. Experimental, 333 K (□); predicted, 333 K and 313 K (—).*

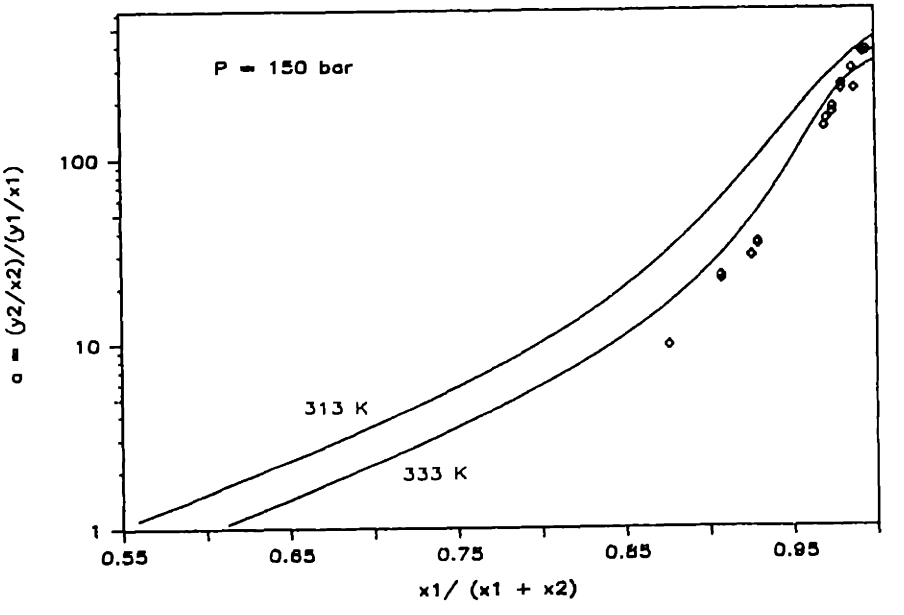

Figure 4.5 *Selectivity factor for acetone over water for the system water (1) - acetone (2) - carbon dioxide (3) system at P = 15.0 MPa, as a function of the water concentration in the lower phase. Experimental, 333 K (◊); predicted, 333 K and 313 K (—).*

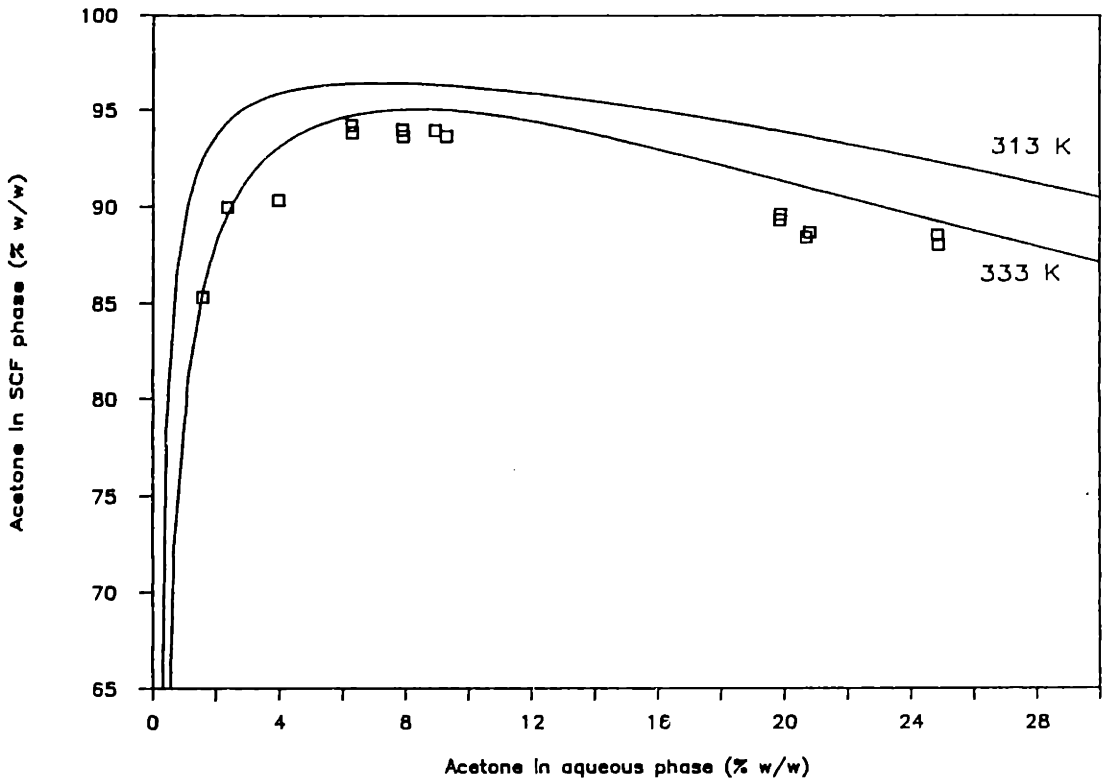

Figure 4.6 *Concentration of acetone in the supercritical fluid phase as a function of the concentration of acetone in the liquid phase at P = 15.0 MPa. Concentrations are expressed in % w/w on a CO_2-free basis. Experimental, 333 K (□); predicted, 333 K and 313 K (—).*

would be depressurized after extraction with the supercritical solvent. This results in removal of most of the solvent (CO_2). The curve necessarily passes through the origin at zero acetone concentration in the aqueous phase (for which no acetone can be present in the supercritical phase),but shows a broad maximum at a range of concentrations of acetone in the aqueous phase between 3% and 16% w/w. The maximum concentration of acetone in the supercritical phase is close to 95% w/w. We can, therefore, obtain almost pure acetone from a dilute aqueous solution using a single-step extraction with supercritical carbon dioxide. The dilute concentration range is exactly the concentration range of greatest interest for the recovery of fermentation products.

4.3. n-Butanol - water - carbon dioxide

4.3.1 Two- and three-phase equilibria

The experimentally observed phase behavior at 313 and 333 K is shown in Figures 4.7 and 4.8 (experimental data are shown as square points, and experimentally observed tie lines as dark lines). Let us follow the phase evolution by starting at a low pressure, e.g. 2.0 MPa in Figure 4.7. Since all three components are mutually immiscible at this temperature and pressure, the ternary phase diagram shows an extensive three-phase equilibrium region. As pressure is increased, the immiscibility gap between CO_2 and *n*-butanol decreases, whereas the immiscibility gaps between water and CO_2 or *n*-butanol do not change appreciably on the scale of the graph. As pressure is further increased above the critical pressure of the binary CO_2-*n*-butanol (Figure 4.7, P = 10 MPa), the phase diagram changes drastically, with the extent of the three-phase regions decreasing with pressure. The system can be classified as Type 3 according to the notation of Elgin and Weinstock (1959). Similar results are obtained at 333 K (Figure 4.8), with the scale of pressures shifted to higher values. No three phase regions were observed experimentally above 9.0 MPa at 313 K and 13.0 MPa at 333 K.

In Figures 4.7 and 4.8, we also present results from the density-dependent model (light lines). The model parameters for the CO_2 - water and the *n*-butanol - water binaries were determined solely from literature data. No literature data were available for the *n*-butanol - CO_2 binary system, but they were measured in this study. We used these data for the regression of the *n*-butanol - CO_2 parameters. The predicted phase diagram at high pressure was found to be quite sensitive to the values of the *n*-butanol - CO_2 interaction parameters. For the two temperatures studied, no temperature dependence of the parameters was necessary. The values of the interaction parameters used are given in Appendix D.

The agreement between experimental data and model predictions is best at low pressures. At the high pressure end, the model predicts a three -

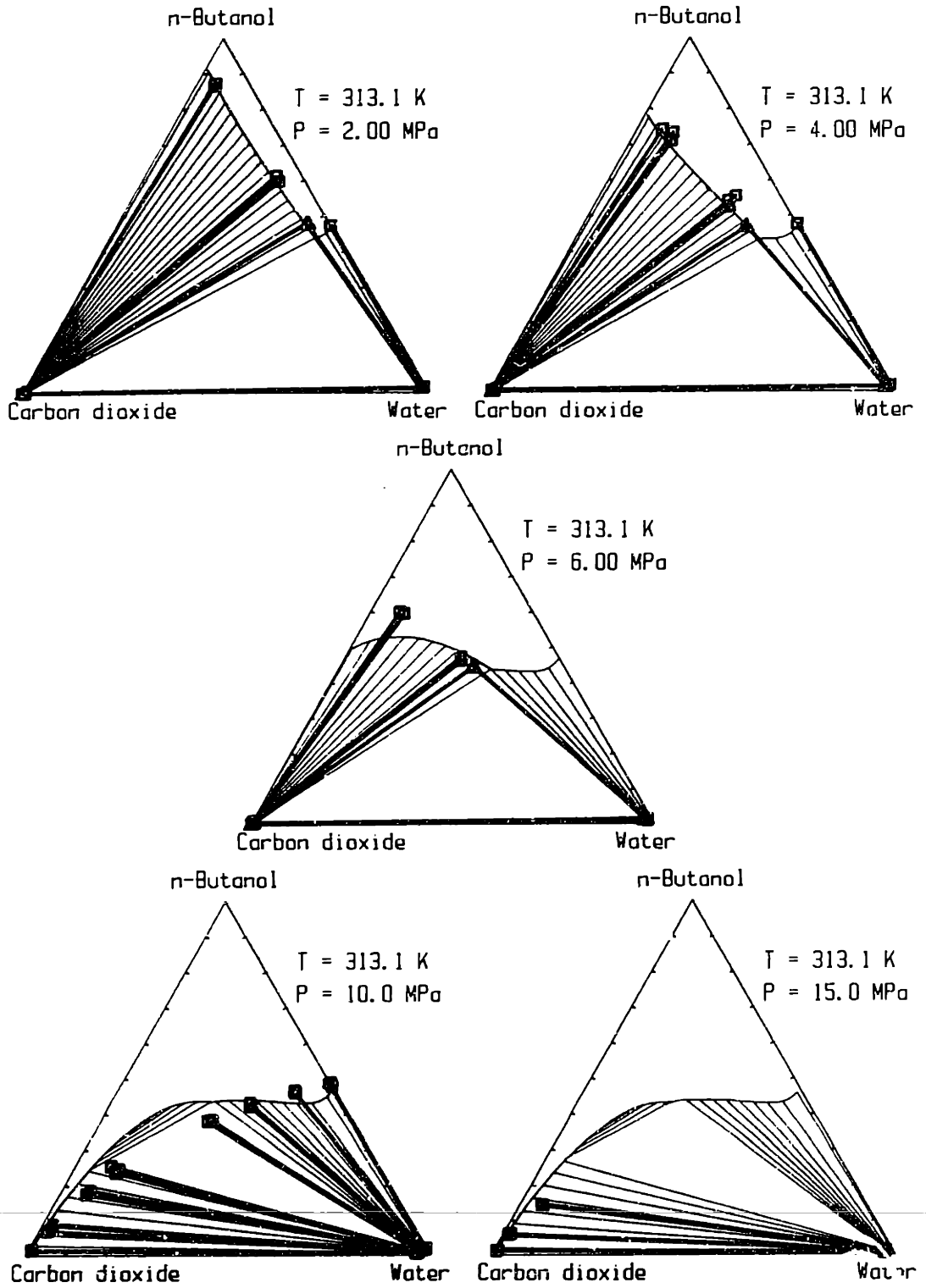

Figure 4.7 Phase equilibrium behavior for the system water - n-butanol - CO_2 at 313 K. Symbols as in Figure 4.2.

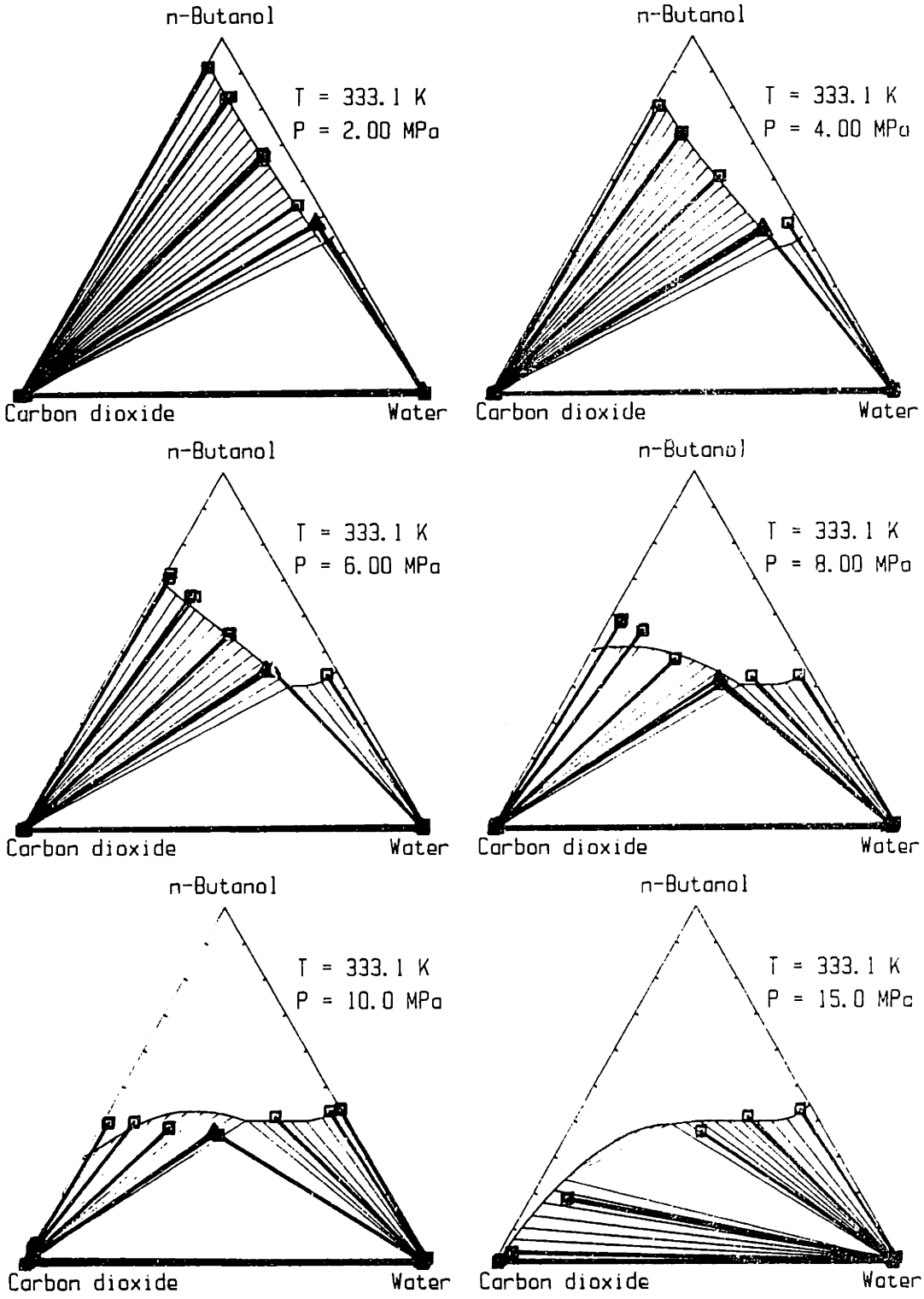

Figure 4.8 *Phase equilibrium behavior for the system water - n-butanol - CO_2 at 333 K. Symbols as in Figure 4.2.*

phase equilibrium region that was not observed experimentally, but the general shape of the phase diagram and its evolution with pressure are well described.

In Fig. 4.9, we present the measured and predicted concentrations of *n*-butanol in the two coexisting phases at the high density region. The results are given on a CO_2-free basis, as for the acetone system. At very low butanol concentrations, the supercritical fluid (SCF) phase is lean in butanol, but the concentration of butanol rises sharply and has a broad maximum at around 2% - 5% w/w concentration in the aqueous phase. It thus appears possible, to enrich a dilute (e.g. 3%) aqueous solution of butanol to better than 90% w/w by a single-step extraction with supercritical CO_2 at 313 K and 15.0 MPa pressure.

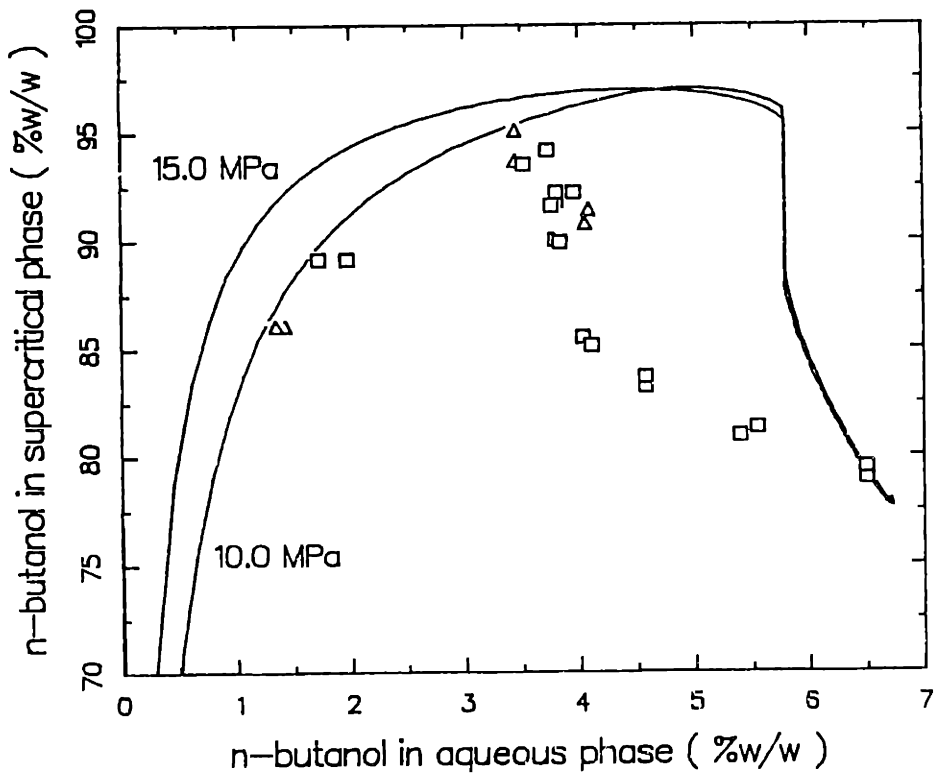

Figure 4.9 *Concentration of n-butanol in the aqueous and supercritical fluid phase on a CO_2-free basis. (□) experimental, 313 K, 10 MPa; (△) experimental, 313 K, 15 MPa; (—) predicted using Eq. 3.6.*

4.3.2 Four-phase equilibria and interpretation

A unique characteristic of the water - *n*-butanol - carbon dioxide system is the presence of a four phase LLLG equilibrium region at 313 K. The experimentally determined phase compositions and densities for the coexisting phases are given in Table 4.2.

Table 4.2 Four-phase equilibrium for the system water - *n*-butanol - carbon dioxide at T = 313.1 K, P = 8.25 MPa

Phase	Composition (mole fraction)			Density
	Water	*n*-Butanol	CO_2	(kg/m^3)
L_1	0.966	0.011	0.023	1002
L_2	0.168	0.285	0.547	846
L_3	0.034	0.039	0.927	793
G	0.013	0.066	0.921	730

As can be seen from Table 4.2, the third liquid (L_3) and "gas" (G) phases have quite similar compositions and all phases have similar densities.

The evolution of the phase behavior with pressure at the vicinity of the four-phase equilibrium point is shown in Figure 4.10. As can be seen, the model correctly predicts the presence of a four-phase equilibrium region at 313 K, but at a slightly different pressure (7.86 MPa, as compared to the experimental value of 8.25 MPa). The predicted phase compositions differ from the measured ones, especially for the (less dense) phases rich in CO_2. It is important to note, however, that no information about the four-phase equilibrium region was incorporated into the model parameters.

The very presence of a four-phase equilibrium region implies the existence of more than one three-phase region in the immediate vicinity of the four-phase point (a point of fixed pressure at constant temperature, according to the phase rule). The evolution of two three-phase regions into a four-phase region and then again into two different three-phase regions, was originally proposed by Gibbs in 1876, based solely on thermodynamic arguments (no data were available). Figure 4.11 presents two schematic three-dimensional diagrams of the topology of Gibbs space at the vicinity of the four-phase equilibrium point, for pressure slightly above and below the four-phase equilibrium pressure at constant temperature.

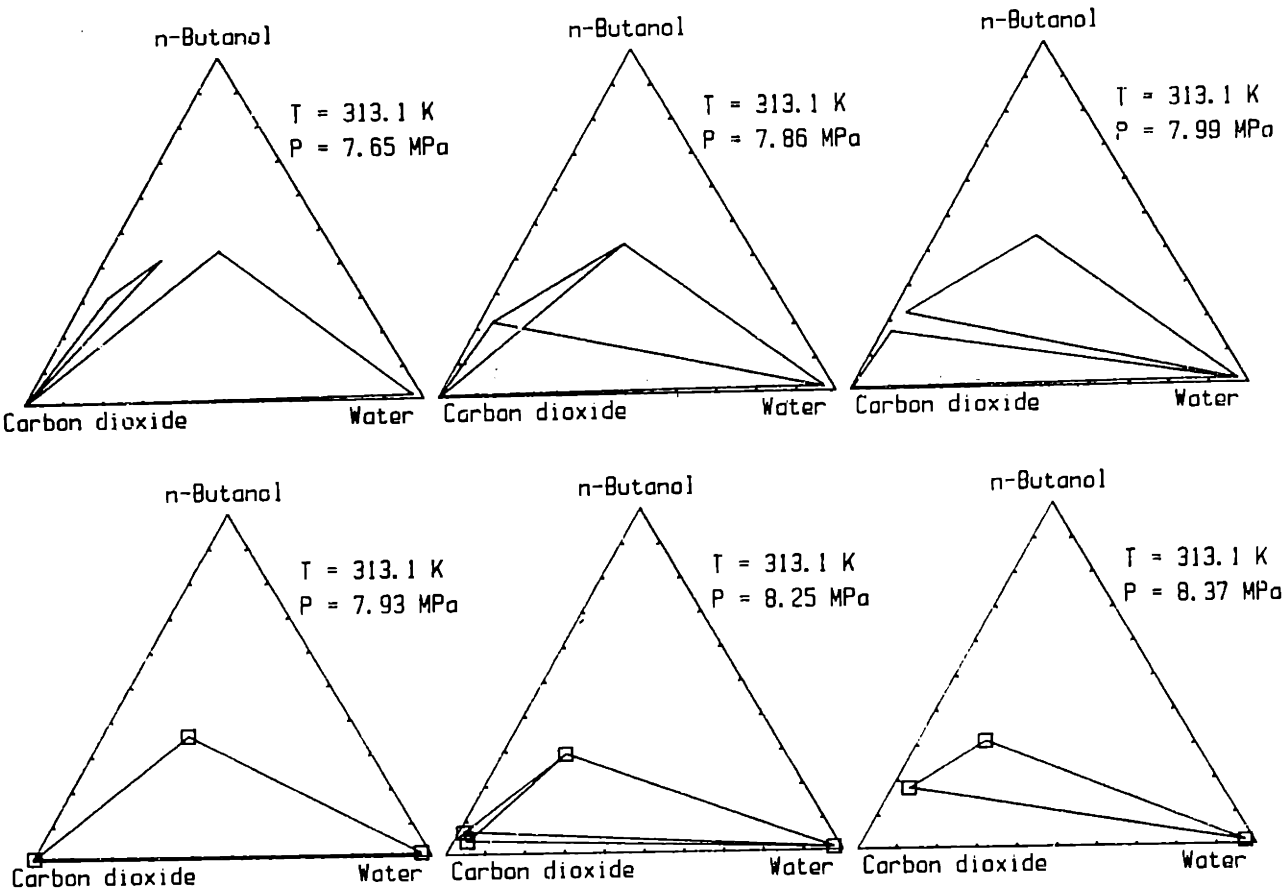

Figure 4.10 *Phase diagrams at the vicinity of the four-phase equilibrium pressure at 313 K. Lower row, experimental; upper row, predicted (Eq. 3.6).*

The appearance of four stable equilibrium phases must necessarily be connected to the appearance of four distinct "peaks" in Gibbs space. The determination of the phase diagram for a given topology is performed by the geometric construction of fitting planes that are tangent to the Gibbs surface, but do not penetrate any part of the surface. Two sets of such planes can be constructed at each pressure, corresponding to the isothermal-isobaric cross sections shown as projections on the X_1-X_2 plane. As pressure is changed, the height of the peaks of the Gibbs energy changes;

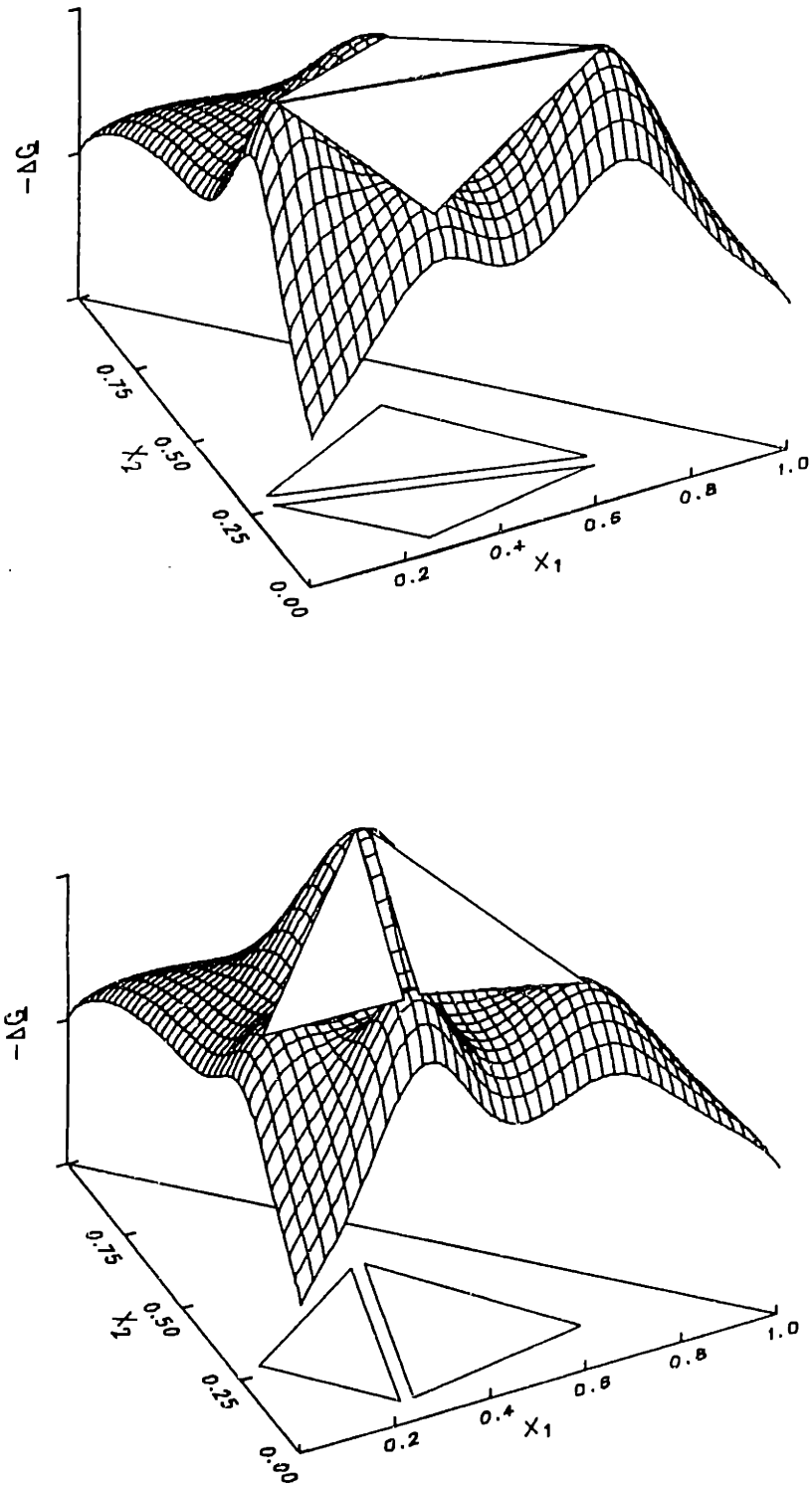

Figure 4.11 *Topology of Gibbs space in the vicinity of a four-phase equilibrium point.*

a four-phase equilibrium point exists when all four peaks are coplanar. In this representation, it is easy to understand why the two distinct three-phase equilibrium regions come together along a diagonal and separate along a different diagonal.

The only other case known to us for equilibrium between four fluid phases in a ternary mixture, is for the system isopropanol - water - CO_2 (DiAndreth and Paulaitis, 1985) at 313 K and 7.6 MPa. It thus would appear that ternary aqueous systems with a supercritical fluid offer unique possibilities for the investigation of multiphase behavior, in addition to their practical applicability in separations.

4.4. Acetic Acid - water - carbon dioxide

In Figures 4.12 and 4.13, the experimentally observed phase equilibrium behavior for the system acetic acid - water - carbon dioxide is presented together with the predictions of the density-dependent model (Eq. 3.6 with the Peng-Robinson form of Eq. 2.7) using parameters derived from binary data. The experimental data for the system are summarized in Appendix C.4.

The phase equilibrium behavior of the system shares several features with the results for previous systems. The ternary diagrams at low pressures are dominated by a two-phase region that represents equilibrium between a liquid mixture of water and acetic acid, and a carbon dioxide-rich phase that contains small amounts of both acid and water. The solubility of CO_2 in the acid phase increases with pressure, with a binary acid-CO_2 critical point at a pressure of approximately 8.5 MPa at 313 K and 10.5 MPa for 333 K. This is similar to the binary critical pressures observed for the binary systems of carbon dioxide with acetone and *n*-butanol. Again, above the binary critical pressure, carbon dioxide and acid form a completely miscible binary.

A three-phase equilibrium region is experimentally observed for this system for a narrow range of pressures just below the binary acid-CO_2 critical pressure (at 7.7-8.1 MPa for T=313 K and 10.2-10.4 MPa for T=333 K, from Table C.7). The model also predicts a three-phase equilibrium region between 6.5 and 8.4 MPa at 313 K. This results in classification of the

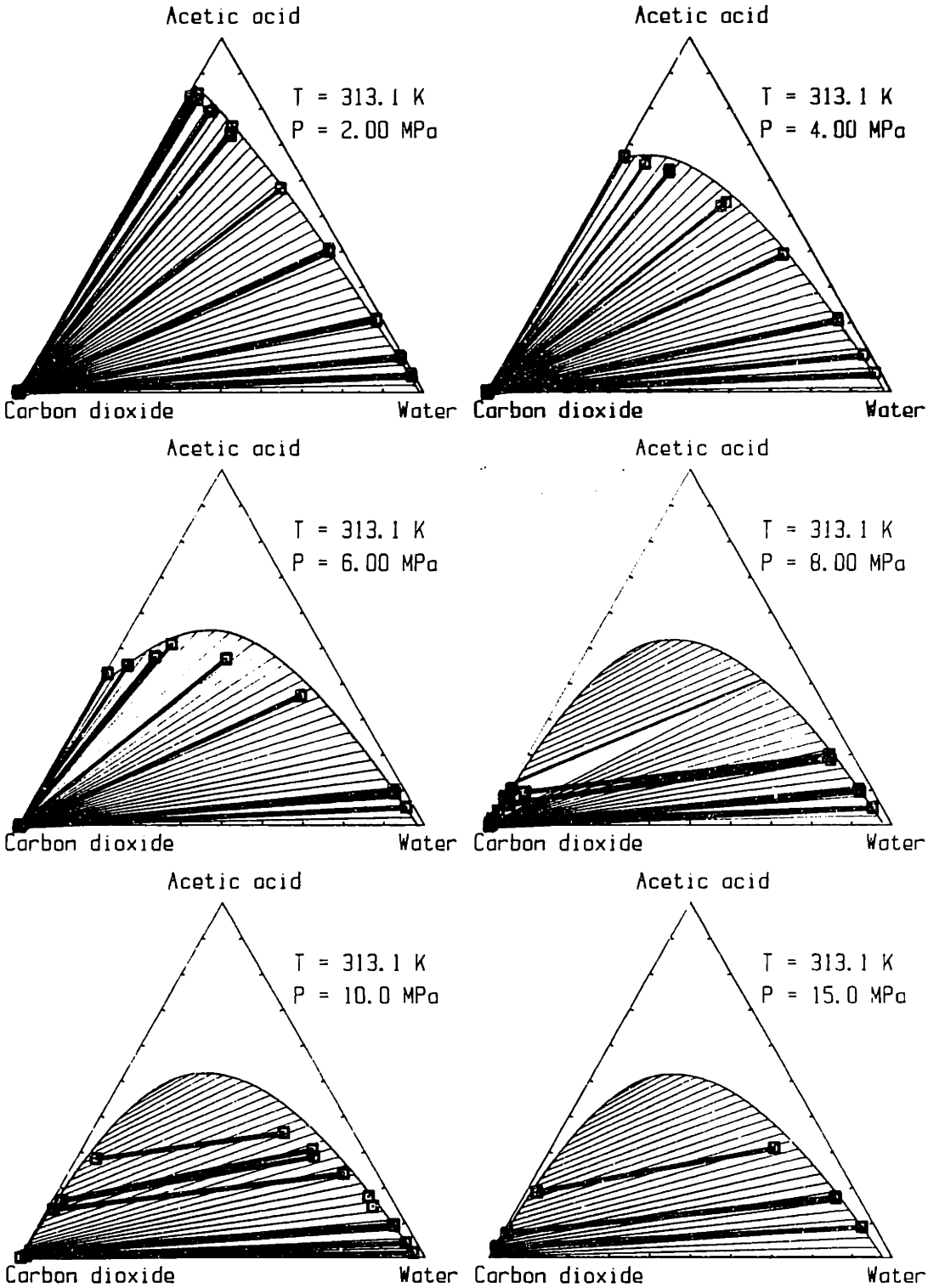

Figure 4.12 *Phase equilibrium behavior for the system water - acetic acid - carbon dioxide at 313 K. Symbols as in Figure 4.2.*

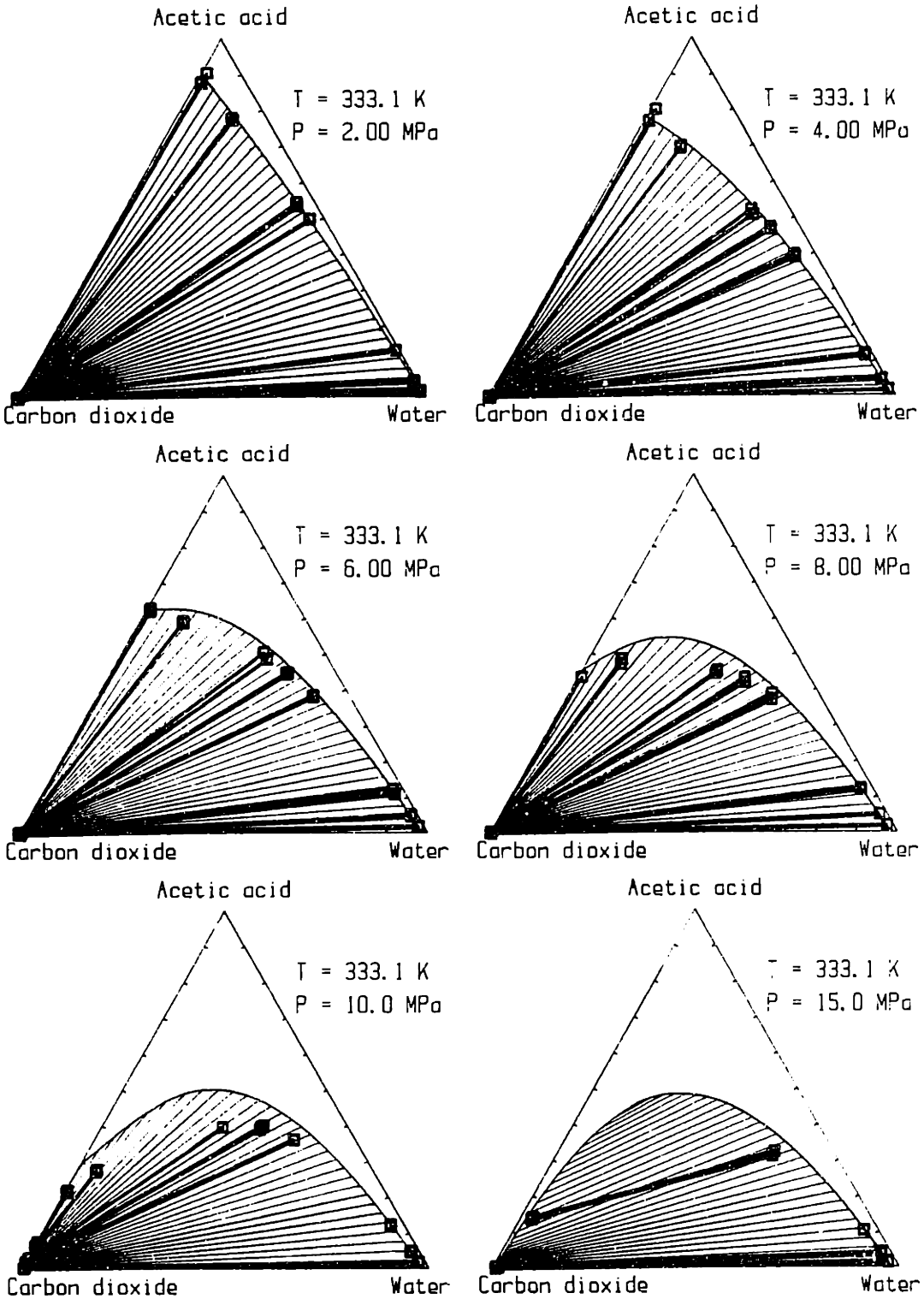

Figure 4.13 *Phase equilibrium behavior for the system water - acetic acid - carbon dioxide at 333 K. Symbols as in Figure 4.2.*

system as "type 2" (according to Elgin and Weinstock, 1959). This system, although qualitatively similar to the ternary acetone system, has a much narrower range of three-phase equilibrium coexistence regions. The behavior of the acetone system can be interpreted as a liquid-phase split between acetone and water at the presence of moderate quantities of carbon dioxide. By contrast, the acetic acid behavior is more seen as equilibrium between two phases rich in carbon dioxide at the presence of a liquid mixture of acetic acid and water.

This contrast in behavior is apparent also at higher pressures: the slope of the tie-lines at high pressures gives a distribution coefficient of acetic acid between the aqueous and the supercritical phase that is significantly less than 1, whereas the acetone system had distribution coefficients at comparable conditions significantly higher that 1. The difference in both high- and low-pressure behavior can be interpreted as an indication of a lower affinity of acetic acid for a carbon dioxide-rich environment relative to acetone. This is consistent with the fact that acetic acid has a high hydrogen-bond formation ability in an aqueous environment that acetone lacks.

The ability of the model to predict the experimentally observed behavior is again best at low pressures. The high pressure prediction is approximately correct for the extent of the two-phase equilibrium region and the slope of the tie-lines at low acid concentrations, but the slope of the tie-lines as the plait-point is approached is less well predicted. It appears, however, that the slope of the tie-lines at the low acid concentration regions is correct.

4.5. *n*-Butyric Acid - water - carbon dioxide

The experimentally observed phase equilibrium behavior for this system at 313 K is shown in Figure 4.14 and presented in tabular form in Appendix C.6. The predictions of the density-dependent model (Eq. 3.6) are also given on the same figure.

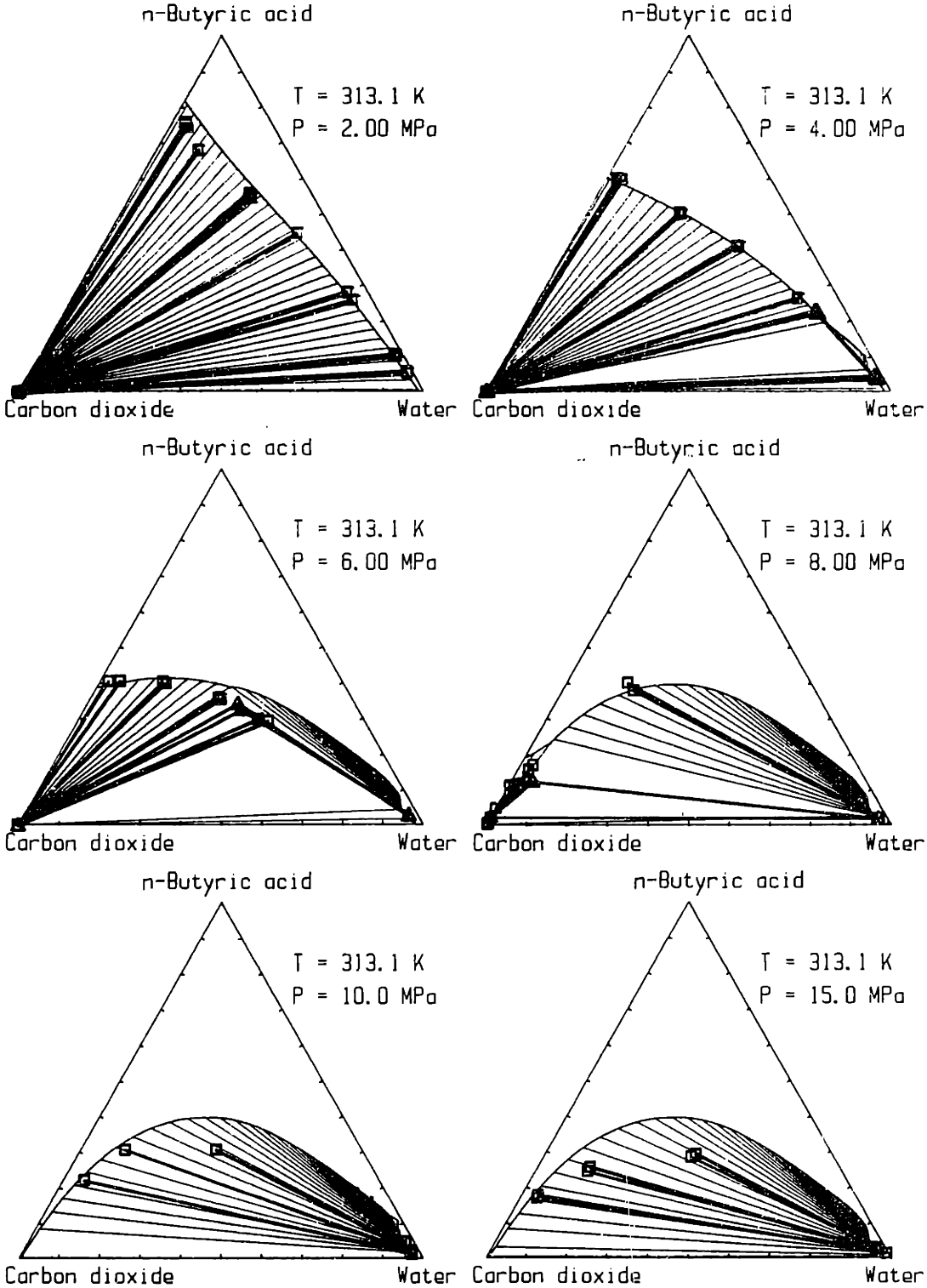

Figure 4.14 *Phase equilibrium behavior for the system water - n-butyric acid - carbon dioxide at 313 K. Symbols as in Figure 4.2.*

The low-pressure behavior of the system is similar to the observed behavior for the acetone-water-CO_2 system. A three-phase equilibrium region appears at a relatively low pressure (between 2.0 and 4.0 MPa experimentally and at a pressure slightly below 2.0 MPa from the model predictions). At high pressures, the system has a single two-phase coexistence region, with tie lines sloping towards the water corner, implying distribution coefficients for *n*-butyric acid higher than 1.

The model predicts the evolution of the three-phase equilibrium region with pressure quite closely and gives correct results for the slope of the tie-line at high pressures, but overpredicts the extent of the two-phase equilibrium region. The dense tie-lines close to the plait point at 15.0 MPa indicate that the binary system *n*-butyric acid - water is close to phase separation.

4.6 Summary and conclusions

4.6.1 Phase equilibrium results

A pronounced effect of the hydrocarbon chain length in a homologous series of organic compounds on the phase diagrams and the selectivity of the supercritical solvent for the organic compound over water was observed. This can be best described by comparing the results for the ternary diagrams at a constant temperature and density for a series of organic acids, as shown in Figure 4.15, comparing the results for the phase equilibrium behavior at 313 K and 15 MPa for acetic, *n*-propionic and *n*-butyric acid in ternary systems with CO_2 and water. Results for acetic and *n*-butyric acid were obtained in this study and discussed before in the appropriate sections; results for *n*-propionic acid were obtained by Willson (1987) using the same experimental apparatus and procedures.

As can be seen in Figure 4.15, the change in hydrocarbon chain length for this series of straight-chain organic acids has the following effects on the phase equilibrium behavior:

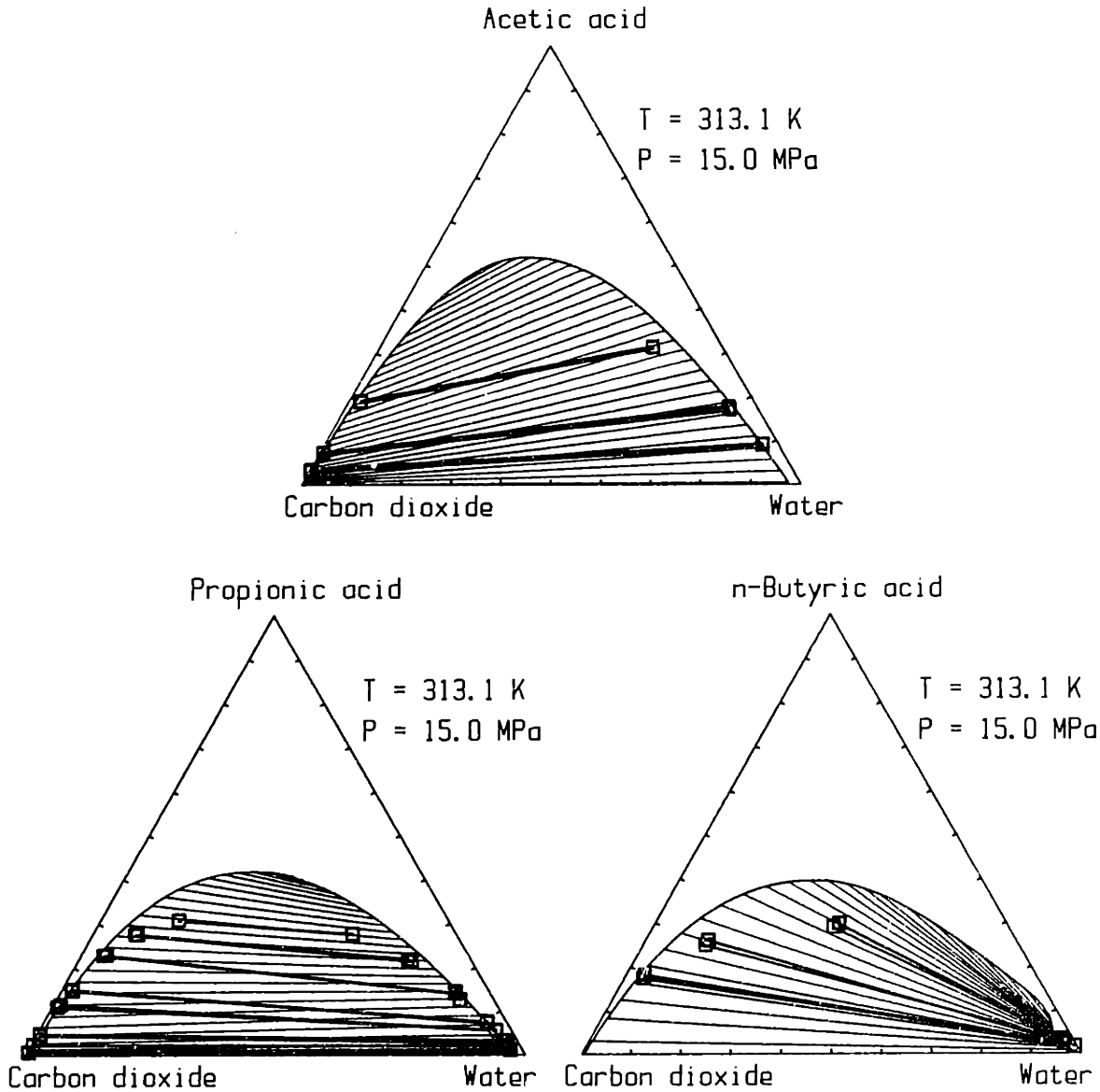

Figure 4.15 *Comparison of the ternary phase equilibrium behavior at 313 K and 15.0 MPa for acetic, propionic and n-butyric acids. Data for propionic acid are from Willson (1987). Symbols as in Figure 4.2.*

a. The slope of the tie-lines, and therefore the distribution coefficient of the organic acid between the supercritical fluid and aqueous phases changes gradually: it is less than 1 (the acid prefers the supercritical phase) for acetic acid, approximately equal to 1 (parallel tie-lines) for *n*-propionic acid, and is greater than 1 (the acid preferentially distributes itself to the supercritical phase) for *n*-butyric acid.
b. The extent of the two-phase envelope (on a mole fraction basis) is less the higher the chain length of the acid.
c. As the hydrocarbon chain length for the acid increases, there is a tendency for phase-separation on the acid-water side of the ternary diagram. This is consistent with the fact that straight-chain organic acids above *n*-pentanoic acid show a liquid-liquid phase split with water at atmospheric pressure that is expected to persist up to high pressures, since liquid-liquid equilibria are relatively insensitive to pressure variations.

A similar behavior can be determined by comparing the results for *n*-butanol (Figures 4.7 and 4.8) and literature results for ethanol (Figure 3.8). Again, increasing the size of the hydrophobic part of a molecule results in an increased tendency of the organic compound to favor the supercritical fluid versus the aqueous phase. This tendency is most likely a direct result of the change in the character of the molecule from hydrophilic at low carbon chain lengths, where the properties of the molecule are primarily determined by the polar oxygen-containing group, to hydrophobic as the carbon chain length increases.

Another observation relates to the sensitivity of the phase diagrams to pressure and temperature. It was observed (Section 4.2) that the shape and extent of the phase coexistence curves for all the systems studied was relatively insensitive to changes in pressure and temperature above the critical pressure of the pure supercritical fluid, for the range of reduced pressures $1.3 \leq P_R \leq 3$ and for reduced temperatures $1.03 \leq T_R \leq 1.10$. This is in agreement with the results of previous investigators for the ethanol system (Gilbert and Paulaitis, 1986); this may not be correct when the system behavior at the high pressure range is complicated by the presence

of three-phase equilibrium regions. An example of this latter case is provided by the system isopropanol - water - carbon dioxide studied by Paulaitis et al. (1984) and Radosz (1984).

The equilibrium between four fluid phases, although theoretically possible, has rarely been observed in the past. The appearance of the four-phase equilibrium region for water - *n*-butanol - carbon dioxide system at 313 K may be related to two factors : 1) the immiscibility gap between water and *n*-butanol, which is enhanced in the presence of CO_2 and 2) the proximity of the critical point of carbon dioxide (T_c = 304.2 K). In the binary system water - CO_2, a three phase equilibrium region is observed at a very narrow temperature interval, up to 304.6 K (Morrison, 1981). The multiphase behavior in the case of butanol and isopropanol extends to temperatures further away from the critical point of CO_2. One would expect this behavior to be quite general, in that several other systems of the type water-organic compound - supercritical fluid may show similar behavior.

The density-dependent model was successful in predicting the qualitative characteristics of the experimentally observed behavior for all the cases studied, including the presence and approximate location of the four-phase equilibrium region in the system water - *n*-butanol - carbon dioxide. The quantitative agreement between model predictions and experimental data is good in most cases, especially for the low-pressure region. For the high pressure region, the model usually overpredicts the extend of the two-phase region and does not accurately reproduce the location of the plait points. However, since only binary parameters regressed from binary data that contain no information about the ternary system behavior were used, the overall performance of the model should be considered satisfactory.

4.6.2 Process implications

The phase equilibrium behavior we observed can form the basis for separation processes that utilize supercritical solvents for the recovery of polar organic compounds from aqueous solutions.

In general, the solvent power of the supercritical fluid, as determined by the loading of the organic compounds in the supercritical phase at a constant concentration of organic compound in the aqueous phase, was found to increase with solvent density. Since an increase in pressure at constant temperature or a decrease in temperature at constant pressure result in an increased density (see Figure 1.1), this would also be the direction of increasing solvent power of the supercritical fluid. The selectivity of the supercritical solvent for the organic compound over water, however, generally increases in the opposite direction: this can be verified from Figures 4.4 - 4.6. A careful optimization of process conditions with respect to both pressure and temperature for the best combination of selectivity and solvent ratio is required.

The ability to use an equation of state that captures most of the important characteristics of the phase equilibrium behavior of the systems should greatly facilitate the design and optimization of separation processes. When only binary data are available, the model predictions for the distribution coefficients are not normally reliable enough for detailed process design, but could serve as guidelines for a preliminary screening of potential solvents and solutes.

4.6.3 Integration with fermentation processes

A conceptual integrated process for the recovery of fermentation products from aqueous solutions using supercritical solvents is shown in Figure 4.16. The basic steps involved are (i) the fermentation that produces a dilute broth containing the growing cells, nutrients and desired product (ii) a supercritical fluid contacting step that recovers part of the product and (iii) separation of the desired product by pressure reduction or a change in temperature and recycling of the supercritical solvent. The success of the process depends on the ability to recover selectively the desired product with a minimum amount of solvent and a low energy consumption, as well as the ability to recycle the stream containing the microorganisms with minimum damage to the growing cells.

It has been observed (Willson, 1986) that under conditions typical for extraction with a supercritical fluids, the growth of propionibacterium freudereuchii is inhibited in the presence of the solvent, but the inhibition may be reversible on removal of the solvent by depressurization. An inverse correlation between solvent power of a supercritical fluid and inhibition effect was observed. The likely cause for the inhibition was found to be the dissolution of the supercritical solvents into the cell membranes. The selection of possible solvents and conditions for an integrated process for the production of low molecular-weight polar organic compounds by biochemical synthesis and recovery with supercritical fluids needs to combine information on the solvent properties and the biological effects of supercritical fluids.

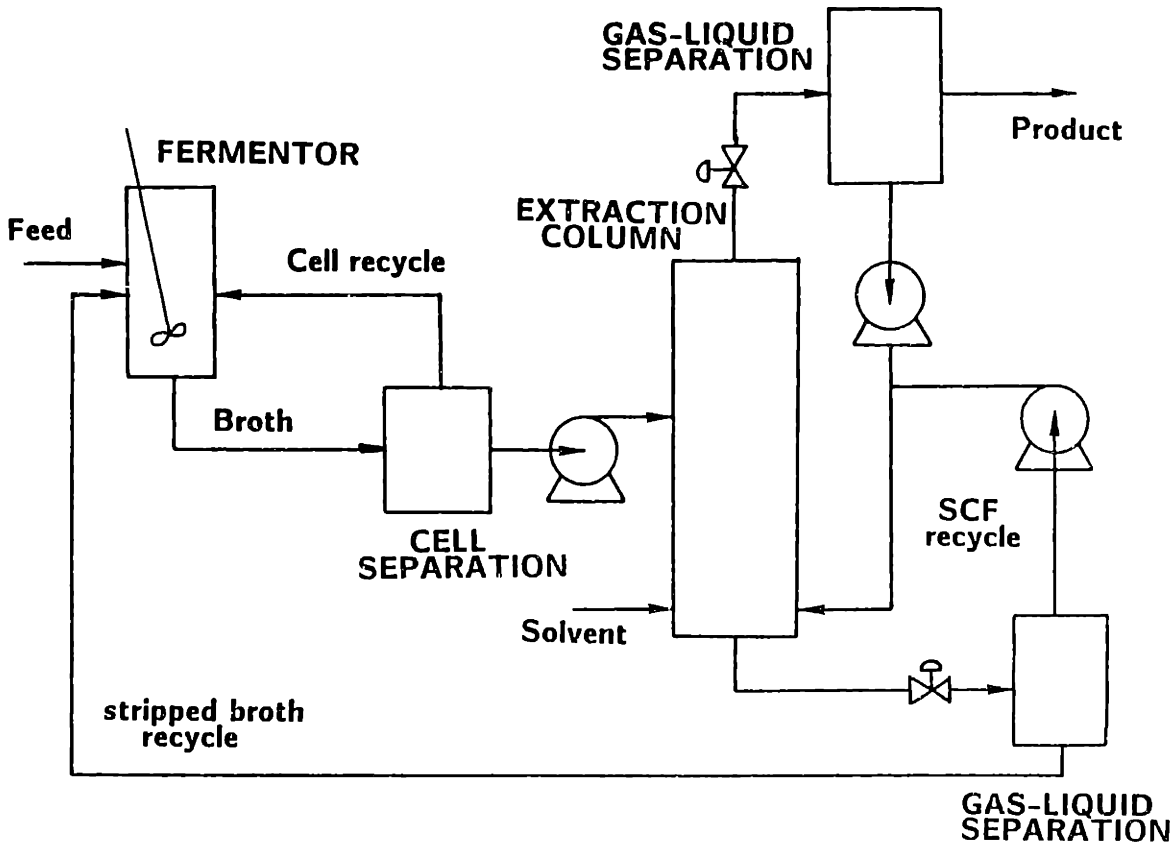

Figure 4.16 *A conceptual integrated process for production of organic compounds using biochemical synthesis and recovery with a supercritical fluid.*

CHAPTER 5
MONTE CARLO SIMULATION - METHODS

5.1 Introduction and research objectives

Direct computer simulation techniques have only recently advanced to the point where the calculation of the properties of realistic mixtures with acceptable accuracy is possible. In recent years, significant advances have been realized in methods to determine the chemical potential of non-ideal mixtures using Monte Carlo simulation (Romano and Singer, 1979; Shing and Gubbins, 1983). The combination of better theoretical techniques and significantly improved computer facilities makes molecular simulation an increasingly attractive tool to understand and predict the behavior of systems of practical importance.

In this work, we focus on the question of predicting the phase equilibrium behavior of non-ideal fluid mixtures using Monte Carlo simulation. The basic goal is the determination of the effects of molecular size and intermolecular potential energy differences in mixtures, on the macroscopic phase behavior and on the microscopic structure.

The ability to determine phase diagrams for fluid mixtures is important both from a theoretical as well as a practical point of view. For binary fluid mixtures, the classification of Scott and van Konynenburg (1970), based on the shape and location of the mixture critical curves, identifies six possible classes of fluids. This classification can serve as a guide to the selection of solvents and process conditions for applications such as supercritical extraction (Paulaitis et al., 1983). It has also been shown using perturbation theory (Gubbins and Twu, 1977a, 1977b) that even a simple potential model, such as the Lennard-Jones with multipolar

interactions, can reproduce a wide range of types of phase equilibrium behavior. However, few calculations of complete phase diagrams of mixtures using direct molecular simulation have been reported.

A discussion of the general questions for the molecular simulation part of this work was given in Section 1.3. The specific issues that need to be addressed are summarized below.

a. We need to select models for the intermolecular potential energy functions which will give a reasonable description of the basic features of molecular interactions, while being simple enough to be tractable using the available computational resources.

b. What are appropriate methods for the estimation of the position of phase transitions in fluid mixtures using Monte Carlo simulation? Are there short-cut methods that avoid the complete chemical potential determination step and still give an indication of the presence of phase transitions?

c. How can we obtain the chemical potential in non-ideal mixtures in an efficient way? What is the range of validity of the Widom test-particle expressions for the calculation of the chemical potential?

d. We need to verify the accuracy and efficiency of our methods using results from previous investigators for both pure-fluids and mixtures.

e. Finally, we would like to obtain results for a representative range of non-ideal mixtures, to investigate the effect of the potential parameters on the mixture phase diagrams and compare the results with corresponding data for real fluids.

In the sections that follow, we present the methodology developed to address questions a. to c. above. Comparisons of the calculated results with literature results and the results from our calculations on mixtures are given in Chapter 6.

5.2 Monte Carlo simulation

5.2.1 Historical background

The availability of the first electronic computing devices in the years immediately following the Second World War, made possible for the first time calculations in which systems with several interacting particles could be followed for a relatively large number of possible configurations. The first use of computing machines for the calculation of thermodynamic properties was made by Metropolis et al. (1953) for the hard sphere fluid. His method became known as the Metropolis importance sampling algorithm, and still forms the basis for Monte-Carlo calculations in statistical physics. The theoretical basis of this method is presented in Section 5.5.2.

In a parallel development, the related method of molecular dynamics was proposed by Alder and Wainwright (1959). In this method, the equations of motion for a system of molecules are integrated in the time domain. The method forms an alternate to the Monte-Carlo technique and offers advantages when dynamic properties (for example, transport coefficients) are of interest. The two methods are completely equivalent for the calculation of equilibrium properties in the so-called ergodic limit, that is when a sufficiently large number of configurations has been sampled (McQuarrie, 1976, p.554).

Despite the theoretical advancements, the capabilities of the early machines were far from sufficient for the simulation of realistic fluid and significant new advances were only made in the recent years with the rapid increase in available computing power. Mixtures, molecules interacting with complicated potentials and even biological macromolecules in solution have been studied in the recent years. The potential for increase in the scope of molecular simulations appears to be expanding at a very rapid pace, driven both by the improvements in hardware and software technology and by advances in theory that make it possible to determine properties of practical importance.

5.2.2 Metropolis importance sampling

The Monte Carlo method (Metropolis et al., 1953) is now a standard technique in statistical physics. A summary of the basic technique is given by Binder (1979) and Binder and Stauffer (1984), and only a brief outline is presented here. In order to use the method, we need first to define the system that will be investigated. We use the canonical (NVT) ensemble, defined by a constant total number of molecules, total volume and temperature. The thermodynamic average of any observable quantity, A, can be written in the following manner :

$$\langle A \rangle = \frac{\int_{\Omega} d\underline{X}\ A(\underline{X})\ e^{-H_N(\underline{X})/k_B T}}{\int_{\Omega} d\underline{X}\ e^{-H_N(\underline{X})/k_B T}} \qquad [5.1]$$

In Eq. 5.1, the numerator is the integral of the observable quantity A over phase space, a 3N-dimensional space in the case of N molecules with spherical symmetry that only have translational degrees of freedom. The integral in the numerator is the canonical partition function. H_N is the Hamiltonian (or configurational energy) of the system and k_B is Boltzmann's constant.

The problem of evaluating the integral in Eq. 5.1 is a formidable one, even for a relatively small ensemble of a few hundred molecules, because of the high dimensionality of the problem. It is important to note, however, that not all regions in configuration space contribute equally to the integrals in Eq. 5.1. In a relatively dense fluid, most of the configurations that would result if we assigned random positions to a system of N molecules (equivalent to sampling a random point of the phase space) would result in the overlap of one or more molecules, with correspondingly very high energy. Because of the negative exponentials in Eq. 5.1, at any reasonable temperature, the contribution of the high-energy configurations to the thermodynamic averages would be negligible. The Metropolis et al. (1953) method of importance sampling is based on taking advantage of this property

of the problem, and concentrating the evaluation of the integrals in Eq. 5.1 at points that are most likely to contribute to the thermodynamic averages. In general, if we generate a set of configurations $\{\underline{x}_\nu\}$ with an associated set of probabilities $\{P(\underline{x}_\nu)\}$, the expressions appropriate for the approximation of Eq. 5.1 are :

$$\langle A \rangle \approx \frac{\sum_{\nu=1}^{M} A(\underline{x}_\nu) P^{-1}(\underline{x}_\nu)\ e^{-H_N(\underline{x}_\nu)/k_B T}}{\sum_{\nu=1}^{M} P^{-1}(\underline{x}_\nu)\ e^{-H_N(\underline{x}_\nu)/k_B T}} \qquad [5.2]$$

where we have simply divided each point with the associated probability to correct for the biased sampling. If we now select our sampling points with the probability

$$P(\underline{x}_\nu) = e^{-H_N(\underline{x}_\nu)/k_B T} \qquad [5.3]$$

then Eq. 5.2 becomes simply

$$\langle A \rangle \approx \frac{1}{M} \sum_{\nu=1}^{M} A(\underline{x}_\nu) \qquad [5.4]$$

and we can obtain thermodynamic averages by simply taking the unweighted average of the observable quantity over all configurations generated.

It can be shown that a sufficient but not necessary condition (Wood, 1968) for the Markov chain to have the desired property that $P(\underline{x}_\nu)$ converges towards the equilibrium probability given in Eq. 5.3, is:

$$\frac{\text{Probability of transition } (\underline{x}_\nu \rightarrow \underline{x}_{\nu'})}{\text{Probability of transition } (\underline{x}_{\nu'} \rightarrow \underline{x}_\nu)} = \frac{P(\underline{x}_{\nu'})}{P(\underline{x}_\nu)} = e^{-\Delta H/k_B T} \qquad [5.5]$$

where $\Delta H = H(\underline{x}_{\nu'}) - H(\underline{x}_\nu)$.

Eqn. 5.5 does not specify uniquely the probability of transition between states $\underline{x}_\nu$ and $\underline{x}_{\nu'}$. A common choice for the transition probabilities that we have used in this work, is:

$$\text{Probability of transition } (\underline{x}_\nu \rightarrow \underline{x}_{\nu'}) = \begin{cases} 1 & \text{if } \Delta H \leq 0 \\ e^{-\Delta H/k_B T} & \text{if } \Delta H > 0 \end{cases} \qquad [5.6]$$

No constraint is placed upon the particular method used to generate configuration $\underline{x}_\nu'$ from configuration $\underline{x}_\nu$, other than the requirement of not biasing the Markov chain by favoring some particular types of configurations. The basic step is repeated using the generated configuration as the new starting point, and a large number of steps ($\sim 10^6$ in this study) are executed and used to calculate the ensemble average properties of the fluid via Eq. 5.4.

5.3 Determination of the chemical potential

5.3.1 Background

The determination, using molecular simulation, of those of the properties of a fluid that can easily be calculated for a given configuration (such as the energy, pressure or radial distribution functions) follows directly from the application of Eq. 5.4. This is not so for <u>derived</u> properties, those properties that in classical thermodynamics cannot be associated with a single state of a system, but instead must be calculated by performing a change to a state of known or assumed properties. Examples of the last set of properties would be the entropy S, or the chemical potential of a component in a mixture, μ_i. The calculation of such properties has been performed up to recently, by using specialized simulation techniques such as the grand canonical ensemble Monte Carlo technique (Adams, 1976; 1979), or umbrella sampling (Shing and Gubbins, 1981). A major disadvantage of these techniques, is that the calculation of the derived properties is made

on artificial systems; a separate series of simulations is necessary to obtain the observable properties of the fluid.

5.3.2 The test particle method

The calculation of the chemical potential of a fluid based on the potential energy distribution functions was first proposed by Widom (1963) and extended by Shing and Gubbins (1981, 1982, 1983). It has been used recently for the determination of the chemical potential in fluids (Romano and Singer, 1980; Powles et al., 1982; Fincham et al., 1986). Eq. 5.7 relates the residual chemical potential of a component i in a mixture to the ensemble average of the energy of a "test" particle that does <u>not</u> take part in the evolution of the system, but is inserted at a random position in the fluid.

$$\beta\mu_{i,r} = -\ln \langle \exp(-\beta u_i^f) \rangle \qquad [5.7]$$

u_i^f is the potential energy of interaction of the test particle with the rest of the particles of the fluid (a simple sum of the corresponding interaction energies). The residual chemical potential $\mu_{i,r}$ is the difference between the chemical potential of component i in the fluid, and the same component in an ideal gas mixture at the same density, composition and temperature. It is useful to define the configurational chemical potential of a component as:

$$\mu_{i,c} = \mu_{i,r} + k_B T \ln\rho \qquad [5.8a]$$

The chemical potential can then be calculated from :

$$\mu_i = \mu_{i,c} + k_B T \ln X_i \qquad [5.8b]$$

The chemical potential defined by Eq. 5.8b is the difference between the chemical potential at the state of interest and a pure component ideal gas reference state; it is equal for a component in all coexisting phases at equilibrium.

The inverse Widom relationship (de Oliveira, 1979; Shing and Gubbins, 1981) provides a similar expression where only the interaction energies of real particles enter:

$$\beta\mu_{i,r} = \ln \langle \exp(+\beta u_i^g) \rangle \qquad [5.9]$$

Here u_i^g is the interaction energy of a real particle (that is, a particle that is a member of the ensemble during the simulation) with the rest of the particles in the fluid.

The expressions shown above can be interpreted in physical terms as follows: the chemical potential of a component is directly related to the energy required to insert a molecule at a <u>random</u> position within a fluid (Eq. 5.7); it is also directly related to the energy required to remove a molecule of this component from a position in the fluid (Eq. 5.9). In the latter case, the position of a molecule is strongly correlated with the positions of the other molecules in the system.

The energy distribution function $f_i(u)$ for the <u>test particle</u> of species i is:

$$f_i(u) = \frac{\int \delta(\beta u - \beta u_i^f) \exp(-\beta u_i^f) dq^{N-1}}{\int \exp(-\beta u_i^f) dq^{N-1}} \qquad [5.10]$$

where δ is the Kronecker delta. In Eq. 5.10, it is assumed that N-1 real particles take part in the simulation. The integral in the numerator of Eq. 5.10 is a constrained ensemble average so that the interaction energy between the test particle and the N-1 real particles is always u. Similarly, the energy distribution function $g_i(u)$ for a real particle of species i is:

$$g_i(u) = \frac{\int \delta(\beta u - \beta u_i^g) \exp(-\beta u_i^g) dq^{N}}{\int \exp(-\beta u_i^g) dq^{N}} \qquad [5.11]$$

Note that Eq. 5.11 is written for a system of N real particles, whereas Eq. 5.10 was written for a simulation with N-1 real particles. When the

two systems have the same total volume and temperature, it can been shown (Shing and Gubbins, 1981) that f(u) and g(u) are related through the following expression:

$$\ell n \frac{f_i(u)}{g_i(u)} = \beta u - \beta \mu_{i,r} \qquad [5.12]$$

The test and real particle distribution functions describe the frequency of occurrence of a given interaction energy. As such, they are interesting in themselves for the determination of the dominant energy interactions in a fluid. It follows directly from Eq. 5.10 and 5.11 that:

$$\exp(\beta \mu_{i,r}) = \left[\int f(u) \exp(-\beta u) du \right]^{-1} = \int g(u) \exp(+\beta u) du \qquad [5.13]$$

Eq. 5.13 implies that we can calculate the chemical potential from an integration of the functions f(u) and g(u). The integrands in Eq. 5.13 represent the contribution of a given energy of interaction to the chemical potential of the fluid; these functions also provide information about the structure of the fluid.

Both expressions (Eq. 5.7 and 5.9) for the calculation of the chemical potential fail at high densities because of inefficient sampling of configurations of favorable (negative) energies in Eq. 5.7 and of repulsive (positive) energies in Eq. 5.9. An asymmetry exists, however, in the accuracy of the two expressions in a practical simulation. It appears (and we have verified that in the course of the simulations performed), that Eq. 5.7, averaging over the interaction energies for the test particles, gives much better results than Eq. 5.9 that averages over the real particles. The causes for this fundamental asymmetry were discussed by Powles (1982) and appear to be related to the inadequate normalization of the real particle distribution function for positive-energy (repulsive) energies in a simulation of limited length. Because the positioning of the test particle is random, this is much less of a problem for Eq. 5.7.

Shing and Gubbins (1981) proposed using the region of overlap of the two distributions and then integrating (via Eq. 5.13) each distribution separately up to that point. The method requires the determination of the appropriate proportionality constant between the integrands of Eq. 5.13, which depends on the unknown chemical potential itself. Shing and Gubbins have argued, however, that the use of both the test- and real-particle distribution functions minimizes the effect of the uncertainties associated with the tails of the energy-distribution functions that are not well sampled.

Powles et al. (1982), on the other hand, used Eq. 5.12 to obtain the value of the chemical potential directly. It has been shown (and we also verify this for our simulations) that this method and the direct integration of the test particle distribution function give results that are very close to each other. The direct method (Eq. 5.12) is the approach preferred here, because (i) an independent verification of the validity of the simulation and the efficiency of sampling the relevant configuration space is possible by plotting $\ell n[f(u)/g(u)]$ vs u and comparing the best slope of the line to $\beta = 1/k_B T$, and (ii) one can obtain error estimates for the chemical potential from the standard deviation of the points around that line. For most of the cases studied in this work, the results of this method and the direct usage of Eq. 5.7 agree to within the estimated uncertainty of the chemical potential.

5.4 Fluctuation theory and its applications

In the vicinity of phase instabilities (i.e., close to spinodal curves), the accurate calculation of the thermodynamic properties of a mixture using Monte Carlo simulation is hindered by large fluctuations in local density and energy. In a truly macroscopic system, complete phase separation into distinct homogeneous regions would result, but for a microscopic model system with a small number of molecules and spacially periodic boundary conditions no phase separation is possible. Specialized techniques that restrict the maximum allowed fluctuations in density within subregions of the simulation cell have been used (Hansen and Verlet, 1969) to allow

for a continuous integration of the pressure-volume relationship for a pure fluid through the unstable region.

Little attention has been paid, however, to the possibility of utilizing fluctuations to detect the presence of phase transitions in a mixture. The equations relating principal fluctuations in macroscopic systems to thermodynamic derivatives (Landau and Lifshitz, 1980; Debenedetti, 1986; Panagiotopoulos and Reid, 1986) are:

$$\text{For a pure fluid : } \langle \delta N \delta N \rangle_V = k_B T \left[\frac{\partial N}{\partial \mu} \right]_{T,V} = - \frac{k_B T N^2}{V^2} \left[\frac{\partial V}{\partial P} \right]_{T,N} \quad [5.14]$$

$$\text{For a multicomponent mixture : } \langle \delta N_k \delta N_j \rangle_V = k_B T \left[\frac{\partial N_k}{\partial \mu_j} \right]_{T,V,\mu_{[j]}} \quad [5.15]$$

Eqs. 5.14 and 5.15 describe the fluctuations of the number of molecules in a fixed volume containing a macroscopic number of particles at equilibrium with an infinite energy and mass reservoir. The fluctuations would diverge at the limit of intrinsic stability (the spinodal point), since the derivatives at the right-hand side of Eqs. 5.14 and 5.15 diverge. In the canonical NVT ensemble used in the simulation, the total number of molecules in the simulation volume is constant and the above expressions clearly do not hold; one way of obtaining a measure of the intensity of the fluctuations, however, is to subdivide the simulation volume into smaller subcells and observe the number of molecules of each species for a series of configurations. The size of the subcells should be significantly smaller than the total cell size so that the influence of the periodic boundaries and the constant total number of molecules would be minimized, but should also contain as large a number of molecules as possible to allow for meaningful statistics. The requirements for strict validity of Eqs. 5.14 and 5.15 can never be met when a phase transition is approached. In these cases, the correlation length for the density or concentration fluctuations in the macroscopic system grows without bound and exceeds the length of the simulation cell. What we hoped to obtain, despite this limitation, is an indication of the presence of a phase transition.

5.5 Intermolecular potentials and selection of systems

5.5.1 Intermolecular forces

For matter at normal conditions, the intermolecular forces determining the structure and physical properties are entirely due to the electromagnetic interactions between the charged particles, electrons and protons, which make up an atom or a molecule (Maitland, 1981). It is convenient to classify the contributions to intermolecular forces between neutral species into several distinct categories:

a. Overlap forces At short ranges relative to the dimensions of atoms and molecules, as determined by the volume per particle for dense liquid and solid phases, the dominant intermolecular interactions result in strong repulsive forces. These forces have their origin to the partial overlap of the electronic clouds of the molecules: according to the Pauli exclusion principle, some electrons will be prevented from occupying the overlap region, and the nucleic positive charges become incompletely shielded from each other. Although the qualitative features of these forces are well understood, the exact calculation of the dependence of force on distance for short distances is extremely complex.

b. Electrostatic contributions Molecules possessing permanent multipole moments (dipole, quadrupole etc), interact at all distances without distortion of the electron clouds. These forces become dominant at large distances, since the decay of the force with distance is of a lower order than for the overlap (short-range) forces. These forces can be both repulsive and attractive, depending on the relative orientation of the molecules.

c. Induction contributions The interaction of a molecule with a permanent dipole (or higher-order) moment and a polar or non-polar molecule results in a distortion of the electronic cloud of the second molecule due to the electric field of the first. This interaction is always

attractive and usually lower in magnitude than the direct contribution for polar molecules.

d. Dispersion contributions For the interaction between non-polar molecules, the only source of the long-range attractive contributions to the intermolecular energy result from dispersion contributions. These forces, first treated by London (1930), are due to instantaneous fluctuations in the electron density that result in fluctuating electric multipoles that in turn induce corresponding multipoles to the other molecule. The forces are attractive, do not depend on orientation for large distances, and are also present for the interactions between polar molecules.

Even as the qualitative features of the intermolecular forces are now well understood, accurate intermolecular potentials are not available, except for some of the inert gases. For the interactions in dense phases, it is now accepted, that multibody (non pair-wise additive) forces play a role in determining the properties of a fluid. By appropriately selecting "effective" pair-wise additive potential energy parameters, however, it is possible to represent the properties of simple atomic fluids using potentials (such as the Lennard-Jones potential) that contain terms representing overlap and dispersion forces only. For the purpose of determining the effect of the basic molecular parameters on the thermodynamic properties of fluid, such a potential appears to be a good starting point.

For representing the intermolecular interactions, we selected to use the simple, spherically symmetric Lennard-Jones (6,12) potential energy function to represent interactions between like and unlike molecules. We selected this energy function for two reasons: (i) a large number of theoretical and computer simulation studies employed this potential, thus providing a basis for comparisons and (ii) the Lennard-Jones potential incorporates both repulsive (size exclusion) and attractive interactions and should be able to account for a wide range of observed phase equilibrium characteristics. In addition, since only these two kinds of interactions are incorporated, it would be easier to investigate the effect of each

separately, as well as the combined effect, on the calculated chemical potentials and the mixture phase diagrams. Additional refinements of the potential used, with the incorporation of non-spherical repulsive cores or multipolar interactions, can be introduced at a later stage.

5.5.2 The Lennard-Jones potential

The Lennard-Jones (6,12) potential energy function is written as

$$u_{ij}(r) = 4\epsilon_{ij}\left[\left(\frac{\sigma_{ij}}{r}\right)^{12} - \left(\frac{\sigma_{ij}}{r}\right)^{6}\right] \qquad [5.16]$$

where ϵ is the potential well depth and σ the characteristic length-scale of the potential.

We can use the two potential parameters σ and ϵ to reduce the thermodynamic variables to non-dimensional form. The definitions of the reduced variables (denoted by *) are given below, using component 1 as the basis for the scaling. By convention, component 1 is the one with the largest size parameter σ:

$$\epsilon_{ij}^* = \epsilon_{ij}/\epsilon_{11} \qquad \sigma_{ij}^* = \sigma_{ij}/\sigma_{11} \qquad T^* = \frac{k_B T}{\epsilon_{11}} \qquad \mu_i^* = \frac{\mu_i}{\epsilon_{11}}$$

$$u^* = \frac{u}{\epsilon_{11}} \qquad U^* = \frac{U}{N\epsilon_{11}} \qquad P^* = \frac{P\sigma_{11}^3}{\epsilon_{11}} \qquad \rho^* = \rho\sigma_{11}^3 = \frac{N\sigma_{11}^3}{L^3} \qquad [5.17]$$

For the representation of the interactions between unlike molecules, a common practice is to use "combining rules", that express the unlike potential parameters in terms of the pure component parameters. A commonly used set of such combining rules is the Lorenz rule for σ

$$\sigma_{ij} = (\sigma_{ii}+\sigma_{jj})/2 \qquad [5.18]$$

and the Berthelot rule for ϵ

$$\epsilon_{ij} = (\epsilon_{ii}\epsilon_{jj})^{1/2} \qquad [5.19]$$

Neither rule is exact, and especially the Berthelot rule appears to systematically overestimate the magnitude of the unlike potential well depth (Maitland et al., 1981, pp.519); because of this, an empirical correction factor is usually incorporated into Eq. 5.19. Since it is difficult to estimate a priori the magnitude of the correction, experimental data are normally used to guide the selection of appropriate values for the cross parameters.

5.5.3 Selection of systems

The selection of systems was made based on the stated goal of obtaining results for the phase equilibrium behavior for a representative set of molecular size and energy parameters. Three types of mixtures were selected for the investigation, covering respectively (i) the case of components of equal sizes that deviate from the Berthelot geometric-mean rule for the unlike-pair interaction, (ii) the case of a mixture with components that differ significantly in size but have similar potential well depths and (iii) a case with pure components that differ both in size and potential energies of interaction with unlike-pair interactions that follow Eqs. 5.18 and 5.19. This last case represents a simple model of a realistic mixture and we can directly compare the results from the simulation with experimental phase equilibrium data. For simplicity, a single temperature, $T^*=1.15$, was investigated for all systems. In addition, a temperature range was investigated for Mixture III to obtain results for the mixture critical curve as a function of temperature. Table 5.1 summarizes the potential parameters used for these three mixtures, and the temperature (or temperature range) at which the mixture phase diagram was investigated.

Table 5.1 Lennard-Jones (6,12) potential parameters for the mixtures studied

Mixture	ϵ^*_{11}	ϵ^*_{12}	ϵ^*_{22}	σ^*_{11}	σ^1_{*2}	σ^*_{22}	T^*
I	1	0.75	1	1	1	1	1.15
II	1	1	1	1	0.885	0.769	1.15
III	1	0.773	0.597	1	0.884	0.768	0.93-1.19

5.6 Computational procedures

5.6.1 Spatially periodic boundary conditions

The simulation of a truly macroscopic system (that is, incorporating a number of molecules of $O(10^{23})$ is impossible and even undesirable in practice. The memory and execution speed limits of modern computers generally impose a limit on the maximum size for a system to be investigated of a few hundred to a few thousand molecules. A system of this size, if isolated, would be only a few times larger that the characteristic size of the molecules. Because of this, surface effects, with a relative significance inversely proportional to the system size, would completely dominate the behavior of the system.

One method of overcoming this difficulty, is the use of periodic boundary conditions. Figure 5.1 gives a schematic representation of the periodic boundary conditions in two dimensions. The extension to three dimensions is direct. In essence, when a molecule leaves the boundary of the simulation volume and ends up to one of the neighboring cells, a new image of it is made to appear in the basic simulation cell. The molecules interact with all their nearest neighbors, including the molecules belonging to cells other than the basic cell. The effect of the artificial periodicity is minimized when the potential energy functions used are of limited range; ideally, no interactions should exist that extend beyond a distance equal to half the basic cell edge. For the Lennard-Jones potential, this condition is well satisfied, provided that the basic cell has a linear dimension more than a few σ (the hard-core diameter of a molecule).

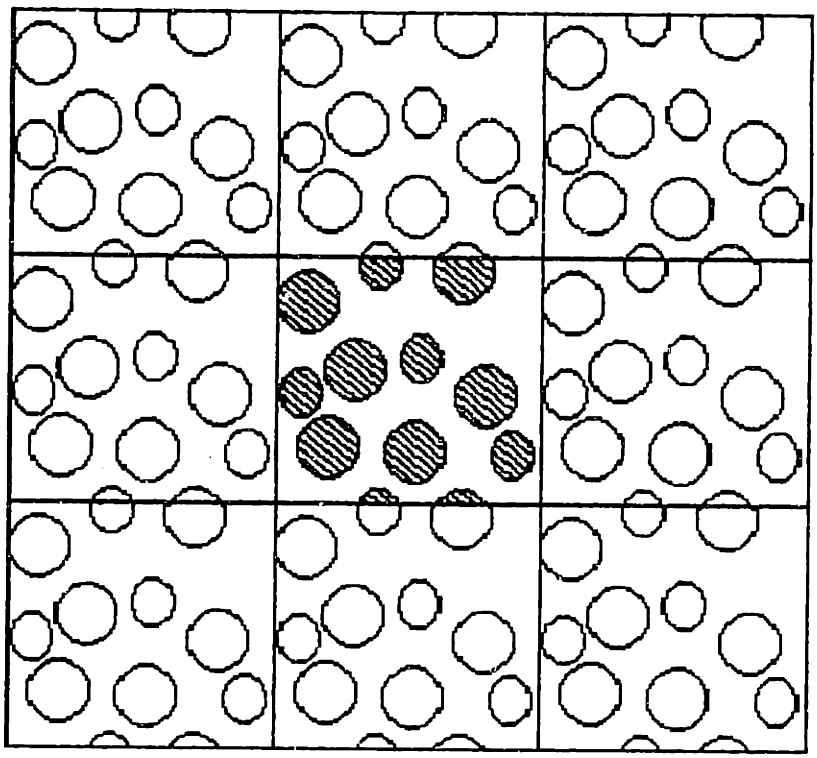

Figure 5.1 *Spatially periodic boundary conditions in two dimensions.*

The periodic boundaries make the simulated system appear as if embedded in an infinite medium, but they give rise to an artificial periodicity not found in real systems. Fortunately, the effect of this artificial periodicity on the properties of the fluid is small, except in regions where large-scale correlations would exist in a macroscopic fluid, e.g., close to a critical point.

The practical implementation of the condition that each particle should interact directly with only its nearest neighbor is based on the "minimum image convention". This is a computationally efficient method of deciding which of the 27 possible nearest-neighbors (for a cubic basic cell) is the nearest one, based on the requirement that the absolute

differences in the values of the particle coordinates should not exceed half the box size for the nearest-neighbor pair.

5.6.2 Cutoff radius and long-range corrections

It was indicated in the preceding section that the range of the potential cannot be allowed to exceed half the box size, because of the periodic boundary conditions. In addition, for computational convenience, it is preferable to use a discretized, rather than continuous, form of the potential. This is so because the "table look-up" operation required to obtain the value of the potential at a given distance when the potential is in discretized form, is orders of magnitude faster than the calculation of the full potential (for the Lennard-Jones potential). Because of these requirements, a discretized and truncated form of the potential was used. The truncation was made at the maximum permitted distance equal to 1/2 the box edge length. There is one exception: at low densities, the length of the simulation cell with the fixed number of molecules used, greatly exceeds the characteristic length of the potential. To prevent large discretization errors in this case, we imposed a maximum limit on the cutoff radius equal to $4\sigma_{11}$.

The long-range corrections to the thermodynamic properties are based on the assumption of uniform distribution of pairs beyond the cut-off radius, an assumption that is confirmed by the radial distribution functions that we obtained (e.g. Figure 6.17). The following expressions were used for the calculation of the long-range corrections to the energy, pressure and chemical potential (adapted from Hansen and Verlet, 1976, pp. 40)

$$\frac{\Delta U}{N} = 2\pi\rho \sum_{i=1}^{n} \sum_{j=1}^{n} \int_{r_c}^{\infty} u_{ij}(r) g_{ij}(r) r^2 dr \qquad [5.20]$$

$$\frac{\beta \Delta P}{\rho} = \frac{2}{3} \pi\beta\rho \sum_{i=1}^{n} \sum_{j=1}^{n} \int_{r_c}^{\infty} \frac{du_{ij}(r)}{dr} g_{ij}(r) r^3 dr \qquad [5.21]$$

$$\Delta\mu_i = 4\pi\rho \sum_{j=1}^{n} \int_{r_c}^{\infty} u_{ij}(r) g_{ij}(r) r^2 dr \qquad [5.22]$$

Assuming a uniform density of pairs beyond the cutoff radius, and substituting the potential from eq 11, we obtain, in reduced quantities:

$$\Delta U^* = 8\pi\rho^* \sum_{i=1}^{n} \sum_{j=1}^{n} \epsilon_{ij}^* X_i X_j \left[\frac{(\sigma_{ij}^*)^{12}}{9(r_c^*)^9} - \frac{\sigma_{ij}^{*\,6}}{3(r_c^*)^3} \right] \qquad [5.23]$$

$$\Delta P^* = \frac{8}{3} \pi(\rho^*)^2 \sum_{i=1}^{n} \sum_{j=1}^{n} \epsilon_{ij}^* X_i X_j \left[\frac{(\sigma_{ij}^*)^{12}}{3(r_c^*)^9} - \frac{2(\sigma_{ij}^*)^6}{(r_c^*)^3} \right] \qquad [5.24]$$

$$\Delta\mu_i^* = 16\pi\rho^* \sum_{j=1}^{n} \epsilon_{ij}^* X_j \left[\frac{(\sigma_{ij}^*)^{12}}{9(r_c^*)^9} - \frac{\sigma_{ij}^{*\,6}}{3(r_c^*)^3} \right] \qquad [5.25]$$

Because of the relatively large cutoff radius, the required corrections to the energy, pressure and chemical potential were always below 2% of the calculated value.

5.6.3 Particle interchange technique

In the simulation of mixtures, particularly when the components differ greatly in size or interaction energies, ensemble averages converge much more slowly than for pure fluids. The reason for this is that at high densities, only very small displacements of the larger particles are allowed by Eq. 5.6 for a large particle interacting with several other molecules. One way to improve this situation, is to introduce the possibility of "jumps" by the large particles, by randomly interchanging the positions of two particles. In the case of a pure fluid, the new configuration is identical to the old, and there is no benefit in performing such an

interchange. In the case of a mixture, however, the new configuration is different from the old if the two particles selected are of different types. The acceptance ratio of this interchange step for the case of mixtures of Lennard-Jones molecules is relatively high even at liquid-like densities because the removal of a particle at a position opens up a hole that may accommodate a larger molecule (detailed results for the acceptance ratios for the interchange steps obtained for the mixtures studied are given in Appendix G.). No biasing is introduced, since the selection of the pair to be interchanged is completely random. The sampling of configuration space becomes significantly more efficient with only modest increases in the computational time per configuration. Numerical examples of the advantages gained by using the particle interchange technique are given in Chapter 6.

This interchange possibility is an example of the potential advantages of the Monte Carlo method relative to molecular dynamics for the calculation of equilibrium properties. The introduction of artificial "jumps" that helps to sample a larger region of configuration space and thus speed up the calculation of equilibrium properties is not possible when the evolution of the system is dictated by the equations of motion.

Simulations with periodic attempts to move a particle by a relatively large distance using interchange have been proposed in the past (Fixman, 1983), but, to the best of our knowledge, this is the first time an interchange method is applied for the calculation of the properties of a mixture of dissimilar components.

5.6.4 Simulation parameters

All simulations were performed using the Metropolis Monte Carlo method in the NVT ensemble with particle interchange for the binary mixtures at high densities. A total number of 256 molecules was used in a cubic box with spatially periodic boundaries. The relatively large number of molecules used makes the application of Eq. 5.7 - 5.13 easier because the difference between the system with N and N-1 molecules at the same total volume is negligible, corresponding on the average to a density change of less than

0.4%. This agrees with the observations of Powles et al. (1982) and Fincham et al. (1986).

The starting configuration for all runs was a faced-centered cubic lattice with a random assignment of the type of molecules to either of type 1 or 2 in the case of binary mixtures. Between 6×10^5 and 1.5×10^6 "composite" steps (an attempted displacement and interchange) were performed for a single density-composition point. The requirements for computer time were of the order of 0.5 - 1.0 ms per configuration on a CYBER-205 supercomputer using explicitly vectorized code. A minimum of 10^5 initial configurations from each run were rejected to allow for equilibration. It was determined that this number was more than sufficient to allow for complete "loss of memory" of the initial non-random configuration.

For the application of the test particle method, a total of 256 static test particles were used. These were placed on a faced-centered cubic lattice (as for the starting configuration of the real particles). No sampling problems related to the correlation between the initial particle positions and the test particle positions were encountered. Equal numbers of test molecules of type 1 and 2 were used for all mixtures studied in order that the number of samples for the test particle distribution functions would not decrease for the dilute mixtures (as would have been the case if the overall mixture composition was used to determine the number of test particles). The energy distribution functions for the real and test particles were recorded every 250 simulation steps, discretized into bins of 0.2 reduced units width, for energies between -20 to +20 in reduced units. More frequent sampling did not improve the statistics because of the correlation in positions between successive configurations. For the real particle interaction energies this energy range was sufficient to cover all events; for the test particle interaction energies, events with $u^* \geq +20$ were simply counted for the purpose of normalizing the test particle distribution function.

The simulation volume was subdivided into 8 cubic subcells, each with edge length half that of the total simulation volume. The number of particles in each subcell was traced by a bookkeeping algorithm, and the total number of molecules of each species, the total energy and the virial of the force in each of the subcells were recorded every 250 "composite"

steps. From this record, a post-run analysis for the average fluctuations was performed.

5.6.5 Determination of the phase diagrams

The calculation of the phase diagram of a fluid or fluid mixture proceeded according to the following methodology: (i) a broad picture of the regions in thermodynamic space was obtained by testing for large fluctuations; these would be regions of possible phase separation, (ii) detailed results for the thermodynamic properties of a series of state conditions that bound the region of phase separation were calculated and (iii) a numerical solution was found for the thermodynamic conditions for phase equilibrium, namely that:

$$\begin{aligned} p^{I} &= p^{II} \\ \mu_i^{I} &= \mu_i^{II} \quad , \; i = 1,n \end{aligned} \qquad [5.26]$$

where I and II denote the coexisting phases. The procedure for the solution of this set of non-linear equations is based on an iterative graphical calculation. The simulation results for the pressure and chemical potential as functions of density and mole fraction are plotted, and smooth curves are fitted to the simulation points. An initial guess for the composition and density of the coexisting phases is made, and the solution is refined until the conditions given by Eqs. 5.26 are satisfied to within the estimated accuracy of our results. Linear interpolation between the simulation points is utilized for conditions where no simulation results were available.

In certain cases, the calculation of the properties of one of the coexisting phases may be carried out by theoretical methods, without need for simulation; this would be the case for low density gas phases where the virial expansion would adequately describe the properties of the mixture. However, even for the pure Lennard-Jones (6,12) fluid using the first five virial coefficients (Barker et al., 1966), the convergence of the virial series is quite slow. The conditions for satisfactory convergence

of the virial series (Nicolas et al., 1979) were not met for most of the conditions studied in this work, so a full calculation of the properties at low (gas-like) conditions was necessary.

5.6.6 Programming and computational time considerations

Modern supercomputers, base their speed on the ability to operate, in the central processing unit, on a series of items (a "vector") without need to interrupt continuously for the slower memory retrieval and storage operations. Because of this, the efficient usage of these machines requires the "vectorization" of the computer programs used. In Appendix F, we present the listings of the FORTRAN programs written for the simulations. Complete vectorization of the internal loops for the Monte Carlo simulation program was achieved by using explicit vector operation statements. The computational time requirements are of the order of 0.5 - 1.0 μs/configuration generated, on a CYBER 205 supercomputer. The computer time requirements for the unvectorized code was approximately 4 times as large. The computational time required increases with the interchange efficiency (the fraction of successful interchange steps) because of the need to update the position and interaction energy vectors.

For the generation of the pseudo-random number sequence, we used the intrinsic CYBER 205 random number generator (function RANF). This is a fast, 64-bit mixed congruential random number generator that was tested for correlations among successive triads of generated random numbers and found satisfactory. Use of a different 32-bit mixed congruential random number generator or changing the initial "seed" did not affect the results for the calculated properties or the chemical potential.

CHAPTER 6
MONTE CARLO SIMULATION: RESULTS

6.1 Pure Lennard-Jones (6,12) fluid

6.1.1 Thermodynamic properties and comparison with literature

The Lennard-Jones (6,12) fluid has been widely studied by theoretical and computer simulation methods. A thorough review of the available results up to 1979 is given by Nicolas et al. (1979). Here, this fluid is used to verify the accuracy of our procedures and to illustrate the new methods we propose.

Table 6.1 presents a summary of the comparison between the calculated results for the properties of the pure Lennard-Jones (6,12) fluid and literature results. The Nicolas et al. (1979) equation of state, a 32-parameter equation fitted to the literature results available up to 1979, is used for the comparisons when no directly comparable results are available. The agreement between the sets of results is satisfactory for all properties, including the chemical potential at high densities. Occasional discrepancies, e.g., for the reduced energy at ρ^*=0.050 and the chemical potential at ρ^*=0.800 at T^*=1.15, may be due to an inadequacy of the equation for these state conditions as evidenced by the much better agreement with direct literature results. The estimated statistical uncertainty of our calculated results is, in most cases, similar to the observed deviations between the results from different sources. The statistical uncertainty of the chemical potential rises rapidly with density, being approximately ±0.3 for ρ^* = 0.800. Beyond this density, specialized sampling techniques such as the test particle method with umbrella sampling (Shing and Gubbins, 1982) are needed for the accurate determination of the chemical potential.

Table 6.1 Comparison of the properties of the pure Lennard-Jones (6,12) fluid

ρ^*	T^*	This study			Equation of state[1]			Other studies			
		$-U^*$	P^*	$-\mu^*$	$-U^*$	P^*	$-\mu^*$	$-U^*$	P^*	$-\mu^*$	Source
0.025	0.928	0.224	0.0201	3.67	0.233	0.0199	3.69				
0.050	0.928	0.460	0.0334	3.28	0.459	0.0334	3.31				
0.600	0.928	4.265	-0.456	4.52	4.289	-0.486	4.70				
0.700	0.928	4.939	-0.250	4.01	4.971	-0.227	4.31				
0.750	0.928	5.288	0.046	3.73	5.296	0.113	3.84				
0.800	0.928	5.602	0.626	2.92	5.608	0.655	3.14				
0.050	1.15	0.431	0.0461	3.92	0.402	0.0464	3.90	0.431	0.0460	3.93	[2]
0.100	1.15	0.372	0.0699	3.55	0.789	0.0724	3.52	0.86	0.07		[3]
0.600	1.15	4.118	0.000	3.68	4.144	-0.012	3.83	4.14	0.05		[3]
0.700	1.15	4.792	0.480	2.52	4.803	0.481	3.08	4.83	0.508	2.65	[4]
0.800	1.15	5.406	1.708	0.63	5.403	1.704	1.46	5.40	1.90		[3]
0.050	1.556	0.367	0.0691	5.00	0.357	0.0693	5.01				
0.200	1.556	1.405	0.201	3.71	1.380	0.197	3.72				
0.400	1.556	2.682	0.344	3.28	2.649	0.316	3.32				
0.600	1.556	3.932	0.892	2.15	3.924	0.822	2.36				
0.800	1.556	5.093	3.445	1.44	5.066	3.471	1.34				

[1] Nicolas et al., (1979)
[2] Interpolated from Adams (1979)
[3] Hansen and Verlet (1969); the data at ρ^*=0.80 are interpolated
[4] Interpolated from Adams (1976)

In Figure 6.1, a graphical comparison is made for the pressure-density relationship at two temperatures. Quite different methods have been used by the various studies, including canonical and grand-canonical ensemble Monte Carlo as well as molecular dynamics. The size of the ensemble used also varies between 108 and several thousand molecules. In the reduced units used, the critical temperature of the Lennard-Jones (6,12) fluid is approximately T^*=1.35. The isotherm shown at T^*=1.15 then corresponds to subcritical conditions, whereas that at T^*=1.56 is supercritical. One basic difference between the two isotherms is the fact that for the subcritical isotherm a van-der-Waals "loop" is observed, with the pressure passing through a local maximum, then decreasing with increasing density in the

mechanically unstable region and then increasing again on the liquid, high-density side of the isotherm. This behavior is a natural consequence of the limited size of the simulated system; in a macroscopic fluid, the pressure-density relationship in the coexistence region would be flat.

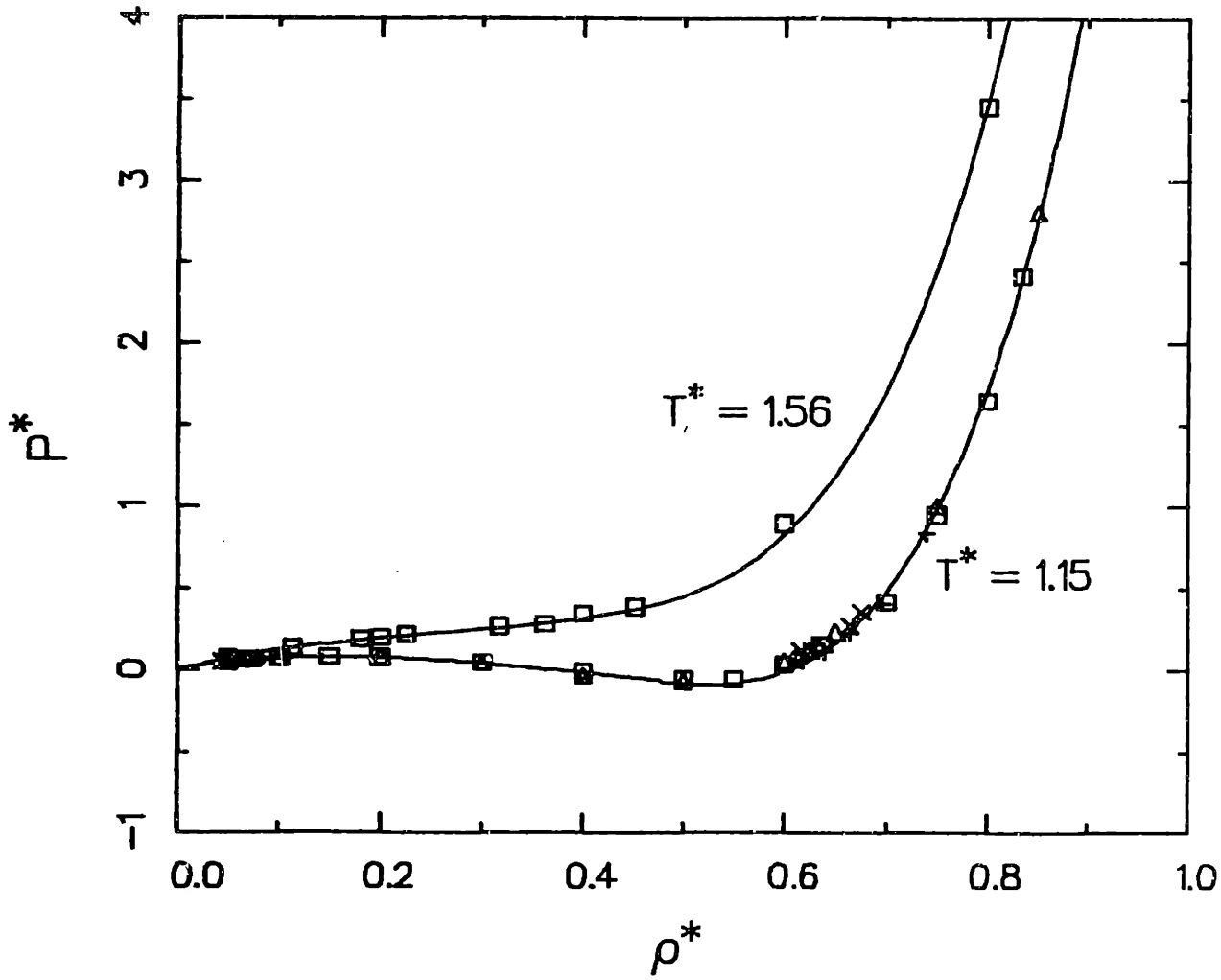

Figure 6.1 *Pressure-density relationship for the pure Lennard-Jones (6,12) fluid.* (□) *This study ;* (△) *Hansen and Verlet (1969) ;* (+) *Adams (1976) ;* (×) *Adams (1979);* (◇) *Yao et al. (1982);* (—) *Equation of state, Nicolas et al. (1979).*

6.1.2 Fluctuations

We use the pure Lennard-Jones fluid to illustrate the possibility of determining the presence of a phase transition based on the microscopic fluctuations. In Figure 6.2, we show a typical configuration for the system at $T^*=1.15$ and $\rho^*=0.20$, a state condition that corresponds to an unstable region according to Figure 6.1. This configuration was obtained in an early run using N = 128 molecules. As may be observed in Figure 6.2, the fluid aggregates into regions of relatively high density (liquid-like) and regions of relatively low density (gas-like). These regions are not static; the aggregates form and dissolve rapidly as the simulation evolves, but the overall picture remains similar to Figure 6.2 when the simulation is performed inside regions where a macroscopic fluid would phase separate.

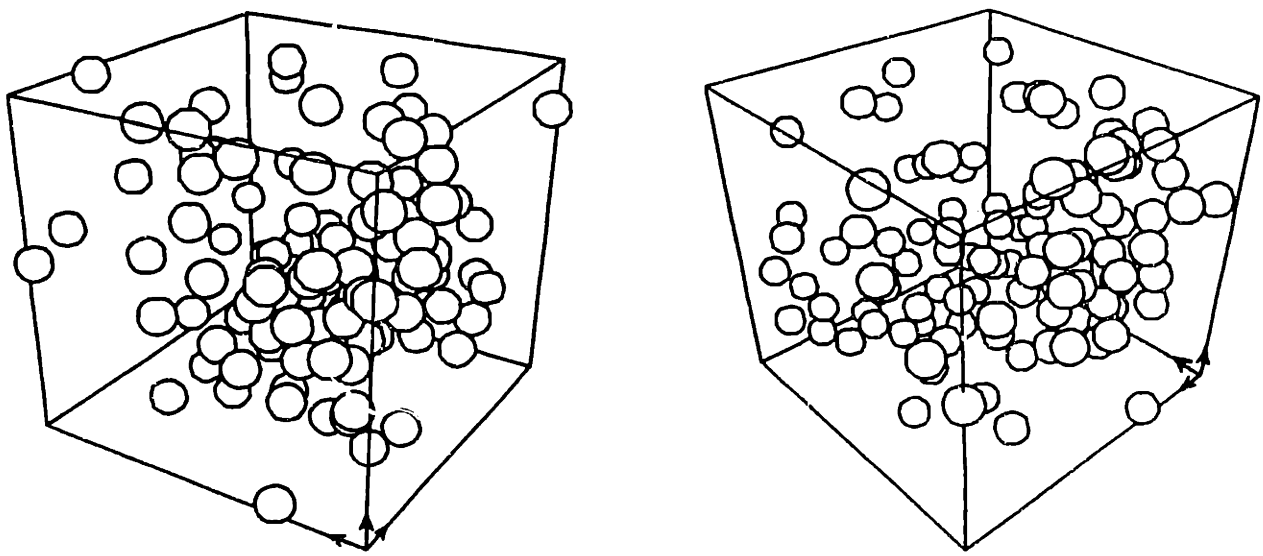

Figure 6.2 *Three dimensional representation of one instantaneous configuration for the pure Lennard-Jones fluid at $T^*=1.15$ and $\rho^*=0.20$, with N=108 molecules. The molecules are drawn at a distance equal to 0.8σ. The same configuration is represented in both halves with the origin of the coordinate system (indicated by the arrows) rotated by 90°.*

To quantify this behavior, we have determined the fluctuations in number density within each subcell of our basic cell. The observed fluctuations in number density in 1/8 of our simulation volume, averaged over all subcells for every run, are presented in Figure 6.3a. A distinct difference in the fluctuation behavior is observed between the subcritical and supercritical isotherm. The subcritical isotherm shows a pronounced increase in the level of the fluctuations inside the phase coexistence region, whereas no such effect is present for the supercritical isotherm. The fluctuations at high densities are less pronounced than at low densities because of the lower compressibility of the liquid. In Figure 6.3b, the expected values for the fluctuations in an infinite system are shown, as obtained from differentiation of the equation of state of Nicolas et al. (1979), according to Eq. 5.14. The fluctuations for the subcritical isotherm diverge at the limit of stability for the fluid which, of course, cannot be observed in the simulations. The fluctuations for the supercritical isotherm, however, are also more pronounced than observed in the simulations. This is due to the fact that the fluctuations in the subcells are influenced by the boundary conditions (constant total number of particles) and the average number of molecules in each subcell is rather small (32 molecules). The conditions for exact validity of the fluctuation relations do not hold. This limits the usefulness of the determination of fluctuations in fluids to qualitative indications of the presence or absence of a phase transition, as well as its approximate location within the phase diagram. The determination of the location of phase transitions requires the calculation of the chemical potential, as discussed in Section 5.3.

Contrary to the behavior at intermediate densities, the fluctuations in the high density range ($\rho^*>0.700$) from Monte Carlo simulation are higher that the theoretical prediction based on Eq. 5.12. The explanation for this discrepancy is again related to the small subcell size. At the limit where the subcell is so small as to contain just 1 molecule on the average, the simulation results would indicate large fluctuations even at close-packing densities, since the center of a molecule may or may not be found inside a subcell. A correction for this discretization effect may be possible by modifying the counting technique so as to take into account the presence of fractional molecules, or by using a larger subcell.

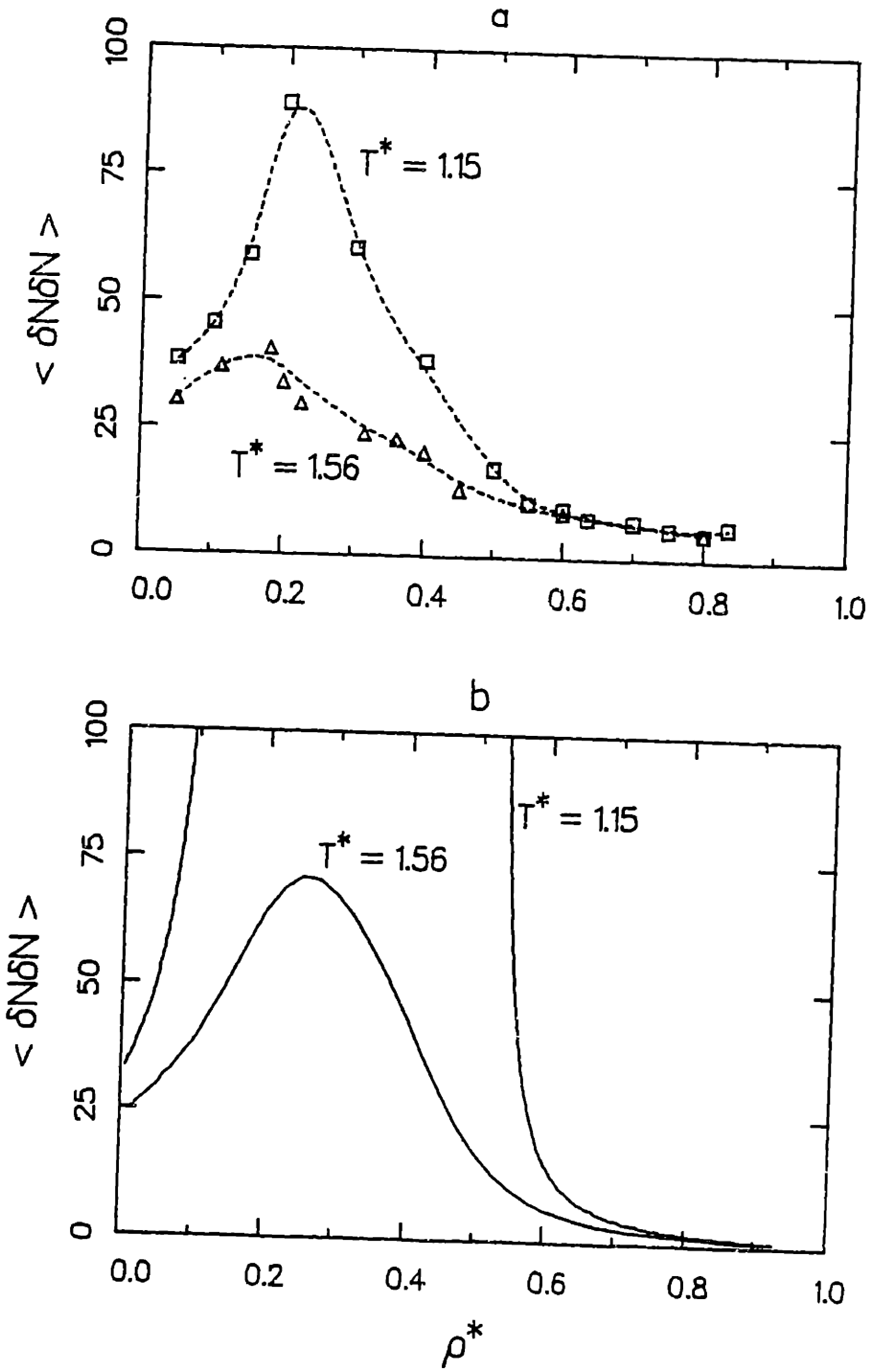

Figure 6.3 *Fluctuation of the number of molecules in a region of the simulation cell containing on the average 32 molecules. a: as determined from the fluctuations in 1/8 of the simulation volume (□) T^*=1.15; (△) T^*=1.56. b: prediction based on the fluctuation expression (Eq. 5.14) and the Nicolas et al. (1979) equation of state.*

6.1.3 Energy distribution functions

Figure 6.4 presents the results for the test-particle energy-distribution function for the pure Lennard-Jones fluid at $T^*=1.56$. Figure 6.5 presents the corresponding results for the real-particle energy distribution function. Comparable results, but at a lower reduced temperature, have been presented by Powles et al. (1982). Several observations can be made at this point :

a. At low densities, both real and test particle energy distribution functions show a sharp peak at $u^* = 0$, corresponding to an isolated particle. A peak is also observed at a value of $u^* = -1$, corresponding to a pair of interacting particles. The distribution functions drop off rapidly for positive values of u^*, since repulsive interactions in the low density gas are uncommon. The functions also decrease rapidly at lower (more negative) values of u^*, since it is unlikely that a single particle will interact with more than one other particle at a time. The real and test particle distribution functions are quite similar at the lower densities.

b. As density is increased, the maximum value of the test particle distribution function decreases significantly, and the peak becomes less sharp and shifts towards lower energy values. This is explained by the fact that the probability of accommodating a test particle in a "hole" of suitable size, without overlap with any of the real particles becomes smaller as the density increases. On the other hand, if such a configuration should occur during the simulation, the test particle is likely to be surrounded by several real particles, thus interacting with a large negative energy. The error (statistical uncertainty) in the determination of the test particle distribution function increases as density increases; it is greatest at the tail of the distributions. This is due to the fact that only a limited sample is available. A value of the test particle distribution function of 10^{-5} would imply that only one in every 100,000 samples contains a test particle in a configuration

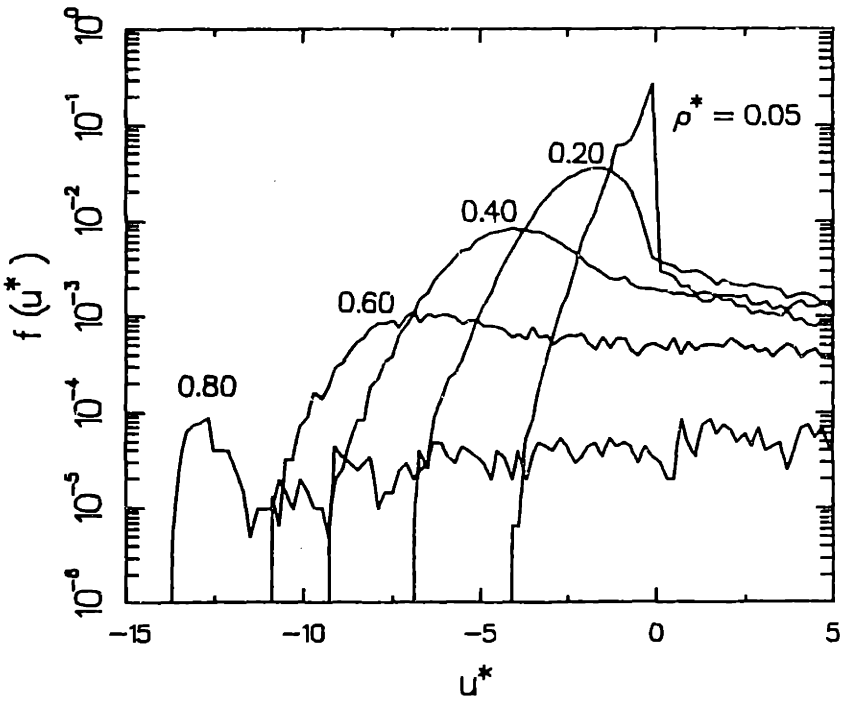

Figure 6.4 *Test-particle energy-distribution functions for the pure Lennard-Jones fluid at T^*=1.56 for a series of reduced densities.*

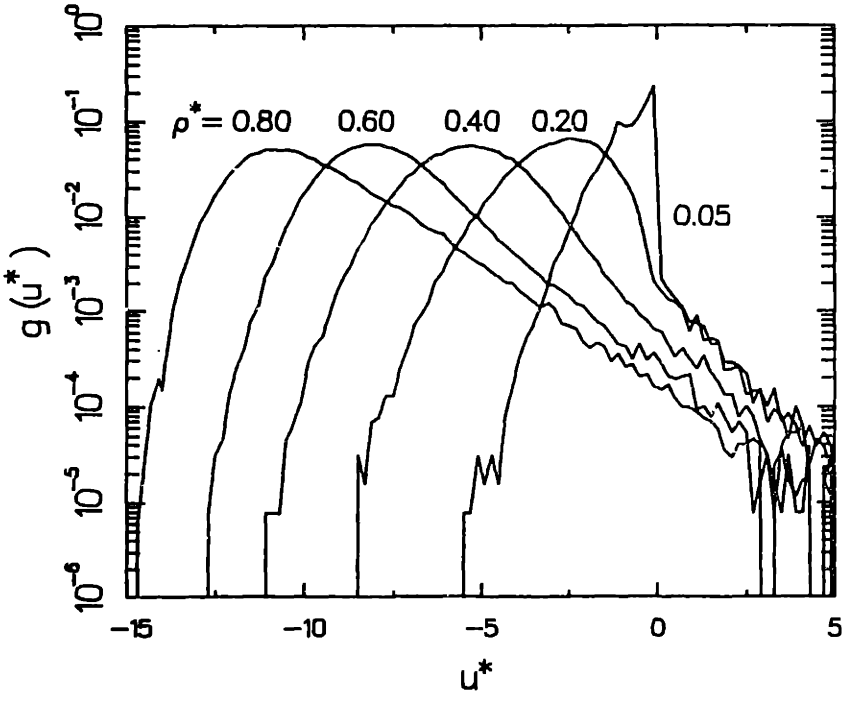

Figure 6.5 *Real-particle energy-distribution functions for the pure Lennard-Jones fluid at T^*=1.56 for a series of reduced densities.*

within 1 unit of a given energy. Such events are too rare to be evaluated with good accuracy in a simulation of reasonable length.

c. The real particle distribution functions show similar trends towards less sharp peaks and lower energies as density increases, but the value of the distribution function at the maximum (and thus the relative probability of occurrence of favorable energy configurations) remains constant. In a macroscopic fluid, or during a simulation, a real particle is not likely to find itself in a configuration of high positive energy. The statistical problems mentioned above for the test particle distribution functions are also present for the tail of the distributions.

A test of the validity of Eq. 5.12, as well as a test of the ability to obtain representative configurations that allow the chemical potential to be estimated is obtained by plotting the distribution functions $f(u^*)$ and $g(u^*)$ as $\ell n[f(u^*)/g(u^*)]$ versus u^*. This is done in Figure 6.6 for $\rho^* = 0.60$ and two temperatures, $T^* = 0.93$ and $T^* = 1.56$. The straight lines in Figure 6.6 are drawn with slopes exactly equal to $\beta = 1/k_B T$; the y-intercept was fitted to the points at each temperature. The data lie remarkably close to the straight line with the correct theoretical slope, except at the end of the distributions where the statistical accuracy of the determination of the f(u) and g(u) functions is lower. The y-intercept (at $u^*=0$) of these lines is directly related, according to Eq. 5.12, to the residual chemical potential at this state point. The estimated statistical uncertainty for the chemical potential at this density is approximately $\pm$ 0.05 reduced units, as calculated from the scatter of the data around the straight line.

It was observed that for densities up to approximately $\rho^*=0.7$, application of Eq. 5.12 (plotting $\ell n[f(u^*)/g(u^*)]$ versus u^*) gives results virtually identical to the ones obtained by the simple test particle expression (Eq. 5.7). Since the latter method is easier to implement computationally, we have used Eq. 5.7 for most conditions studied, and tested a representative sample of the high-density results using Eq. 5.12.

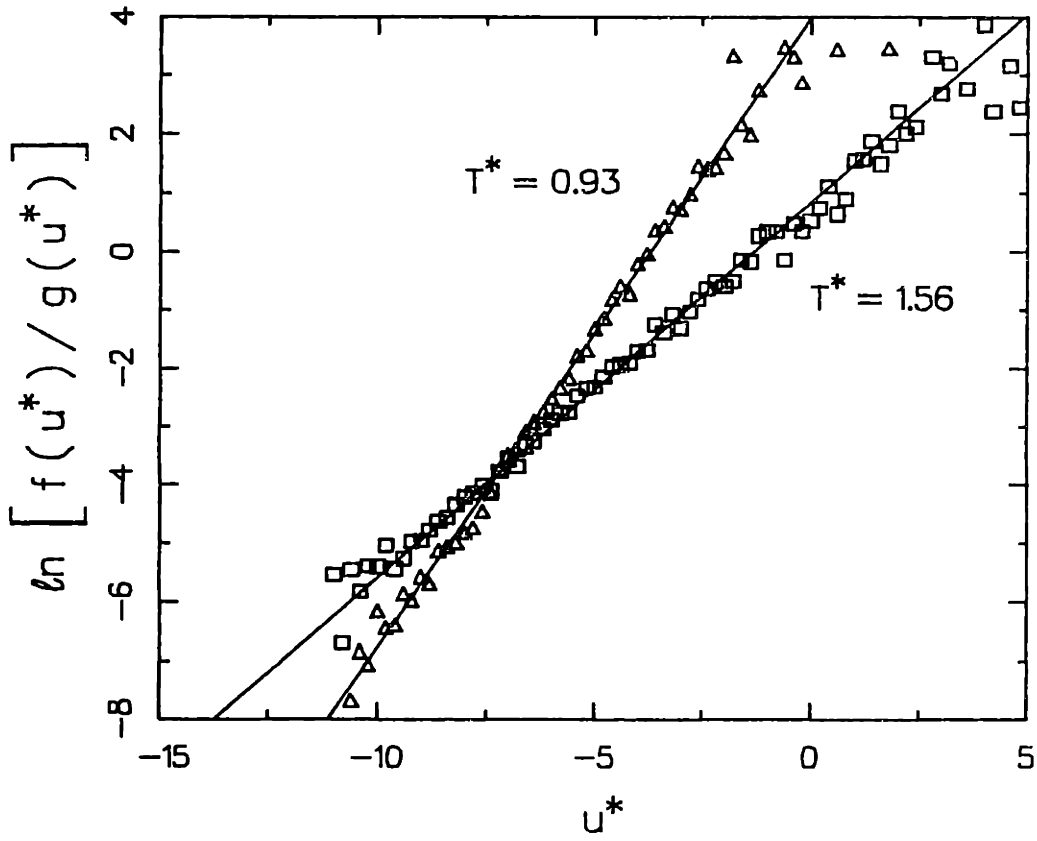

Figure 6.6 *The function* $\ell n[f(u^*)/g(u^*)]$ *vs. the energy* u^* *for the pure Lennard-Jones fluid at* $\rho^* = 0.60$. *The line has slope exactly equal to* $\beta = 1/k_B T$ *and intercept fitted to the points .* (△) $T^* = 0.93$; (□) $T^* = 1.56$.

6.2 Calculation of the chemical potential for mixtures and comparisons

In the previous sections, we presented results for the calculation of the chemical potential for the pure Lennard-Jones fluid and demonstrated the agreement with literature results for the properties of the pure fluid. In order to ascertain the validity of our mixture calculations, we also performed a comparison of our results with literature results for the chemical potential in mixtures. We chose to compare our findings with the results of Shing and Gubbins (1983) for a mixture of Lennard-Jones molecules at conditions similar to the ones we have studied. The comparison is

given in Table 6.2, and graphically depicted in Figure 6.7. As can be seen, the agreement between the two sets of results is good for all compositions. There are small systematic deviations (our results tend to be slightly higher), especially for the chemical potential of component 2, but the agreement is probably within the accuracy of the results (shown in parentheses for our results; the results of Shing and Gubbins have a claimed accuracy of 5%). The systematic differences may be due to the difference in ensemble size (128 molecules for Shing and Gubbins versus 256 molecules for our results). The results agree well with the predictions of the van der Waals 1-fluid mixing rule, shown as dashed lines in Figure 6.7. The complete results for the thermodynamic properties of the fluid at the conditions investigated are presented in Appendix G.2.

A typical example of the calculation of the chemical potential in a mixture using Eq. 5.12 is given in Figure 6.8, where the results for the function $L(u^*) = \ell n[f(u^*)/g(u^*)]$ versus u^* for the mixture with $X_1=0.5$ are presented. The data for both components fall on a straight line with the correct theoretical slope, except close to the two ends of the distributions, where there is significant scatter due to statistical inaccuracies in determining the energy-distribution functions (see Section 6.1.3).

Table 6.2 Comparison of calculated results for the chemical potential of a mixture with $\epsilon^*_{12}=1.41, \epsilon^*_{22}=2, \sigma^*_{12}=\sigma^*_{22}=1$ at $T^*=1.2, \rho^*=0.70$

	This work		Shing and Gubbins (1983)	
X_2	$\mu^*_{1,r}$	$\mu^*_{2,r}$	$\mu^*_{1,r}$	$\mu^*_{2,r}$
0			-2.39†	
0.0195	-2.19 (5)	-6.39(10)	-2.40	-6.65
0.0741			-2.55	-7.00
0.1484	-2.71 (5)	-7.18(10)	-2.82	-7.51
0.3320	-3.53 (5)	-8.30 (5)	-3.45	-8.42
0.5	-4.10 (5)	-9.29 (5)	-4.25	-9.30
0.6111			-4.55	-10.2
0.7226	-4.99(10)	-10.38 (5)	-5.25	-10.6
0.8515	-5.41(10)	-11.16 (5)	-5.61	-11.7
1				-12.3†

† Calculated from the Lennard-Jones equation of state (Nicolas et al., 1979)

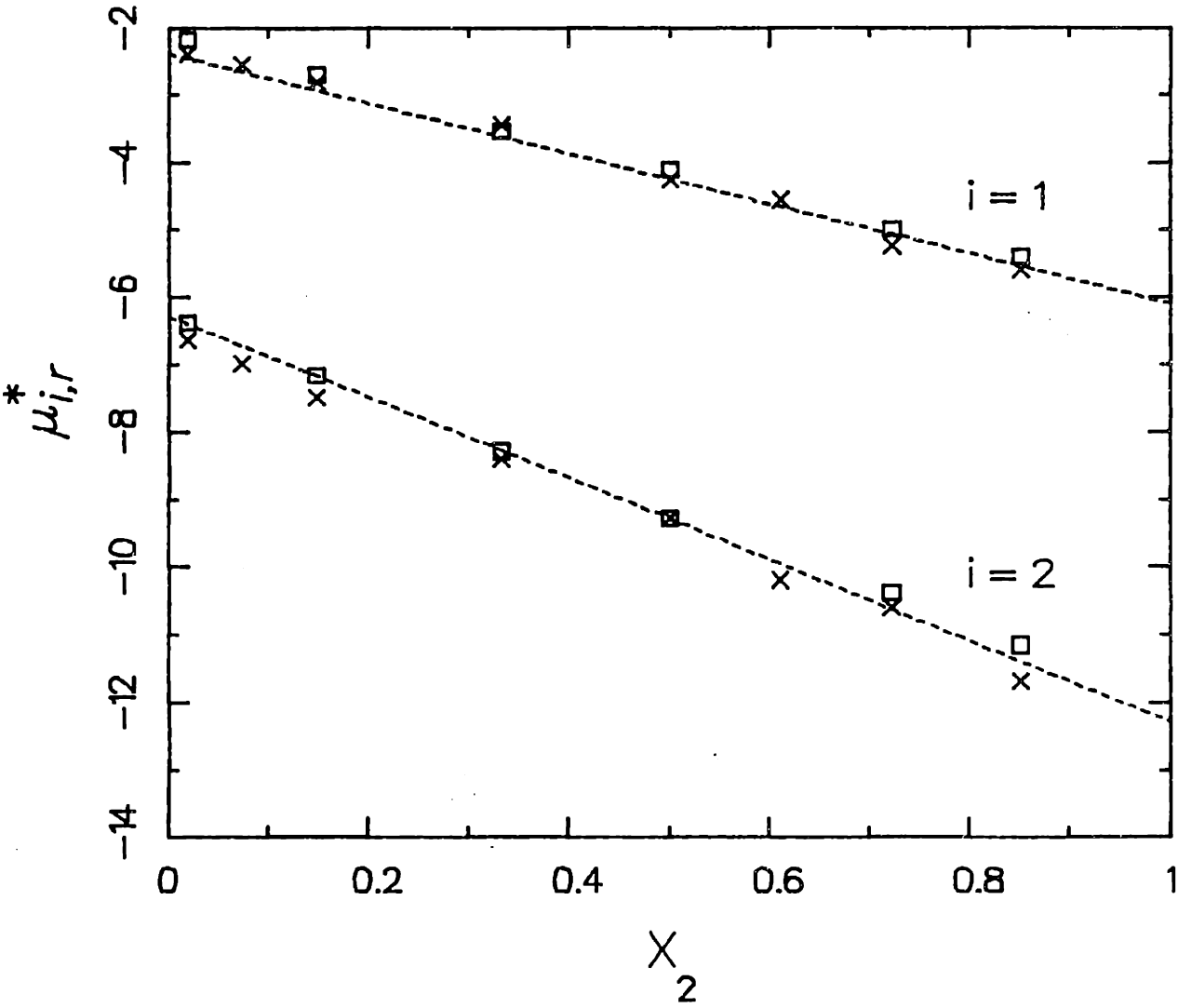

Figure 6.7 *Comparison of the results for the chemical potential for a mixture with* ϵ^*_{12}=1.41, ϵ^*_{22}=2, σ^*_{12}=σ^*_{22}=1 *at* T^*=1.2, ρ^*=0.70. (□) *this work;* (×) *Shing and Gubbins (1983).*

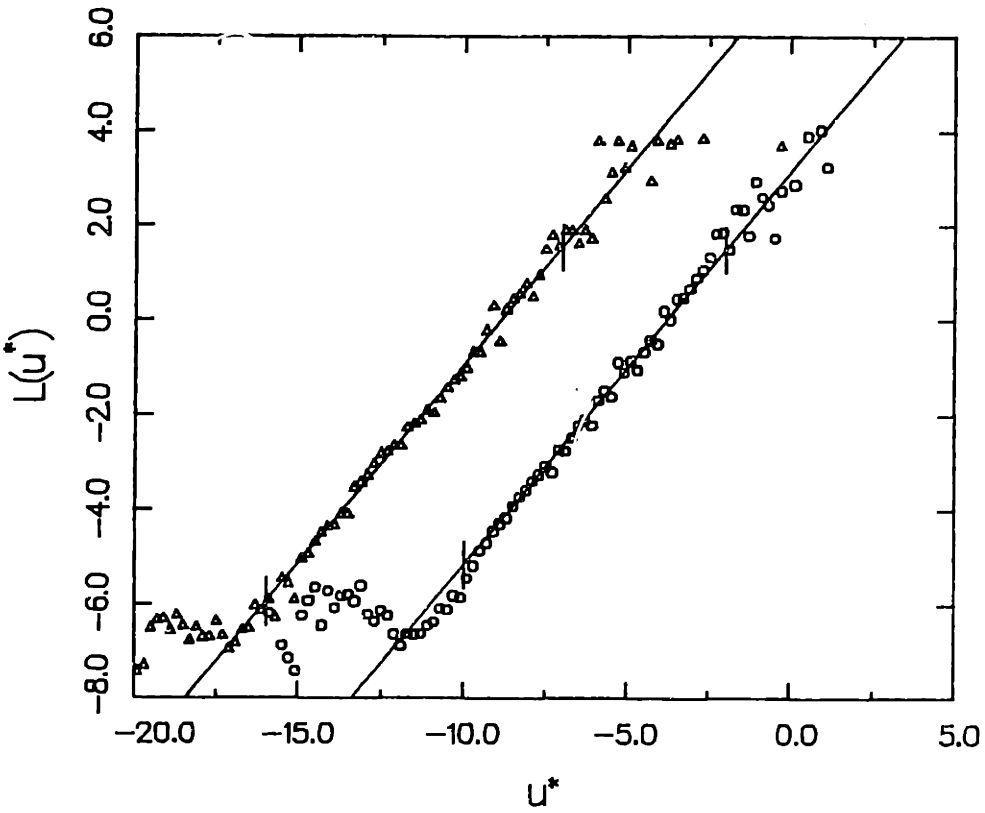

Figure 6.8 *The function* $L(u^*) = \ell n[f(u^*)/g(u^*)]$ *versus the energy* u^* *for a mixture with* $\epsilon^*_{12}=1.41, \epsilon^*_{22}=2, \sigma^*_{12}=\sigma^*_{22}=1$ *at* $T^*=1.2, \rho^*=0.70$. *The lines have slopes exactly equal to* $\beta=1/k_BT$ *and y-intercepts fitted to the points.* (□) *component 1;* (△) *component 2.*

6.3 Mixture I: Effect of different interaction energies

An interesting class of mixtures is one in which the components have similar sizes, but interact with specific forces that lead to unlike-pair energy interactions different from like-pair interactions. To investigate the effect of changing unlike-pair interactions, we calculated the properties of a mixture of molecules with unlike-pair parameters only 75% of the like-pair parameters, as shown in Table 5.1. The molecules in their pure state are completely identical, so the mixture is symmetric. Because the unlike-pair interactions are less favorable than the like-pair interactions, we expect the mixture to show positive deviations from Raoult's law and,

since the pure components have the same vapor pressures, positive azeotropy is suggested.

6.3.1 Thermodynamic properties

The results for the properties of the system at the state conditions studied are given in Appendix G.3. First, let us examine the dependence of the main thermodynamic quantities on mixture composition and density.

Internal Energy: The dependence of the mixture internal energy on composition for a series of reduced densities at $T^*=1.15$ is shown in

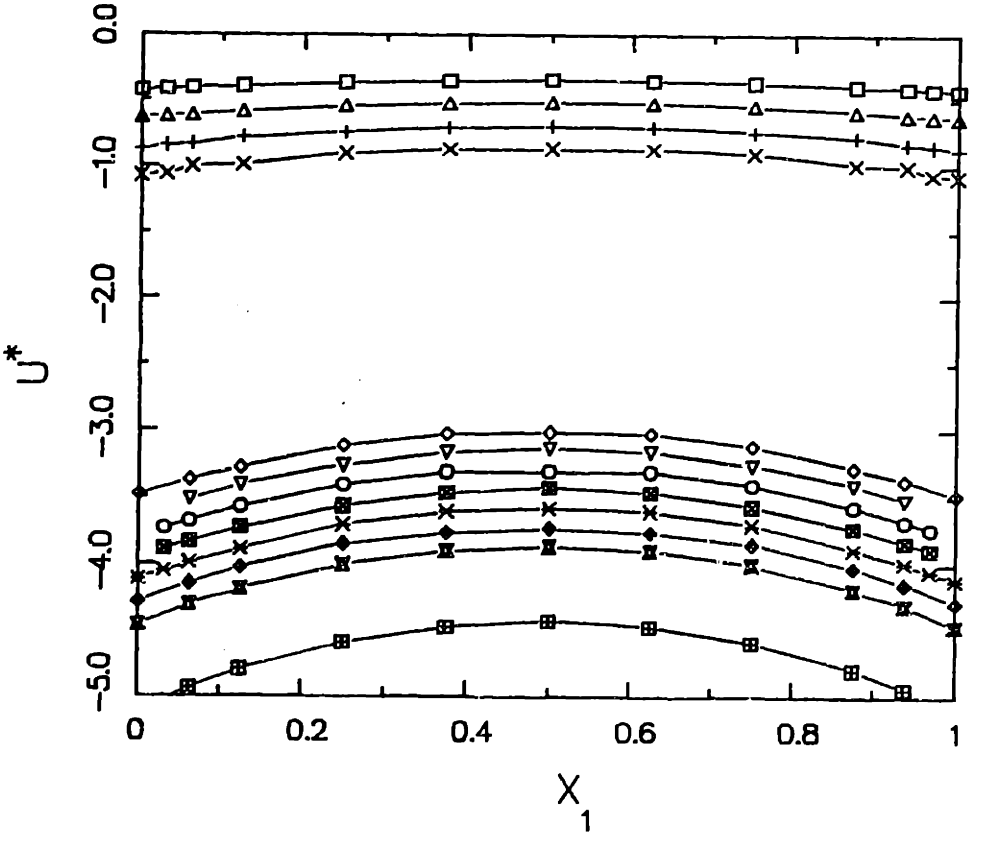

Figure 6.9 *Reduced internal energy versus composition for Mixture I at $T^*=1.15$ and a series of reduced densities:* (□) $\rho^* = 0.050$; (△) *0.075;* (+) *0.100;* (×) *0.125;* (◇) *0.500;* (▽) *0.525;* (○) *0.550;* (⊠) *0.575;* (✳) *0.600;* (♦) *0.625;* (⧗) *0.650;* (⊞) *0.750.*

Figure 6.9. The mixture internal energy appears to be a parabolic function of composition. The increase in internal energy as the equimolar composition is approached is easily explained by the fact that for the equimolar mixture, the unfavorable unlike-pair interactions are maximized. The effect increases as density is increased.

Pressure: Again, a near-parabolic dependence is observed in Figure 6.10 for the total pressure as a function of mixture composition. For clarity, we have omitted the results for some densities from Figure 6.10. The magnitude of the effect of composition on pressure at constant density is significant. For the equimolar mixture at ρ^*=0.650, the maximum pressure (at X_1=0.5) is 0.5, or three times the pure component critical pressure. This can be understood as follows: the pure components at T^* = 1.15 are quite close to

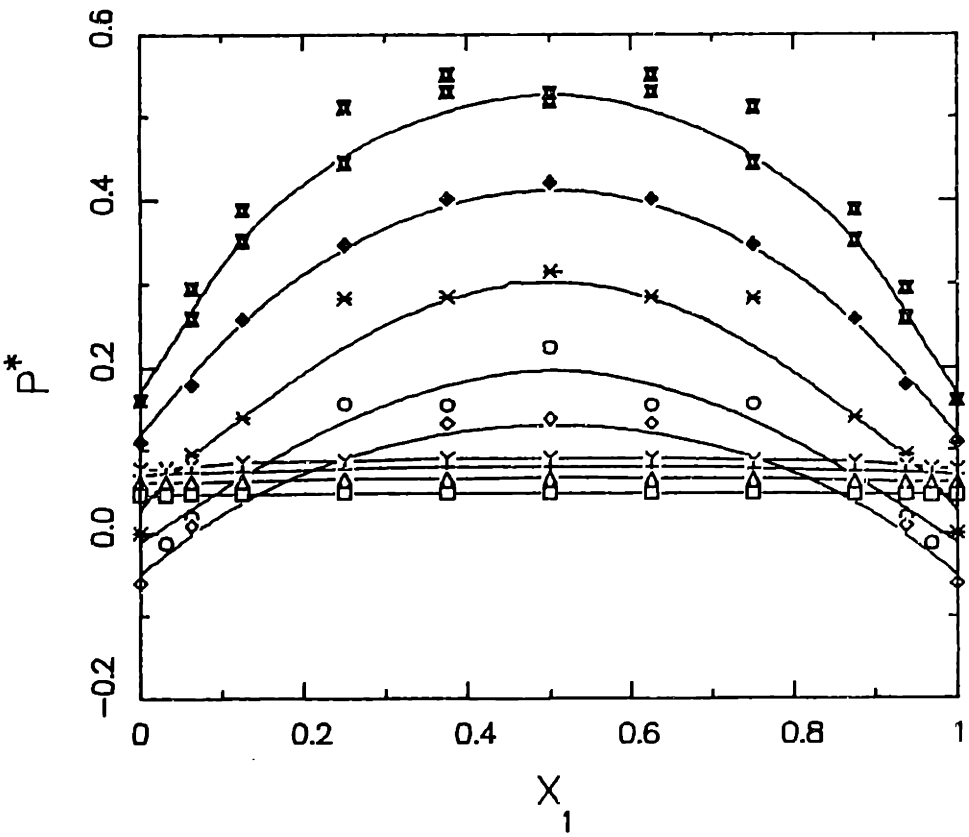

Figure 6.10 *Reduced pressure versus composition for Mixture I at T^*=1.15 and a series of densities. Symbols are as in Figure 6.9.*

the vapor-liquid critical point (T_c^*=1.35). For the equimolar mixture, however, the effective reduced temperature is much lower, due to the unfavorable unlike-pair interactions. Mixtures close to the equimolar composition have the character of compressed liquids, and show significantly higher resistance to compression.

Chemical potential: The dependence of the configurational chemical potential of component 1, $\mu_{1,c}^*$, on the mixture composition is shown in Figure 6.11. Since the mixture is symmetric, the configurational chemical potential of component 2 is identical to that of component 1, when a comparison is made at the same concentration (this was also obtained during the simulations of the equimolar mixtures, as shown in Appendix G.3). The configuration chemical potential is, to a good approximation, a linear function of composition for all densities, as was also observed from the

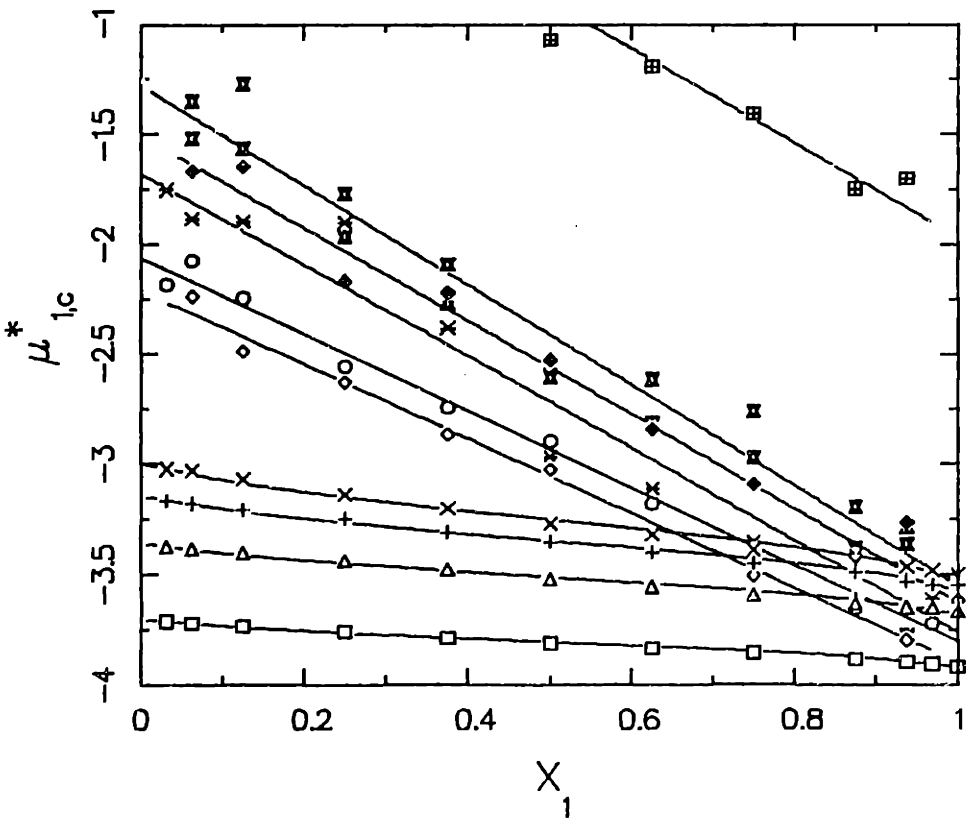

Figure 6.11 *Reduced configurational chemical potential of component 1, $\mu_{1,c}^*$ at T^*=1.15, versus composition for Mixture I at a series of reduced densities. Symbols are as in Figure 6.9.*

results of Shing and Gubbins (1983) for a mixture with the same size parameters but unequal potential well depths. For the calculation of the mixture phase diagrams, the simulation results for the chemical potential were smoothed by linear regression to facilitate their use.

6.3.2 Effect of particle interchange

The calculation of the fluctuations of the number of molecules in subcells of the basic equilibrium cell, as described in Section 6.1.3, entails severe difficulties when the conventional Metropolis procedure (Eq. 5.6 without particle interchange) is used. The difficulties are related to the slow movement of molecules during a simulation at high densities: the average distance travelled by a molecule is less than the box edge length for simulations of reasonable duration (10^6 or so configurations for N=256 molecules). This has the following effect: if, because of random deviations, a subcell starts with significantly different number of molecules of one species than the expected average, it is likely that it will still have some of the same molecules (and therefore, a significantly higher number of molecules of one species) at the end of the simulation. This results in very large apparent fluctuations of the number of molecules across cells, that only reflect the initial random assignment of molecules to positions rather than the properties of the fluid.

In order to illustrate this effect, two simulations were performed for Mixture I at $T^*=1.15$, $\rho^*=0.750$, $X_1=0.50$, without and with particle interchange. For the simulation without particle interchange, twice as many steps (1.2×10^6) were performed to compensate for the fact that both an attempted displacement and an interchange are performed per simulation step when the particle interchange method is applied. The simulations required approximately equal amounts of computer time, as shown in Table 6.3. The average number of molecules in each of the eight subcells and the mean-squared fluctuation of the number of molecules in each subcell for the two simulation runs are presented in Table 6.3. The expected average number of molecules of each species (for an infinite number of configurations generated) in each of

the eight subcells is 16. As can be seen, for the run without particle interchange, there are large deviations in the average number of molecules of each species (values range between 12.36 and 19.57). In addition, the mean-squared deviation of the number of molecules in each subcell show significant variation across cells. The problem cannot be easily solved by generating a larger number of configurations, since the average distance travelled by a molecule only increases with the square root of the number of configurations generated. By contrast, the average number of molecules

Table 6.3 Effects of particle interchange for Mixture I at T^*=1.15, ρ^*=0.750, X_1=0.50.

Property	no interchange	with interchange
Configurations generated	1600000	800000
CPU time (min)	760	780
Interchange efficiency	-	0.634
U^*	-4.41	-4.43
P^*	1.377	1.381
$\mu^*_{1,c}$	-1.04	-1.07
$\mu^*_{2,c}$	-1.03	-1.09

Cell number	no interchange			with interchange		
	$\langle N \rangle$	$\langle N_1 \rangle$	$\langle N_2 \rangle$	$\langle N \rangle$	$\langle N_1 \rangle$	$\langle N_2 \rangle$
	$\langle \delta N \delta N \rangle$	$\langle \delta N_1 \delta N_1 \rangle$	$\langle \delta N_2 \delta N_2 \rangle$	$\langle \delta N \delta N \rangle$	$\langle \delta N_1 \delta N_1 \rangle$	$\langle \delta N_2 \delta N_2 \rangle$
1	32.07	15.63	16.44	31.82	16.11	15.70
	5.27	3.69	3.71	5.02	15.61	14.86
2	30.96	14.74	16.22	32.29	16.19	16.10
	5.52	4.56	5.06	5.70	14.91	15.02
3	31.93	19.57	12.36	32.84	16.46	16.38
	5.65	6.57	7.24	5.46	16.29	15.96
4	32.37	16.59	15.78	31.28	15.59	15.68
	5.76	3.97	3.93	5.22	14.88	14.75
5	32.06	13.85	18.21	32.71	16.17	16.54
	5.73	5.10	7.06	6.24	16.13	16.21
6	31.94	18.50	13.44	31.58	15.69	15.89
	5.50	7.05	6.71	6.19	16.15	15.24
7	32.32	16.03	16.29	31.77	15.94	15.83
	5.55	8.33	7.37	5.06	14.89	14.60
8	32.36	13.09	19.27	31.71	15.84	15.86
	5.64	5.30	5.71	5.90	16.12	16.64

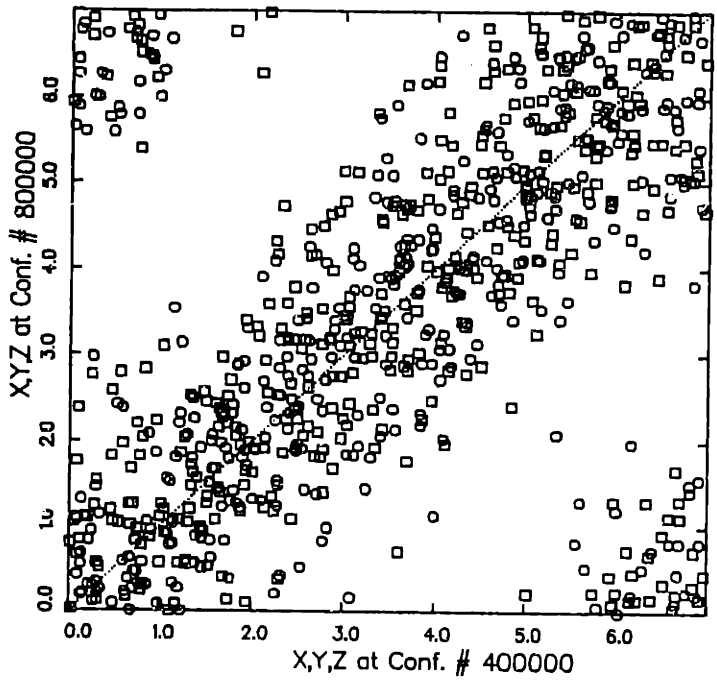

Figure 6.12 *Correlation of the position of molecules for two configurations during a simulation without particle interchange. X,Y and Z are, respectively, the x- y- and z-coordinates of a molecule.*

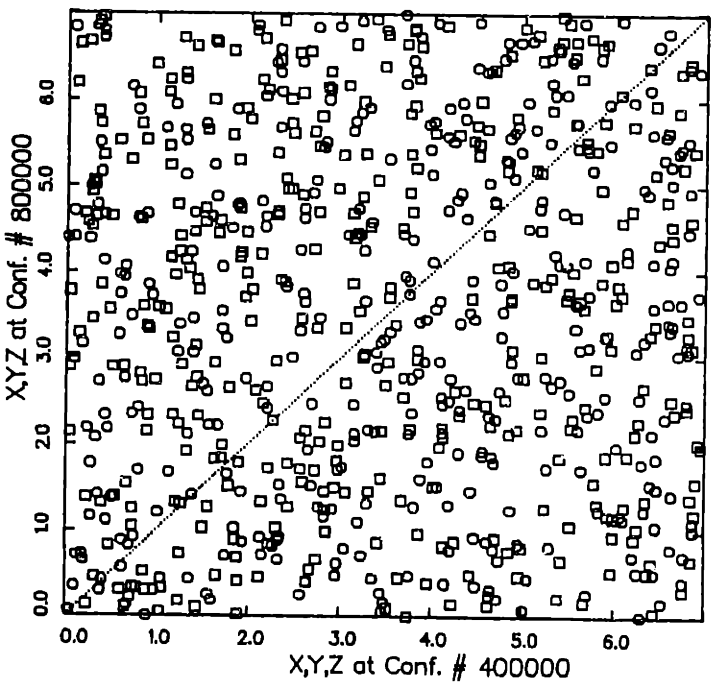

Figure 6.13 *Correlation of the position of molecules for two configurations during a simulation with particle interchange. Labels as in Figure 6.12.*

of each species for the run with particle interchange are very close to their theoretical values, and the fluctuation of the number of molecules of each species is almost constant across cells, and significantly higher than the values obtained without interchange.

Figures 6.12 and 6.13 represent graphically the correlation of position of the particles between two configurations. For the run without particle interchange, after 400000 simulation steps, the particles have only travelled an average distance of approximately 1 reduced unit, or 1/7 of the simulation box edge length. By contrast, there is no correlation of the position of two configurations for the run with particle interchange.

The results for the thermodynamic properties (energy, pressure and chemical potentials) are not significantly different for the two runs with and without interchange. This is probably due to the fact that for both cases the number of configurations generated is sufficient for the calculation of the thermodynamic properties. However, it is expected that for different cases, and especially at higher densities or for mixtures that phase-separate, the calculation of the thermodynamic properties should be more rapid when particle interchange is used.

6.3.3 Energy and radial distribution functions

In Figure 6.14, we illustrate the behavior of the radial distribution function for this mixture at a fixed density, $\rho^*=0.500$. For mixtures dilute in component 1, there is significant clustering of molecules of type 1, as evidenced by the first peak of the radial distribution function which is highest for 1-1 pairs. As the composition of the mixture approaches the equimolar point, the peak becomes less pronounced, although there is still more clustering than for the pure components at the same state conditions ($g_{22}(r)$ for $x_1=0.0625$ is practically identical to $g(r)$ for the pure components at the same conditions). 1-2 pairs occur less frequently than any other type of pairs because of the less favorable energy of an unlike pair interaction. Studies of local compositions in Lennard-Jones fluids have been performed by Nakanishi and his coworkers (Gierycz and Nakanishi, 1984).

A set of energy distribution functions for this mixture at $T^* = 1.15$, $\rho^* = 0.50$, is shown in Figure 6.15. The reason the functions $f(u^*)\exp(-\beta u)$ and $g(u^*)\exp(+\beta u)$ are plotted rather than $f(u^*)$ and $g(u^*)$, is that the chemical potential of the corresponding species can be directly obtained from the integral under the curves (Eq. 5.13). The peak of the functions as plotted in Figure 6.15 correspond to the interaction energy contributing most to the chemical potential of the component. At low concentrations of component 1, the peaks of the test and real particle energy distribution functions are shifted to positive values relative to component 2. This is a direct consequence of the unfavorable unlike-pair interactions.

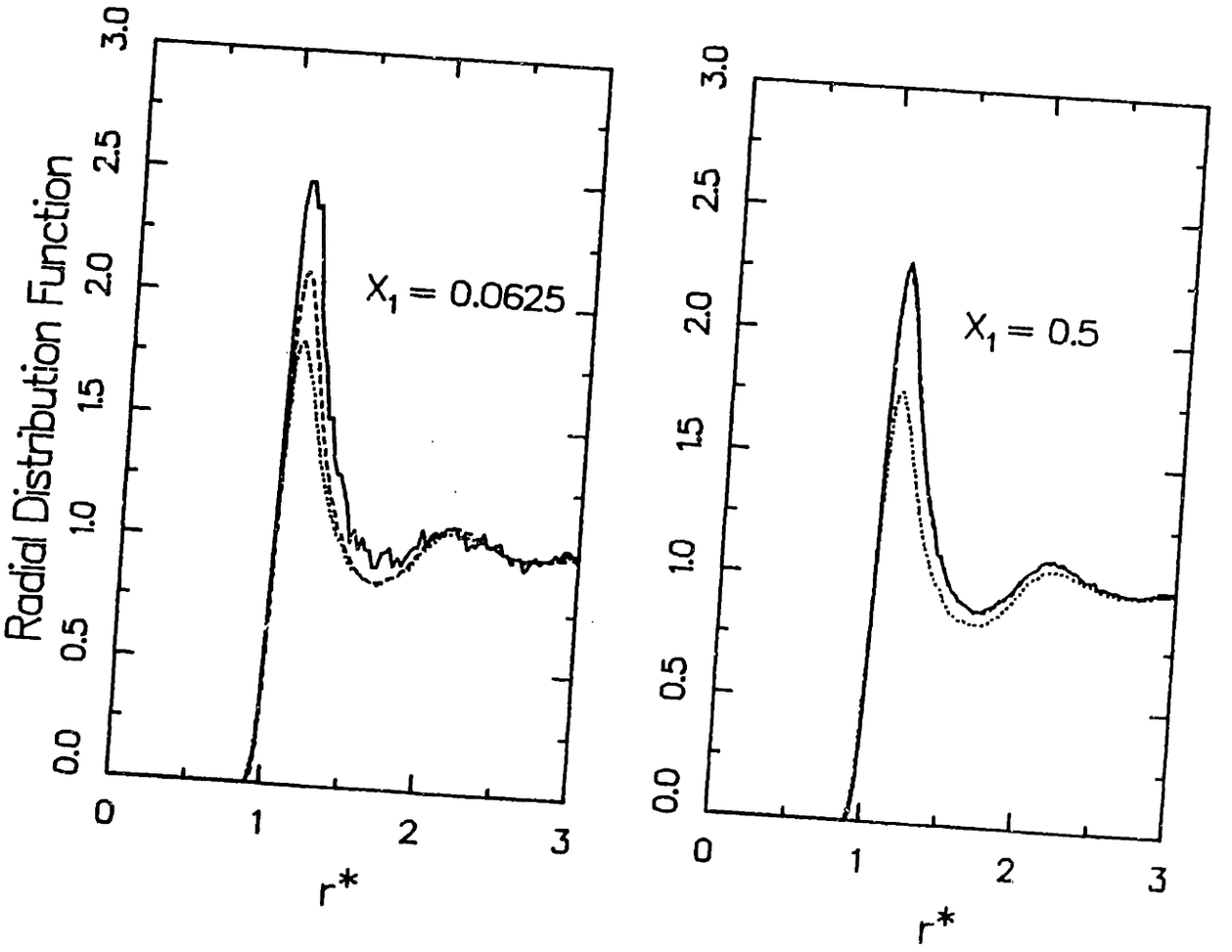

Figure 6.14. *Radial distribution functions for mixture I at $T^*=1.15$, $\rho^*=0.500$. (——) 1-1 pairs; (...) 1-2 pairs;* (---) 2-2 pairs.

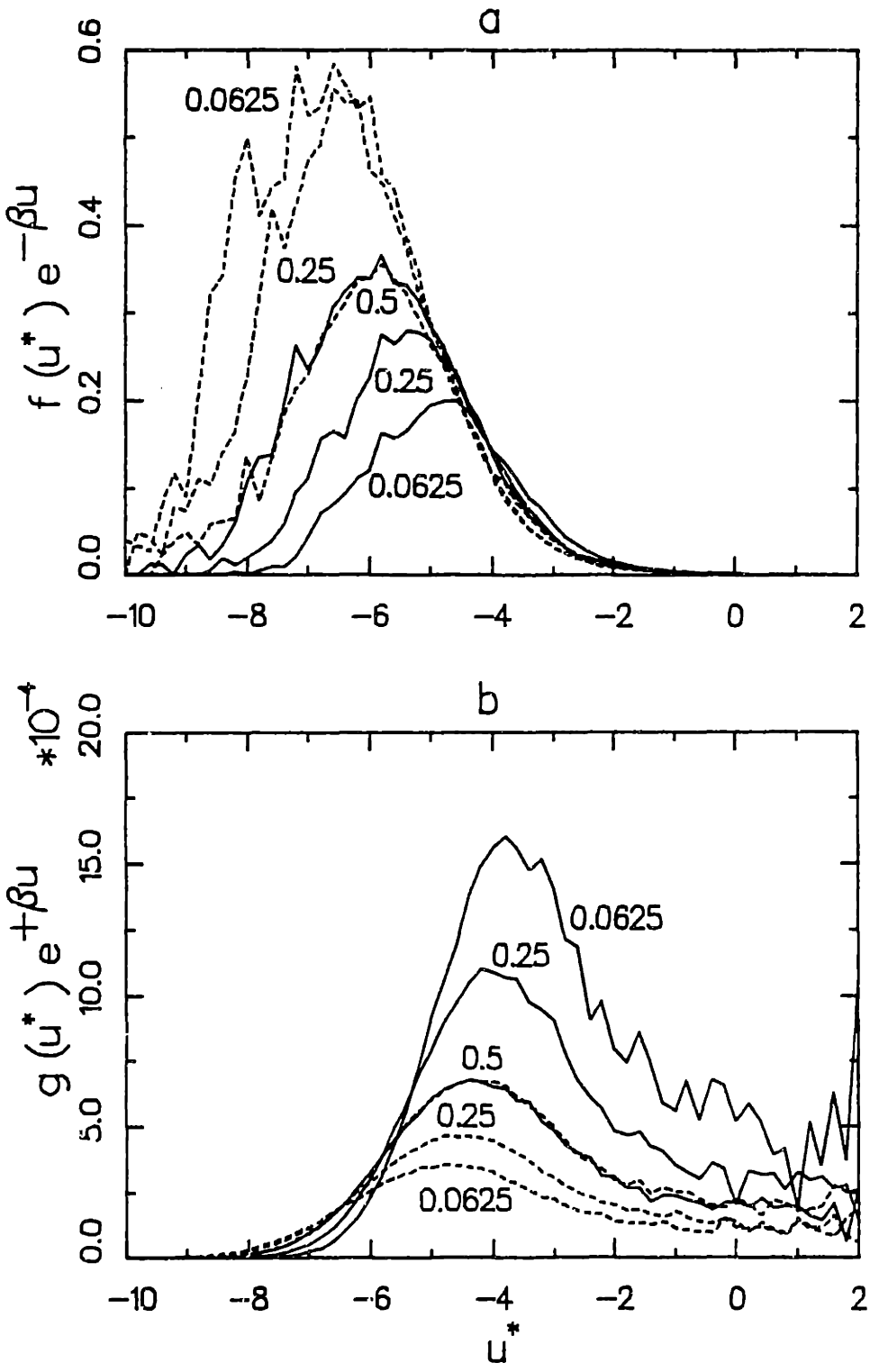

Figure 6.15. *Test- and real-particle energy-distribucion functions for mixture I at T^*=1.15, ρ^*= 0.500. (——) component 1; (---) component 2. The parameter on the curves is the mole fraction of component 1, X_1.*

6.3.4 Phase behavior

Figure 6.16 presents the calculated phase diagram for this mixture at $T^* = 1.15$. There is, as expected, an azeotrope at equimolar composition. In addition, a liquid-liquid phase split at higher pressures is hinted by the dashed curve in Figure 6.16. The presence of a liquid-liquid phase split for a Lennard-Jones mixture with this set of unlike pair interactions has been suggested by Torrie and Valleau (1977) and recently verified by Schoen and Hoheisel (1984). At $T^* = 1.15$, the mixture is very close to the upper critical solution temperature and an accurate determination of very small differences of the chemical potential between the two liquid phases is difficult; this leads tc large uncertainties in the liquid-liquid coexisting phase compositions.

Table 6.4 summarizes the results for the phase coexistence curve, including the chemical potential and densities of the coexisting phases. The results at $X_1 = 0$ (pure component) were calculated from in the present study and are in excellent agreement with the results given by Adams (1979).

As can be seen in Table 6.4, there is a very pronounced decrease in the saturated liquid density of the mixture as the azeotropic point is approached.

Table 6.4† Phase coexistence properties for mixture I at $T^* = 1.15$

		Vapor - Liquid Equilibrium				
$X_{1,L}$	$X_{1,v}$	P_s^*	ρ_L^*	ρ_v^*	μ_1^*	μ_2^*
0	0	0.063 (2)	0.613 (3)	0.077 (2)	-	-3.65 (5)
0.0313	0.13 (2)	0.067 (3)	0.599 (3)	0.083 (4)	-5.71 (5)	-3.75 (5)
0.0625	0.21 (3)	0.078 (3)	0.574 (3)	0.095 (4)	-5.23 (5)	-3.82 (5)
0.125	0.28 (2)	0.086 (3)	0.554 (3)	0.118 (4)	-4.65 (5)	-3.75 (5)
0.250	0.40 (2)	0.099 (3)	0.513 (3)	0.145 (4)	-4.23 (5)	-3.79 (5)
		Liquid - Liquid Equilibrium				
$X_{1,L1}$	$X_{1,L2}$	P_s^*	ρ_{L1}^*	ρ_{L2}^*	μ_1^*	μ_2^*
0.29 (7)	0.71 (7)	1.3 (1)	0.750[2]	0.750‡	-1.3 (1)	-1.3 (1)

† The numbers in parentheses indicate the estimated error in the last decimal digit: 0.063 (2) means 0.063 ± 0.002

‡ This calculation was performed at fixed density

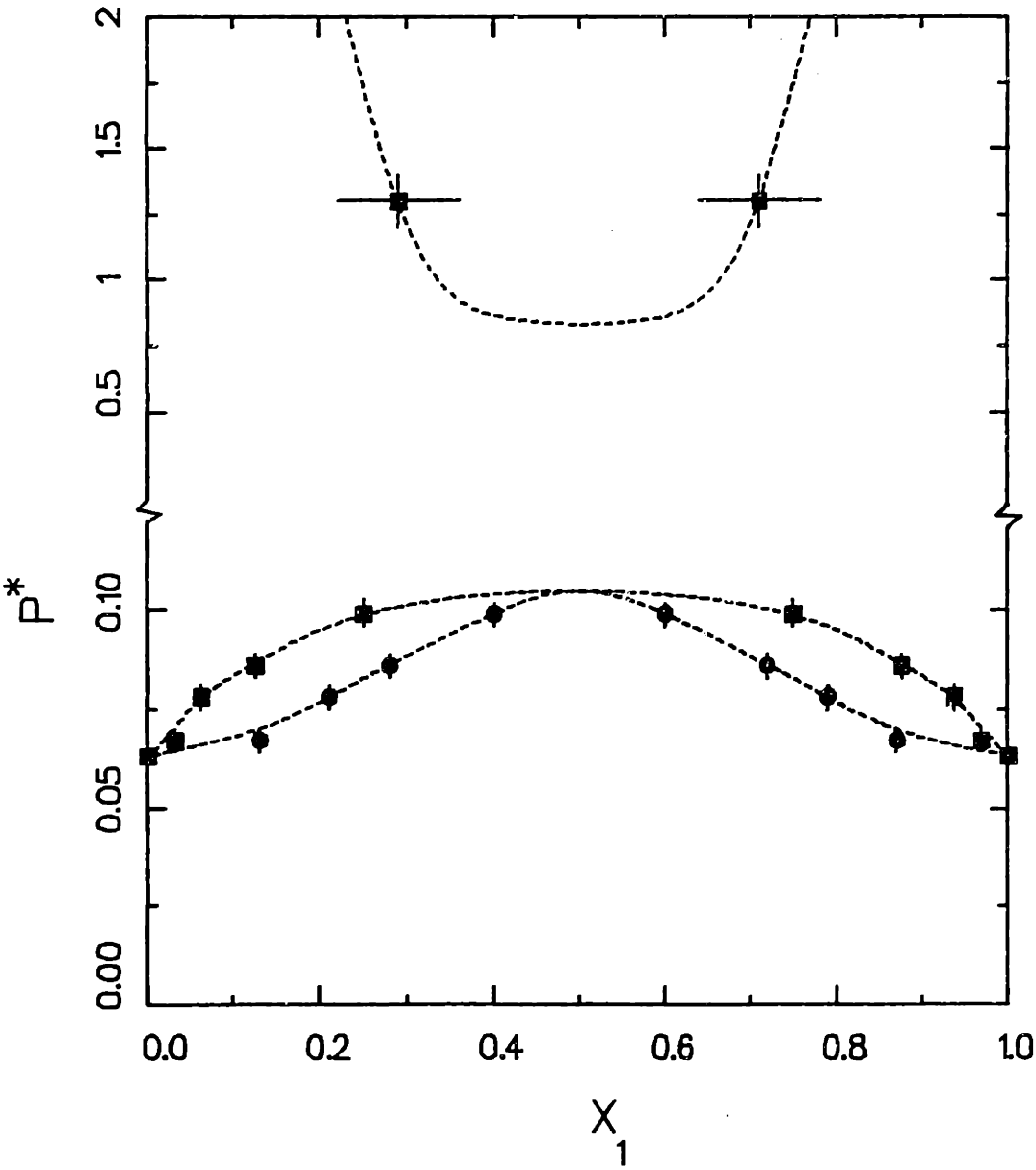

Figure 6.16 *Phase-coexistence curves for mixture I at $T^* = 1.15$. (■) liquid phase compositions; (•) gas phase compositions. The dashed lines are drawn through the points for visual clarity. The solid lines at the points indicate estimated errors for the pressure and concentration.*

This unexpected decrease is most likely due to the proximity of a mixture liquid-vapor critical point. The pure component critical temperature is approximately $T^* = 1.35$; the unfavorable unlike-pair interactions tend to decrease this temperature, with a resulting decrease in liquid molar density as the equimolar composition is approached.

6.4 Mixture II: Effect of different size

The case of mixtures of molecules of unequal sizes but similar potential well depths is not very common for real fluids, since increasing size of a molecule usually results in larger effective ϵ. Exceptions are fluorocarbon molecules that have low attractive well parameters. The ratio of volumes of the two components chosen for mixture II is equal to $(\sigma_{22}/\sigma_{11})^3 = 0.45$, so the two components have a significant size disparity. The unlike size parameter, σ_{12}, is taken as the average of the pure-component size parameters (Lorenz rule). A summary of the potential parameters used is given in Table 5.1. A summary of the simulation results for this mixture is given in Appendix G.4.

6.4.1 Energy and radial distribution functions

Figure 6.17 shows results for the radial distribution functions for the mixture at a $T^*=1.15$, $\rho^*=0.950$ and $X_1=0.500$. The behavior illustrated for these conditions is representative for the high-density conditions studied. The three pair-distribution functions are displaced with respect to the radial position of the peaks, reflecting the difference in the size parameter characterizing the corresponding interactions. The height of the first (nearest-neighbor) peak of the radial distribution function is the lowest for the 1-1 pairs. This may be related to the fact that the potential well depth for 1-1 pairs is the same as for the 2-2 pairs, but the size of molecules of type 1 is significantly larger. Fewer nearest neighbors of type 1 can then be accommodated in the first-nearest neighbor cell of a molecule of type 1.

Figure 6.18 shows the test-particle energy distribution functions for this mixture at $T^* = 1.15$ as a function of composition. Because of the difference in size of the two components, changes in composition at a constant reduced density result in significant changes in absolute density; to compensate for this effect, a constant volume fraction of $\rho(X_1\sigma_{11}^3+X_2\sigma_{22}^3)$

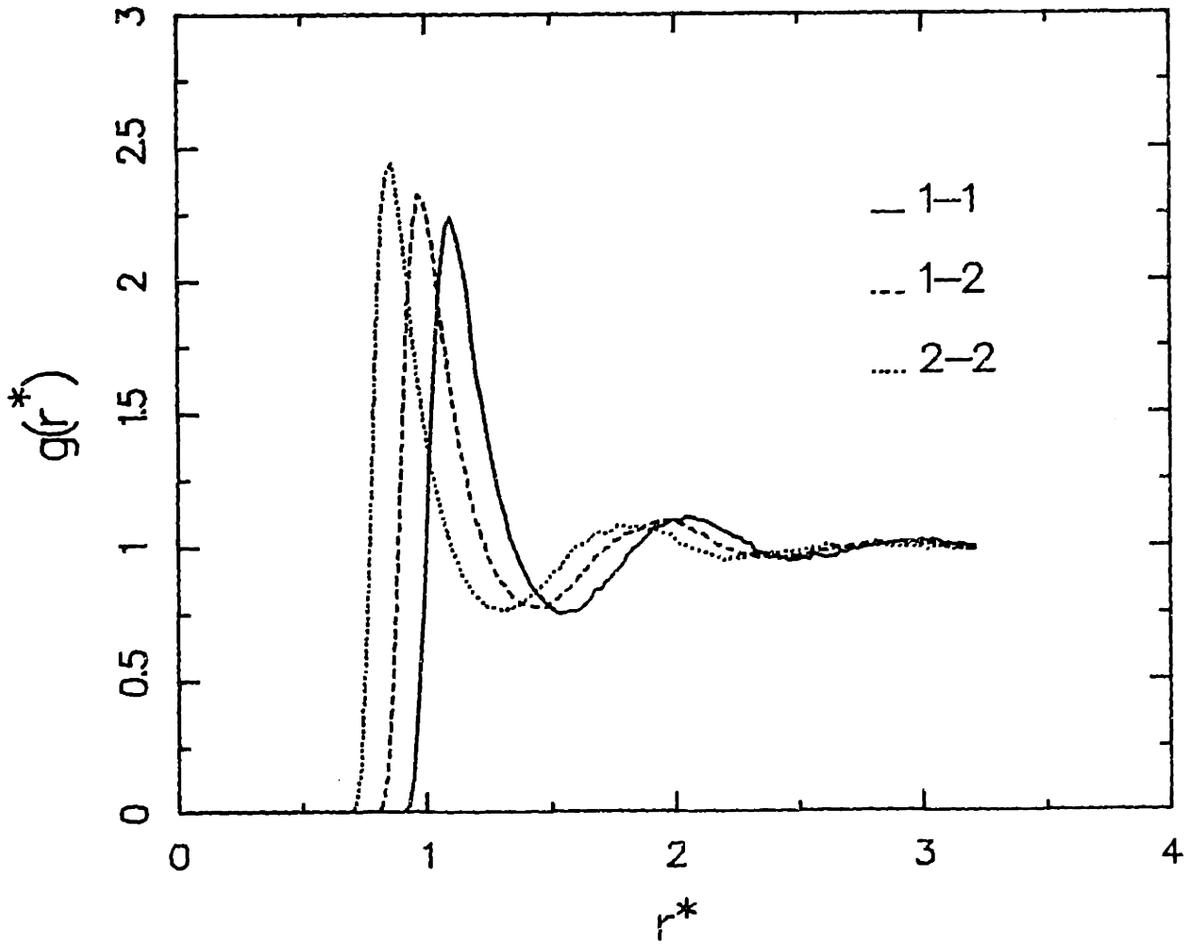

Figure 6.17 *Radial distribution functions for Mixture II at* $T^*=1.15$, $\rho^*=0.950$, $X_1=0.500$. (——) *1-1 pairs;* (---) *1-2 pairs;* (...) *2-2 pairs.*

= 0.63, rather than a constant density, was used in Figure 6.18. As in Figure 6.15, the integrals under the curves are related to the chemical potentials of the components *via* Eq. 5.13. For the larger component (component 1), the peak of the test-particle distribution function is shifted to more negative values relative to the smaller component, because the greater exposed area of the large molecules results in more attractive average interaction energies. This effect is stronger at low concentrations of component 1 because of the more efficient packing of the

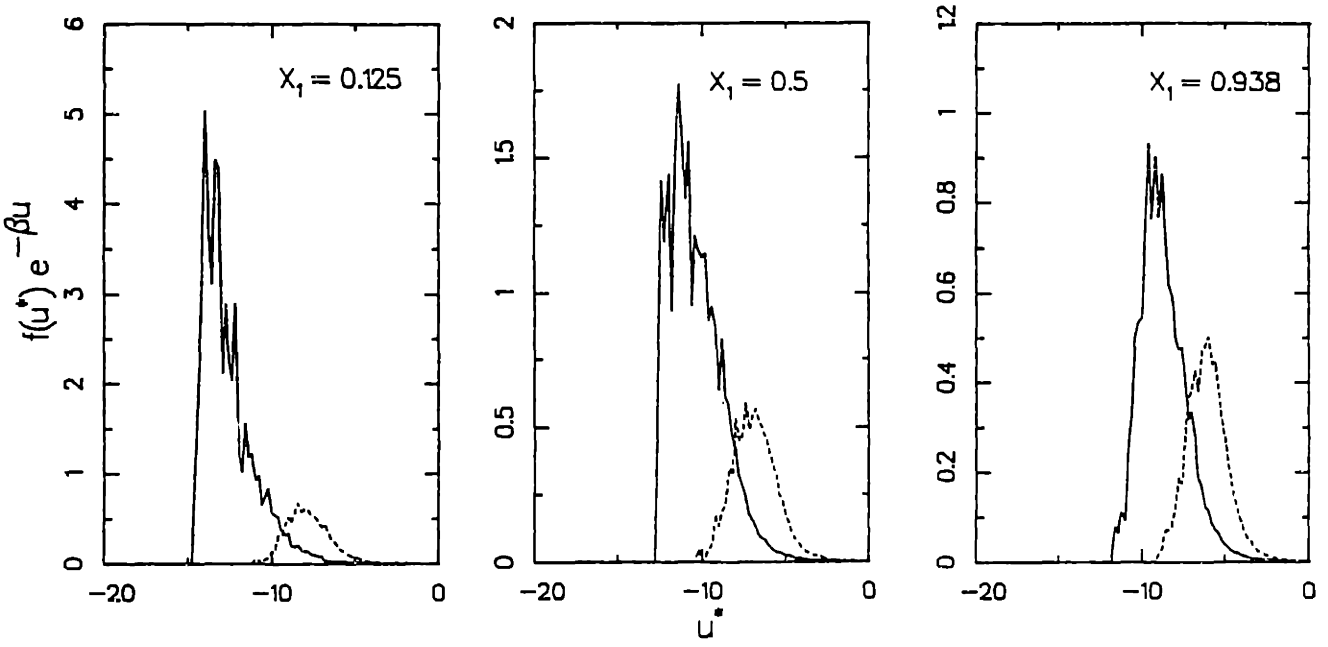

Figure 6.18 *Test-particle energy-distribution functions for mixture II at* $T^*=1.15$, $\rho(X_1\sigma_{11}^3+X_2\sigma_{22}^3) = 0.63$. (——) *component 1;* (---) component 2.

small molecules around a center of type 1. No such shifting of the position of the peak of the test-particle energy-distribution function is seen for component 2.

6.4.2 Phase coexistence curves

Figure 6.19 and Table 6.5 summarize the phase coexistence properties of this mixture. Despite the large size difference, the phase behavior of the mixture is close to ideal, with a narrow coexistence envelope. The calculation of the mixture phase diagram from Monte Carlo simulation is possible, despite this relatively narrow coexistence region.

Table 6.5† Phase coexistence properties for mixture II at $T^* = 1.15$

$X_{1,L}$	$X_{1,V}$	P_s^*	ρ_L^*	ρ_V^*	μ_1^*	μ_2^*
0	0	0.139 (4)	1.348 (5)	0.169 (4)	–	-2.74 (5)
0.125	0.08 (2)	0.120 (5)	1.159 (5)	0.140 (5)	-6.11 (5)	-3.00 (5)
0.25	0.19 (2)	0.102 (5)	1.037 (5)	0.120 (5)	-5.26 (5)	-3.25 (5)
0.375	0.27 (2)	0.095 (5)	0.927 (5)	0.110 (5)	-4.82 (5)	-3.36 (5)
0.5	0.37 (2)	0.083 (5)	0.854 (5)	0.095 (5)	-4.61 (5)	-3.72 (5)
0.625	0.52 (2)	0.078 (5)	0.771 (5)	0.090 (5)	-4.18 (5)	-4.06 (5)
0.75	0.67 (2)	0.072 (4)	0.717 (5)	0.087 (4)	-3.95 (5)	-4.50 (5)
0.875	0.84 (2)	0.067 (2)	0.666 (5)	0.082 (2)	-3.73 (5)	-5.35 (5)
0.9375	0.91 (1)	0.064 (2)	0.635 (5)	0.078 (2)	-3.66 (5)	-6.21 (5)
1	1	0.063 (2)	0.613 (3)	0.077 (2)	-3.65 (5)	–

† See footnote to Table 6.4 for the notation used for the errors

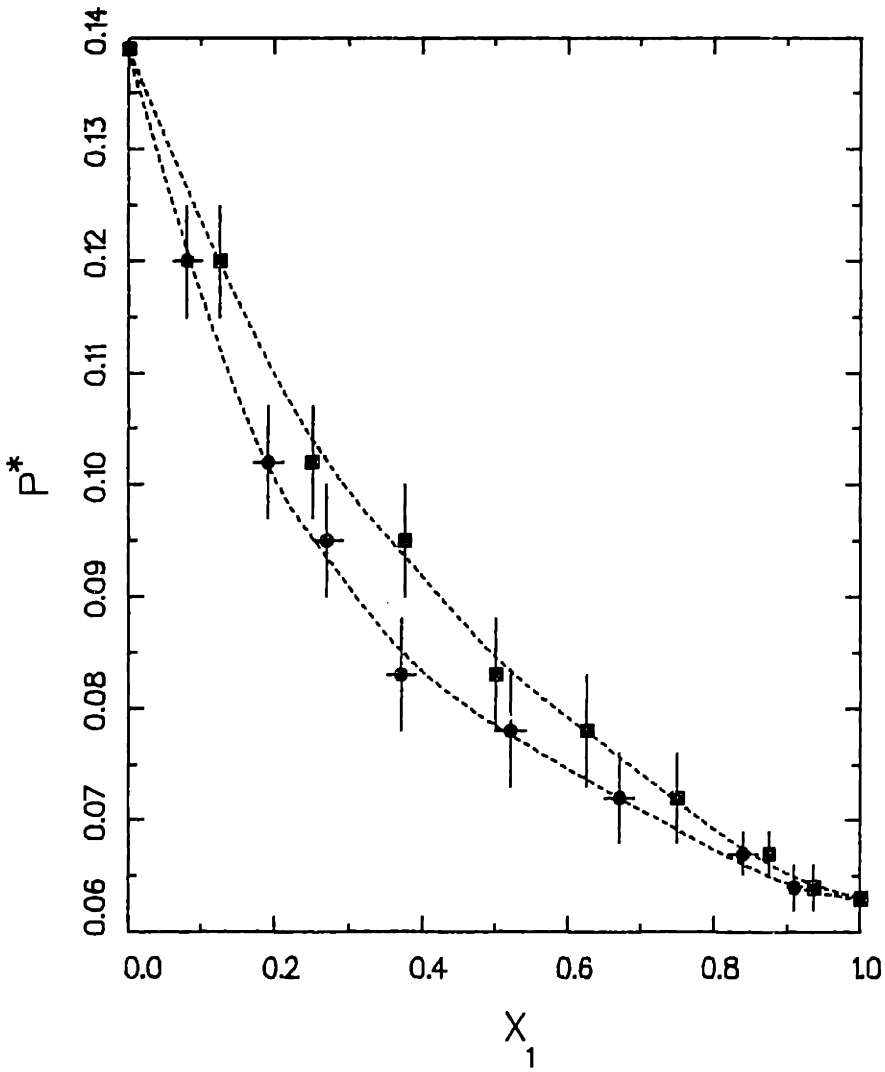

Figure 6.19. *Phase-coexistence curve for mixture II at T^*=1.15. For an explanation of the symbols, see legend of Figure 6.15.*

6.5 Mixture III: Simulation of a realistic mixture

6.5.1 Selection of potential parameters

As a test of the case where both size and energy interaction parameters are different, and also to test the ability of the simulation to reproduce phase diagrams of real mixtures, we performed a series of simulations for a mixture that is a simple model of a real asymmetric system, namely the acetone - carbon dioxide system at temperatures above the critical temperature of carbon dioxide. Experimental results for this system are presented in Section 4.2 and Appendix C.2. To obtain the potential parameters we fitted the critical temperature and critical volume of the corresponding components using values from Reid et al. (1977). The critical parameters for the pure Lennard-Jones fluid were taken to be $T_c^* = 1.35$, $\rho_c^* = 0.35$, $P_c^* = 0.142$ (Nicolas et al., 1979). The resulting parameters are shown in Table 6.6 and correspond to the ratios given in Table 5.1. The Lorenz-Berthelot rules were used for the unlike pair parameters (arithmetic mean of the pure component parameters for σ_{12} and geometric mean for ϵ_{12}).

Table 6.6 Lennard-Jones (6,12) potential parameters for mixture III: acetone (1) - carbon dioxide (2)

ϵ_{11}/k_B	ϵ_{12}/k_B (K)	ϵ_{22}/k_B	σ_{11}	σ_{12} (Å)	σ_{22}
377	291	225	4.95	4.38	3.80

6.5.2 Thermodynamic properties

The calculated results for the thermodynamic properties of this mixture are given in Appendix G.5. Here, we present a summary of the basic results in graphical form.

Energy: The energy *versus* composition for this mixture at $T^*=1.15$ for a series of reduced densities is shown in Figure 6.20. There is an almost linear dependence of internal energy on composition at constant density.

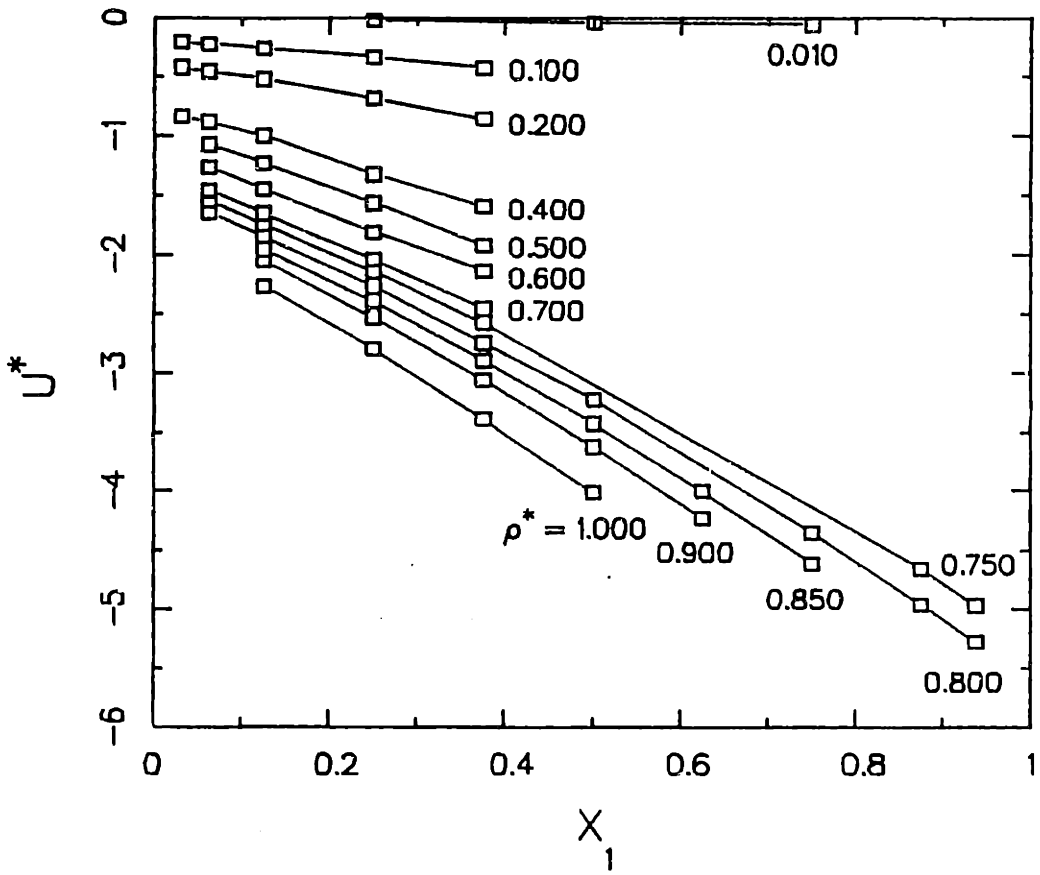

Figure 6.20 *Reduced internal energy as a function of compositions for a series of reduced densities for Mixture III at T^*=0.928. The parameter on the curves is the reduced density, ρ^*.*

For the larger component (component 1) the absolute value of the energy is significantly higher at a given reduced density. Because of the large difference in size of the two components, a constant reduced density corresponds to much higher absolute densities for the mixtures rich in component 1.

Pressure: A plot of the pressure (in bar) *versus* density for a series of compositions is given in Figure 6.21. For the mixture rich in component 2 (carbon dioxide) the behavior closely approximates the behavior of a pure supercritical component (e.g. T^*=1.556 in Figure 6.1), with a monotonic increase in pressure with increasing density. As the mixture becomes more concentrated in component 1, the behavior changes gradually to that of a subcritical liquid, and a van der Waals loop appears. For the mixtures

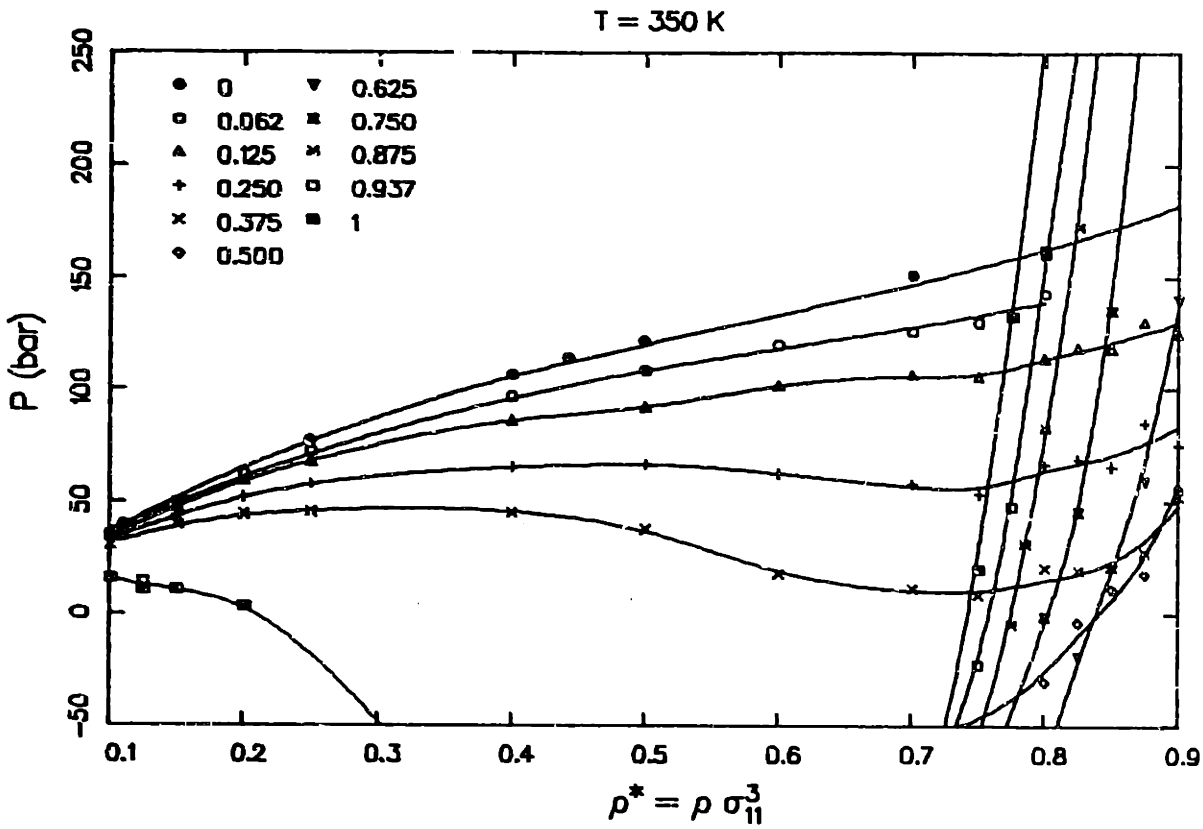

Figure 6.21 *Pressure versus reduced density for Mixture III at T^*=0.928 (T=350K). The legend on the figure gives the mole fraction of component 1, X_1.*

rich in component 1, the behavior is more typical of a subcritical liquid. The compressibility at high densities is low, and pressure increases rapidly with increasing density. A pronounced van der Waals loop is present (only partly shown in Figure 6.21).

Chemical potentials: In Figure 6.22, we present the chemical potentials, μ_i^* for the two components at the conditions investigated. Close to the two ends of the composition scale, the chemical potentials change rapidly, reflecting the effect of concentration on the chemical potential (via Eq. 5.8b). Some scatter in the data is evident, especially for the higher densities, but the accuracy of the results is sufficient for the calculation of the mixture phase diagrams by the graphical construction explained in Section 5.6.5.

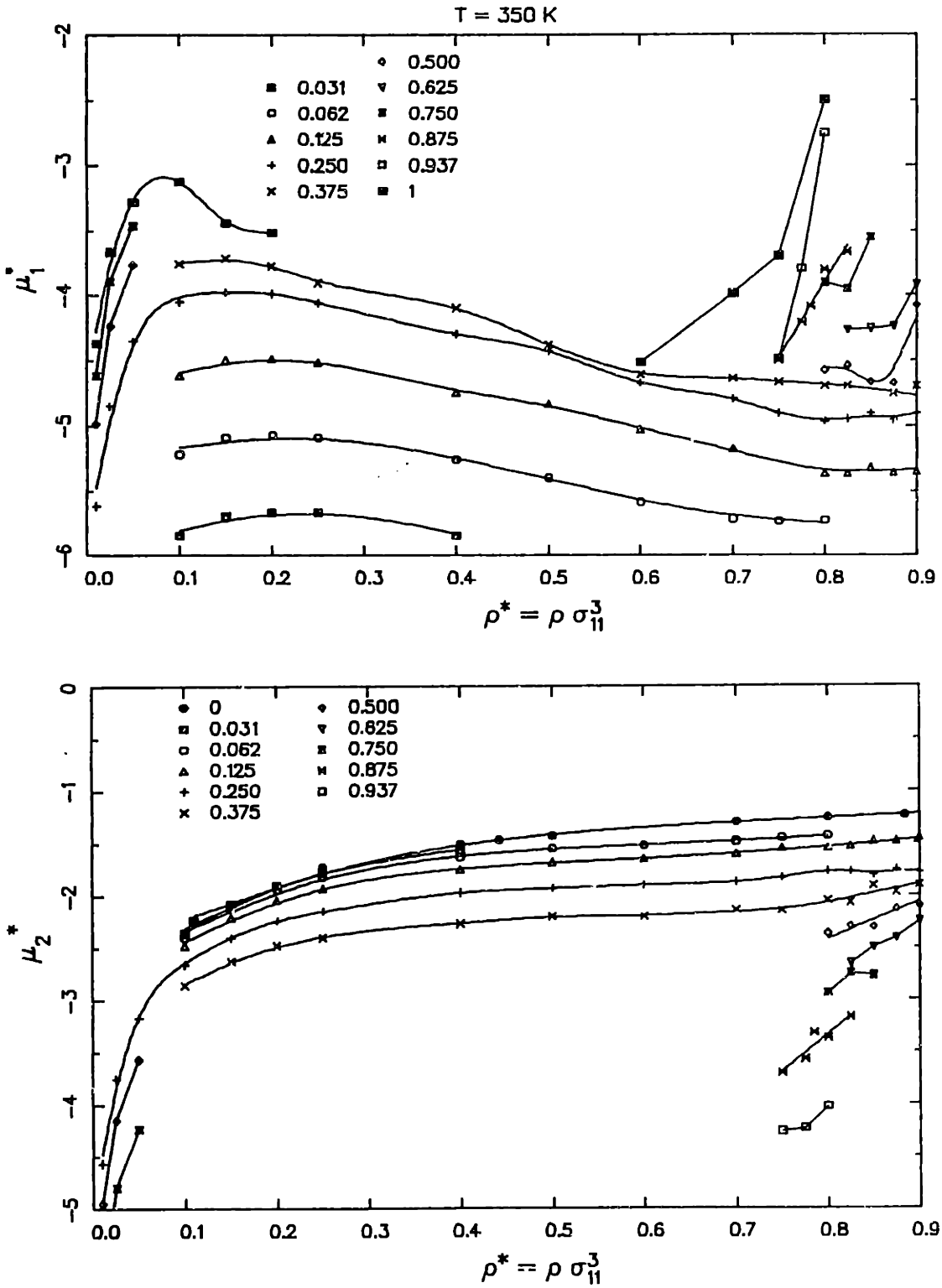

Figure 6.22 *Reduced chemical potentials as a function of composition at a series of reduced densities for Mixture III at T^*=0.928 (T=350 K). The legend on the figures give the mole fraction of component 1, X_1.*

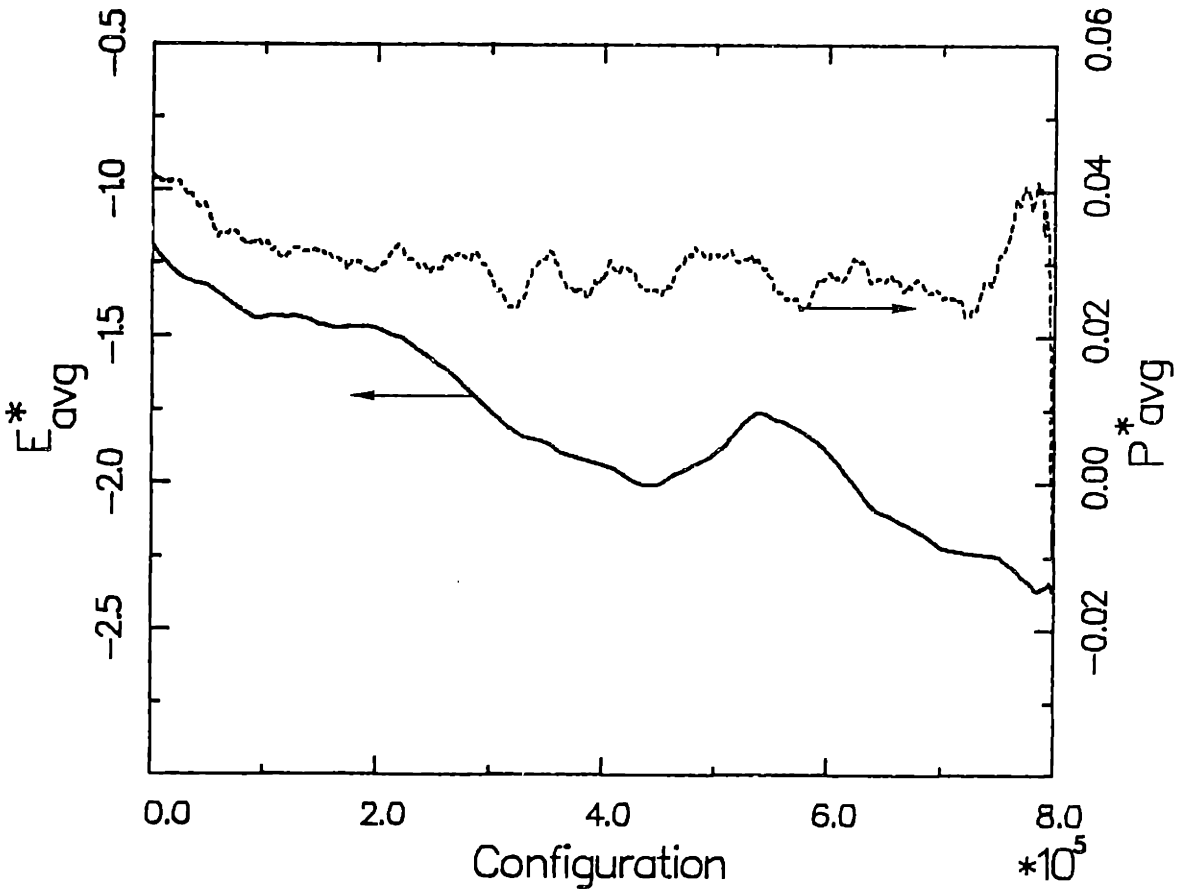

Figure 6.23 *Average energy versus configuration generated for a simulation of Mixture III at T_*=0.928, ρ^*=0.125, X_1=0.938. A running average of 100000 configurations was performed.*

An example of a case where the calculation of the properties of the fluid becomes difficult because the fluid is in a materially unstable region, is given in Figures 6.23 and 6.24, from the results from a simulation at T^*=0.928, ρ^*=.125, X_1=0.938. In Figure 6.23, the average value of the energy versus the number of configurations generated shows a substantial downward trend, and large fluctuations in pressure are present. In addition, the radial distribution function for component 1 (Figure 6.24) shows a very pronounced first peak, and decreases very slowly, being significantly above unity even for r^*=4.0. This behavior of the radial distribution was also observed by Shoen and Hoheisel (1984) for unstable mixtures. Despite the large fluctuations of energy and local density, the energy distribution functions appear to be well-behaved, and a good straight line was obtained

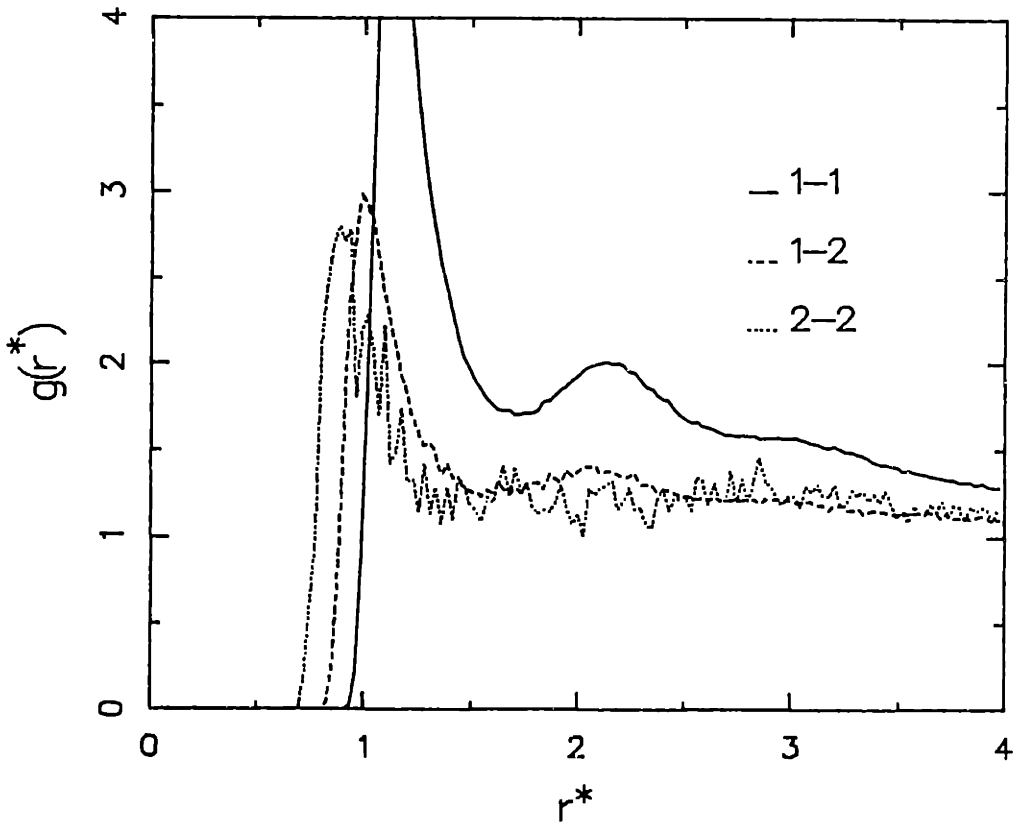

Figure 6.24 *Radial distribution functions for Mixture III at T^*=0.928, ρ^*=0.125, X_1=0.938.*

during calculation of the chemical potential (this may be related to the fact that changes in density do not affect the chemical potential at constant composition close to the spinodal limit). For the same conditions, the fluctuations in the number of molecules are extremely large (Appendix G.4), verifying the presence of phase instability.

6.5.3 Radial and energy distribution functions

A typical example of the radial distribution functions obtained for this mixture for the high-density simulation runs is given in Figure 6.26 for T^*=0.928, ρ^*=0.800, X_1=0.500. The behavior resembles closely the behavior observed for Mixture II (Figure 6.17), with the first peak displaced along the radial direction because of the difference of the characteristic size parameter for the interactions of the 1-1, 1-2 and 2-2 pairs. The height

of the first peak, however is now highest for the 1-1 pairs (the largest component), whereas in the case of Mixture II it was highest for component 2 (the smallest component). It is interesting to note that the shape of the radial distribution function for the pairs 1-1 is virtually identical for Mixtures II and III. The height of the first peak of the 2-2 pair distribution function, however, is significantly higher for Mixture II, reflecting the deeper potential well depth for component 1 (ϵ_{22}=0.597 for Mixture III versus ϵ_{22}=1 for Mixture II).

The energy distribution functions for this mixture were qualitatively similar to the corresponding functions for Mixture II (Figure 6.18), reflecting the significant disparity in size of the two components.

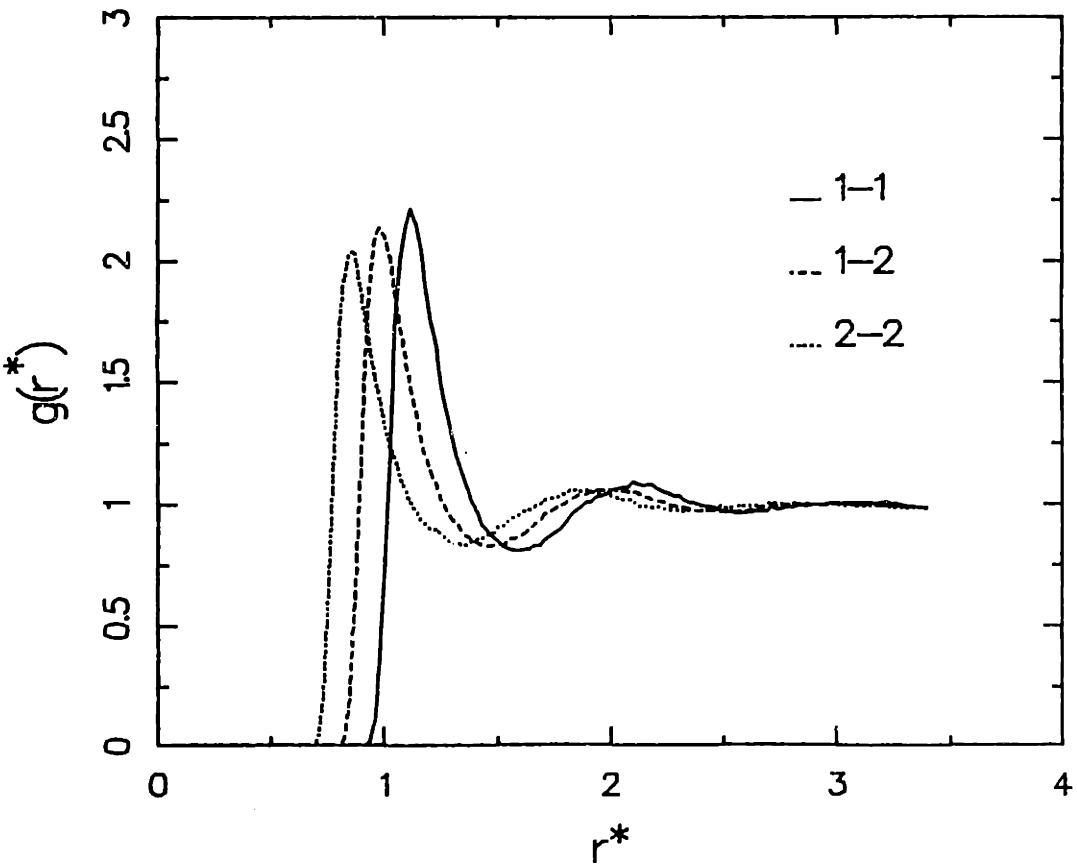

Figure 6.25 *Radial distribution functions for MIxture III at T^*=0.928, ρ^*=0.800, X_1=0.500.*

6.5.4 Phase behavior and comparison with experiment

The calculated phase coexistence properties for this mixture at $T^* = 0.928$ ($T = 350$ K) are presented in Table 6.7. The calculated phase diagram at the same temperature is shown in Figure 6.26a, together with experimental data for the mixture acetone - carbon dioxide at three temperatures in Figure 6.26b. Only results from the correlation are available for the experimental properties at 350 K, but they are expected to be of comparable accuracy to the results at the lower temperatures. The mixture critical pressure is lower than the experimental value ($P_c = 91$ bar from Monte Carlo; $P_c = 115$ bar from the extrapolation of the experimental data) and the solubility of acetone in the supercritical phase is higher than what is experimentally observed, but the general shape of the coexistence curve is well reproduced. This agreement is all the more significant since this is a completely a priori prediction of the properties of the mixture with no fitting of the potential parameters to experimental data. This agreement is at first surprising given the fact that the Lennard-Jones potential does not give a realistic representation of the molecular structure of either acetone or carbon dioxide. Both molecules have a distinctly non-spherical shape and a significant dipole moment (acetone) or quadrupole moment (carbon dioxide). The inability of the Lennard-Jones potential to give a good description of the properties of the pure components is evidenced in Figure 6.26 by the fact that at $X_2 = 0$ (pure acetone) the pure component vapor pressure for the Lennard-Jones fluids is almost twice the experimental value. It appears, however, that the properties of the mixture are primarily influenced by the difference in size and energy parameters and not by the detailed shape

Table 6.7† Phase coexistence properties for mixture III at $T^* = 0.928$

$X_{1,L}$	$X_{1,V}$	P_s^*	ρ_L^*	ρ_V^*	μ_1^*	μ_2^*
0.625	0.19 (3)	0.072 (9)	0.86 (1)	0.09 (1)	-4.3 (1)	-2.55 (5)
0.50	0.12 (3)	0.100 (9)	0.88 (1)	0.13 (1)	-4.5 (1)	-2.19 (5)
0.375	0.10 (2)	0.163 (9)	0.92 (1)	0.24 (1)	-4.7 (1)	-1.90 (5)
0.25	0.15 (2)	0.196 (9)	0.91 (1)	0.55 (1)	-4.9 (1)	-1.72 (5)
0.20‡ (2)	0.20‡ (3)	0.212 (9)	0.68 (3)	0.68 (3)	-4.8 (1)	-1.70 (5)

† See footnote to Table 6.4 for the notation used for the errors
‡ Mixture critical point

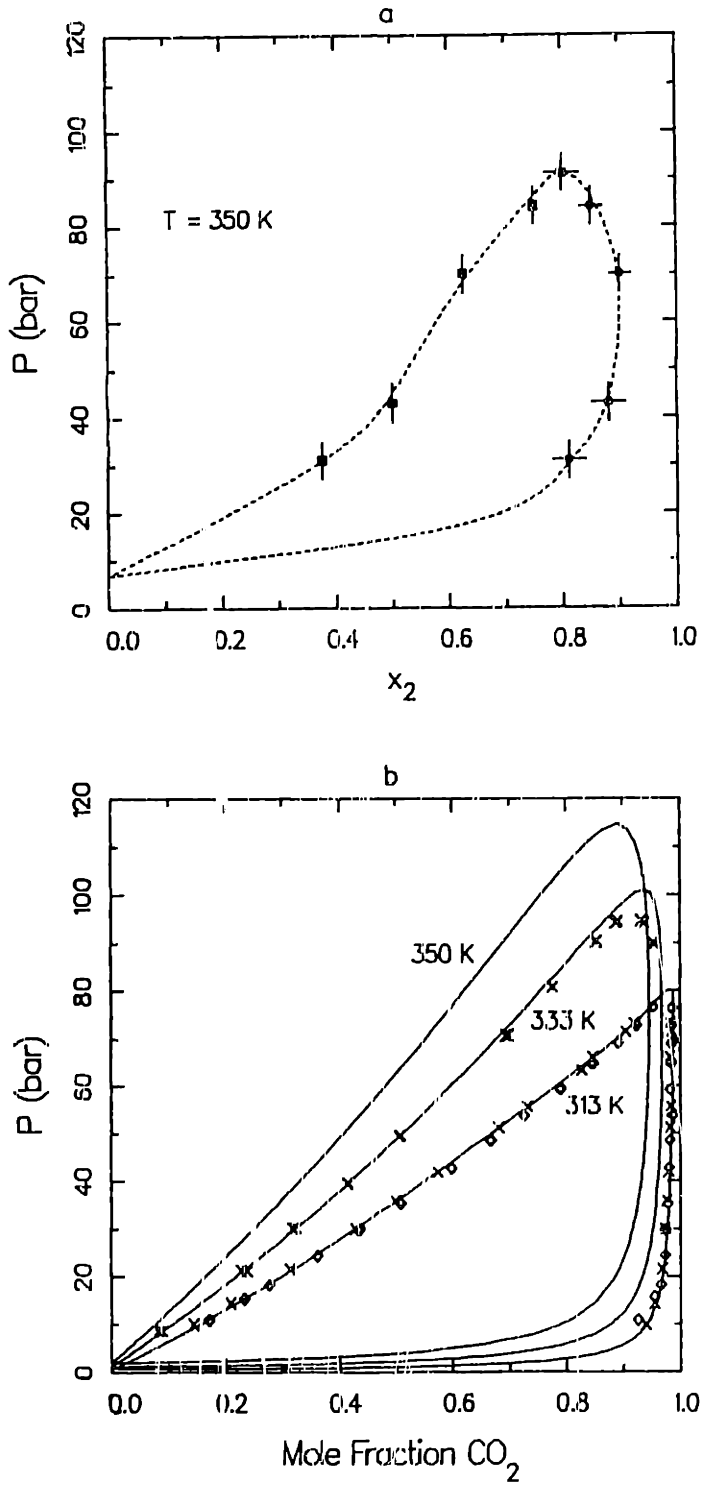

Figure 6.26. *Phase-coexistence curve for mixture III. a: Monte Carlo simulation results at T = 350 K (for an explanation of the symbols, see legend of Figure 15). b: (×, ◊) experimental and (—) equation of state results for the mixture carbon dioxide - acetone at 313, 333 and 350 K.*

or multipolar moments of the molecules. The ability to obtain direct information on the factors responsible for a given type of macroscopic behavior is a distinct advantage of molecular simulation methods.

6.5.5. Mixture critical curves

An important parameter characterizing fluid mixtures is the shape and location of the mixture critical curve. Close to critical points, the accurate calculation of properties of fluids from molecular simulation is impossible because of the very large correlation lengths. We can, nevertheless, obtain the approximate location of the critical point (in the classical mean-field approximation) by determining the point beyond which no solution to the two-phase equilibrium problem can be found. We performed a series of simulations for mixture III to obtain the mixture critical curve at several temperatures. Figure 6.27 presents the results of these calculations (no comparable set of experimental data is available). The mixture critical curve is continuous from the critical point of one to the critical point of the other component; therefore this is a type I mixture according to the classification by Scott and van Konynenburg (1970). This is in agreement with the results of the perturbation theory of Gubbins and Twu (1977).

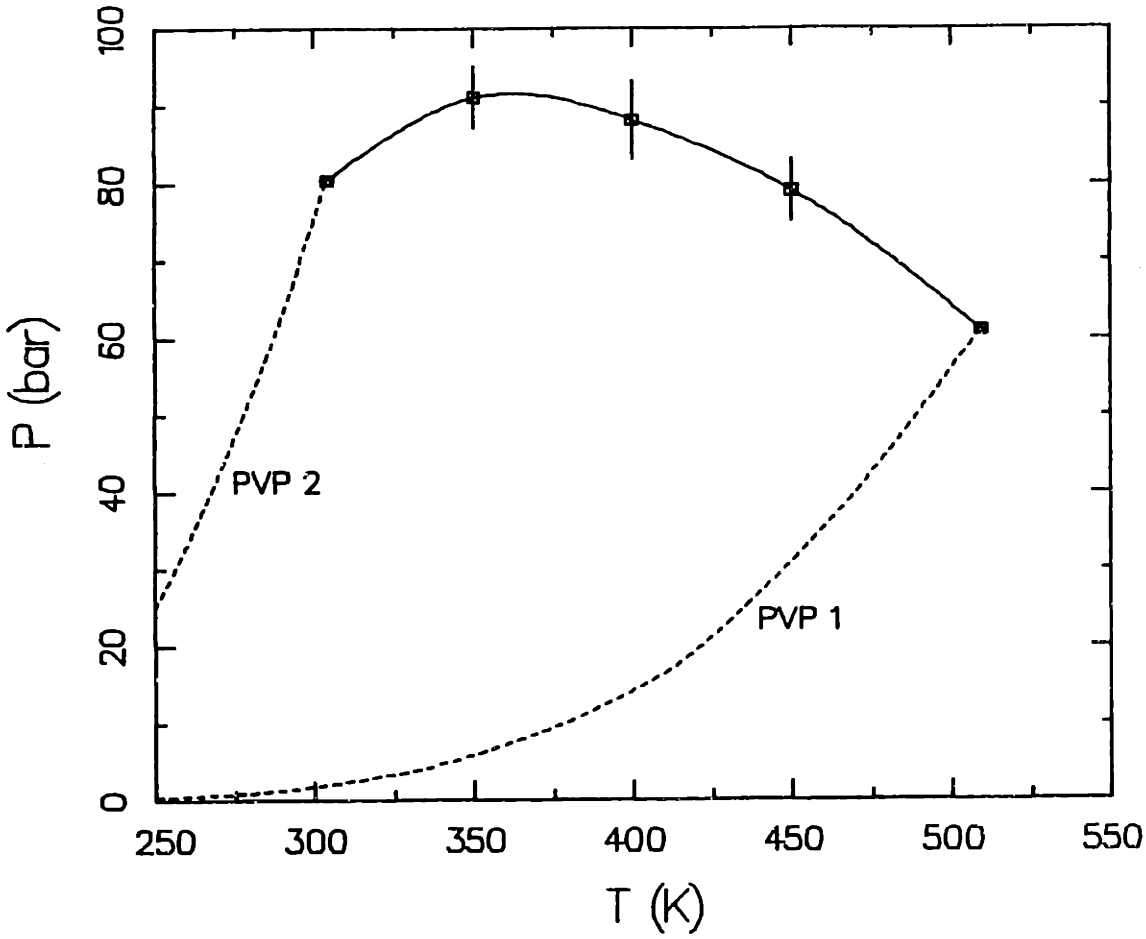

Figure 6.27. *Mixture critical curve for mixture III from Monte Carlo simulation.* (---) *pure component vapor pressures;* (□) *calculated mixture critical points;* (——) *interpolated mixture critical line.*

CHAPTER 7
CONCLUSIONS AND SIGNIFICANCE

7.1 Experimental and correlation

7.1.1 Summary of present work

The experimental data obtained in this work demonstrate the basic characteristics of phase equilibrium behavior in ternary systems containing water, a polar organic compound and a supercritical fluid. It was shown that a drastic change in phase equilibrium behavior occurs as pressure is increased above the supercritical component critical pressure. This change in behavior can be exploited for developing separation methods between polar organic compounds and water.

A common feature of the phase equilibrium behavior in the systems studied is the presence of multiphase equilibrium regions. Three-phase equilibrium regions occur over a range of pressures comparable to the critical pressures of the supercritical fluid-organic compound binaries. The presence of a three-phase region at relatively low pressures is associated with a high selectivity of the supercritical fluid for the organic compound over water at high pressures. Equilibria between four fluid phases were observed for one of the systems studied (*n*-butanol - water-carbon dioxide). This type of multiphase equilibria has rarely been reported in the past.

A summary of the phase equilibrium results and their possible implications for the development of new separation methods is given below:

- Organic compounds of moderate polarity can be extracted from dilute aqueous mixtures with high selectivity and favorable solvent capacities. For example, single-step extraction of a 4% w/w aqueous solution of acetone with carbon dioxide at 333 K and 15 MPa results in approximately 93% w/w acetone in the solvent phase.

- Organic compounds, such as acetic acid, that strongly associate with water can still be selectively extracted, but the distribution coefficients between the solvent and the aqueous phase are significantly less than 1.

- Increasing the hydrocarbon chain length in a homologous series of polar organic compounds results in improved separation efficiency, at least for the lower molecular weight compounds. It is known, however, that the solvent capacity also diminishes with increasing molecular weight of the solute.

The development of new methods for recovery of fermentation products from aqueous solutions using supercritical fluids needs to take into account both the solvent ability to extract selectively the desired compound, and, in the case of in situ extraction, the solvent effect on the growing microorganisms. The results from this study suggest that the type of compounds best suited for consideration in supercritical fluid recovery processes would be compounds of low to moderate polarity and relatively low molecular weight.

A new density-dependent mixing rule for cubic equations of state was developed for modelling the experimental results. The model, in conjunction with a novel technique to obtain pure component parameters for equations of state, can quantitatively reproduce phase equilibrium data for highly non-ideal systems at both low and high pressures. Ternary data were predicted with parameters determined from binary data only. The methods developed can thus be used for the extension of limited experimental information and can greatly facilitate process design and optimization.

7.1.2 Possible extensions

Several possible improvements and extensions of the experimental and correlation techniques developed in this work, and the range of systems covered can be identified:

Experimental technique: The experimental techniques used in this work was found to be accurate, reliable and rapid. The techniques can be improved, however, in several ways:

- Better temperature control of the equilibrium apparatus is important. Isothermal operation of all parts of the equipment, including the recirculation and sampling section, can be achieved by using a totally enclosed system and air for temperature control. This should improve the stability of conditions and the reproducibility of the experimental results.

- Direct chromatographic sampling using switching valves was found to be an efficient and rapid method of obtaining composition measurements in multicomponent systems. The sampling technique employed (using a gas chromatograph) cannot be used for non-volatile or heat-labile components. Use of a liquid or supercritical fluid chromatograph and thus sampling to a high-pressure environment without depressurization of the sample should greatly extend the range of applicability of the sampling technique.

- Continuous calibration of the gas chromatograph with mixtures of known composition close to the compositions being measured should eliminate the most likely source of systematic error in the measurements, namely the uncertainties in the relative response factors of the components. This could be achieved using a special sampling compartment and gravimetric preparation of calibration mixtures.

Modelling: The use of cubic equations of state with higher-order, density-dependent mixing rules appears to be a promising way to correlate

experimental data for highly asymmetric systems, at both low and high pressures. Several areas for possible future work can be identified:

- Determination of the behavior of the models for a large number of systems, including highly polar systems at high and low pressures. The objective of this investigation may be the generalization of the model parameters (e.g. using group contribution methods) to facilitate use of the models when no appropriate data are available.

- Testing of existing mixing rules and development of new methods based on incorporation of results from well-defined model systems using molecular simulation methods. This may significantly improve certain aspects of current equations of state, for example the transition from the low-density to the high density region using arbitrary interpolation functions.

- Incorporation of specific interactions and chemical association (for example for the hydrogen-bonding species) may extend the range of validity of the correlation methods developed in this work. The incorporation of additional adjustable parameters, however, should be avoided whenever possible.

Extensions to different systems: The range of systems covered in this and previous studies of high pressure phase equilibria in ternary fluid mixtures is sufficient to demonstrate the feasibility of separations between polar organic compounds and water using supercritical fluids. The basic needs for additional studies may be summarized as follows:

- Investigation of the phase equilibrium behavior for ternary systems with water, a polar organic compound and a range of different solvents (for example light hydrocarbons and halogenated hydrocarbons). This should demonstrate the effect of the solvent chemical character on the system behavior.

- Extension of the phase equilibrium data for solutes of higher molecular weight. We have determined in this study that extraction efficiency appears to be increasing with hydrocarbon chain length. Equilibrium data are needed for higher molecular weight compounds, in order to determine the upper limits of molecular size for the practical use of supercritical solvents.

- Data for higher order systems (quaternary and multicomponent) are needed for the investigation of possible deviations from the behavior expected based on the corresponding ternary and binary systems. The investigation of the effect of added electrolytes should help the development of new separation processes for biochemical products.

7.2 Molecular simulation

7.2.1 Summary of present work

The Monte Carlo simulation technique provides a means of directly obtaining results for the macroscopic behavior of fluids and fluid mixtures when the intermolecular interactions are known. Phase envelopes, solubilities and mixture critical curves can be obtained with sufficient accuracy to permit practical use of the results. Since no empirical approximations are involved, this is a method for *a priori* calculation of the properties of mixtures. The technique is only limited by the lack of knowledge for the intermolecular potentials acting between real fluids, but it can still be used to elucidate the effect of the primary molecular parameters (size, specific attractive interactions) on the macroscopic behavior of mixtures. Direct molecular simulation also provides detailed information at the molecular level that cannot be obtained in any other way.

The Widom test-particle expression provides a direct route for the calculation of the chemical potential from simulation. The method has limitations at high densities, but is adequate for fluids over a wide range of densities of practical importance. The energy-distribution

functions obtained with this technique provide useful information on the microscopic structure and energetic interactions in fluid mixtures.

Two specialized techniques used in this work can facilitate the calculation of thermodynamic properties of non-ideal fluid mixtures. The first is based on the observation of microscopic fluctuations and enables a qualitative determination of the presence or absence of a phase transition. The second involves a particle interchange technique that enables a faster and more accurate calculation of the properties of mixtures of dissimilar components.

Calculated phase diagrams for a range of mixtures using simple Lennard-Jones potential energy functions show significant variety, including azeotropes and liquid-liquid immiscibilities. Simulation of a model system of the mixture acetone-carbon dioxide demonstrates that a simple potential gives a good representation of the phase equilibrium behavior of this non-ideal mixture.

7.2.2 Possible extensions

The methodologies developed in this work are quite general and can be used for the investigation of a wide range of questions related to the prediction of macroscopic properties of mixtures from information at the molecular level. In particular, the following problems are of significant interest:

- Computation of the phase diagrams and critical curves for binary mixtures that include the effects of: a) a wider variation in size and potential energy b) non-spherical potentials c) multipolar terms, such as dipolar and quadrupolar interactions d) molecules with internal degrees of freedom (rotation, vibration) and e) molecules with strong specific forces, such as hydrogen bonding.

- A detailed comparison of results from simulation with existing perturbation theories and possibly incorporation of the results into new versions of the theories needs to be performed.

- The Monte Carlo simulation methodology developed in this work can be used for the determination of the chemical potential in systems with an interface. Of particular interest are the equilibrium properties and molecular organization at the vicinity of a solid surface for a fluid or mixture interacting with the surface. Another area of possible application is the study of fluids at the vicinity of a liquid-gas interface.

- An important area of possible application for molecular simulation techniques relates to systems with organized aggregates that contain a large number of molecules, in particular micellar systems. An improved understanding of the molecular mechanisms for micelle formation, structure and solubilization behavior is of considerable practical and theoretical interest.

- Nucleation from liquids and gases may also be studied using molecular simulation methods. Understanding the microscopic mechanisms for nucleation and crystal growth can result in significant practical benefits, since these processes are widely used but not well described by phenomenological methods.

NOTATION

a = energy parameter in an equation of state, J m^3 mol^{-2}
A = molar Helmholtz energy, J mol^{-1}
$\underline{A}$ = total Helmholtz energy, J
B = second virial coefficient, m^3 mol^{-1}
b = volume parameters in an equation of state, m^3 mol-1
f = fugacity of component, N/m^2
f(u) = test particle energy distribution function (dimensionless)
g(u) = real particle energy distribution function (dimensionless)
g(r) = radial pair distribution function
G = Gibbs energy, J mol^{-1}
H = system Hamiltonian, J
k_B = Boltzmann's constant, 1.3805×10^{-23} J/K
k_{ij} = binary interaction parameter in Eqs 2.10 or 3.6 (dimensionless)
L = edge length of the cubic simulation volume
L(u) = the function $\ell n[f(u)/g(u)]$
M = number of coexisting phases at equilibrium; also number of configurations genarated during a simulation run
n = number of components in a mixture
N = number of molecules
P = pressure, Pa ($=Jm^{-3}$); also probability in Eq. 5.2
R = universal gas constant, 8.31429 J K^{-1} mol^{-1}
q = configuration space integration variable
r = distance from the center of a molecule, m or Å
S = entropy, J/K
T = thermodynamic temperature, K
u = energy parameter, J
U = internal energy of a system, J
u,w = arithmetic constants in a cubic EOS represented in Eq. 2.7
V = specific volume, m^3 mol^{-1}
$\underline{V}$ = total system volume, m^3
$\underline{x}$ = configuration of a system
X = mole fraction
y = Legendre-transformed function

Greek Letters

β = $1/k_BT$, J^{-1}
δ = fluctuation quantity; also Kronecker delta in Eqs. 5.10 and 5.11
Δ = difference
ϵ = energy parameter in Lennard-Jones potential (Eq. 5.16), J
λ_{ij} = binary interaction parameter in Eq. 3.6, J^2 m^3 mol^{-3}
μ = chemical potential, J
ρ = density, m^{-3}
σ = size parameter in Lennard-Jones potential (Eq. 5.16), m or Å
Ω = phase space

Subscripts

c = configurational property (for chemical potential); also cutoff distance (for potential energy function)
cr = critical property
G = gas-phase property
i,j = component i or j
[k] = in partial differentiation, indicates that all component variables except for those of component k are held constant
L = liquid-phase property
m = mixture property
r = residual property
R = reduced property (e.g $T_R = T/T_{cr}$)
s = saturation property
ν = configuration count
VP = vapor pressure

Superscripts

* = reduced property (see Eq. 5.17 for definitions)
+ = reference state
0 = ideal-gas property
f = test-particle property
g = real-particle property
(n)= n-th order Legendre transform

LITERATURE CITED

Abrams, D.S. and J.M. Prausnitz, 1975. Statistical Thermodynamics of liquid mixtures: A new expression for the excess Gibbs energy of partly or completely miscible systems, *AIChE J.*, 21: 116-128.

Adams, D.J., 1976. Calculating the low temperature vapour line by Monte Carlo, *Molec. Phys.* 32: 647-657.

Adams, D.J., 1979. Calculating the high-temperature vapour line by Monte Carlo, *Molec. Phys.* 37: 211-221.

Alder, B.J. and T.E. Wainwright, 1959. Studies in molecular dynamics. I. general method, *J. Chem. Phys.*, 31: 459-466.

Baker, L.C.W. and T.F. Anderson, 1957. Some phase relationships in the three-component liquid system CO_2-H_2O-C_2H_5OH at high pressures, *J. Amer. Chem. Soc.*, 80:, 2071-2074

Barker, J.A and D.J. Henderson, 1967. Perturbation theory and equation of state for fluids. II. A successful theory of liquids. *J. Chem. Phys.*, 47: 4714-4721.

Barker, J.A., P.J. Leonard and A. Pompe, 1966. Fifth virial coefficients, *J. Chem. Phys.*, 44: 4206-4211.

Beegle, B.L , M. Modell and R.C. Reid, 1974. Legendre transforms and their application in thermodynamics, *AIChE J.*, 20: 1194-1200.

Binder, K. 1979. Chapter 1 in "Monte Carlo methods in statistical physics", *Topics Curr. Phys.*, 7: 1-45.

Binder, K. and D. Stauffer, 1984. Chapter 1 in "Monte Carlo methods in statistical physics", *Topics Curr. Phys.*, 35: 1-36.

Callen, H.B., 1960. "Thermodynamics", Wiley, New York.

Chaudhry, M.M., H.C. van Ness and M.M. Abbott, 1980. Excess thermodynamic functions for ternary systems. 6. Total-pressure data and G^E for acetone-ethanol-water at 50 °C, *J. Chem. Eng. Data*, 25: 254-257.

Coan, C.R. and A.D. King, Jr., 1971. Solubility of water in compressed carbon dioxide, nitrous oxide, and ethane. Evidence of hydration of carbon dioxide and nitrous oxide in the gas phase, *J. Am. Chem. Soc.* 93: 1857-62.

Cotterman, R.L., B.J. Schwartz and J.M. Prausnitz, 1985. Molecular thermodynamics for fluids at high and low densities. Part 1. Pure fluids containing small or large molecules, *AIChE J.*, submitted for publication.

Cotterman, R.L. and J.M. Prausnitz, 1985. Molecular thermodynamics for fluids at high and low densities. Part 2. Phase equilibria for mixtures containing components with large differences in molecular size or potential energy, *AIChE J.*, submitted for publication.

Debenedetti, P.G.,1984. Diffusion and mass transfer in supercritical fluids, Ph.D. Dissertation, Massachusetts Institute of Technology, Cambridge, MA.

Debenedetti, P.G., 1986. On the relationship between principal fluctuations and stability coefficients in multicomponent systems, *J. Chem. Phys.*, 84: 1778-1787.

De Oliveira, M.J., 1979. private communication to J.S. Rowlinson.

DiAndreth, J.R. and M.E. Paulaitis, 1985. Multiphase behavior in ternary systems at elevated pressures. *Amer. Chem. Soc. Division Fuel Chem. Prepr.*, 30: 57-61.

DiAndreth, J.R., 1985. "Multiphase behavior in ternary fluid mixtures", Doctoral Dissertation, Department of Chemical Engineering, University of Delaware, Newark, DE.

Diepen, G.A.M. and F.E.C. Scheffer, 1948. On critical phenomena of saturated solutions in binary systems. *J. Am. Chem. Soc.*, 70: 4081-85.

Dietz, W.A., 1967. Response factors for gas chromatographic analyses, *J. Gas Chrom.* 5: 68-71.

Elgin, J.C. and J.J. Weinstock, 1959. Phase equilibrium at elevated pressures in ternary systems of ethylene and water with organic liquids. Salting out with a supercritical gas. *J. Chem. Eng. Data*, 4: 3 - 12.

Evelein, K.A., R.G. Moore and R.A. Heidemann, 1976. Correlation of the phase behavior in the systems hydrogen sulfide - water and carbon dioxide -water, *Ind. Eng. Chem. Process Des. Dev.*, 15, 423-428.

Fincham, D., N. Quirke, D.J. Tildesley, 1986. Computer simulation of molecular liquid mixtures. I. A diatomic Lennard-Jones model mixture for CO_2/C_2H_6, *J. Chem. Phys.*, 84: 4535-4546.

Fixman, M., 1983. Direct simulation of the chemical potential, *J. Chem. Phys.* 78: 4223-4226.

Fleck, R.N., 1967. "Ternary fluid-phase equilibria at high pressures with one normally gaseous component", Doctoral Dissertation, University of California, Berkeley, CA.

Francis, A.W., 1954. Ternary systems of liquid carbon dioxide, *J. Phys. Chem.* 58: 1099-1114.

Gibbs, J.W. 1876. On the equilibrium of heterogeneous substances. Reprinted in "The collected works of J. Willard Gibbs", vol. I, Yale University Press, 1948.

Gierycz, P. and K. Nakanishi, 1984. Local composition in binary mixtures of Lennard-Jones fluids with differing sizes of components, *Fluid Phase Equilibria* 16: 255-273.

Gilbert, M.L. and M.E. Paulaitis, 1986. Gas-liquid equilibrium for ethanol-water-carbon dioxide mixtures at elevated pressures, *J. Chem. Eng. Data*, 31: 296-298.

Goral, M., A. Maczynski, G. Schmidt and H. Wenzel, 1981. Vapor-liquid equilibrium calculations in binary systems of hydrocarbons + related compounds not containing oxygen. Comparison between methods using equations of state and activity coefficients, *Ind. Eng. Chem. Fundam.*, 20: 267-277.

Gray, C.G. and K.E. Gubbins, 1984. "Theory of molecular fluids", vol 1, Clarendon Press, Oxford.

Gubbins, K.E. and C.H. Twu, 1977a. Thermodynamics of polyatomic fluid mixtures - I. Theory, *Chem. Eng. Sci.* 33: 863-878.

Gubbins, K.E. and C.H. Twu, 1977b. Thermodynamics of polyatomic fluid mixtures - II. Polar, quadrupolar and octopolar mixtures, *Chem. Eng. Sci.* 33: 863-878.

Gubbins, K.E., 1983. Equations of state - New theories, *Fluid Phase Equilibria*, 13: 35-57.

Hannay, J.B., 1880. On the solubility of solids in gases, *Proc. Roy. Soc. (London)*, 30: 484-489.

Hannay, J.B. and J. Hogarth, 1879. On the solubility of solids in gases, *Proc. Roy. Soc. (London)*, 29: 324-326.

Hansen, J.P. and I.R. McDonald, 1976. "Theory of simple liquids", Academic Press, London.

Hansen, J.P. and L. Verlet, 1969. Phase transitions of the Lennard-Jones system, *Phys. Rev.* 184: 151-161.

Henderson, D., 1974. *Ann. Rev. Phys. Chem.*, 25: 461-483.

Henderson, D., 1979. *Adv. Chem. Ser.*, 182: 1-30.

Hill, T.L., 1956. "Statistical Mechanics", McGraw-Hill, New York.

Hirschfelder, J.O., C.F. Curtiss and R.B. Bird, 1954. "Molecular theory of gases and liquids", John Wiley, New York.

Huron, M.J. and J. Vidal, 1979. New mixing rules in simple equations of state for representing vapour-liquid equilibria of strongly non-ideal mixtures., *Fluid Phase Equilibria*, 3: 255-271.

Irani, C.A. and E.W. Funk, 1977. Separations using supercritical fluids, CRC Handbook: Recent development in separation science, CRC Press, Boca Raton, FL., Vol III, Part A, pp. 171-177.

Joffe J., G.M. Schroeder and D. Zudkevitch, 1970. Vapor-liquid equilibria with the Redlich-Kwong equation of state, *AIChE J.* 16: 496-498.

Joffe, J. and D. Zudkevitch, 1970. Prediction of liquid-phase enthalpies with the Redlich-Kwong equation of state, *Ind. Eng. Chem. Fundam.* 9: 545-548.

Katayama, T., K. Oghaki, G. Maekawa, M. Goto and T. Nagano, 1975. Isothermal vapor-liquid equilibria of acetone - carbon dioxide and methanol-carbon dioxide systems at high pressures, *J. Chem. Eng. Jpn.* 8: 89-92.

Kuk, M.S. and J.C. Montagna, 1983. Chapter 4 in Paulaitis et al. (ed.), "Chemical Engineering at Supercritical Fluid Conditions", Ann Arbor Science Publishers, Ann Arbor, Michigan, pp. 101-111.

Kumar, K. and R.C. Reid, 1986. Derivation of the relatioships between partial derivatives of Legendre transforms, *AIChE J.* 32: 1224-26.

Kurnik, R.T., S.J. Holla and R.C. Reid, 1982. Solubility of solids in supercritical carbon dioxide and ethylene, *J. Chem. Eng. Data* 26: 47-51.

Landau, L.D. and E.M. Lifshitz, 1980. "Statistical Physics", 3d ed., Part 1, Pergamon Press, Oxford.

Lieberwirth, I. and H Schuberth, 1979. Das isotherme Dampf-Flüssigkeits-Phasengleichgewichtsverhalten des Systems Aceton/Wasser bei 35 °C, *Z. phys. Chemie, Leipzig*, 260: 669-672.

London, F., 1930. *Z. phys. Chem. (B)*, 11: 222.

Lüdecke, D. and J.M. Prausnitz, 1985. Phase equilibria for strongly nonideal mixtures with an equation of state with density-dependent mixing rules. *Fluid Phase Equilibia.*, 22: 1 - 19.

Maitland, G.C., M. Rigby, E.B. Smith, and W.A. Wakeham, 1981. "Intermolecular Forces", Clarendon Press, Oxford.

Mathias, P.M., 1986. Personal communication (Air Products and Chemicals, Inc., Box 538, Alletown, PA 18105).

Mathias, P.M. and T.W. Copeman, 1983. Extension of the Peng-Robinson equation of state to complex mixtures: Evaluation of the various forms of the local composition concept, *Fluid Phase Equilibria* 13: 91-108.

Matous, J., J. Sobr, J.P. Novak and J. Pick, 1969. Solubility of carbon dioxide in water at pressures up to 40 atm, *Coll. Czech. Chem. Commun.* 34: 3982-85.

McHugh, M.A., M.W. Mallett, and J.P. Kohn, 1981. High Pressure Fluid Phase Equilibria of Alcohol - Water - Supercritical Solvent Mixtures, paper presented at the 1981 annual AIChE meeting, New Orleans, Louisiana, Nov. 9, 1981.

McQuarrie, D.A, 1976. "Statistical Mechanics", Harper-Row, New York.

Metropolis, N., A.W. Rosenbluth, M.N. Rosenbluth, A.H. Teller, and E. Teller, 1953. Equation of state calculations by fast computing machines, *J. Chem. Phys.*, 21(6): 1087-1092.

Modell, M. and R.C. Reid, 1983. "Thermodynamics and its applications", 2d ed., Prentice-Hall, Englewood Cliffs, N.J.

Mollerup, J., 1981. A note on excess Gibbs energy models, equations of state and the local composition concept, *Fluid Phase Equilibria*, 7: 121-138.

Morrison, G., 1981. Effect of water upon the critical points of carbon dioxide and ethane, *J. Phys. Chem.*, 85: 759 - 761.

Nicolas, J.J., K.E. Gubbins, W.B. Street, and D.J. Tildesley, 1979. Equation of state for the Lennard-Jones fluid, *Molec. Phys.*, 37: 1429-1454.

Oellrich L.R., Knapp H. and Prausnitz J.M., 1978. A simple perturbed-hard-sphere equation of state applicable to subcritical and supercritical temperatures, *Fluid Phase Equilibria*, 2: 163-171.

Panagiotopoulos, A.Z. and S. Kumar, 1985. A generalized technique to obtain pure component parameters for two-parameter equations of state, *Fluid Phase Equilibria*, 22: 77-88.

Panagiotopoulos, A.Z. and R.C. Reid, 1985. High pressure phase equilibria in ternary mixtures with a supercritical component, *Prepr. Pap. Amer. Chem. Soc. Division Fuel Chem.* 30: 46-56.

Panagiotopoulos, A.Z. and R. C. Reid, 1986a. On the relationship between pair-wise fluctuations and thermodynamic derivatives, accepted for publication, *J. Chem. Phys.*

Panagiotopoulos, A.Z. and R.C. Reid, 1986b. Multiphase high-pressure equilibria in ternary aqueous systems, accepted for publication, *Fluid Phase Equilibria.*

Panagiotopoulos, A.Z. and R.C. Reid, 1986c. New mixing rule for cubic equations of state for highly polar, asymmetric systems, Chap. 28 in K.C. Chao and R.L. Robinson, "Equations of state - Theories and applications", *Amer. Chem. Soc. Symposium Ser.*, 300: 571-582.

Panagiotopoulos, A.Z., U.W. Suter and R.C. Reid, 1986. Phase diagrams of non-ideal fluid mixtures from Monte Carlo simulation, accepted for publication, *Ind. Eng. Chem. Fundam.*

Paulaitis, M.E., M.L. Gilbert and C.A. Nash, 1981. Separation of Ethanol - Water Mixtures with Supercritical Fluids, paper presented at the 2nd World Congress of Chemical Engineering, Montreal, Canada.

Paulaitis, M.E., R.G. Kander and J.R. DiAndreth, 1984. Phase equilibria related to supercritical solvent extractions, *Ber. Bunsenges. Phys. Chem.*, 88: 869 - 875.

Paulaitis, M.E., V.J. Krukonis, R.T. Kurnik R.T. and R.C. Reid, 1983. Supercritical fluid extraction, *Rev. Chem. Eng.*, 1: 181-250.

Pemberton, R.C. and C.J. Mash, 1978. Thermodynamic properties of aqueous non-electrolyte mixtures. II. Vapour pressures and excess Gibbs energies for water+ethanol at 303.15 to 363.15 K determined by an accurate static method, *J. Chem. Thermodynamics* 10: 867-888.

Peng, D-Y. and D.B. Robinson, 1976. A new two-constant equation of state, *Ind. Eng. Chem. Fundam.*, 15: 59-64.

Powles, J.G., 1982. The computation of the chemical potential of a fluid, *Chem. Phys. Letters*, 86: 335-339.

Powles, J.G., W.A.B. Evans and N. Quirke, 1982. Non-destructive molecular-dynamics simulation of the chemical potential of a fluid, *Molec. Phys.* 46: 1347-1370.

Radosz, M., 1984. Variable-volume recirculation apparatus for measuring high-pressure fluid-phase equilibria, *Ber. Bunsenges. Phys. Chem.* 88: 859-862.

Randall, L.G., 1982. The present status of dense (supercritical) gas extraction and dense gas chromatography: Impetus for DGC/MS development, *Sep. Sci. Tech.*, 17: 1-118.

Redlich, O. and J.N.S. Kwong, 1949. On the thermodynamics of solutions. V. An equation of state. Fugacities of gaseous solutions, *Chem. Rev.*, 44: 233-243.

Reid, R.C., J.M. Prausnitz and T.K. Sherwood, 1977. "The properties of gases and liquids", 3d ed., McGraw-Hill, New York.

Renon, H. and J.M. Prausnitz, 1968. Local compositions in thermodynamic excess functions for liquid mixtures, *AIChE J.*, 14: 135-144.

Richon, D. and H. Renon, 1983. New methods of experimental determinations of volumetric properties and vapor-liquid equilibria at high pressures, *Fluid Phase Equilibria*, 14: 235-243.

Robinson, D.B., D.-Y. Peng and C.Y.-K. Chung, 1984. The Development of the Peng - Robinson Equation and its Application to Phase Equilibrium in a System containing Methanol, paper presented at the Annual AIChE meeting in San Fransisco, CA, November 1984. See also Peng, D.-Y. and D.B. Robinson, *Amer. Chem. Soc. Symposium Ser.*, 133: 393-414.

Romano, S. and K. Singer, 1979. Calculation of the entropy of liquid chlorine and bromine by computer simulation, *Molec. Phys.* 37: 1765-1772.

Rowlinson, J.S. and F.L. Swinton, 1982. "Liquids and liquid mixtures", 3d ed., Butterworth, London.

Schmidt G. and H. Wenzel, 1980. A modified van der Waals type equation of state, *Chem. Eng. Sci.*, 35: 1503-1512.

Schofield, P., 1966. Wavelength-dependent fluctuations in classical fluids. I. The long wavelength limit, *Proc. Phys. Soc.*, 88: 149-170.

Schultz, W.G. and J.N. Randall, 1970. Liquid carbon dioxide for selective aroma extraction, *Food Tech.*, 24: 94-98.

Scott, R.L. and P.H. van Konynenburg, 1970. Static properties of solutions. Van der Waals and related models for hydrocarbon mixtures. *Discuss. Faraday Soc.* 1970, 49: 87-97.

Semenova, A.I., E.A. Emel'yanova, S.S. Tsimmerman and D.S. Tsiklis, 1979. Phase equilibria in the methanol - carbon dioxide system, *Russ. J. Phys. Chem.*, 53: 1428-1430.

Shing, K.S. and K.E. Gubbins, 1981. The chemical potential from computer simulation. Test particle method with umbrella sampling, *Molec. Phys.* 43: 717-721.

Shing, K.S. and K.E. Gubbins, 1982. The chemical potential in dense fluids and fluid mixtures via computer simulation, *Molec. Phys.* 46: 1109-1128.

Shing, K.S. and K.E. Gubbins, 1983a. The chemical potential in non-ideal liquid mixtures. Computer simulation and theory, *Molec. Phys.* 49: 1121-1138.

Shing, K.S. and K.E. Gubbins, 1983b. A review of methods for predicting fluid phase equilibria: Theory and computer simulation, chapter 4 in

J.M. Haile and G.A. Mansoori (ed.), "Molecular-based Study of fluids", *Amer. Chem. Soc. Adv. Chem. Ser.*, 204: 73-106.

Shoen, M. and C. Hoheisel, 1984. Static and dynamic cross correlation in thermodynamically stable and unstable mixtures. I. A molecular dynamics simulation study using Lennard-Jones (12,6) pair potential functions with identical σ parameters, *Molec. Phys.* 53: 1367-1380.

Shvarts, A.V. and G.D. Efremova, 1970. Higher-order critical phenomena in the system ethanol-water-carbon dioxide, *Russ. J. Phys. Chem.*, 44: 614-615

Snedeker, R.A., 1955. "Phase equilibrium in systems with supercritical carbon dioxide", Ph.D. Dissertation, Princeton University, Princeton, NJ.

Soave, G., 1972. Equilibrium constants from a modified Redlich-Kwong equation of state, *Chem. Eng. Sci.* 27: 1197-1203.

Stryjek, R. and J.H. Vera, 1986a. PRSV - An improved Peng-Robinson equation of state with new mixing rules for strongly non-ideal mixtures, *Can. J. Chem. Eng.* 64: 334-40.

Stryjek, R. and J.H. Vera, 1986b. Vapor-liquid equilibrium of hydrochloric acid solutions with the PRSV equation of state, *Fluid Phase Equilib.*, 25: 279-90.

Todd, D.B., 1952. Ph.D. Dissertation, Princeton University, Princeton, N.J.

Topliss, R.J., D. Dimitrellis and J.M. Prausnitz, 1982. High-pressure vapor-liquid equilibria in ternary systems containing two immiscible liquids and one supercritical gas, paper presented at the Industrial Physical Chemistry Group meeting of the Royal Society of Chemistry, Faraday Division, Cambridge, U.K. September 13-15, 1982.

Torrie, G.M. and J.P. Valleau, 1977. Monte Carlo simulation of a phase-separating liquid miture by umbrella sampling, *J. Chem. Phys.* 66: 1402-1408.

Tsekhanskaya, Yu.V., M.B. Iomtev and E.V. Muskina, 1962. Solubility of napthalene in ethylene and carbon dioxide under pressure, *Russ. J. Phys. Chem.* 38: 1173-1176.

Tsekhanskaya, Yu.V., M.B. Iomtev and E.V. Muskina, 1964. Solubility of diphenylamine and napthalene in carbon dioxide under pressure, *Russ. J. Phys. Chem.* 36: 1177-1181.

Tsiklis, D.C., A.I. Kulikova and L.H. Shenderei, 1960. *Khim. Prom.*, 401-406.

Van der Waals, J.D., 1873. Over de continuiteit van den gas- en vloeistoftoestand. Doctoral dissertation, University of Leiden, The Netherlands.

Van Welie, G.S.A. and G.A.M. Diepen, 1961. The PTx model of the system ethylene-napthalene (III), *Rec. Trav. Chim.* 80: 673-680.

Weeks, J.D, D. Chandler and H.C. Anderson, 1971. Role of repulsive forces in determining the equilibrium structure of simple liquids, *J. Chem. Phys.* 54: 5237-5247.

Whiting, W.B. and J.M. Prauznitz, 1982. Equations of state for strongly nonideal fluid mixtures: application of local compositions toward density-dependent mixing rules, *Fluid Phase Equil.* 9: 119-147.

Widom, B., 1963. Some topics in the theory of fluids, *J. Chem. Phys.* 39: 2808-2812.

Wiebe, R. and V.L. Gaddy, 1941. Vapor phase composition of carbon dioxide-water mixtures at various temperatures and at pressures to 700 atmospheres, *J. Am. Chem. Soc.* 63: 475-77.

Wiebe, R., 1941. The binary system carbon dioxide-water under pressure, *Chem. Rev.* 29: 475-81.

Williams, D.F., 1981. Extraction with supercritical gases, *Chem. Eng. Sci.*, 36: 1769-1788.

Willson, R.C., 1987. Ph.D. Dissertation, Massachusetts Institute of Technology, Cambridge, MA (in preparation).

Willson, R.C., J.-F.P. Hamel and C.L. Cooney, 1986. The effect of supercritical solvents on growth and metabolism of *Propionibacterium freudenreichii*. *Appl. Environ. Microbiology*, to be submitted.

Wilson, G., 1964. Vapor-Liquid Equilibrium. XI. A new expression for the excess free energy of mixing, *J. Amer. Chem. Soc.*, 86: 127-130.

Wood, W.W., 1968. In H.N.V. Temperlay, J.S. Rowlinson and G.S. Rushbrooke, "Physics of simple liquids", North-Holland, Amsterdam, 115.

Yao, J., R.A. Greenkorn and K.C. Chao, 1982. Monte carlo simulation of the grand canonical ensemble, *Molec. Phys.* 46: 587-594.

Zawisza, A. and B. Malesinska, 1981. Solubility of carbon dioxide in liquid water and of water in gaseous carbon dioxide in the range 0.2-5 Mpa and at temperatures up to 473 K, *J. Chem. Eng. Data* 26: 388-391.

Zosel K., 1978. Separation with supercritical gases: Practical applications, *Angew. Chem. Int. Ed. Engl.* 17: 702-715.

APPENDIX A. PURE COMPONENT PARAMETER DETERMINATION FOR TWO-PARAMETER EQUATIONS OF STATE

When using the equation of state approach for determining phase equilibria in mixtures, as described in Section 2.3.4, a method must be devised to obtain the pure component parameters of the equations. The methods available from the literature for the pure component parameter evaluation are summarized below; a new method is then proposed, based on the technique of Joffe and Judkevitch (1970).

Corresponding States Approach.

One of the simplest ways to obtain a and b for a pure component is to use a general cubic equation of state (Eq. 2.7) with the thermodynamic critical point criteria for a pure material,

$$\left(\frac{\partial P}{\partial V} \right)_{T=T_{cr}} = \left(\frac{\partial^2 P}{\partial V^2} \right)_{T=T_{cr}} = 0 \qquad [A.1]$$

We can define two dimensionless parameters Ω_a and Ω_b so that

$$a_{cr} = \Omega_a \times (R^2 T_{cr}^2 / P_{cr}) \qquad [A.2]$$

$$b_{cr} = \Omega_b \times (R\, T_{cr} / P_{cr}) \qquad [A.3]$$

Application of Eqs. A.1 - A.3 then yields the following result:

$$3Z_{cr} - [1 - \Omega_b\ (u-1)\ ] = 0 \qquad [A.4a]$$

$$3Z_{cr}^2 - \Omega_b\ [w\Omega_b - u\Omega_b - u] - \Omega_a = 0 \qquad [A.4b]$$

$$Z_{cr}^3 - \Omega_b\ [w\Omega_b^2 + w\Omega_b + \Omega_a] = 0 \qquad [A.4c]$$

Z_{cr} is the critical compressibility. In principle, Eqs. A.4a through A.4c can be solved analytically to give

$$\Omega_a = \Omega_a(u,w)$$

$$\Omega_b = \Omega_b(u,w) \qquad [A.5]$$

$$Z_{cr} = Z_{cr}(u,w)$$

In the van der Waals EOS (u=w=0 in Eq. 2.7), it is assumed that a and b, as calculated at T_{cr} and P_{cr} are applicable at all temperatures. In general, however, to obtain better agreement with experimental data, Eqs. A.2 and A.3 are modified to apply at temperatures other than the critical point, i.e.,

$$a = \alpha\Omega_a \times (R^2 T_{cr}^2 / P_{cr}) \qquad [A.6]$$

$$b = \beta\Omega_b \times (RT_{cr}/P_{cr}) \qquad [A.7]$$

where α and β are functions of the reduced temperature, and frequently other component-dependent parameters such as the acentric factor ω. In most cases, at the critical point α=1 and β=1. Some values of α, β, Ω_a and Ω_b for a few of the common EOS are shown in Table A.1.

While Table A.1 could be expanded to include other cubic EOS, the point being emphasized is that there are many generalized, but approximate, techniques in use for estimation of a and b away from the critical point for a selected EOS. These methods were developed to obtain a good fit of saturation pressures and volumetric properties for a wide range of components and temperatures.

Direct Approach.

In many cases of interest, one has available the vapor pressure and saturated liquid molar volumes for the pure components over the temperature range of interest. Critical properties may be unknown or of questionable accuracy. This can especially be the case for compounds of low volatility. If vapor pressure and liquid volume data are available, then it is possible to use these along with Eq. 2.7 to obtain values of a and b at each temperature. Joffe and Zudkevitch (1970) and Zudkevitch et al.(1970) developed a procedure wherein data on vapor pressure and liquid volume were

Table A.1 Parameters for some common cubic equations of state

Equation of State	u	w	Ω_a	Ω_b	Z_c	α	β
van der Waals (1873)	0	0	27/64	1/8	3/8	1	1
Redlich-Kwong (1949)	1	0	$[9(2^{1/3}-1)]^{-1}$	$\frac{2^{1/3}-1}{3}$	1/3	$T_r^{-1/2}$	1
Soave (1972)	1	0	$[9(2^{1/3}-1)]^{-1}$	$\frac{2^{1/3}-1}{3}$	1/3	$[1+K_S(1-T_r^{1/2})]^2$	1
Peng-Robinson (1976)	2	-1	0.45724	0.0778	0.308	$[1+K_{PR}(1-T_r^{1/2})]^2$	1

$$K_S = 0.480 + 1.574\,\omega - 0.176\,\omega^2$$

$$K_{PR} = 0.37464 + 1.54226\,\omega - 0.26992\,\omega^2$$

used to obtain temperature-dependent values for a and b. Their technique involved the formulation of the criterion of phase equilibrium between the liquid and the vapor, i.e.,

$$f_V = f_L \qquad [A.8]$$

Eq. A.8 was then solved along with Eq. 2.7 using a Newton-Raphson technique, in order to obtain values for a and b that would reproduce the saturated liquid volume and vapor pressure at the temperature of interest. Their procedure is widely used (see for example Oellrich et al., 1978), but the need to solve a system of non-linear equations for each component at each temperature somewhat limits its usefulness.

New method

The technique discussed below (Panagiotopoulos and Kumar, 1985) is an extension of the technique of Joffe and Zudkevitch (1970), and allows one to determine component values of a and b for any two parameter EOS, given the vapor pressure and the liquid volume of a component at the temperature of interest. The results can be put in an analytic, substance-independent form, in contrast to the method of Joffe and Zudkevitch.

A pressure explicit, two parameter EOS can be written as:

$$P = P(V, RT; a,b) \qquad [A.9]$$

where a and b are temperature dependent parameters. For the particular form given in Eq. 2.7, parameter a has the units of (mass) $\times$ (length)^5 $\times$ (time)$^{-2}$ $\times$ (mole)$^{-2}$ and b has the units of (length)^3 $\times$ (mole)$^{-1}$, but for a different form of the EOS, the parameters will have different dimensions. From dimensional analysis of Eq. 2.7 the minimum number of dimensionless groups to reduce this equation to a dimensionless form is three. We have chosen:

$$\epsilon = bP/RT \qquad [A.10]$$

$$\eta = aP/(RT)^2 \qquad [A.11]$$

$$Z = PV/RT \qquad [A.12]$$

For an EOS of different form, the choice of the dimensionless groups may have to be modified, but the groups shown above are valid for most of the common forms of the currently available two-parameter EOS.

Using these groups, Eq. A.9 becomes:

$$g_1(\epsilon,\eta,Z) = 0 \qquad [A.13]$$

Any two parameter EOS can be reduced to the form represented by Eq. [A.14], with an appropriate choice for the dimensionless groups. All thermodynamic properties that can be derived from Eq. A.9 may also be expressed in terms of ϵ, η, and Z, when non-dimensionalized in an appropriate way. For example, for the fugacity of a pure substance,

$$\ell n(f/P) = \ell n\ \nu = g_2\ (\epsilon,\eta,Z) \qquad [A.14]$$

If the pure component is in a state at which the vapor and the liquid are at equilibrium, Eq. A.13 must have at least two real roots for Z, one of which can be assigned to the saturated liquid state and the other to the saturated vapor state. In addition, the fugacities of the two phases must be equal. These conditions result in the following system of non linear equations:

$$g_1(\epsilon,\eta,Z_L) = 0 \qquad [A.15a]$$

$$g_1(\epsilon,\eta,Z_V) = 0 \qquad [A.15b]$$

$$g_2(\epsilon,\eta,Z_L) = g_2(\epsilon,\eta,Z_V) \qquad [A.15c]$$

where Z_L and Z_V refer to the compressibility of the saturated liquid and vapor phases.

Eqs. A.15a through A.15c form a system of equations with unknowns ϵ, η, Z_L and Z_V. If this system can be solved, then three of the unknowns may be obtained as a function of the fourth. A particular choice, in accordance with our objective to obtain the parameters of the EOS when saturated liquid volume and vapor pressure are known, is to express ϵ, η and Z_V in terms of Z_L:

$$\begin{aligned} \eta &= \eta(Z_L) \\ \epsilon &= \epsilon(Z_L) \\ Z_V &= Z_V(Z_L) \end{aligned} \qquad [A.16]$$

Up to this point, the analysis is valid for any two parameter EOS. When applied to the cubic form represented by Eq. 2.7, the equations corresponding to Eqs. A.13 and A.14 are:

$$Z^3 + Z^2[\epsilon(u-1) - 1\ ] + Z[\epsilon^2(w-u) - u\epsilon + \eta] - (w\epsilon^3 + w\epsilon^2 + \epsilon\eta) = 0 \qquad [A.17]$$

$$\ell n\ \nu = Z - 1 - \ell n(Z - \epsilon) + (\eta/\epsilon q)\ \ell n\ (2Z+u\epsilon-\epsilon q/2Z+u\epsilon+\epsilon q) \qquad [A.18]$$

where $q = (u^2 - 4w)^{1/2}$

For any value of Z_L up to Z_{cr}, once an EOS of the form of Eq. 2.7 is selected to define u and w, one can employ numerical methods to obtain ϵ and η. This only needs to be done once for any particular two-parameter equation of state, since the results are substance independent.

Using this method, we carried out the calculations for the van der Waals form (u=w=0), the Redlich-Kwong or Soave form (u=1,w=0) and the Peng-Robinson form (u=2, w=1) of cubic EOS. In Figures A.1 and A.2, $\ell n\epsilon$ and η/ϵ are shown as functions of ℓnZ_L for the three forms of Eq. 2.7 listed above. From Figure A.1 it is clear that $\ell n\epsilon$ is an almost linear function of ℓnZ_L, except in the critical region. A more interesting fact is that in the same region the curves for the three EOS considered, essentially coincide (at the scale of the graph), leading to the conclusion that at low vapor pressures the "volume parameter", b, is EOS independent to a good approximation. For example at $Z_L \sim 10^{-4}$, the variation among the three EOS is less than four percent.

In Figure A.2, η/ϵ is again a nearly linear function of ℓnZ_L except close to the critical point.

It is important to note that the values of ϵ and η obtained by the numerical solution of Eqs. 16a through 16c approach the values Ω_b and Ω_a respectively, as the compressibility approaches Z_{cr}.

In order to facilitate the use of the numerical results, ϵ and η need to be obtained as analytical functions of Z_L. A standard least squares regression technique was used to obtain polynomial approximations to $\epsilon(Z_L)$ and $\eta(Z_L)$ functions. The final form of the correlation selected was based on the following observations:

a. It was found that expressing $\epsilon/(Z_L - \epsilon)$ and η/ϵ as a power series in $\ell n\ Z_L$ was superior to any of the other correlating schemes attempted.
b. It was found that a single polynomial function of a reasonable order, could not give sufficiently accurate results for the whole range of Z_L desired ($7\times10^{-13} \leq Z_L \leq Z_{cr}$). The polynomial fitting was thus performed in two parts, one for low Z_L and the other for higher Z_L, up to and including the predicted value of Z_{cr}.

The coefficients of the polynomial expansions are listed in Table A.2.

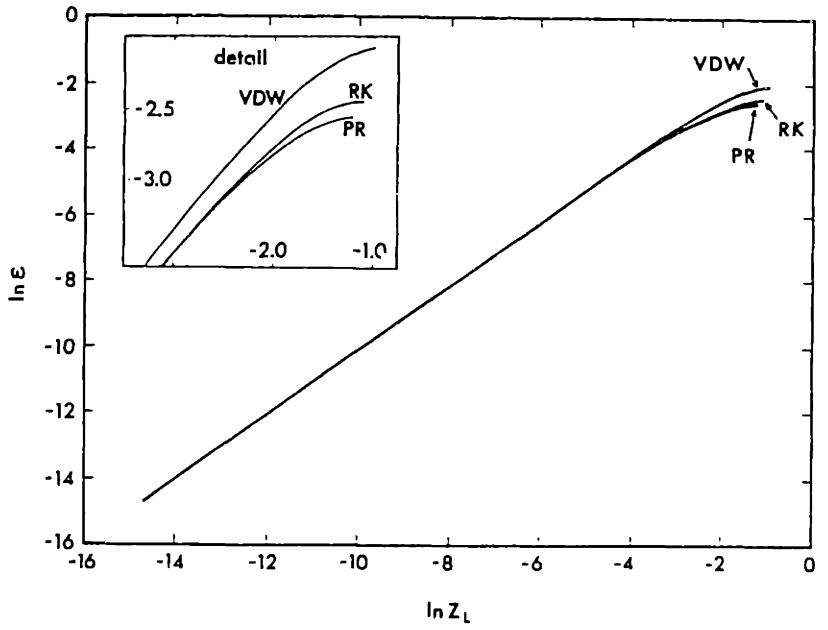

Figure A.1 *The dependence of $\ell n\epsilon$ on ℓnZ_L for the van der Waals (VDW), Redlich-Kwong or Soave (RK) and Peng-Robinson (PR) forms of the general cubic EOS.*

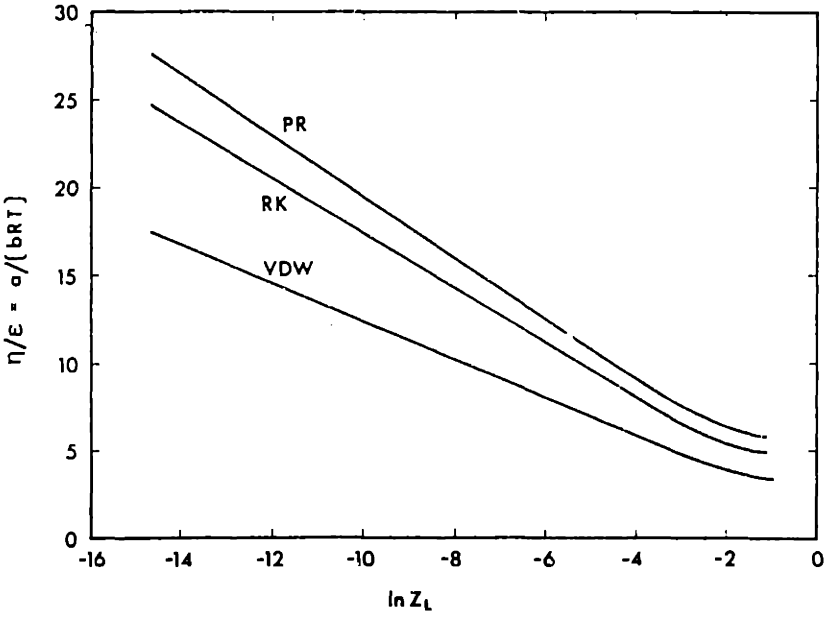

Figure A.2 *The dependence of η/ϵ on ℓnZ_L for the van der Waals (VDW), Redlich-Kwong or Soave (RK) and Peng-Robinson (PR) forms of the general cubic EOS.*

In order to use the table, one needs to know the vapor pressure and liquid volume of a component at a given (subcritical) temperature. One can then calculate Z_L as

$$Z_L = P_{VP}V_L/RT$$

and use Table A.2 to obtain ϵ and η. The parameters a and b are then easily calculated from equations A.10 and A.11.

Limitations

Cubic EOS with two parameters cannot produce a substance dependent value for Z_{cr}. Also, the phase coexistence curve tends to flatten in a non-analytic fashion in the critical region, a feature that that cannot be captured by any analytic EOS. The first fact implies that in most cases the value of Z_{cr} predicted by the EOS will be incorrect; and the second fact suggests that large divergences in the values for the a and b parameters in the vicinity of the critical point are needed to follow the saturated liquid volume changes in this regime.

The difference between the true critical compressibility of a substance and the value for Z_{cr} predicted by an EOS, also results in a "shift" of the critical point, when the new method is applied close to the critical temperature of a substance. That is, the condition $Z_L=Z_V$ is no longer valid at $T=T_{cr}$ for the new method. For this reason, use of the new method is not recommended at the immediate vicinity of the critical point.

Notation specific to Appendix A

α temperature functionality of parameter a ($\alpha = a/a_c$)
β temperature functionality of parameter b ($\beta = b/b_c$)
ϵ dimensionless b parameter, $\epsilon = bP/RT$
η dimensionless a parameter, $\eta = aP/(RT)^2$)
ν pure component fugacity coefficient
Ω_a η at the critical point
Ω_b ϵ at the critical point
ω acentric factor

Table A.2 Approximate expressions for the functions $\epsilon(Z_L)$ and $\eta(Z_L)$

$$\epsilon = Z_L \cdot \frac{\sum_i [\, A_i \cdot (\ell n\, Z_L)^i \,]}{1 + \sum_i [\, A_i \cdot (\ell n\, Z_L)^i \,]} \qquad \eta = \epsilon \cdot \sum_i [\, B_i (\ell n\, Z_L)^i \,]$$

a. van der Waals Form ($u = w = 0$, $Z_{cr} = 0.375$)

i	$6.91 \cdot 10^{-13} \le Z_L \le 0.011$		$0.011 \le Z_L \le Z_{cr}$	
	A_i	B_i	A_i	B_i
0	-.844962	1.28092	-.125484	3.89522
1	-1.15067	-1.17014	-.471148	1.32552
2	$-2.50956 \cdot 10^{-3}$	$-5.21032 \cdot 10^{-3}$	.182880	.966997
3	-	$-6.81575 \cdot 10^{-5}$	$1.61945 \cdot 10^{-2}$	.178266
4	-	-	-	$1.26439 \cdot 10^{-2}$

b. Redlich-Kwong (or Soave) Form ($u = 1$, $w = 0$, $Z_{cr} = 0.333$)

i	$6.91 \cdot 10^{-13} \le Z_L \le 0.011$		$0.011 \le Z_L \le Z_{cr}$	
	A_i	B_i	A_i	B_i
0	-.874084	1.50479	$-3.66182 \cdot 10^{-2}$	5.88848
1	-.827262	-1.66630	-.203841	2.07104
2	$-1.74216 \cdot 10^{-3}$	$-6.30280 \cdot 10^{-3}$	.147671	1.31927
3	-	$-7.68315 \cdot 10^{-5}$	$1.19456 \cdot 10^{-2}$	.226604
4	-	-	-	$1.52897 \cdot 10^{-2}$

c. Peng-Robinson Form ($u = 2$, $w = -1$, $Z_{cr} = 0.308$)

i	$6.91 \cdot 10^{-13} \le Z_L \le 0.011$		$0.011 \le Z_L \le Z_{cr}$	
	A_i	B_i	A_i	B_i
0	-1.21190	1.82378	$2.14469 \cdot 10^{-2}$	7.09646
1	-.918850	-1.84430	$-5.87391 \cdot 10^{-2}$	2.41021
2	$-1.91042 \cdot 10^{-3}$	$-5.75993 \cdot 10^{-3}$	.195961	1.41294
3	-	$-2.90784 \cdot 10^{-5}$	$1.53575 \cdot 10^{-2}$	.229028
4	-	$8.43108 \cdot 10^{-7}$	-	$1.47396 \cdot 10^{-2}$

APPENDIX B: PROGRAM DESCRIPTION - PHASE EQUILIBRIUM CALCULATIONS

The phase equilibrium programs need to perform a variety of different tasks, such as to calculate the fugacities of the components in a mixture when the pure component parameters and mixture compositions are known, to solve the non-linear system of equations describing phase equilibria (Eq. 2.7), to perform a calculation of a complete phase diagram for a range of pressures or mixture compositions, and to regress experimental data for the determination of the mixture parameters. It was decided that the development of a single program that performs all of these tasks would be unnecessarily complicated. Instead, a modular approach was chosen, that uses a relatively small number of common subroutines that perform recurring tasks (e.g. the fugacity coefficient calculations) and a number of main programs to perform the overall calculations. Table B.1 summarizes the modules used and their general function. Table B.2 gives a summary of the function of the main (calling) programs and their required subroutines.

The programs are implemented in the FORTRAN 77 programming language for an IBM XT or AT microcomputer (8088 or 80286 processor with an 8087 or 80287 arithmetic co-processor; the IBM Professional FORTRAN compiler that provides a full implementation of the FORTRAN 77 standard was used). The requirements for execution time are modest: a single calculation of phase equilibrium between two phases for a ternary system generally takes less that 2 seconds (the exact timing depends on the initial guess).

Complete listing of the programs (30 pp.) are available from the author and from Professor Robert C. Reid, Rm. 66-540, Massachusetts Institute of Technology, Cambridge, MA 02139.

Table B.1 Summary of subroutines

Name	Function
NEWTON	Solves a general non-linear system of equations
LU	Lower-upper decomposition of a matrix
BACK	Solution of a system of linear equations by back-substitution
CUBSOLV	Analytical solution of a general cubic equation
FUNCT	Provides the residuals of the phase-equilibrium equations
TRANSFOR	Transformation of the vector of component mole fractions from the domain [0,1] to [$-\infty$,$+\infty$] and the reverse
STABIL	Determination of stability coefficients for a mixture
INPTEMP	Input parameters and conditions
OUTP	Output results
MIXCALC	Mixture parameter calculation (mixing-rule dependent)
ALOGFUG	Fugacity coefficient calculation (mixing-rule dependent)
SETPAR	Set-up of parameters for optimization routines (mixing-rule dependent)
UPDPAR	Update parameters in optimization step (mixing-rule dependent)

Table B.2 Summary of calling programs

Name	Function
PHASE	Performs phase equilibrium calculations for a multicomponent system at constant temperature T, and a series of pressures (normally used for two-phase equilibrium calculations for binary systems and three-phase equilibrium calculations in ternary systems). Uses first-order continuation to provide initial guesses for the Newton-Raphson method.
PHASEX	Performs phase equilibrium calculations for a multicomponent system at constant temperature T and pressure P (normally used for two-phase equilibrium calculations in ternary systems). Uses first-order continuation to provide initial guesses for the Newton-Raphson method.
OPTIM	Parameter regression program. Uses a simple amoeba method to find an optimum set of parameters from experimental phase equilibrium data.

APPENDIX C: EXPERIMENTAL DATA

C.1 Chromatograph calibration

The chromatograph calibration procedure for the compounds of interest was performed as follows:

Water - organic compound mixtures

Mixtures with known concentrations of water and organic compound were prepared by weighing appropriate quantities of material in 25 ml glass jars, using a calibrated balance with a weighing accuracy of ±0.01 g. The error in composition because of the weighing uncertainties is negligible relative to the error due to impurities. The purity of the organic compounds used in this study was stated to be in the 99.5- 99.8 %w/w by the suppliers, with water being the major impurity, as determined by gas-liquid chromatographic analysis. Because of this, the purity of the pure components used for the preparation of the calibration mixtures was determined in the course of the calibration runs. This requires the unknown values of the relative response factors, and therefore an iterative calculation was necessary. Starting values for the response factors were obtained from Dietz (1967). The calibration runs were performed before, during and after the corresponding ternary system measurements to ensure chromatograph stability. No appreciable drift was observed.

In Table C.1, the calculated values of the response factors for each water - organic compound pair are shown, for the series of calibration mixtures used for the various liquid components. The response factors are based on a (arbitrary) value for the RRF for water of 33 (this value was selected for consistency with the values reported by Dietz, 1967). An average response factor for each component was then determined and is reported in Table C.2; this value was used for all the determination of composition of the ternary mixtures. The error in the calculated mole fractions using

these average response factors is also shown in Table C.1. The errors are usually below 2%, with an average error of approximately 0.6% in mole fraction.

Determination of the carbon dioxide and air response factors

Air may be present in our system either as an impurity accompanying CO_2, or as a result of inadequate purging or degassing. The response factors between air and CO_2 were determined by injecting known volumes of each gas at atmospheric pressure, using a precision gas syringe. The relative response factors were found to be identical to the values given by Dietz (1967) and are reported in Table C.2.

Table C.1 Chromatograph calibration with water (1) - organic compound (2) mixtures

Compound	volume injected (μl)	concentration calc.† X_2	concentration true X_2	RRF‡	Error (true-calc.)
acetone	0.06	0.084	0.094	87	0.010
	1.00	0.087	0.094	91	0.006
	0.40	0.088	0.094	91	0.006
	0.20	0.102	0.094	108	-0.009
	0.20	0.307	0.313	96	0.006
	0.20	0.322	0.313	102	-0.009
	0.20	0.125	0.133	91	0.008
	0.20	0.127	0.133	92	0.007
	0.10	0.139	0.133	103	-0.005
	0.20	0.409	0.439	87	0.030
	0.10	0.412	0.439	88	0.027
	0.10	0.432	0.439	95	0.007
	0.20	0.449	0.439	102	-0.010
ethanol	0.20	0.061	0.063	76	0.002
	0.10	0.061	0.063	76	0.001
	0.20	0.062	0.063	77	0.001
	0.10	0.063	0.063	78	-0.000
	0.20	0.063	0.063	79	-0.001
	0.10	0.069	0.063	86	-0.006
	0.20	0.239	0.244	76	0.005
	0.10	0.249	0.244	80	-0.005

(continued on next page)

Table C.1 (continued)

Compound	volume injected (μl)	concentration calc.† X_2	concentration true X_2	RRF‡	Error (true-calc.)
ethanol	0.10	0.250	0.244	80	-0.006
	0.10	0.262	0.244	86	-0.018
	0.20	0.467	0.482	73	0.015
	0.20	0.470	0.482	74	0.012
	0.20	0.471	0.482	74	0.011
	0.20	0.473	0.482	75	0.009
	0.10	0.476	0.482	76	0.006
	0.10	0.483	0.482	78	-0.001
n-butanol	0.20	0.550	0.544	107	-0.006
	0.20	0.691	0.693	103	0.002
	0.20	0.534	0.544	100	0.009
	0.20	0.687	0.693	101	0.006
	0.50	0.900	0.889	118	-0.011
	0.30	0.900	0.889	118	-0.012
	0.50	0.012	0.010	123	-0.002
	0.50	0.011	0.010	112	-0.001
	0.20	0.548	0.549	104	0.001
	0.40	0.543	0.549	102	0.006
	0.20	0.887	0.857	138	-0.031
	0.30	0.883	0.857	132	-0.026
	0.40	0.007	0.005	145	-0.002
	0.20	0.017	0.012	144	-0.005
	0.20	0.017	0.012	146	-0.005
acetic acid	0.20	0.012	0.019	46	0.007
	0.20	0.090	0.100	65	0.010
	0.20	0.085	0.100	61	0.015
	0.20	0.089	0.100	64	0.011
	0.20	0.093	0.100	68	0.007
	0.17	0.894	0.907	63	0.014
	0.20	0.915	0.907	81	-0.008
	0.20	0.916	0.907	82	-0.009
	0.20	0.579	0.593	69	0.015
	0.20	0.611	0.593	79	-0.018
	0.10	0.610	0.593	78	-0.016
	0.20	0.118	0.118	73	0.000
	0.20	0.110	0.118	67	0.008
	0.20	0.115	0.118	71	0.004
	0.20	0.101	0.100	74	-0.001

(continued on next page)

Table C.1 (continued)

Compound	volume injected (μl)	concentration calc.† X_2	concentration true X_2	RRF‡	Error (true-calc.)
acetic acid	0.20	0.100	0.100	73	0.000
	0.20	0.019	0.019	69	0.001
	0.20	0.019	0.019	69	0.001
	0.20	0.090	0.100	65	0.010
butyric acid	0.20	0.723	0.791	83	0.068
	0.20	0.795	0.791	107	-0.003
	0.20	0.047	0.050	86	0.002
	0.20	0.053	0.050	85	-0.003
	0.20	0.043	0.050	69	0.007
	0.20	0.050	0.050	80	-0.000
	0.20	0.798	0.791	110	-0.007
	0.20	0.797	0.791	109	-0.005
	0.20	0.048	0.050	86	0.002
	0.20	0.429	0.441	95	0.012
	0.20	0.015	0.015	82	-0.000
	0.20	0.015	0.015	81	-0.000
	0.20	0.014	0.015	78	0.000
	0.20	0.431	0.441	96	0.009
	0.20	0.446	0.450	88	0.005
	0.20	0.431	0.441	96	0.010
	0.20	0.805	0.791	114	-0.014
	0.20	0.051	0.050	93	-0.001
	0.20	0.051	0.050	93	-0.002
	0.20	0.470	0.450	98	-0.020
	0.20	0.714	0.716	89	0.002
	0.20	0.723	0.716	104	-0.007
	0.20	0.804	0.791	114	-0.013
	0.20	0.050	0.050	90	-0.000
	0.20	0.050	0.050	91	-0.001
	0.20	0.051	0.050	92	-0.001
	0.20	0.814	0.791	116	-0.023
	0.20	0.714	0.716	99	0.001

† Calculated using the final average values for the relative response factors shown in Table C.2.

‡ RRF: calculated value for relative response factor on a molar basis (water = 33). The final average values of the relative response factors are shown in Table C.2.

The problem of determining the relative response factors between a volatile and non-volatile component is more complicated, since it is more difficult to prepare and sample a mixture of known composition. For the determination of these response factors, an indirect approach was used. We obtained equilibrium data for the binary systems acetone - carbon dioxide (Table C.3) and methanol - carbon dioxide, using the response factors reported by Dietz for the initial chromatographic analyses. We then compared the results with literature values, obtained with a direct technique (Katayama et al., 1976; Semenova et al., 1979). An adjustment of the relative response factor for carbon dioxide was required to bring the measured and literature data into complete agreement. Since two different literature sources were used, this constitutes a reasonable consistency test for the values of the response factors used. Additional continuous tests of the validity of the relative response factors is provided by comparisons of the results close to the sides of the ternary diagrams (for example, water and CO_2 at low *n*-butanol concentrations for the ternary water - *n*-butanol - CO_2) with available literature results for the binary system CO_2 - water. Still, the main source of systematic error in our reported experimental results are the values of the relative response factors. The final values of the relative response factors thus obtained are presented in Table C.2.

Table C.2 Values of the relative response factors (molar basis)

Component	RRF used	Dietz (1967)
air	59	42
carbon dioxide	68	48
water	33	33
ethanol	78	72
acetone	98	86
n-butanol	104	117
acetic acid	73	-
n-butyric acid	90	-

C.2 Acetone - water - carbon dioxide

The primary experimental results for the system water - acetone-carbon dioxide are presented below in Tables C.3. and C.4. Each line in the table (and the tables that follow) represents the results of a single chromatographic analysis for the composition of one of the equilibrium phases. The conditions in the cell (temperature, pressure, number of coexisting phases) at the time of sampling are indicated on the table. In addition, the "run numbers" (runs for each ternary system at each temperature were numbered sequentially) are indicated under the column "run". During each such run, the total composition inside the cell was constant. Pressure variations occur because of slight changes in environmental conditions, or small leaks.

At pressures below approximately 70-80 bar, entrainment and adsorption on the supercritical phase sampling loop was a problem, resulting in abnormally high, and irreproducible, concentrations of water and organic compound in the supercritical phase. These results were eliminated from the table, since they are not considered reliable.

Table C.3 Experimental results for the mixture water(1) - acetone(2) - carbon dioxide(3) at 40 °C (313.1 K)

T °C	P bar	run[‡]	phase	M	mole fractions[†] X_1	X_2	X_3
39.72	10.29	1	LIQ	2	0.214	0.689	0.097
39.74	10.37	1	LIQ	2	0.218	0.691	0.091
40.10	10.45	22	LIQ	2	0.001	0.877	0.119
40.10	10.46	22	LIQ	2	0.001	0.877	0.119
40.20	10.48	57	LIQ	2	0.746	0.233	0.019
40.15	10.72	57	LIQ	2	0.745	0.235	0.020
39.73	10.81	8	LIQ	2	0.019	0.810	0.170
39.76	10.88	8	LIQ	2	0.021	0.809	0.171
39.74	10.89	8	SCF	2	0.000	0.073	0.925
40.10	14.48	24	LIQ	2	0.002	0.779	0.216
40.10	14.50	24	LIQ	2	0.002	0.777	0.219
40.10	14.48	24	LIQ	2	0.001	0.778	0.217
40.10	14.48	24	LIQ	2	0.002	0.778	0.217

(continued on next page)

Table C.3 (continued)

T °C	P bar	run†	phase	M	mole fractions† x_1	X_2	X_3
40.10	14.44	27	LIQ	2	0.937	0.054	0.009
40.10	14.52	27	LIQ	2	0.941	0.051	0.008
40.10	14.57	27	SCF	2	0.006	0.023	0.969
39.22	15.30	9	LIQ	2	0.032	0.734	0.233
39.22	15.31	9	LIQ	2	0.034	0.734	0.232
39.30	15.31	9	SCF	2	0.002	0.040	0.956
39.73	15.77	9	SCF	2	0.004	0.040	0.955
39.24	18.31	10	LIQ	2	0.031	0.691	0.277
39.24	18.28	10	LIQ	2	0.032	0.691	0.277
39.23	18.29	10	SCF	2	0.000	0.033	0.966
39.21	18.29	10	SCF	2	0.000	0.025	0.974
40.10	18.28	42	LIQ	2	0.875	0.115	0.010
40.10	18.30	42	LIQ	2	0.888	0.103	0.009
40.10	19.45	23	LIQ	2	0.001	0.772	0.224
40.10	19.45	23	LIQ	2	0.001	0.772	0.224
39.76	20.19	2	LIQ	2	0.160	0.503	0.315
39.80	20.38	2	LIQ	2	0.221	0.606	0.172
40.10	20.37	26	LIQ	2	0.947	0.043	0.010
40.10	23.93	28	SCF	2	0.003	0.014	0.981
40.10	23.96	28	SCF	2	0.002	0.015	0.981
40.10	23.98	28	SCF	2	0.004	0.017	0.978
40.10	24.03	28	LIQ	2	0.936	0.051	0.013
40.10	24.32	25	LIQ	2	0.004	0.889	0.103
40.10	24.31	25	LIQ	2	0.004	0.888	0.104
40.10	24.14	25	LIQ	2	0.006	0.646	0.346
40.10	24.12	25	SCF	2	0.003	0.039	0.955
40.10	24.14	25	SCF	2	0.019	0.032	0.946
39.25	24.31	11	LIQ	2	0.028	0.611	0.361
39.24	24.33	11	LIQ	2	0.027	0.611	0.362
39.24	24.35	11	SCF	2	0.006	0.020	0.973
39.23	24.39	11	SCF	2	0.000	0.028	0.971
40.20	24.63	58	SCF	2	0.006	0.023	0.937
40.20	24.72	58	LIQ	2	0.692	0.245	0.062
40.15	24.82	58	LIQ	2	0.697	0.247	0.055
40.20	29.27	59	LIQ2	3	0.291	0.455	0.250
40.20	29.37	59	LIQ2	3	0.297	0.452	0.248
40.15	29.40	59	SCF	3	0.005	0.025	0.954
40.20	29.51	59	LIQ	3	0.812	0.153	0.034
40.20	29.61	59	LIQ	3	0.808	0.154	0.037
39.23	29.65	12	SCF	2	0.000	0.025	0.974
39.23	29.68	12	SCF	2	0.000	0.033	0.967
39.23	29.71	12	LIQ	2	0.024	0.542	0.433

(continued on next page)

Table C.3 (continued)

T °C	P bar	run‡	phase	M	mole fractions† X_1	X_2	X_3
39.24	29.81	12	LIQ	2	0.023	0.540	0.436
39.80	33.37	3	LIQ	2	0.177	0.485	0.338
39.80	33.40	3	SCF	2	0.004	0.025	0.970
39.80	33.41	3	SCF	2	0.002	0.020	0.977
39.80	33.46	3	LIQ	2	0.172	0.478	0.349
39.24	35.15	13	SCF	2	0.000	0.025	0.974
39.26	35.16	13	SCF	2	0.000	0.021	0.978
39.24	35.26	13	LIQ	2	0.020	0.471	0.508
39.23	35.36	13	LIQ	2	0.021	0.473	0.506
40.15	35.80	60	LIQ2	3	0.179	0.435	0.380
40.15	35.86	60	SCF	3	0.007	0.020	0.906
40.15	35.88	60	SCF	3	0.005	0.017	0.965
40.15	35.95	60	LIQ	3	0.866	0.104	0.028
40.15	35.95	60	LIQ2	3	0.215	0.420	0.362
40.15	35.98	60	LIQ	3	0.862	0.108	0.029
40.10	36.78	43	LIQ	2	0.892	0.089	0.019
40.10	36.81	43	LIQ	2	0.887	0.090	0.024
40.10	36.91	43	SCF	2	0.002	0.023	0.974
40.10	37.01	43	SCF	2	0.002	0.023	0.975
40.10	38.58	30	SCF	2	0.008	0.013	0.978
40.10	38.68	30	SCF	2	0.002	0.014	0.984
40.10	38.83	30	LIQ	2	0.931	0.050	0.019
40.10	39.13	30	LIQ	2	0.923	0.056	0.021
39.80	41.10	4	SCF	2	0.002	0.015	0.982
39.80	41.23	4	SCF	2	0.002	0.020	0.976
39.80	41.46	4	LIQ	2	0.150	0.383	0.466
39.80	41.67	4	LIQ	2	0.131	0.390	0.479
39.24	42.55	14	LIQ	2	0.016	0.386	0.598
39.24	42.58	14	LIQ	2	0.016	0.386	0.598
39.24	42.59	14	SCF	2	0.000	0.018	0.981
39.24	42.71	14	SCF	2	0.000	0.017	0.982
40.10	42.86	44	SCF	3	0.002	0.017	0.980
40.10	42.94	44	SCF	3	0.004	0.019	0.976
40.10	42.97	44	SCF	3	0.003	0.018	0.978
40.10	43.07	44	LIQ	3	0.906	0.072	0.021
40.10	43.21	44	LIQ	3	0.909	0.072	0.019
40.10	43.21	44	LIQ	3	0.894	0.084	0.023
40.10	43.31	44	LIQ	3	0.907	0.073	0.020
40.10	46.11	35	LIQ2	3	0.135	0.333	0.532
39.25	48.22	15	SCF	2	0.000	0.019	0.980
39.24	48.33	15	SCF	2	0.000	0.017	0.982
39.28	48.36	15	SCF	2	0.000	0.022	0.978
39.28	48.36	15	LIQ	2	0.013	0.320	0.667

(continued on next page)

Table C.3 (continued)

T °C	P bar	run‡	phase	M	mole fractions† X_1	X_2	X_3
39.24	48.41	15	LIQ	2	0.013	0.319	0.668
39.80	48.73	5	SCF	2	0.002	0.016	0.982
39.80	48.81	5	SCF	2	0.002	0.021	0.977
39.80	48.85	5	LIQ	2	0.101	0.307	0.591
39.80	48.94	5	LIQ	2	0.114	0.302	0.584
40.10	49.51	45	SCF	3	0.001	0.016	0.983
40.10	49.61	45	SCF	3	0.003	0.017	0.980
40.10	49.61	45	SCF	3	0.002	0.017	0.981
40.10	49.66	45	LIQ	3	0.913	0.063	0.023
40.10	49.66	45	LIQ	3	0.917	0.060	0.022
39.26	53.53	16	SCF	2	0.000	0.015	0.985
39.26	53.60	16	LIQ	2	0.011	0.263	0.726
39.26	53.61	16	SCF	2	0.000	0.013	0.986
40.10	55.12	51	LIQ2	3	0.081	0.238	0.681
40.10	55.90	31	SCF	3	0.002	0.016	0.982
40.10	55.91	31	LIQ	3	0.918	0.054	0.028
40.10	55.93	31	LIQ	3	0.922	0.051	0.027
40.10	56.99	51	LIQ	3	0.919	0.052	0.030
40.10	56.62	51	LIQ2	3	0.139	0.226	0.635
40.10	56.47	51	LIQ2	3	0.099	0.234	0.667
40.12	56.28	51	SCF	3	0.003	0.015	0.982
40.10	56.32	51	SCF	3	0.001	0.008	0.990
40.10	57.06	46	LIQ	3	0.928	0.045	0.027
40.10	57.54	36	LIQ	3	0.928	0.046	0.026
40.10	57.54	36	LIQ	3	0.936	0.041	0.023
40.10	57.61	36	LIQ	3	0.938	0.040	0.023
40.10	57.31	36	LIQ2	3	0.108	0.222	0.670
40.10	57.31	36	LIQ2	3	0.153	0.208	0.639
40.10	57.51	36	SCF	3	0.001	0.016	0.982
40.10	57.61	36	SCF	3	0.002	0.015	0.982
40.10	57.51	34	LIQ	3	0.934	0.041	0.025
40.10	55.97	34	LIQ	3	0.939	0.036	0.025
40.10	58.07	34	LIQ	3	0.938	0.039	0.023
40.10	56.31	34	LIQ2	3	0.137	0.222	0.640
40.10	57.47	33	LIQ	2	0.951	0.026	0.023
39.80	56.31	6	LIQ	2	0.086	0.225	0.688
39.80	56.23	6	LIQ	2	0.073	0.232	0.694
39.80	56.56	6	SCF	2	0.001	0.015	0.984
40.10	58.15	32	SCF	2	0.003	0.010	0.986
40.10	58.36	32	SCF	2	0.001	0.023	0.974
40.10	58.46	32	SCF	2	0.001	0.013	0.986
40.10	58.52	32	SCF	2	0.001	0.013	0.985
40.10	58.63	32	LIQ	2	0.940	0.035	0.025

(continued on next page)

Table C.3 (continued)

T °C	P bar	run‡	phase	M	mole fractions† X_1	X_2	X_3
40.10	58.68	32	LIQ	2	0.935	0.038	0.027
40.10	58.72	32	LIQ	2	0.941	0.035	0.025
39.27	59.13	17	SCF	2	0.000	0.015	0.984
39.29	59.19	17	SCF	2	0.000	0.017	0.983
39.26	59.19	17	LIQ	2	0.007	0.203	0.790
39.26	59.50	17	LIQ	2	0.008	0.202	0.790
40.10	60.80	52	LIQ2	3	0.083	0.199	0.718
40.10	60.80	52	LIQ2	3	0.145	0.183	0.672
40.10	60.80	52	LIQ2	3	0.116	0.195	0.688
40.10	60.90	52	LIQ2	3	0.129	0.188	0.683
40.10	60.95	52	LIQ	3	0.939	0.039	0.022
40.10	61.16	52	SCF	3	0.002	0.015	0.983
40.10	61.16	52	SCF	3	0.005	0.015	0.979
40.10	61.22	52	LIQ	3	0.945	0.034	0.021
39.80	62.09	7	SCF	2	0.002	0.014	0.984
39.80	62.18	7	SCF	2	0.002	0.017	0.981
39.80	62.23	7	LIQ	2	0.060	0.171	0.769
39.80	62.28	7	LIQ	2	0.053	0.169	0.777
40.10	63.31	37	LIQ2	3	0.112	0.160	0.728
40.10	63.31	37	LIQ2	3	0.140	0.155	0.706
40.10	63.31	37	LIQ2	3	0.144	0.155	
40.10	63.81	37	SCF	3	0.001	0.015	0.984
40.10	64.01	37	SCF	3	0.002	0.015	0.983
40.10	65.80	53	LIQ	3	0.940	0.034	0.025
40.10	65.80	53	LIQ	3	0.948	0.030	0.022
40.10	65.26	53	LIQ2	3	0.123	0.148	0.729
40.10	64.95	53	LIQ2	3	0.136	0.148	0.716
40.10	64.97	53	LIQ2	3	0.141	0.139	0.719
40.10	65.50	53	SCF	3	0.002	0.014	0.983
40.10	65.50	53	SCF	3	0.001	0.015	0.984
39.30	64.68	18	LIQ	2	0.005	0.147	0.848
39.32	64.68	18	LIQ	2	0.006	0.149	0.845
39.30	65.11	18	SCF	2	0.000	0.015	0.985
39.30	64.68	18	SCF	2	0.000	0.015	0.985
40.10	66.51	47	LIQ2	3	0.163	0.126	0.711
40.10	66.61	47	LIQ2	3	0.151	0.118	0.731
40.10	67.71	47	SCF	3	0.001	0.015	0.984
40.10	67.71	47	SCF	3	0.000	0.015	0.985
40.10	67.71	47	SCF	3	0.002	0.015	0.983
40.10	67.81	47	LIQ	3	0.942	0.029	0.029
40.10	68.01	47	LIQ	3	0.951	0.025	0.025
40.10	68.01	47	LIQ	3	0.942	0.030	0.028

(continued on next page)

Table C.3 (continued)

T °C	P bar	run†	phase	M	mole fractions† X_1	X_2	X_3
39.10	68.92	19	SCF	2	0.000	0.014	0.986
39.10	68.96	19	SCF	2	0.000	0.014	0.986
39.10	69.03	19	SCF	2	0.000	0.014	0.985
39.10	69.09	19	LIQ	2	0.004	0.105	0.891
39.00	69.19	19	LIQ	2	0.004	0.105	0.891
40.12	69.36	54	LIQ	3	0.943	0.032	0.025
40.12	69.40	54	LIQ	3	0.944	0.032	0.025
39.10	72.67	20	LIQ	2	0.003	0.074	0.923
39.10	72.78	20	LIQ	2	0.003	0.073	0.924
39.10	72.78	20	SCF	2	0.000	0.014	0.986
39.10	72.88	20	SCF	2	0.000	0.014	0.986
40.10	74.41	48	LIQ2	3	0.023	0.069	0.907
40.10	74.51	48	LIQ2	3	0.016	0.069	0.915
40.10	74.51	48	LIQ2	3	0.043	0.067	0.891
40.10	75.01	48	SCF	3	0.002	0.015	0.983
40.10	75.01	48	SCF	3	0.002	0.014	0.983
40.10	75.21	48	LIQ	3	0.962	0.016	0.023
40.10	75.21	48	LIQ	3	0.956	0.019	0.026
39.14	76.37	21	SCF	2	0.000	0.014	0.986
39.12	76.39	21	SCF	2	0.000	0.014	0.985
39.10	76.49	21	LIQ	2	0.001	0.046	0.952
39.10	76.55	21	LIQ	2	0.002	0.045	0.953
40.10	77.22	49	LIQ2	3	0.035	0.047	0.917
40.10	77.82	49	LIQ	3	0.965	0.013	0.023
40.10	77.82	49	LIQ2	3	0.045	0.047	0.908
40.10	77.82	49	SCF	3	0.001	0.014	0.984
40.10	77.87	49	SCF	3	0.001	0.015	0.984
40.15	79.02	50	LIQ2	3	0.048	0.035	0.916
40.10	79.12	50	SCF	3	0.001	0.015	0.984
40.10	79.12	50	SCF	3	0.004	0.015	0.981
40.10	79.52	50	LIQ	3	0.967	0.011	0.022
40.10	79.52	50	LIQ2	3	0.049	0.035	0.915
40.10	79.62	50	LIQ	3	0.964	0.011	0.025
40.15	79.62	55	LIQ	2	0.950	0.026	0.024
40.15	79.62	55	SCF	2	0.023	0.145	0.832
40.15	79.72	55	LIQ	2	0.948	0.027	0.025
40.15	79.82	55	SCF	2	0.023	0.162	0.815
40.15	95.92	56	SCF	2	0.021	0.145	0.834
40.15	96.72	56	SCF	2	0.022	0.143	0.835
40.15	97.72	56	LIQ	2	0.948	0.026	0.026
40.15	99.32	56	LIQ	2	0.949	0.026	0.026

(continued on next page)

Table C.3 (concluded)

T °C	P bar	run‡	phase	M	mole fractions† X_1	X_2	X_3
40.17	115.01	38	LIQ	2	0.945	0.026	0.029
40.17	119.01	38	LIQ	2	0.947	0.027	0.026
40.10	127.51	38	LIQ	2	0.938	0.032	0.030
40.17	151.01	39	LIQ	2	0.947	0.025	0.028
40.17	154.51	39	LIQ	2	0.947	0.026	0.028
40.12	207.51	40	LIQ	2	0.940	0.028	0.033
40.12	213.51	40	LIQ	2	0.951	0.024	0.025
40.12	253.01	41	LIQ	2	0.942	0.027	0.031
40.15	263.01	41	LIQ	2	0.943	0.028	0.030

† The sum of the three mole fractions in usually slightly lower than 1.000, because of the presence of small quantities of impurities (usually air) detected during the chromatographic analysis.

‡ The serial number of the run is included so as to permit the determination of the tie-lines from the data given in the table. Data with the same run number were taken for a constant composition, temperature and pressure (small pressure variations did occur, as shown in the table) .

Table C.4 Experimental results for the mixture water(1) - acetone(2) - carbon dioxide(3) at 60 °C (333.1 K)

T °C	P bar	run‡	phase	M	mole fractions† X_1	X_2	X_3
60.00	8.62	39	LIQ	2	0.023	0.895	0.082
60.00	8.53	39	LIQ	2	0.032	0.879	0.089
60.00	19.47	1	LIQ	2	0.989	0.005	0.006
60.00	19.46	1	LIQ	2	0.990	0.005	0.006
60.05	20.04	28	LIQ	2	0.583	0.356	0.062
60.10	20.10	28	LIQ	2	0.581	0.360	0.060
60.00	20.29	23	LIQ	2	0.753	0.218	0.030
60.00	20.32	23	LIQ	2	0.753	0.218	0.030
60.10	20.31	17	LIQ	2	0.750	0.221	0.030

(continued on next page)

Table C.4 (continued)

T °C	P bar	run‡	phase	M	mole fractions† X_1	X_2	X_3
60.10	20.52	17	LIQ	2	0.744	0.225	0.031
60.00	21.10	40	LIQ	2	0.019	0.743	0.237
60.00	21.20	40	LIQ	2	0.020	0.753	0.227
60.00	30.00	41	LIQ	2	0.019	0.663	0.317
60.00	30.12	41	LIQ	2	0.018	0.658	0.324
60.00	38.56	22	LIQ	2	0.842	0.131	0.027
60.00	38.56	22	LIQ	2	0.841	0.131	0.028
60.00	38.25	7	SCF	2	0.004	0.020	0.972
60.00	38.55	7	SCF	2	0.012	0.013	0.975
60.00	39.08	7	LIQ	2	0.965	0.024	0.011
60.00	39.09	24	LIQ	3	0.793	0.164	0.044
60.00	39.15	24	LIQ2	3	0.394	0.402	0.204
60.00	39.15	24	LIQ2	3	0.394	0.399	0.207
60.00	39.09	24	LIQ	3	0.794	0.164	0.043
60.10	39.25	29	LIQ2	3	0.414	0.390	0.196
60.10	39.20	29	SCF	3	0.018	0.049	0.931
60.10	39.07	29	LIQ2	3	0.397	0.402	0.201
60.00	40.98	18	LIQ2	3	0.446	0.373	0.181
60.00	39.03	18	LIQ	3	0.795	0.164	0.042
60.00	39.03	18	LIQ2	3	0.437	0.380	0.183
60.00	39.03	18	SCF	3	0.015	0.036	0.948
60.00	38.96	18	LIQ	3	0.797	0.161	0.043
60.00	39.36	42	LIQ	2	0.017	0.568	0.415
60.00	39.50	42	LIQ	2	0.016	0.569	0.415
60.00	39.86	2	LIQ	2	0.982	0.006	0.012
60.00	40.54	2	LIQ	2	0.985	0.005	0.009
60.00	39.65	2	LIQ	2	0.984	0.005	0.010
60.00	39.52	2	SCF	2	0.010	0.005	0.984
60.00	40.74	12	LIQ	2	0.844	0.127	0.029
60.00	39.85	12	SCF	2	0.426	0.054	0.520
60.00	40.31	12	LIQ	2	0.845	0.129	0.026
60.00	42.49	36	LIQ2	2	0.401	0.477	0.122
60.00	41.49	36	LIQ2	2	0.432	0.487	0.082
60.00	42.49	36	LIQ	2	0.816	0.146	0.038
60.00	42.99	36	LIQ	2	0.813	0.149	0.039
60.00	49.28	43	SCF	2	0.001	0.068	0.928
60.00	49.25	43	SCF	2	0.001	0.064	0.932
60.00	49.32	43	LIQ	2	0.014	0.481	0.505
60.00	49.40	43	LIQ	2	0.014	0.479	0.507
60.00	51.36	31	LIQ	3	0.881	0.090	0.028
60.00	50.77	31	LIQ2	3	0.183	0.431	0.385

(continued on next page)

Table C.4 (continued)

T °C	P bar	run†	phase	M	mole fractions† X_1	X_2	X_3
60.00	50.77	31	LIQ2	3	0.180	0.405	0.414
60.00	51.31	31	LIQ	3	0.879	0.091	0.030
60.00	51.32	31	SCF	3	0.022	0.060	0.917
60.05	58.14	25	LIQ2	3	0.178	0.360	0.461
60.05	58.34	25	LIQ2	3	0.175	0.360	0.465
60.00	59.03	25	LIQ	3	0.903	0.070	0.027
60.00	59.15	8	LIQ	2	0.962	0.022	0.016
60.00	59.01	8	LIQ	2	0.961	0.023	0.016
60.00	59.01	8	SCF	2	0.009	0.014	0.978
60.00	59.06	3	LIQ	2	0.979	0.006	0.016
60.00	59.44	3	LIQ	2	0.976	0.006	0.018
60.00	58.78	3	SCF	2	0.007	0.020	0.973
60.05	59.33	19	SCF	3	0.006	0.030	0.964
60.00	59.00	19	LIQ2	3	0.166	0.358	0.476
60.00	59.88	19	LIQ	3	0.905	0.068	0.027
60.00	59.93	19	LIQ	3	0.904	0.068	0.028
60.00	60.02	44	SCF	2	0.001	0.043	0.955
60.00	60.03	44	SCF	2	0.001	0.042	0.955
60.00	60.67	13	LIQ	3	0.909	0.066	0.025
60.00	60.48	13	SCF	3	0.006	0.029	0.963
60.00	60.54	13	SCF	3	0.007	0.032	0.961
60.00	60.75	13	LIQ	3	0.909	0.066	0.025
60.00	64.39	37	LIQ	2	0.843	0.127	0.031
60.00	63.79	37	LIQ	2	0.839	0.131	0.030
60.00	59.49	37	LIQ2	2	0.298	0.421	0.280
60.00	58.39	37	LIQ2	2	0.297	0.432	0.271
60.00	68.97	32	LIQ2	3	0.114	0.297	0.589
60.00	68.67	32	LIQ2	3	0.121	0.303	0.576
60.00	71.07	32	LIQ	3	0.925	0.050	0.025
60.00	70.82	32	SCF	3	0.008	0.035	0.956
60.00	70.87	32	SCF	3	0.089	0.032	0.878
60.00	71.24	32	LIQ	3	0.925	0.049	0.026
60.00	70.68	45	LIQ	2	0.009	0.292	0.699
60.00	70.69	45	SCF	2	0.001	0.039	0.959
60.00	70.72	45	SCF	2	0.001	0.037	0.962
60.00	70.68	45	LIQ	2	0.008	0.299	0.693
60.00	79.43	20	LIQ	2	0.908	0.065	0.027
60.00	72.73	20	LIQ2	2	0.149	0.433	0.418
60.00	76.93	20	LIQ	2	0.908	0.065	0.027
60.00	74.48	20	LIQ2	2	0.140	0.386	0.474
60.00	79.91	14	LIQ	3	0.938	0.040	0.022

(continued on next page)

Table C.4 (continued)

T °C	P bar	run‡	phase	M	mole fractions† X_1	X_2	X_3
60.00	79.82	14	SCF	3	0.007	0.032	0.961
60.00	79.97	14	LIQ	3	0.939	0.038	0.023
60.00	78.02	14	LIQ2	3	0.081	0.242	0.677
60.00	78.02	14	LIQ2	3	0.097	0.227	0.676
60.00	79.72	14	SCF	3	0.005	0.032	0.962
60.00	80.58	46	SCF	2	0.001	0.057	0.941
60.00	80.64	46	LIQ	2	0.006	0.217	0.776
60.00	80.53	46	SCF	2	0.001	0.039	0.960
60.10	80.61	26	LIQ2	2	0.087	0.259	0.654
60.10	80.61	26	LIQ2	2	0.128	0.356	0.516
60.10	80.61	26	LIQ	2	0.911	0.062	0.027
60.00	80.46	9	SCF	2	0.005	0.017	0.978
60.00	81.60	9	LIQ	2	0.957	0.022	0.021
60.00	80.49	9	SCF	2	0.005	0.017	0.978
60.00	80.07	9	LIQ	2	0.957	0.021	0.022
60.00	81.93	4	SCF	2	0.003	0.005	0.991
60.00	82.01	4	LIQ	2	0.974	0.005	0.020
60.00	81.93	4	LIQ	2	0.979	0.005	0.017
60.00	81.92	4	SCF	2	0.004	0.005	0.990
60.00	89.88	47	SCF	2	0.001	0.045	0.953
60.00	89.70	47	SCF	2	0.000	0.043	0.956
60.00	90.07	47	LIQ	2	0.004	0.143	0.852
60.00	90.33	47	LIQ	2	0.004	0.143	0.853
60.00	93.03	33	LIQ	3	0.945	0.029	0.026
60.00	91.82	33	LIQ2	3	0.089	0.129	0.782
60.00	93.03	33	LIQ	3	0.946	0.028	0.025
60.00	93.03	33	SCF	3	0.009	0.046	0.944
60.00	93.03	33	SCF	3	0.011	0.047	0.942
60.00	91.82	33	LIQ2	3	0.079	0.126	0.795
60.00	94.21	48	LIQ	2	0.003	0.110	0.887
60.00	94.13	48	SCF	2	0.002	0.060	0.938
60.00	94.89	38	LIQ	2	0.848	0.122	0.030
60.00	96.49	38	LIQ	2	0.851	0.121	0.029
60.00	91.29	38	LIQ2	2	0.299	0.415	0.286
60.00	94.59	49	LIQ	2	0.003	0.106	0.891
60.00	94.39	49	LIQ	2	0.004	0.107	0.889
60.00	94.66	49	SCF	2	0.002	0.065	0.932
60.00	94.69	49	SCF	2	0.002	0.066	0.931
60.00	99.87	34	LIQ	2	0.958	0.020	0.022
60.00	98.57	34	SCF	2	0.015	0.072	0.913
60.00	98.57	34	SCF	2	0.014	0.072	0.913
60.00	99.84	34	LIQ	2	0.957	0.020	0.023

(continued on next page)

Table C.4 (concluded)

T °C	P bar	run‡	phase	M	mole fractions† X_1	X_2	X_3
60.00	101.49	10	LIQ	2	0.965	0.012	0.022
60.00	101.29	10	SCF	2	0.006	0.026	0.968
60.00	101.46	10	SCF	2	0.008	0.024	0.967
60.00	101.46	10	LIQ	2	0.965	0.014	0.021
60.00	100.67	15	SCF	2	0.033	0.161	0.806
60.00	101.92	15	LIQ	2	0.949	0.029	0.023
60.00	102.40	15	LIQ	2	0.946	0.030	0.024
60.00	101.22	15	SCF	2	0.049	0.226	0.725
60.00	102.42	5	SCF	2	0.004	0.007	0.985
60.00	102.48	5	LIQ	2	0.972	0.005	0.023
60.00	101.92	5	SCF	2	0.004	0.007	0.989
60.00	143.82	16	LIQ	2	0.952	0.025	0.023
60.00	146.73	16	LIQ	2	0.951	0.025	0.024
60.00	141.32	16	SCF	2	0.031	0.143	0.826
60.00	139.82	16	SCF	2	0.030	0.148	0.821
60.00	143.32	11	SCF	2	0.009	0.024	0.967
60.00	143.32	11	SCF	2	0.009	0.025	0.966
60.00	143.32	11	SCF	2	0.009	0.025	0.966
60.00	144.32	11	LIQ	2	0.969	0.007	0.024
60.00	143.82	11	LIQ	2	0.968	0.007	0.025
60.00	147.22	6	SCF	2	0.000	0.003	0.996
60.00	147.80	6	LIQ	2	0.976	0.002	0.021
60.10	158.51	27	LIQ	2	0.902	0.069	0.029
60.10	156.01	27	LIQ	2	0.903	0.069	0.028
60.10	153.01	27	SCF	2	0.136	0.353	0.510
60.10	151.01	27	SCF	2	0.132	0.356	0.513
60.00	155.02	35	SCF	2	0.152	0.365	0.483
60.00	154.02	35	LIQ	2	0.876	0.090	0.034
60.00	154.02	35	SCF	2	0.161	0.367	0.471
60.00	156.02	35	LIQ	2	0.876	0.090	0.035
60.05	155.03	21	SCF	2	0.152	0.362	0.485
60.05	157.03	21	SCF	2	0.150	0.364	0.487
60.00	163.03	21	LIQ	2	0.899	0.073	0.028
60.00	165.53	21	LIQ	2	0.896	0.073	0.031

†‡ See footnotes to Table C.3

C.3 *n*-Butanol - water - carbon dioxide

The methodology described previously in Section C.2 was followed for the presentation of the experimental results in this system in Tables C.5 and C.6. In addition, results from the density measurements using the vibrating tube density meter (as described in Section 4.1.1) are presented in the tables that follow.

Table C.5 Experimental results for the mixture water(1) - n-butanol(2) - carbon dioxide(3) at 40 °C (313.1 K)

T °C	P bar	run†	phase	M	mole fractions† X_1	X_2	X_3	density kg/m^3
39.98	2.61	22	LIQ2	2	0.527	0.471	0.002	834
39.98	2.65	22	LIQ	2	0.984	0.016	0.000	
39.98	2.68	22	LIQ	2	0.984	0.016	0.000	981
39.98	3.96	22	LIQ2	2	0.527	0.471	0.002	
39.98	18.60	5	LIQ	3	0.979	0.014	0.007	
39.98	18.20	5	LIQ2	3	0.467	0.476	0.057	839
39.98	18.40	5	LIQ	3	0.978	0.014	0.007	988
39.96	18.50	14	LIQ	2	0.044	0.862	0.094	
39.96	18.39	14	LIQ	2	0.044	0.870	0.086	807
39.91	19.19	25	SCF	2	0.012	0.009	0.966	
39.91	19.22	25	SCF	2	0.007	0.008	0.977	
39.91	19.10	25	LIQ	2	0.336	0.595	0.069	825
39.91	19.14	25	LIQ	2	0.323	0.610	0.066	
39.95	38.39	16	SCF	2	0.002	0.004	0.993	
39.95	38.52	16	LIQ	2	0.090	0.730	0.181	
39.95	38.48	16	LIQ	2	0.097	0.707	0.196	819
39.98	38.75	6	SCF	3	0.004	0.004	0.989	
39.98	39.22	6	LIQ	3	0.975	0.013	0.013	993
39.98	37.89	6	LIQ	3	0.974	0.013	0.013	
39.98	38.70	6	LIQ2	3	0.404	0.464	0.132	844
39.92	38.20	26	SCF	2	0.002	0.005	0.989	
39.92	38.25	26	SCF	2	0.002	0.005	0.989	
39.90	39.58	26	LIQ	2	0.335	0.551	0.114	
39.90	39.41	26	LIQ	2	0.324	0.538	0.138	836
39.90	38.34	26	LIQ	2	0.335	0.519	0.146	
39.96	38.94	15	LIQ	2	0.060	0.739	0.201	
40.08	58.25	1	LIQ	2	0.978	0.008	0.014	

(continued on next page)

Table C.5 (continued)

T °C	P bar	run‡	phase	M	mole fractions† X_1	X_2	X_3	density kg/m³
40.03	58.60	1	LIQ	2	0.978	0.008	0.013	
40.08	58.20	1	SCF	2	0.005	0.003	0.992	
40.08	58.08	1	SCF	2	0.003	0.002	0.995	
40.03	58.60	1	SCF	2	0.004	0.001	0.994	
40.03	58.70	1	LIQ	2	0.975	0.010	0.015	
39.92	58.53	27	LIQ	2	0.293	0.458	0.249	846
39.92	58.56	27	LIQ	2	0.288	0.468	0.245	
39.92	58.40	27	SCF	2	0.001	0.006	0.991	
39.98	59.30	7	LIQ	3	0.972	0.011	0.017	
39.98	58.40	7	SCF	3	0.002	0.013	0.983	
39.98	58.90	7	LIQ	3	0.968	0.013	0.019	999
39.98	58.40	7	SCF	3	0.002	0.003	0.992	
39.98	58.10	7	LIQ2	3	0.331	0.441	0.228	850
39.98	58.40	7	LIQ2	3	0.351	0.420	0.229	
39.95	58.87	17	LIQ	2	0.071	0.596	0.333	
39.95	60.11	18	LIQ	2	0.085	0.591	0.325	831
39.96	59.84	18	SCF	2	0.001	0.002	0.997	
39.96	60.14	18	SCF	2	0.001	0.005	0.994	
39.92	79.20	28	LIQ	2	0.188	0.337	0.474	
39.92	79.00	28	LIQ	2	0.199	0.338	0.463	849
39.92	79.40	28	SCF	2	0.003	0.006	0.989	
39.92	58.37	28	SCF	2	0.002	0.003	0.993	
39.92	79.40	28	SCF	2	0.003	0.008	0.989	
39.92	79.50	28	SCF	2	0.002	0.004	0.993	
39.98	77.60	8	LIQ2	3	0.216	0.340	0.444	
39.98	77.50	8	LIQ2	3	0.216	0.357	0.427	853
39.98	78.70	8	SCF	3	0.003	0.014	0.982	
39.98	78.80	8	SCF	3	0.003	0.006	0.991	
39.98	78.84	8	LIQ	3	0.966	0.011	0.023	1002
39.96	78.60	19	LIQ	2	0.044	0.296	0.660	827
39.96	78.40	19	SCF	2	0.001	0.006	0.992	
39.96	78.76	19	LIQ	2	0.045	0.294	0.661	
39.96	78.40	19	SCF	2	0.001	0.007	0.991	
40.08	79.66	2	LIQ	2	0.975	0.008	0.018	
40.08	79.31	2	SCF	2	0.003	0.005	0.992	
40.08	79.49	2	LIQ	2	0.975	0.008	0.018	
40.08	79.31	2	SCF	2	0.003	0.004	0.993	
39.96	80.49	20	LIQ	2	0.024	0.145	0.831	784
39.96	80.00	20	LIQ	2	0.031	0.172	0.797	
39.96	79.95	20	SCF	2	0.002	0.015	0.983	
39.96	79.91	20	SCF	2	0.002	0.009	0.988	
39.96	80.73	21	SCF	2	0.015	0.062	0.923	
39.96	80.72	21	LIQ	2	0.019	0.104	0.877	760

(continued on next page)

Table C.5 (continued)

T °C	P bar	run‡	phase	M	mole fractions† X_1	X_2	X_3	density kg/m³
39.96	80.74	21	SCF	2	0.010	0.067	0.923	
39.96	80.59	21	LIQ	2	0.016	0.095	0.889	
40.08	80.08	46	LIQ	2	0.099	0.278	0.623	825
40.08	80.80	46	SCF	2	0.016	0.077	0.908	
40.08	80.95	46	LIQ	2	0.093	0.274	0.633	
40.08	81.15	46	SCF	2	0.016	0.076	0.908	730
40.06	81.18	40	SCF	3	0.015	0.081	0.903	
40.05	81.29	40	LIQ	3	0.969	0.010	0.021	
40.05	81.10	40	SCF	3	0.022	0.072	0.906	
40.05	81.11	40	LIQ2	3	0.174	0.305	0.520	
40.03	80.80	40	LIQ	3	0.966	0.011	0.023	955
40.08	81.19	40	SCF	3	0.012	0.062	0.926	
40.05	81.10	40	LIQ2	3	0.172	0.314	0.514	832
39.90	81.45	10	LIQ3	4	0.045	0.046	0.908	
39.90	81.45	10	LIQ3	4	0.056	0.043	0.901	669
39.90	81.63	9	LIQ2	4	0.187	0.280	0.533	
39.91	81.40	9	LIQ	4	0.969	0.009	0.021	
39.91	81.45	9	LIQ2	4	0.168	0.285	0.547	
39.91	81.35	9	LIQ	4	0.966	0.011	0.023	1000
39.90	81.45	9	SCF	4	0.012	0.065	0.922	
39.90	81.48	9	LIQ2	4	0.160	0.289	0.551	846
40.08	81.40	41	LIQ	4	0.970	0.010	0.020	
40.08	81.56	41	SCF	4	0.014	0.066	0.920	
40.08	81.54	41	SCF	4	0.015	0.067	0.917	
40.08	81.92	41	LIQ2	4	0.155	0.297	0.548	
40.08	81.60	41	LIQ2	4	0.179	0.287	0.534	841
39.92	81.59	29	SCF	3	0.011	0.079	0.910	
39.92	81.68	29	SCF	3	0.012	0.066	0.921	
39.92	81.61	29	SCF	3	0.009	0.057	0.934	
39.92	81.68	29	LIQ	3	0.150	0.291	0.559	844
39.92	81.68	29	LIQ	3	0.151	0.291	0.558	
40.08	81.80	42	LIQ3	4	0.034	0.039	0.927	
40.08	81.80	42	LIQ3	4	0.036	0.039	0.926	
40.08	81.66	42	LIQ3	4	0.035	0.041	0.924	793
39.90	81.90	30	LIQ	2	0.970	0.010	0.020	999
39.90	81.50	30	LIQ	2	0.970	0.010	0.020	
39.90	81.90	30	SCF	2	0.283	0.402	0.315	
39.90	81.90	30	SCF	2	0.295	0.424	0.281	853
40.08	81.85	45	LIQ2	3	0.038	0.040	0.922	
40.08	81.99	45	SCF	3	0.024	0.085	0.890	
40.08	81.80	45	LIQ2	3	0.020	0.042	0.938	790
40.08	81.82	45	LIQ2	3	0.038	0.042	0.920	
40.08	81.95	45	LIQ	3	0.158	0.288	0.554	831
40.08	81.95	45	LIQ	3	0.158	0.292	0.550	

(continued on next page)

Table C.5 (continued)

T °C	P bar	run‡	phase	M	mole fractions† X_1	X_2	X_3	density kg/m³
40.08	81.93	45	SCF	3	0.020	0.087	0.892	
40.08	81.95	45	SCF	3	0.030	0.113	0.856	753
40.08	82.07	47	LIQ	3	0.166	0.309	0.525	
40.08	82.12	47	LIQ	3	0.190	0.297	0.513	
39.92	82.10	11	LIQ2	3	0.165	0.286	0.549	850
39.92	82.60	11	LIQ	3	0.966	0.011	0.023	1002
39.92	83.40	11	LIQ	3	0.966	0.011	0.024	
39.92	82.10	11	LIQ2	3	0.165	0.290	0.545	
39.92	83.20	11	SCF	3	0.044	0.175	0.780	
40.08	84.80	43	LIQ2	3	0.144	0.268	0.588	
40.08	84.98	43	LIQ2	3	0.148	0.249	0.603	
40.08	85.50	43	LIQ	3	0.970	0.010	0.020	
40.08	85.50	43	LIQ	3	0.971	0.010	0.020	964
40.08	88.80	48	LIQ2	3	0.147	0.242	0.610	
40.08	86.89	48	SCF	3	0.085	0.294	0.620	
40.08	89.25	48	LIQ	3	0.971	0.009	0.020	
40.08	86.69	48	SCF	3	0.059	0.188	0.752	
40.08	86.90	48	SCF	3	0.064	0.235	0.701	
40.08	86.90	48	SCF	3	0.071	0.243	0.686	
40.08	89.05	48	LIQ2	3	0.162	0.240	0.598	
40.08	89.70	48	LIQ	3	0.971	0.009	0.021	
40.08	100.5	44	LIQ	2	0.975	0.013	0.011	958
40.08	90.7	44	LIQ2	2	0.442	0.456	0.101	820
40.08	94.6	44	LIQ2	2	0.437	0.461	0.102	
40.08	101.0	44	LIQ	2	0.975	0.014	0.011	
39.98	97.5	13	SCF	2	0.082	0.206	0.712	
39.98	93.4	13	SCF	2	0.087	0.250	0.663	
39.92	99.6	13	LIQ	2	0.969	0.009	0.022	
39.92	99.9	13	LIQ	2	0.970	0.010	0.020	1003
40.08	97.8	3	SCF	2	0.007	0.013	0.980	
40.08	98.0	3	LIQ	2	0.968	0.004	0.028	
40.08	97.7	3	LIQ	2	0.963	0.005	0.033	1008
40.08	97.7	3	SCF	2	0.004	0.014	0.982	
39.90	98.1	35	LIQ	2	0.969	0.009	0.021	
39.90	98.1	35	LIQ	2	0.970	0.010	0.020	
39.90	99.6	36	LIQ	2	0.971	0.010	0.019	
39.90	100.4	36	LIQ	2	0.970	0.010	0.020	
39.90	97.0	36	SCF	2	0.278	0.378	0.344	
39.90	97.5	36	SCF	2	0.263	0.376	0.361	
39.90	98.0	32	SCF	2	0.019	0.067	0.913	750
39.90	99.2	32	LIQ	2	0.970	0.009	0.021	
39.90	99.9	32	LIQ	2	0.969	0.009	0.022	1003
39.90	99.0	32	SCF	2	0.022	0.085	0.893	
39.90	99.7	34	SCF	2	0.228	0.413	0.359	

(continued on next page)

Table C.5 (concluded)

T °C	P bar	run‡	phase	M	mole fractions† X_1	X_2	X_3	density kg/m³
39.90	99.6	34	SCF	2	0.107	0.233	0.660	
39.90	99.5	34	SCF	2	0.110	0.241	0.649	841
39.90	98.0	34	SCF	2	0.196	0.366	0.438	
39.90	99.1	34	SCF	2	0.178	0.327	0.495	
39.90	103.1	33	LIQ	2	0.970	0.009	0.021	1001
39.90	99.7	34	SCF	2	0.143	0.271	0.585	
39.90	101.0	34	LIQ	2	0.971	0.009	0.020	
39.90	101.5	34	LIQ	2	0.971	0.009	0.020	
39.88	102.7	33	SCF	2	0.065	0.172	0.763	
39.88	103.5	33	SCF	2	0.066	0.182	0.752	810
39.90	103.2	33	LIQ	2	0.969	0.009	0.021	
39.90	103.1	33	LIQ	2	0.971	0.009	0.020	
39.92	109.3	23	LIQ2	2	0.514	0.484	0.002	
39.92	98.1	23	LIQ	2	0.983	0.017	0.000	
39.92	97.1	23	LIQ	2	0.983	0.017	0.000	985
39.92	109.8	23	LIQ2	2	0.522	0.476	0.002	
39.90	105.0	37	SCF	2	0.344	0.427	0.229	
39.90	106.9	37	SCF	2	0.348	0.419	0.233	
39.90	100.0	37	LIQ	2	0.970	0.011	0.018	
39.90	128.4	31	LIQ	2	0.969	0.008	0.022	
39.90	143.3	31	SCF	2	0.012	0.057	0.931	
39.90	134.5	31	SCF	2	0.016	0.058	0.926	804
40.08	143.4	4	SCF	2	0.006	0.009	0.984	
40.08	144.6	4	LIQ	2	0.969	0.003	0.028	
40.08	144.0	4	LIQ	2	0.969	0.003	0.028	
39.92	150.0	12	SCF	2	0.054	0.140	0.806	851
39.92	150.6	12	SCF	2	0.057	0.137	0.805	
39.92	152.8	12	LIQ	2	0.965	0.010	0.025	1008
39.92	154.0	12	LIQ	2	0.966	0.010	0.025	
39.94	260.5	24	LIQ2	2	0.545	0.453	0.002	
39.94	265.5	24	LIQ	2	0.982	0.017	0.000	
39.94	265.5	24	LIQ	2	0.982	0.018	0.000	993
39.94	244.5	24	LIQ2	2	0.547	0.451	0.002	854

†‡ See footnotes to Table C.3

Table C.6 Experimental results for the mixture water(1) - *n*-butanol(2) - carbon dioxide(3) at 60 °C (333.1 K)

T °C	P bar	run‡	phase	M	mole fractions† X_1	X_2	X_3	density kg/m³
60.00	1.01	13	LIQ2	2	0.436	0.465	0.099	
59.90	18.36	43	LIQ	2	0.007	0.914	0.079	
59.90	18.30	43	LIQ	2	0.007	0.914	0.079	786
58.90	19.05	5	LIQ	2	0.991	0.004	0.005	
58.90	19.00	5	LIQ	2	0.991	0.004	0.004	987
59.90	19.75	37	LIQ	2	0.094	0.828	0.078	
60.00	19.68	37	LIQ	2	0.104	0.832	0.064	791
60.00	19.52	37	LIQ	2	0.096	0.828	0.076	
59.70	20.14	1	LIQ	2	0.992	0.003	0.005	
59.70	20.17	1	LIQ	2	0.992	0.003	0.005	983
59.82	20.18	1	SCF	2	0.004	0.000	0.996	
59.82	20.19	1	SCF	2	0.020	0.003	0.977	
60.07	20.71	11	LIQ	3	0.982	0.014	0.004	
60.07	20.70	11	LIQ	3	0.982	0.014	0.004	978
60.07	20.65	11	LIQ2	3	0.492	0.476	0.033	
60.07	20.65	11	LIQ2	3	0.482	0.486	0.032	839
60.07	20.23	11	SCF	3	0.010	0.002	0.987	
60.00	20.83	31	LIQ	2	0.270	0.655	0.064	
60.00	20.83	31	LIQ	2	0.260	0.675	0.065	
59.85	20.30	31	LIQ	2	0.268	0.666	0.065	805
59.85	21.15	23	LIQ	2	0.416	0.530	0.053	
59.85	21.15	23	LIQ	2	0.418	0.530	0.052	817
60.00	36.71	53	LIQ	2	0.983	0.015	0.002	
60.00	34.98	53	LIQ	2	0.983	0.016	0.002	
60.00	30.99	53	LIQ2	2	0.556	0.427	0.016	
60.00	25.72	53	LIQ2	2	0.552	0.434	0.014	
38.90	39.03	6	LIQ	2	0.987	0.004	0.009	
58.90	38.67	6	LIQ	2	0.986	0.004	0.009	991
58.90	38.39	6	SCF	2	0.004	0.002	0.986	
59.82	39.08	24	LIQ	2	0.423	0.525	0.052	
59.82	38.73	24	LIQ	2	0.421	0.527	0.052	823
59.85	40.14	32	LIQ	2	0.257	0.609	0.134	
59.85	39.98	32	LIQ	2	0.258	0.608	0.134	811
59.85	40.40	38	LIQ	2	0.105	0.732	0.163	
59.85	40.17	38	LIQ	2	0.107	0.723	0.170	799
60.08	40.05	12	LIQ	3	0.977	0.013	0.010	
60.00	40.26	12	LIQ	3	0.978	0.013	0.010	
59.90	40.17	12	LIQ	3	0.977	0.013	0.010	982
59.98	40.83	44	LIQ	2	0.013	0.804	0.183	

(continued on next page)

Table C.6 (continued)

T °C	P bar	run‡	phase	M	mole fractions† X_1	X_2	X_3	density kg/m³
60.02	40.59	44	LIQ	2	0.014	0.805	0.181	793
60.00	40.46	13	LIQ2	3	0.446	0.454	0.100	
60.00	40.41	13	LIQ2	3	0.436	0.465	0.099	825
60.00	40.61	13	SCF	3	0.009	0.021	0.955	
60.00	40.59	13	SCF	3	0.004	0.003	0.991	
59.80	57.92	2	LIQ	2	0.985	0.003	0.013	
59.80	58.73	2	SCF	2	0.002	0.001	0.997	
59.80	58.09	2	SCF	2	0.002	0.001	0.998	
59.82	59.00	25	LIQ	2	0.419	0.487	0.094	
59.82	58.46	25	LIQ	2	0.418	0.486	0.097	827
60.00	58.99	14	LIQ	3	0.975	0.012	0.013	
60.00	58.70	14	LIQ	3	0.975	0.012	0.013	985
60.00	57.81	14	LIQ2	3	0.394	0.447	0.159	
60.00	58.74	39	LIQ	2	0.090	0.656	0.254	
60.00	58.54	39	LIQ	2	0.102	0.652	0.246	804
60.00	58.46	39	SCF	2	0.003	0.004	0.992	
60.00	60.59	45	LIQ	2	0.013	0.704	0.282	
60.00	59.29	45	LIQ	2	0.011	0.717	0.271	799
59.85	60.01	54	LIQ	2	0.979	0.015	0.006	978
59.85	60.21	54	LIQ2	2	0.532	0.435	0.033	832
59.80	60.49	7	LIQ	2	0.983	0.004	0.013	991
59.80	60.70	7	LIQ	2	0.983	0.004	0.012	
59.80	60.12	7	SCF	2	0.004	0.001	0.994	
59.85	60.85	33	LIQ	2	0.237	0.549	0.214	
59.88	60.73	33	LIQ	2	0.241	0.546	0.213	817
59.80	61.04	15	LIQ2	3	0.385	0.443	0.172	
59.80	60.97	15	LIQ2	3	0.375	0.452	0.173	827
59.85	61.60	15	SCF	3	0.003	0.003	0.993	
59.85	61.48	15	SCF	3	0.004	0.004	0.991	
59.85	79.81	58	LIQ	2	0.971	0.011	0.018	988
59.85	73.01	58	LIQ2	2	0.423	0.427	0.150	
59.80	78.34	40	LIQ	2	0.094	0.554	0.351	
59.80	78.21	40	LIQ	2	0.094	0.554	0.352	811
59.80	78.13	40	SCF	2	0.003	0.014	0.971	
59.80	78.13	40	SCF	2	0.003	0.008	0.989	
59.80	78.11	40	SCF	2	0.003	0.011	0.986	
59.85	79.30	26	LIQ	2	0.417	0.485	0.097	
59.85	79.10	26	LIQ	2	0.397	0.478	0.126	
59.85	78.65	26	LIQ	2	0.401	0.476	0.123	830
59.85	78.50	26	SCF	2	0.005	0.008	0.987	
59.90	78.98	8	LIQ	2	0.981	0.004	0.015	
59.15	79.18	8	LIQ	2	0.981	0.004	0.015	

(continued on next page)

Table C.6 (continued)

T °C	P bar	run‡	phase	M	mole fractions† X_1	X_2	X_3	density kg/m³
59.85	79.60	8	SCF	2	0.003	0.001	0.995	
59.85	79.30	8	SCF	2	0.003	0.001	0.995	
59.90	80.74	16	LIQ	3	0.973	0.011	0.016	
59.90	80.68	16	LIQ	3	0.973	0.010	0.016	988
59.90	78.50	16	LIQ2	3	0.359	0.404	0.238	
59.90	76.36	16	LIQ2	3	0.347	0.420	0.233	831
59.90	80.22	16	SCF	3	0.004	0.006	0.990	
59.90	79.87	47	LIQ	2	0.028	0.578	0.394	
59.90	79.89	47	LIQ	2	0.028	0.584	0.388	806
59.90	79.81	47	SCF	2	0.001	0.013	0.986	
59.90	79.81	47	SCF	2	0.001	0.008	0.991	
59.90	79.81	47	SCF	2	0.001	0.011	0.988	
59.85	80.81	55	LIQ	2	0.980	0.015	0.004	
59.85	80.21	55	LIQ2	2	0.538	0.429	0.032	833
59.80	81.46	34	LIQ	2	0.212	0.475	0.313	
59.85	81.51	34	LIQ	2	0.213	0.475	0.312	820
59.85	81.37	34	SCF	2	0.006	0.015	0.979	
59.85	81.33	34	SCF	2	0.005	0.010	0.985	
60.00	100.8	51	LIQ	2	0.983	0.016	0.001	975
60.00	98.9	51	LIQ2	2	0.563	0.433	0.004	
59.90	94.1	51	LIQ2	2	0.560	0.436	0.004	832
59.55	98.1	28	SCF	2	0.005	0.013	0.981	
59.95	98.0	28	SCF	2	0.005	0.012	0.983	
59.85	98.7	27	LIQ	2	0.377	0.471	0.152	
59.85	98.5	27	LIQ	2	0.360	0.470	0.170	830
59.90	99.0	9	LIQ	2	0.980	0.004	0.017	
59.90	98.9	9	LIQ	2	0.979	0.004	0.017	
59.90	98.7	9	SCF	2	0.005	0.003	0.991	
59.90	97.8	9	SCF	2	0.004	0.003	0.993	
59.90	99.1	17	LIQ	3	0.973	0.010	0.018	
59.90	99.1	17	LIQ	3	0.973	0.010	0.017	991
59.90	98.5	17	LIQ2	3	0.290	0.367	0.342	
89.90	98.3	17	LIQ2	3	0.284	0.372	0.344	741
59.90	98.9	17	SCF	3	0.005	0.017	0.976	
89.90	98.7	17	SCF	3	0.005	0.010	0.985	
59.85	98.0	59	LIQ	2	0.974	0.012	0.015	
59.85	101.0	59	LIQ2	2	0.412	0.413	0.174	840
59.90	100.3	48	SCF	2	0.002	0.042	0.955	
59.90	100.2	48	SCF	2	0.002	0.046	0.951	
59.85	99.9	56	LIQ	2	0.979	0.015	0.006	980
59.85	100.6	56	LIQ2	2	0.538	0.430	0.032	836
59.85	101.4	41	LIQ	2	0.075	0.399	0.527	
59.85	101.7	41	LIQ	2	0.075	0.400	0.525	810

(continued on next page)

Table C.6 (continued)

T °C	P bar	run‡	phase	M	mole fractions† X_1	X_2	X_3	density kg/m^3
59.85	101.7	41	SCF	2	0.007	0.052	0.940	
59.85	101.8	41	SCF	2	0.007	0.043	0.950	
59.85	101.7	41	SCF	2	0.010	0.061	0.928	
59.90	102.1	46	LIQ	2	0.013	0.395	0.592	
59.90	102.1	46	LIQ	2	0.014	0.398	0.589	801
59.90	102.0	46	SCF	2	0.002	0.053	0.941	
59.90	102.0	46	SCF	2	0.002	0.062	0.936	
59.90	101.9	46	SCF	2	0.002	0.051	0.947	
59.85	102.2	35	LIQ	2	0.170	0.382	0.448	
59.85	102.2	35	LIQ	2	0.167	0.384	0.449	821
59.90	102.2	35	SCF	2	0.011	0.034	0.949	
59.90	102.1	35	SCF	2	0.012	0.033	0.955	
59.85	102.2	62	LIQ	2	0.973	0.010	0.017	991
59.85	102.2	62	LIQ2	2	0.299	0.363	0.338	844
59.80	104.5	3	LIQ	2	0.980	0.002	0.018	
59.80	104.4	3	LIQ	2	0.980	0.002	0.017	994
59.80	104.5	3	SCF	2	0.004	0.002	0.993	
59.80	104.5	3	SCF	2	0.005	0.002	0.993	
60.00	100.9	50	LIQ	2	0.984	0.016	0.000	
59.90	110.6	50	LIQ	2	0.018	0.272	0.710	
59.90	110.4	49	LIQ	2	0.015	0.272	0.713	
59.90	110.2	49	LIQ	2	0.015	0.273	0.711	782
59.90	110.1	49	SCF	2	0.003	0.062	0.935	
59.90	110.1	49	SCF	2	0.004	0.074	0.922	
59.85	113.5	42	LIQ	2	0.054	0.265	0.681	
59.85	113.3	42	LIQ	2	0.054	0.269	0.676	790
59.85	113.2	42	SCF	2	0.009	0.059	0.931	538
59.90	117.2	36	LIQ	2	0.120	0.285	0.595	
59.90	117.1	36	LIQ	2	0.119	0.286	0.595	810
60.00	117.2	36	SCF	2	0.030	0.111	0.859	
60.00	116.8	36	SCF	2	0.031	0.110	0.859	575
59.90	120.8	18	LIQ	3	0.972	0.010	0.018	
59.90	120.5	18	LIQ	3	0.972	0.009	0.018	992
59.90	119.0	18	LIQ2	3	0.203	0.294	0.504	
59.90	118.8	18	LIQ2	3	0.199	0.297	0.505	830
60.00	119.0	18	SCF	3	0.037	0.126	0.837	
60.00	119.9	18	SCF	3	0.032	0.100	0.868	
59.95	123.3	29	LIQ	2	0.329	0.452	0.218	
59.95	123.2	29	LIQ	2	0.313	0.437	0.250	
60.00	123.4	29	SCF	2	0.045	0.147	0.803	
60.00	121.7	29	SCF	2	0.043	0.144	0.813	640
59.85	125.2	21	LIQ2	3	0.168	0.265	0.567	

(continued on next page)

Table C.6 (continued)

T °C	P bar	run‡	phase	M	mole fractions† X_1	X_2	X_3	density kg/m³
39.85	125.0	21	LIQ2	3	0.154	0.272	0.574	
60.00	127.0	30	LIQ	2	0.348	0.463	0.189	
60.00	126.9	30	LIQ	2	0.347	0.460	0.194	805
60.00	126.4	30	SCF	2	0.057	0.164	0.779	
60.00	126.4	30	SCF	2	0.055	0.163	0.782	704
60.00	127.6	19	SCF	3	0.061	0.165	0.774	
59.90	144.3	10	LIQ	2	0.979	0.002	0.019	
59.90	142.6	10	LIQ	2	0.979	0.002	0.019	998
59.90	146.9	10	SCF	2	0.007	0.006	0.985	
59.90	148.4	10	SCF	2	0.007	0.006	0.988	
60.00	150.0	20	LIQ	2	0.972	0.009	0.019	
60.00	149.2	20	LIQ	2	0.971	0.009	0.020	994
60.00	146.6	20	SCF	2	0.091	0.184	0.724	798
60.00	142.0	20	SCF	2	0.086	0.182	0.731	
59.85	148.9	65	LIQ	2	0.974	0.006	0.019	997
59.85	146.7	65	SCF	2	0.029	0.032	0.939	
59.85	146.8	65	SCF	2	0.025	0.033	0.942	688
58.80	145.5	4	LIQ	2	0.980	0.001	0.019	
59.80	149.6	4	LIQ	2	0.980	0.001	0.019	
59.80	150.7	4	SCF	2	0.006	0.005	0.988	
59.80	150.2	4	SCF	2	0.007	0.005	0.989	
60.00	149.5	57	LIQ	2	0.980	0.016	0.004	
60.00	149.6	57	SCF	2	0.536	0.432	0.033	838
59.85	150.2	60	LIQ	2	0.973	0.012	0.015	
59.85	149.3	60	SCF	2	0.416	0.412	0.171	
59.85	150.4	67	LIQ	2	0.977	0.003	0.020	
59.85	150.7	67	LIQ	2	0.978	0.003	0.019	1000
59.85	149.9	67	SCF	2	0.040	0.011	0.948	
59.85	149.7	67	SCF	2	0.015	0.011	0.974	
59.85	149.5	67	SCF	2	0.011	0.011	0.978	
59.85	149.5	67	SCF	2	0.009	0.011	0.980	
59.85	149.5	67	SCF	2	0.009	0.011	0.980	
59.85	152.0	63	LIQ	2	0.971	0.010	0.019	992
59.85	151.6	63	SCF	2	0.324	0.371	0.306	849
59.85	202.2	22	LIQ	2	0.971	0.009	0.020	
59.85	200.6	22	LIQ	2	0.971	0.008	0.020	997
59.90	194.5	22	SCF	2	0.063	0.143	0.760	821
59.95	192.5	22	SCF	2	0.066	0.146	0.788	
59.85	199.5	64	LIQ	2	0.971	0.010	0.019	995
59.85	199.5	64	SCF	2	0.320	0.372	0.307	854
59.90	204.0	52	LIQ	2	0.982	0.017	0.001	
59.90	199.0	52	LIQ	2	0.983	0.017	0.001	979

(continued on next page)

Table C.6 (concluded)

T °C	P bar	run‡	phase	M	mole fractions† X_1	X_2	X_3	density kg/m^3
59.90	200.5	52	SCF	2	0.564	0.432	0.003	839
59.90	195.5	52	SCF	2	0.560	0.436	0.004	
59.85	199.5	68	LIQ	2	0.976	0.002	0.021	
59.85	199.5	68	LIQ	2	0.977	0.002	0.021	1002
59.85	200.2	68	SCF	2	0.010	0.011	0.979	
59.85	200.2	68	SCF	2	0.010	0.011	0.979	
59.85	200.0	61	LIQ	2	0.972	0.013	0.015	992
59.85	200.2	61	SCF	2	0.433	0.405	0.162	
59.85	200.0	66	LIQ	2	0.974	0.005	0.021	
59.85	199.5	66	LIQ	2	0.974	0.005	0.020	1001
59.85	203.0	66	SCF	2	0.014	0.032	0.952	
59.85	203.0	66	SCF	2	0.014	0.033	0.953	784

†‡ See footnotes to Table C.3

C.4 Acetic acid - water - carbon dioxide

The methodology described in the previous section was followed for the presentation of the data for this system in Tables C.7 and C.8.

Table C.7 Experimental results for the mixture water(1) - acetic acid(2) - carbon dioxide(3) at 40 °C (313.1 K)

T °C	P bar	run‡	phase	M	mole fractions† X_1	X_2	X_3	density kg/m^3
40.05	19.48	35	LIQ	2	0.894	0.096	0.010	1037
40.05	19.04	35	LIQ	2	0.887	0.102	0.011	
39.60	19.42	1	LIQ	2	0.029	0.820	0.151	
39.60	19.41	1	LIQ	2	0.023	0.838	0.139	
40.05	19.72	26	LIQ	2	0.778	0.206	0.016	1051
40.05	19.68	26	LIQ	2	0.779	0.204	0.017	

(continued on next page)

Table C.7 (continued)

T °C	P bar	run‡	phase	M	mole fractions† X_1	X_2	X_3	density kg/m³
40.05	20.12	42	LIQ	2	0.947	0.044	0.009	1026
40.05	20.02	42	LIQ	2	0.941	0.051	0.009	
40.05	19.95	20	LIQ	2	0.561	0.402	0.037	
40.05	20.28	20	LIQ	2	0.568	0.395	0.037	1060
40.05	20.80	16	LIQ	2	0.359	0.573	0.069	1056
40.05	20.84	8	LIQ	2	0.075	0.787	0.138	1038
40.05	20.89	8	LIQ	2	0.081	0.787	0.132	
40.25	20.91	2	LIQ	2	0.010	0.827	0.163	
40.05	20.87	2	LIQ	2	0.013	0.820	0.166	
40.05	20.86	2	LIQ	2	0.009	0.830	0.160	
40.05	21.07	11	LIQ	2	0.158	0.728	0.114	
40.05	21.18	11	LIQ	2	0.155	0.744	0.101	1046
40.05	21.17	11	LIQ	2	0.162	0.721	0.117	
40.05	38.85	27	LIQ	2	0.767	0.201	0.032	1054
40.05	38.75	27	LIQ	2	0.763	0.206	0.031	
40.05	39.75	3	LIQ	2	0.008	0.659	0.334	
40.05	39.35	3	LIQ	2	0.008	0.663	0.329	1010
40.05	39.83	20a	LIQ	2	0.538	0.385	0.077	1061
40.05	39.58	20a	LIQ	2	0.537	0.388	0.075	
40.05	39.93	36	LIQ	2	0.877	0.104	0.019	1042
40.05	39.77	36	LIQ	2	0.878	0.103	0.019	
40.05	40.07	9	LIQ	2	0.068	0.641	0.291	
40.05	39.72	9	LIQ	2	0.068	0.645	0.287	1024
40.05	40.04	43	LIQ	2	0.934	0.051	0.016	1030
40.05	39.83	43	LIQ	2	0.932	0.052	0.015	
40.05	40.16	12	LIQ	2	0.139	0.617	0.245	1034
40.05	40.01	12	LIQ	2	0.138	0.624	0.238	
40.05	40.22	17	LIQ	2	0.321	0.534	0.145	1052
40.05	39.95	17	LIQ	2	0.314	0.523	0.163	
40.05	59.00	13	LIQ	2	0.098	0.473	0.430	1003
40.05	58.60	13	LIQ	2	0.099	0.476	0.425	
40.05	59.01	18	LIQ	2	0.276	0.469	0.256	1040
40.05	58.61	18	LIQ	2	0.276	0.470	0.254	
40.05	58.95	44	LIQ	2	0.927	0.053	0.020	1033
40.05	58.71	44	LIQ	2	0.927	0.053	0.020	
40.05	59.05	4	LIQ	2	0.005	0.428	0.588	962
40.05	58.86	4	LIQ	2	0.004	0.430	0.566	
40.05	59.31	10	LIQ	2	0.042	0.451	0.507	982
40.05	58.96	10	LIQ	2	0.043	0.452	0.505	
40.05	59.61	21	LIQ	2	0.511	0.366	0.123	1060
40.05	59.13	21	LIQ	2	0.511	0.368	0.121	
40.05	60.02	37	LIQ	2	0.881	0.091	0.028	
40.05	59.84	37	LIQ	2	0.872	0.101	0.027	1045
40.05	59.21	37	SCF	2	0.001	0.000	0.998	

(continued on next page)

Table C.7 (continued)

T °C	P bar	run‡	phase	M	mole fractions† X_1	X_2	X_3	density kg/m^3
40.05	59.15	37	SCF	2	0.001	0.000	0.999	
40.05	60.68	28	LIQ	2	0.753	0.199	0.048	1057
40.05	69.61	28	LIQ	2	0.745	0.201	0.054	1058
40.05	68.73	28	LIQ	2	0.745	0.200	0.054	
40.05	69.01	55	LIQ	2	0.705	0.228	0.068	1062
40.05	68.55	55	LIQ	2	0.700	0.235	0.065	
40.05	68.38	55	SCF	2	0.001	0.017	0.983	
40.05	69.70	22	LIQ	2	0.492	0.363	0.145	1059
40.05	67.92	22	LIQ	2	0.495	0.360	0.145	
40.05	69.83	5	LIQ	2	0.003	0.262	0.735	895
40.05	69.26	5	LIQ	2	0.003	0.265	0.733	895
40.05	69.07	5	SCF	2	0.000	0.021	0.979	
40.05	69.88	14	LIQ	2	0.063	0.320	0.618	945
40.05	69.65	14	LIQ	2	0.062	0.329	0.609	
40.05	69.54	14	SCF	2	0.000	0.022	0.978	
40.05	69.28	14	SCF	2	0.000	0.012	0.988	
40.05	70.11	18a	LIQ	2	0.228	0.399	0.373	
40.05	69.80	18a	LIQ	2	0.232	0.402	0.366	
40.05	70.37	10a	LIQ	2	0.023	0.280	0.697	915
40.05	69.75	10a	LIQ	2	0.025	0.283	0.692	
40.05	75.11	6	LIQ	2	0.001	0.165	0.834	820
40.05	74.66	6	LIQ	2	0.001	0.161	0.838	
40.05	74.48	6	SCF	2	0.000	0.026	0.974	
40.05	74.41	6	SCF	2	0.000	0.004	0.996	
40.05	77.77	15	LIQ	2	0.023	0.122	0.855	
40.05	77.83	15	LIQ	2	0.025	0.111	0.864	788
40.05	77.50	15	SCF	2	0.000	0.011	0.989	
40.05	77.44	15	SCF	2	0.001	0.007	0.992	
40.05	77.98	19	LIQ	2	0.032	0.097	0.871	
40.05	77.77	19	LIQ	2	0.029	0.118	0.853	793
40.05	77.75	19	SCF	2	0.010	0.037	0.953	
40.05	77.75	19	SCF	2	0.002	0.016	0.982	
40.05	77.67	19	SCF	2	0.001	0.007	0.991	
40.05	78.03	56	LIQ	3	0.570	0.307	0.123	
40.05	77.90	56	LIQ	3	0.572	0.310	0.118	1062
40.05	77.41	56	LIQ2	3	0.087	0.156	0.757	814
40.05	77.61	56	LIQ2	3	0.028	0.131	0.840	
40.05	77.37	56	LIQ2	3	0.037	0.134	0.830	
40.05	77.92	56	SCF	3	0.000	0.020	0.980	
40.05	78.00	56	SCF	3	0.002	0.008	0.990	
40.05	78.69	10b	LIQ	2	0.007	0.105	0.888	
40.05	78.46	10b	LIQ	2	0.007	0.101	0.893	784
40.05	78.24	10b	SCF	2	0.003	0.042	0.955	

(continued on next page)

Table C.7 (continued)

T °C	P bar	run‡	phase	M	mole fractions† X_1	X_2	X_3	density kg/m³
40.05	78.04	10b	SCF	2	0.001	0.021	0.978	
40.05	77.98	10b	SCF	2	0.001	0.010	0.989	
40.05	79.28	7	LIQ	2	0.001	0.078	0.922	
40.05	79.13	7	LIQ	2	0.001	0.082	0.917	735
40.05	79.02	7	SCF	2	0.000	0.020	0.980	
40.05	78.93	7	SCF	2	0.000	0.007	0.993	
40.05	78.83	7	SCF	2	0.000	0.009	0.991	
40.05	80.38	51	LIQ	2	0.960	0.021	0.019	
40.05	79.98	51	LIQ	2	0.960	0.019	0.021	1021
40.05	79.80	51	SCF	2	0.000	0.004	0.996	
40.05	79.57	51	SCF	2	0.000	0.001	0.999	
40.05	79.99	45	LIQ	2	0.924	0.051	0.024	
40.05	80.30	45	LIQ	2	0.925	0.051	0.024	1036
40.05	79.55	45	SCF	2	0.002	0.014	0.984	
40.05	79.45	45	SCF	2	0.001	0.002	0.997	
40.05	80.46	45	SCF	2	0.001	0.000	0.999	
40.05	80.18	38	LIQ	2	0.871	0.095	0.034	1044
40.05	79.81	38	LIQ	2	0.865	0.102	0.033	
40.05	79.95	38	SCF	2	0.003	0.009	0.988	
40.05	79.93	38	SCF	2	0.005	0.003	0.992	
40.05	81.02	29	LIQ	3	0.743	0.197	0.060	1059
40.05	80.48	29	LIQ	3	0.743	0.199	0.059	
40.05	80.44	30	LIQ	3	0.754	0.184	0.062	
40.05	81.13	30	LIQ	3	0.743	0.199	0.058	1056
40.05	81.13	30	SCF	3	0.043	0.094	0.862	
40.05	81.21	30	SCF	3	0.021	0.059	0.920	
40.05	81.24	30	SCF	3	0.020	0.063	0.917	
40.05	99.23	39	LIQ	2	0.875	0.092	0.033	
40.05	98.68	39	LIQ	2	0.873	0.095	0.032	1048
40.05	98.44	39	SCF	2	0.067	0.039	0.894	
40.05	98.07	39	SCF	2	0.047	0.029	0.924	
40.05	98.02	39	SCF	2	0.076	0.039	0.884	
40.05	100.00	46	LIQ	2	0.931	0.043	0.027	1037
40.05	99.50	46	SCF	2	0.100	0.020	0.880	
40.05	99.02	46	SCF	2	0.107	0.019	0.874	
40.05	98.49	46	SCF	2	0.114	0.017	0.869	
40.05	98.81	46	SCF	2	0.100	0.025	0.875	
40.05	97.32	46	SCF	2	0.071	0.011	0.918	
40.05	96.79	46	SCF	2	0.035	0.007	0.958	
40.05	96.17	46	SCF	2	0.012	0.006	0.982	
40.05	95.73	46	SCF	2	0.061	0.008	0.930	
40.05	99.66	60	LIQ	2	0.471	0.350	0.179	
40.05	99.68	60	LIQ	2	0.473	0.353	0.174	1057
40.05	98.93	60	SCF	2	0.062	0.347	0.590	

(continued on next page)

Table C.7 (continued)

T °C	P bar	run‡	phase	M	mole fractions† X_1	X_2	X_3	density kg/m³
40.05	98.65	60	SCF	2	0.048	0.280	0.672	
40.05	100.23	31	LIQ	2	0.797	0.145	0.058	
40.05	99.43	31	LIQ	2	0.772	0.174	0.054	1060
40.05	100.04	52	LIQ	2	0.962	0.016	0.022	1028
40.05	101.36	52	SCF	2	0.001	0.001	0.997	
40.05	101.16	52	SCF	2	0.004	0.000	0.996	
40.05	100.78	23	LIQ	2	0.581	0.286	0.133	
40.05	101.81	23	LIQ	2	0.568	0.306	0.126	1063
40.05	101.25	23	SCF	2	0.021	0.161	0.818	
40.05	100.81	23	SCF	2	0.022	0.163	0.815	859
40.05	99.92	47	SCF	2	0.095	0.005	0.900	
40.05	100.77	47	SCF	2	0.072	0.011	0.917	
40.05	107.97	47	SCF	2	0.102	0.016	0.882	
40.05	100.91	47	SCF	2	0.094	0.012	0.894	
40.05	102.31	47	SCF	2	0.119	0.021	0.860	
40.05	103.64	47	SCF	2	0.034	0.012	0.954	
40.05	103.90	47	SCF	2	0.024	0.010	0.966	
40.05	104.46	47	SCF	2	0.013	0.008	0.980	
40.05	104.41	47	SCF	2	0.009	0.005	0.986	
40.05	104.38	47	SCF	2	0.008	0.004	0.987	
40.05	102.37	57	LIQ	2	0.687	0.225	0.088	1064
40.05	103.06	57	LIQ	2	0.679	0.238	0.083	
40.05	103.21	57	SCF	2	0.022	0.165	0.813	
40.05	102.99	57	SCF	2	0.015	0.137	0.848	
40.05	102.96	57	SCF	2	0.020	0.168	0.813	
40.05	148.11	32	LIQ	2	0.769	0.173	0.058	
40.05	147.21	32	LIQ	2	0.774	0.168	0.058	1062
40.05	143.28	32	SCF	2	0.039	0.080	0.881	842
40.05	141.51	32	SCF	2	0.010	0.069	0.921	
40.05	148.16	40	LIQ	2	0.879	0.087	0.034	1049
40.05	145.47	40	LIQ	2	0.880	0.088	0.033	
40.05	144.31	40	SCF	2	0.005	0.032	0.963	
40.05	142.51	40	SCF	2	0.004	0.029	0.967	
40.05	149.51	24	LIQ	2	0.550	0.309	0.141	
40.05	146.51	24	LIQ	2	0.551	0.310	0.140	1065
40.05	139.51	24	SCF	2	0.026	0.186	0.788	
40.05	144.41	58	LIQ	2	0.693	0.225	0.082	1066
40.05	148.79	58	SCF	2	0.012	0.103	0.886	
40.05	147.04	58	SCF	2	0.012	0.103	0.885	
40.05	137.13	61	LIQ	2	0.405	0.372	0.223	
40.05	152.41	61	SCF	2	0.067	0.272	0.661	
40.05	148.31	61	SCF	2	0.067	0.260	0.673	
40.05	151.78	61	SCF	2	0.402	0.368	0.231	1056
40.05	147.11	48	LIQ	2	0.926	0.044	0.030	1040

(continued on next page)

Table C.7 (concluded)

T °C	P bar	run‡	phase	M	mole fractions† X_1	X_2	X_3	density kg/m³
40.05	146.91	48	LIQ	2	0.926	0.047	0.027	
40.05	149.66	48	SCF	2	0.006	0.008	0.986	
40.05	148.16	48	SCF	2	0.004	0.008	0.988	
40.05	151.37	53	LIQ	2	0.963	0.014	0.023	1030
40.05	147.61	53	SCF	2	0.003	0.001	0.996	
40.05	147.05	53	SCF	2	0.002	0.001	0.997	
40.05	176.01	25	LIQ	2	0.540	0.312	0.148	
40.05	194.01	25	SCF	2	0.035	0.195	0.771	
40.05	184.01	25	SCF	2	0.034	0.192	0.774	943
40.05	201.01	62	LIQ	2	0.408	0.359	0.233	
40.05	190.01	62	LIQ	2	0.409	0.360	0.231	
40.05	182.01	62	SCF	2	0.071	0.272	0.657	
40.05	175.01	62	SCF	2	0.067	0.268	0.665	
40.05	197.51	33	LIQ	2	0.783	0.158	0.060	1064
40.05	195.51	33	LIQ	2	0.783	0.160	0.057	
40.05	188.01	33	SCF	2	0.011	0.077	0.911	
40.05	185.01	33	SCF	2	0.034	0.077	0.889	
40.05	203.51	41	LIQ	2	0.881	0.085	0.034	1052
40.05	188.01	41	SCF	2	0.007	0.027	0.966	
40.05	185.01	41	SCF	2	0.005	0.031	0.964	
40.05	198.51	34	SCF	2	0.015	0.067	0.917	894
40.05	195.01	34	SCF	2	0.011	0.072	0.917	
40.05	195.01	34	SCF	2	0.019	0.074	0.906	
40.05	199.51	54	LIQ	2	0.959	0.017	0.024	1032
40.05	195.01	54	LIQ	2	0.958	0.018	0.024	
40.05	198.11	54	SCF	2	0.003	0.001	0.997	
40.05	196.01	54	SCF	2	0.003	0.001	0.997	
40.05	201.01	59	LIQ	2	0.709	0.212	0.079	1069
40.05	198.01	59	SCF	2	0.015	0.109	0.876	
40.05	195.01	59	SCF	2	0.013	0.106	0.881	
40.05	200.01	49	LIQ	2	0.927	0.046	0.027	1042
40.05	198.01	49	SCF	2	0.004	0.013	0.983	
40.05	197.01	49	SCF	2	0.004	0.011	0.986	
40.05	252.01	50	SCF	2	0.004	0.011	0.985	

†‡ See footnotes to Table C.3

Table C.8 Experimental results for the mixture water(1) - acetic acid(2) - carbon dioxide(3) at 60 °C (333.1 K)

T °C	P bar	run‡	phase	M	mole fractions† X_1	X_2	X_3	density kg/m³
59.95	19.70	59	LIQ	2	0.979	0.016	0.005	997
59.95	19.60	59	LIQ	2	0.977	0.018	0.005	
59.85	20.29	14	LIQ	2	0.418	0.535	0.047	
59.85	20.20	14	LIQ	2	0.412	0.544	0.044	1024
59.90	20.38	24	LIQ	2	0.467	0.498	0.035	
59.90	20.31	24	LIQ	2	0.467	0.498	0.035	
59.95	20.26	33	LIQ	2	0.566	0.406	0.028	
59.95	20.23	33	LIQ	2	0.562	0.410	0.028	1034
59.95	20.33	71	LIQ	2	0.682	0.297	0.021	1032
60.00	20.34	71	LIQ	2	0.678	0.301	0.021	
59.85	20.41	8	LIQ	2	0.141	0.773	0.086	
59.85	20.40	8	LIQ	2	0.137	0.779	0.085	1001
59.90	20.60	42	LIQ	2	0.860	0.132	0.008	1019
60.00	20.74	1	LIQ	2	0.012	0.907	0.081	
60.00	20.71	1	LIQ	2	0.013	0.877	0.109	1000
60.00	20.74	1	LIQ	2	0.012	0.880	0.108	
60.10	20.95	50	LIQ	2	0.950	0.044	0.006	1004
60.00	20.84	50	LIQ	2	0.947	0.047	0.006	
59.90	38.13	25	LIQ	2	0.460	0.467	0.073	
59.90	38.13	25	LIQ	2	0.455	0.472	0.073	1030
60.00	38.39	72	LIQ	2	0.659	0.303	0.038	1034
60.00	38.31	72	LIQ	2	0.665	0.297	0.038	
59.95	39.04	60	LIQ	2	0.972	0.018	0.009	1000
60.05	38.75	60	LIQ	2	0.971	0.019	0.010	
60.00	40.02	2	LIQ	2	0.006	0.802	0.192	
60.00	39.82	2	LIQ	2	0.011	0.767	0.222	988
60.00	39.59	2	LIQ	2	0.011	0.811	0.178	
60.10	39.69	51	LIQ	2	0.941	0.048	0.011	1008
60.05	39.38	51	LIQ	2	0.939	0.050	0.012	
59.85	39.66	15	LIQ	2	0.394	0.509	0.096	
59.85	39.60	15	LIQ	2	0.383	0.523	0.095	1022
59.85	40.43	9	LIQ	2	0.125	0.694	0.181	
59.85	39.98	9	LIQ	2	0.124	0.697	0.179	993
59.90	40.50	43	LIQ	2	0.864	0.119	0.017	1022
59.90	40.41	43	LIQ	2	0.867	0.116	0.018	
60.10	40.35	43	LIQ	2	0.863	0.119	0.018	
60.10	41.12	34	LIQ	2	0.557	0.390	0.053	
60.10	41.07	34	LIQ	2	0.552	0.396	0.052	1034
59.85	59.47	16	LIQ	2	0.364	0.486	0.149	
59.85	57.74	16	LIQ	2	0.347	0.505	0.148	1019

(continued on next page)

Table C.8 (continued)

T °C	P bar	run‡	phase	M	mole fractions† X_1	X_2	X_3	density kg/m³
59.90	59.41	26	LIQ	2	0.431	0.448	0.121	
59.90	59.06	26	LIQ	2	0.435	0.446	0.119	
60.00	59.93	3	LIQ	2	0.010	0.622	0.368	
60.00	59.75	3	LIQ	2	0.009	0.628	0.363	965
60.05	59.98	52	LIQ	2	0.933	0.052	0.016	
60.05	59.81	52	LIQ	2	0.936	0.048	0.016	1011
59.90	60.06	27	LIQ	2	0.436	0.447	0.117	1028
59.80	60.08	27	LIQ	2	0.434	0.444	0.122	
60.00	60.68	73	LIQ	2	0.650	0.291	0.059	1036
60.00	60.41	73	LIQ	2	0.648	0.293	0.059	
60.10	60.61	44	LIQ	2	0.865	0.110	0.026	
60.10	60.64	44	LIQ	2	0.853	0.122	0.024	1026
60.05	60.75	61	LIQ	2	0.967	0.019	0.014	1004
60.05	60.57	61	LIQ	2	0.968	0.019	0.013	
60.10	60.75	35	LIQ	2	0.530	0.381	0.089	
60.10	60.65	35	LIQ	2	0.528	0.384	0.088	1034
59.85	61.68	10	LIQ	2	0.106	0.589	0.304	
59.85	61.44	10	LIQ	2	0.105	0.592	0.302	977
60.05	79.51	36	LIQ	2	0.506	0.370	0.124	
60.05	78.89	36	LIQ	2	0.498	0.386	0.116	1033
60.05	78.91	36	SCF	2	0.080	0.030	0.890	
60.10	78.61	36	SCF	2	0.119	0.024	0.857	
59.90	79.24	28	LIQ	2	0.416	0.418	0.166	
59.90	78.94	28	LIQ	2	0.409	0.431	0.159	1025
59.90	78.98	28	SCF	2	0.070	0.032	0.898	
59.90	78.84	28	SCF	2	0.103	0.029	0.868	
60.05	79.15	62	LIQ	2	0.964	0.019	0.017	
60.05	78.41	62	LIQ	2	0.964	0.019	0.017	
59.95	79.05	63	SCF	2	0.007	0.001	0.992	
59.95	79.42	63	SCF	2	0.004	0.000	0.996	
60.05	79.01	53	LIQ	2	0.930	0.050	0.020	1013
60.05	79.01	53	LIQ	2	0.930	0.050	0.019	
60.10	80.06	45	LIQ	2	0.852	0.118	0.031	1027
60.10	79.03	45	LIQ	2	0.848	0.122	0.030	
60.00	80.00	74	LIQ	2	0.635	0.288	0.078	1037
60.00	79.35	74	LIQ	2	0.636	0.287	0.077	
60.05	79.06	74	SCF	2	0.003	0.040	0.956	
60.05	78.81	74	SCF	2	0.002	0.012	0.986	
59.85	79.81	11	LIQ	2	0.085	0.470	0.444	
59.85	79.63	11	LIQ	2	0.082	0.483	0.435	949
59.85	79.31	11	SCF	2	0.007	0.090	0.903	
59.85	79.26	11	SCF	2	0.012	0.075	0.913	
59.85	80.11	18	LIQ	2	0.331	0.444	0.225	

(continued on next page)

Table C.8 (continued)

T °C	P bar	run†	phase	M	mole fractions† X_1	X_2	X_3	density kg/m³
59.85	80.11	18	LIQ	2	0.331	0.452	0.217	974
60.05	81.67	5	LIQ	2	0.007	0.434	0.559	
60.05	81.57	5	LIQ	2	0.007	0.448	0.546	
60.05	81.91	4	SCF	2	0.001	0.066	0.933	
60.05	81.81	4	SCF	2	0.001	0.061	0.939	
59.85	89.60	6	LIQ	2	0.007	0.340	0.654	
59.85	89.77	6	LIQ	2	0.006	0.344	0.650	871
59.90	99.15	29	LIQ	2	0.389	0.390	0.221	
59.90	98.98	29	LIQ	2	0.389	0.397	0.214	1018
59.90	98.62	29	SCF	2	0.001	0.029	0.969	
59.90	98.42	29	SCF	2	0.001	0.019	0.979	
59.85	99.34	12	LIQ	2	0.048	0.272	0.681	
59.85	99.25	12	LIQ	2	0.048	0.277	0.675	861
59.85	99.04	12	SCF	2	0.007	0.075	0.918	
59.85	99.05	12	SCF	2	0.007	0.060	0.934	
59.85	99.11	7	LIQ	2	0.003	0.214	0.782	
59.85	99.21	7	LIQ	2	0.004	0.219	0.777	783
59.85	99.93	19	LIQ	2	0.295	0.396	0.308	
59.85	99.61	19	LIQ	2	0.294	0.401	0.306	993
59.85	99.36	19	SCF	2	0.002	0.031	0.967	
59.85	99.11	19	SCF	2	0.001	0.020	0.979	
59.90	100.15	80	LIQ	2	0.166	0.365	0.469	
59.90	100.02	80	LIQ	2	0.266	0.000	0.734	951
59.90	99.95	80	LIQ	2	0.170	0.380	0.450	
59.90	99.46	80	SCF	2	0.010	0.055	0.936	
59.90	99.39	80	SCF	2	0.007	0.057	0.937	
60.08	101.70	37	LIQ	2	0.488	0.360	0.152	
60.08	101.17	37	SCF	2	0.001	0.021	0.978	
60.08	101.18	37	SCF	2	0.001	0.018	0.981	
60.05	102.21	75	LIQ	2	0.631	0.276	0.094	1037
60.05	101.85	75	LIQ	2	0.629	0.278	0.093	
60.05	101.83	75	SCF	2	0.005	0.017	0.977	
60.05	101.03	75	SCF	2	0.003	0.015	0.982	
59.95	102.02	64	LIQ	2	0.964	0.018	0.018	1008
59.95	102.05	64	LIQ	2	0.962	0.019	0.019	
59.95	101.72	64	SCF	2	0.004	0.003	0.993	
59.90	102.59	81	LIQ	3	0.216	0.381	0.402	
59.90	102.56	81	LIQ	3	0.208	0.397	0.395	971
59.90	102.12	81	LIQ2	3	0.089	0.304	0.606	
59.90	102.08	81	LIQ2	3	0.091	0.318	0.591	893
59.90	102.37	81	SCF	3	0.008	0.080	0.911	
59.90	102.37	81	SCF	3	0.009	0.067	0.924	

(continued on next page)

Table C.8 (continued)

T °C	P bar	run‡	phase	M	mole fractions† X_1	X_2	X_3	density kg/m³
60.00	102.59	54	LIQ	2	0.929	0.048	0.023	
60.00	102.48	54	LIQ	2	0.931	0.048	0.021	1016
60.10	103.29	46	LIQ	2	0.844	0.120	0.036	1029
60.10	102.62	46	LIQ	2	0.842	0.123	0.035	
60.10	102.62	46	SCF	2	0.064	0.013	0.923	
60.10	102.60	46	SCF	2	0.064	0.008	0.928	
59.85	103.71	21	LIQ	3	0.272	0.391	0.337	
59.85	103.71	21	LIQ	3	0.255	0.397	0.348	
59.85	108.81	22	LIQ	2	0.284	0.388	0.328	992
39.85	104.57	22	SCF	2	0.053	0.229	0.718	
59.85	104.11	22	SCF	2	0.064	0.227	0.709	820
59.90	108.93	30	LIQ	2	0.423	0.374	0.204	
59.90	108.72	30	LIQ	2	0.415	0.377	0.208	1021
59.90	108.56	30	SCF	2	0.022	0.102	0.876	
59.90	108.45	30	SCF	2	0.021	0.099	0.880	
59.85	109.31	20	LIQ	2	0.371	0.367	0.262	
59.85	108.90	20	LIQ	2	0.361	0.387	0.251	1006
59.85	108.51	20	SCF	2	0.043	0.176	0.782	
59.85	108.11	20	SCF	2	0.051	0.176	0.774	
60.08	110.15	38	LIQ	2	0.511	0.335	0.154	
60.08	110.15	38	LIQ	2	0.508	0.346	0.146	
60.10	109.68	38	SCF	2	0.022	0.063	0.915	
60.10	109.81	38	SCF	2	0.018	0.057	0.925	
60.10	110.96	47	LIQ	2	0.859	0.106	0.035	
60.10	110.31	47	LIQ	2	0.855	0.110	0.035	
60.10	109.60	47	SCF	2	0.057	0.013	0.930	
60.10	109.35	47	SCF	2	0.047	0.007	0.945	
60.05	110.50	76	LIQ	2	0.637	0.269	0.095	
60.05	110.38	76	LIQ	2	0.631	0.274	0.095	1038
60.05	110.03	76	SCF	2	0.031	0.055	0.914	
60.05	109.96	76	SCF	2	0.036	0.059	0.905	
59.95	119.60	65	LIQ	2	0.960	0.020	0.020	
59.95	119.41	65	LIQ	2	0.960	0.020	0.020	1010
59.95	119.11	65	SCF	2	0.004	0.000	0.996	
59.95	118.97	65	SCF	2	0.005	0.000	0.995	
60.05	120.48	77	LIQ	2	0.644	0.263	0.093	
60.05	120.26	77	LIQ	2	0.644	0.265	0.091	1039
60.05	120.11	77	SCF	2	0.031	0.076	0.893	
60.05	119.94	77	SCF	2	0.036	0.070	0.894	
59.90	120.94	31	LIQ	2	0.472	0.352	0.177	
59.90	120.62	31	LIQ	2	0.472	0.353	0.175	1018
59.90	120.02	31	SCF	2	0.027	0.138	0.835	

(continued on next page)

Table C.8 (continued)

T °C	P bar	run†	phase	M	mole fractions† X_1	X_2	X_3	density kg/m³
59.90	119.47	31	SCF	2	0.029	0.133	0.838	
60.05	120.51	55	LIQ	2	0.929	0.046	0.025	
60.05	120.36	55	LIQ	2	0.928	0.048	0.024	1018
60.10	120.74	39	LIQ	2	0.547	0.310	0.143	
60.10	120.61	39	LIQ	2	0.541	0.324	0.136	
60.10	120.82	39	SCF	2	0.026	0.094	0.880	
60.10	120.83	39	SCF	2	0.036	0.094	0.871	
60.05	122.03	68	LIQ	2	0.579	0.292	0.129	
60.05	121.51	68	LIQ	2	0.567	0.308	0.125	1035
60.05	121.47	68	SCF	2	0.024	0.095	0.881	
60.05	121.25	68	SCF	2	0.023	0.094	0.883	
59.85	132.07	23	LIQ	2	0.341	0.375	0.284	
59.85	127.04	23	SCF	2	0.065	0.242	0.693	
60.05	148.35	56	LIQ	2	0.933	0.042	0.025	
60.00	147.50	56	LIQ	2	0.931	0.044	0.025	1019
60.05	138.39	56	SCF	2	0.012	0.003	0.986	
60.05	138.39	56	SCF	2	0.007	0.002	0.991	
60.05	138.39	56	SCF	2	0.010	0.003	0.987	
59.90	149.16	82	LIQ	2	0.318	0.371	0.311	
59.90	147.41	82	LIQ	2	0.312	0.390	0.297	1004
59.90	142.83	82	SCF	2	0.081	0.268	0.651	903
59.90	140.39	82	SCF	2	0.058	0.226	0.716	
60.10	149.01	48	LIQ	2	0.859	0.105	0.036	
60.10	145.40	48	SCF	2	0.071	0.035	0.894	
60.10	145.21	48	SCF	2	0.052	0.021	0.927	
59.90	147.60	57	LIQ	2	0.935	0.040	0.025	
59.90	148.14	57	LIQ	2	0.933	0.043	0.024	
59.90	148.33	57	SCF	2	0.005	0.004	0.991	
59.90	148.02	57	SCF	2	0.006	0.003	0.991	
60.05	149.81	69	LIQ	2	0.581	0.293	0.126	
60.00	148.91	69	LIQ	2	0.580	0.297	0.123	1039
60.05	148.71	69	SCF	2	0.020	0.120	0.860	
60.05	146.27	69	SCF	2	0.024	0.113	0.863	783
59.90	150.41	40	LIQ	2	0.530	0.318	0.152	
59.90	150.41	40	LIQ	2	0.530	0.325	0.145	1036
59.90	149.12	40	SCF	2	0.028	0.141	0.831	
59.90	146.97	40	SCF	2	0.027	0.137	0.837	804
60.05	150.86	78	LIQ	2	0.675	0.238	0.088	
60.05	150.16	78	LIQ	2	0.672	0.242	0.087	1042
60.05	149.37	78	SCF	2	0.013	0.082	0.905	
60.05	148.85	78	SCF	2	0.011	0.077	0.912	
60.10	150.82	66	LIQ	2	0.964	0.016	0.021	
60.10	150.24	66	LIQ	2	0.961	0.018	0.021	1019

(continued on next page)

Table C.8 (concluded)

T °C	P bar	run‡	phase	M	mole fractions† X_1	X_2	X_3	density kg/m³
60.10	150.02	66	SCF	2	0.007	0.000	0.993	
60.10	149.37	66	SCF	2	0.006	0.001	0.993	
59.90	184.01	83	LIQ	2	0.381	0.367	0.252	
59.90	199.01	83	SCF	2	0.075	0.248	0.677	
59.90	194.01	83	SCF	2	0.071	0.248	0.681	917
60.05	197.51	70	LIQ	2	0.596	0.281	0.123	
60.05	195.01	70	LIQ	2	0.594	0.285	0.121	1042
60.05	193.01	70	SCF	2	0.024	0.136	0.840	
60.05	189.01	70	SCF	2	0.024	0.129	0.847	848
60.10	191.01	49	LIQ	2	0.859	0.098	0.043	1032
60.10	195.01	49	LIQ	2	0.858	0.099	0.043	
60.10	202.11	49	SCF	2	0.059	0.035	0.907	768
60.10	189.01	49	SCF	2	0.052	0.028	0.919	
60.10	197.21	67	LIQ	2	0.961	0.016	0.023	
60.10	195.51	67	LIQ	2	0.962	0.017	0.021	1013
59.95	195.01	67	SCF	2	0.006	0.002	0.992	
59.95	193.01	67	SCF	2	0.005	0.000	0.994	
59.95	192.01	67	SCF	2	0.005	0.000	0.994	
60.00	198.51	79	LIQ	2	0.661	0.247	0.092	1044
60.00	195.01	79	SCF	2	0.018	0.104	0.878	
60.00	192.01	79	SCF	2	0.017	0.100	0.883	824
59.90	198.51	58	LIQ	2	0.934	0.040	0.025	1021
59.90	196.51	58	LIQ	2	0.932	0.042	0.026	
59.90	194.51	58	SCF	2	0.007	0.008	0.985	
59.90	194.51	58	SCF	2	0.007	0.006	0.987	751
60.05	200.12	32	LIQ	2	0.459	0.344	0.198	
60.05	199.02	32	LIQ	2	0.453	0.353	0.194	1033
60.05	195.02	32	SCF	2	0.060	0.212	0.728	
60.05	192.02	32	SCF	2	0.040	0.198	0.762	888
59.90	203.01	41	LIQ	2	0.526	0.312	0.162	
59.90	201.51	41	LIQ	2	0.043	0.169	0.787	
59.90	197.01	41	LIQ	2	0.525	0.316	0.159	
59.90	195.51	41	SCF	2	0.041	0.164	0.795	874

†‡ See footnotes to Table C.3

C.5 *n*-Butyric acid - water - carbon dioxide

The methodology described in Sections C.2 and C.3 is followed in the presentation of the experimental data for this system in Table C.9.

Table C.9 Experimental results for the mixture water(1) - *n*-butyric acid(2) - carbon dioxide(3) at 40 °C (313.1 K)

T °C	P bar	run†	phase	M	mole fractions† X_1	X_2	X_3	density kg/m^3
40.05	19.58	16	LIQ	2	0.467	0.446	0.086	974
40.05	19.82	21	LIQ	2	0.698	0.256	0.046	987
40.05	19.91	21	LIQ	2	0.673	0.279	0.048	
40.05	20.13	35	LIQ	2	0.931	0.058	0.011	1007
40.05	20.38	35	LIQ	2	0.933	0.055	0.012	
40.05	20.21	29	LIQ	2	0.876	0.106	0.018	1002
40.05	20.45	29	LIQ	2	0.879	0.103	0.018	
40.05	20.44	6	LIQ	2	0.106	0.679	0.209	954
40.05	20.60	6	LIQ	2	0.333	0.006	0.646	
40.05	20.50	11	LIQ	2	0.302	0.547	0.149	964
40.05	20.63	11	LIQ	2	0.291	0.558	0.146	
40.10	20.55	1	LIQ	2	0.043	0.743	0.204	952
40.10	20.59	1	LIQ	2	0.034	0.756	0.202	
40.05	39.62	7	LIQ	2	0.072	0.570	0.354	
40.10	39.68	2	LIQ	2	0.034	0.596	0.357	951
40.10	39.57	2	LIQ	2	0.025	0.599	0.370	
40.05	39.79	30	LIQ	3	0.939	0.043	0.018	1012
40.05	39.71	30	LIQ	3	0.946	0.036	0.018	
40.05	39.59	30	LIQ2	3	0.704	0.220	0.075	993
40.05	39.49	30	LIQ2	3	0.701	0.225	0.074	
40.05	39.77	12	LIQ	2	0.234	0.498	0.262	964
40.05	39.60	12	LIQ	2	0.226	0.503	0.269	
40.05	39.87	17	LIQ	2	0.415	0.409	0.174	975
40.05	39.72	17	LIQ	2	0.419	0.408	0.173	
40.05	40.46	22	LIQ	2	0.638	0.261	0.100	
40.05	58.84	0	LIQ	2	0.444	0.298	0.257	
40.05	58.83	0	LIQ	2	0.472	0.293	0.235	
40.05	59.75	31	LIQ	3	0.951	0.030	0.019	1015
40.05	58.84	31	LIQ	3	0.952	0.026	0.021	
40.05	58.46	31	LIQ2	3	0.390	0.324	0.286	974
40.05	58.46	31	LIQ2	3	0.373	0.340	0.286	

(continued on next page)

Table C.9 (continued)

T °C	P bar	run‡	phase	M	mole fractions† X_1	X_2	X_3	density kg/m³
40.05	59.65	13	LIQ	2	0.156	0.403	0.435	954
40.05	58.99	13	LIQ	2	0.166	0.398	0.432	
40.05	60.11	18	LIQ	2	0.316	0.359	0.326	969
40.05	59.31	18	LIQ	2	0.325	0.354	0.322	
40.05	60.50	3	LIQ	2	0.022	0.404	0.569	936
40.05	60.54	8	LIQ	2	0.051	0.405	0.538	
40.05	60.48	8	LIQ	2	0.049	0.410	0.538	940
40.05	69.77	19	LIQ	2	0.136	0.334	0.531	929
40.05	68.83	19	LIQ	2	0.158	0.326	0.516	947
40.05	70.08	32	LIQ	3	0.963	0.018	0.020	1017
40.05	68.46	32	LIQ2	3	0.129	0.310	0.561	939
40.05	68.38	32	LIQ2	3	0.130	0.332	0.537	
40.05	70.01	32	SCF	3	0.002	0.112	0.887	
40.05	70.01	32	SCF	3	0.001	0.016	0.983	
40.05	70.04	32	SCF	3	0.002	0.004	0.994	
40.05	70.04	32	SCF	3	0.999	0.001	0.000	
40.05	69.62	9	LIQ	2	0.038	0.318	0.642	918
40.05	69.51	9	LIQ	2	0.033	0.302	0.662	
40.05	69.42	9	SCF	2	0.002	0.086	0.911	
40.05	69.44	9	SCF	2	0.001	0.013	0.986	
40.05	69.86	14	LIQ	2	0.107	0.310	0.579	932
40.05	69.86	14	LIQ	2	0.105	0.317	0.578	
40.05	71.06	4	LIQ	2	0.017	0.274	0.706	906
40.05	70.95	4	LIQ	2	0.016	0.270	0.709	
40.05	79.21	36	LIQ	2	0.957	0.023	0.020	1017
40.05	78.29	36	LIQ	2	0.963	0.017	0.020	
40.05	75.13	36	LIQ	2	0.961	0.019	0.020	
40.05	74.39	36	LIQ2	2	0.176	0.378	0.445	1018
40.05	75.12	36	LIQ2	2	0.152	0.399	0.449	
40.05	78.11	15	LIQ	2	0.032	0.169	0.799	848
40.05	78.02	15	LIQ	2	0.029	0.157	0.815	
40.05	79.37	10	LIQ	2	0.015	0.112	0.868	
40.05	79.04	10	LIQ	2	0.022	0.115	0.863	821
40.05	78.90	10	SCF	2	0.002	0.031	0.967	
40.05	78.91	10	SCF	2	0.002	0.007	0.990	
40.05	78.84	10	SCF	2	0.002	0.003	0.995	
40.05	79.46	31	LIQ	3	0.961	0.018	0.021	1017
40.05	79.21	31	LIQ2	3	0.056	0.122	0.822	832
40.05	79.46	31	LIQ2	3	0.041	0.123	0.835	
40.05	79.90	5	LIQ	2	0.005	0.111	0.882	804
40.05	79.50	5	LIQ	2	0.005	0.109	0.886	
40.05	79.49	5	SCF	2	0.001	0.049	0.951	

(continued on next page)

Table C.9 (concluded)

T °C	P bar	run‡	phase	M	mole fractions† X_1	X_2	X_3	density kg/m³
40.05	79.45	5	SCF	2	0.001	0.022	0.977	
40.05	81.49	20	LIQ	1	0.053	0.255	0.691	
40.05	80.92	20	SCF	2	0.085	0.334	0.577	
40.05	80.31	20	SCF	2	0.070	0.268	0.658	
40.05	79.57	20	SCF	2	0.088	0.334	0.574	
40.05	98.31	25	LIQ	2	0.957	0.023	0.020	
40.05	96.41	25	LIQ	2	0.959	0.021	0.020	1018
40.05	93.31	25	SCF	2	0.334	0.306	0.359	970
40.05	99.01	28	LIQ	2	0.934	0.047	0.019	1014
40.05	99.01	28	LIQ	2	0.935	0.044	0.021	
40.05	101.51	28	SCF	2	0.784	0.157	0.060	999
40.05	98.01	28	SCF	2	0.736	0.181	0.081	
40.05	99.51	32	LIQ	2	0.965	0.014	0.021	1019
40.05	99.82	32	LIQ	2	0.967	0.012	0.021	
40.05	100.05	32	SCF	2	0.052	0.220	0.728	857
40.05	101.30	22	LIQ	2	0.961	0.019	0.020	1019
40.05	101.11	22	LIQ	2	0.961	0.018	0.021	
40.05	100.71	22	SCF	2	0.134	0.265	0.601	
40.05	97.01	22	SCF	2	0.111	0.306	0.583	946
40.05	151.35	23	LIQ	2	0.950	0.029	0.021	
40.05	148.81	23	LIQ	2	0.958	0.020	0.021	1021
40.05	140.51	23	SCF	2	0.129	0.246	0.626	
40.05	143.31	23	SCF	2	0.129	0.257	0.614	955
40.05	151.01	26	LIQ	2	0.948	0.031	0.021	1019
40.05	151.51	26	SCF	2	0.363	0.287	0.329	982
40.05	151.01	26	SCF	2	0.370	0.295	0.335	
40.05	152.01	33	LIQ	2	0.956	0.022	0.021	1021
40.05	150.01	33	LIQ	2	0.963	0.015	0.022	
40.05	153.01	33	SCF	2	0.041	0.171	0.788	915
40.05	153.01	33	SCF	2	0.040	0.179	0.782	
40.05	199.01	34	LIQ	2	0.963	0.015	0.023	1023
40.05	193.01	34	LIQ	2	0.963	0.014	0.022	
40.05	188.01	34	SCF	2	0.052	0.178	0.770	
40.05	185.01	34	SCF	2	0.047	0.179	0.773	932
40.05	194.01	24	LIQ	2	0.954	0.024	0.022	1022
40.05	198.01	24	SCF	2	0.130	0.251	0.619	966
40.05	200.51	27	LIQ	2	0.956	0.022	0.021	
40.05	194.01	27	LIQ	2	0.947	0.026	0.027	1021
40.05	196.01	27	SCF	2	0.433	0.269	0.298	989
40.05	197.01	27	SCF	2	0.404	0.289	0.307	

‡‡ See footnotes to Table C.3

C.6 Carbon dioxide - ethanol

Data for this binary system were obtained in the initial stages of the operation of the equipment. Some water was found present in the system, coming from the ethanol used; the measured concentration is listed in the table. The run number is not listed in the table, since all points correspond closely to the binary system ethanol - carbon dioxide.

Table C.10 Experimental results for the system carbon dioxide(1) - ethanol(2) at 35, 50 and 65 °C.

T °C	P bar	phase	M	mole fractions† X_1	X_2	water
35.08	12.45	LIQ	2	0.078	0.914	0.003
34.95	12.45	LIQ	2	0.077	0.915	0.004
35.08	12.45	LIQ	2	0.078	0.914	0.003
35.10	12.48	SCF	2	0.973	0.018	0.000
34.70	12.63	LIQ	2	0.077	0.915	0.004
35.10	26.45	SCF	2	0.987	0.009	0.000
35.10	26.46	SCF	2	0.987	0.010	0.000
35.10	26.48	SCF	2	0.987	0.010	0.000
35.10	26.54	LIQ	2	0.166	0.825	0.004
35.10	26.75	LIQ	2	0.167	0.826	0.004
35.10	34.77	SCF	2	0.990	0.008	0.000
35.10	34.77	SCF	2	0.989	0.009	0.000
35.10	34.79	SCF	2	0.989	0.009	0.000
35.10	34.85	LIQ	2	0.224	0.768	0.003
35.10	35.14	LIQ	2	0.222	0.770	0.003
35.10	42.36	SCF	2	0.991	0.007	0.000
35.10	42.47	SCF	2	0.991	0.007	0.000
35.10	42.47	LIQ	2	0.283	0.710	0.003
35.10	42.73	LIQ	2	0.283	0.709	0.003
35.10	51.86	SCF	2	0.991	0.007	0.000
35.10	51.88	SCF	2	0.991	0.007	0.000
35.10	51.95	LIQ	2	0.369	0.625	0.003
35.10	52.20	LIQ	2	0.370	0.624	0.003
35.10	63.83	SCF	2	0.991	0.008	0.000
35.10	63.86	SCF	2	0.992	0.008	0.000
35.10	63.87	SCF	2	0.990	0.008	0.001
35.10	64.01	LIQ	2	0.535	0.460	0.002
35.10	64.31	LIQ	2	0.541	0.454	0.002
35.05	69.09	LIQ	2	0.711	0.286	0.001

(continued on next page)

Table C.10 (continued)

T °C	P bar	phase	M	mole fractions† X_1	X_2	water
35.07	69.09	SCF	2	0.991	0.009	0.000
35.10	69.10	SCF	2	0.990	0.010	0.000
35.08	69.13	SCF	2	0.989	0.010	0.000
35.00	69.27	LIQ	2	0.702	0.296	0.000
35.08	71.59	SCF	2	0.989	0.011	0.000
35.08	71.63	SCF	2	0.986	0.011	0.003
35.08	71.66	LIQ	2	0.867	0.131	0.001
35.09	71.72	LIQ	2	0.867	0.131	0.001
35.01	72.34	SCF	2	0.990	0.010	0.000
35.01	72.34	SCF	2	0.989	0.010	0.000
35.00	72.37	SCF	2	0.990	0.009	0.000
35.00	72.43	LIQ	2	0.906	0.092	0.000
35.03	72.53	LIQ	2	0.907	0.091	0.000
50.00	17.17	SCF	2	0.952	0.044	0.000
50.00	17.18	SCF	2	0.958	0.038	0.000
50.00	17.19	SCF	2	0.954	0.043	0.000
50.00	17.21	LIQ	2	0.086	0.910	0.001
50.02	17.23	LIQ	2	0.086	0.909	0.002
50.02	26.66	SCF	2	0.978	0.019	0.000
50.02	26.67	SCF	2	0.978	0.020	0.000
50.02	26.70	SCF	2	0.978	0.019	0.000
50.02	26.72	LIQ	2	0.138	0.857	0.002
50.02	26.75	LIQ	2	0.135	0.860	0.002
50.00	26.77	LIQ	2	0.137	0.859	0.001
50.00	38.00	SCF	2	0.983	0.015	0.000
50.00	38.01	SCF	2	0.985	0.014	0.000
50.00	38.03	SCF	2	0.984	0.015	0.000
50.02	38.07	LIQ	2	0.195	0.801	0.002
50.02	38.10	LIQ	2	0.192	0.804	0.001
50.00	38.42	LIQ	2	0.197	0.799	0.001
50.00	48.32	LIQ	2	0.255	0.741	0.001
50.00	48.37	SCF	2	0.986	0.013	0.000
50.00	48.49	LIQ	2	0.257	0.739	0.001
50.00	62.55	LIQ	2	0.350	0.646	0.001
50.00	62.59	LIQ	2	0.352	0.645	0.001
50.00	62.66	SCF	2	0.986	0.013	0.000
50.00	62.66	SCF	2	0.987	0.013	0.000
50.00	62.69	SCF	2	0.987	0.012	0.000
50.00	75.20	SCF	2	0.983	0.016	0.000
50.00	75.21	SCF	2	0.985	0.015	0.000
50.00	75.33	SCF	2	0.985	0.015	0.000
50.00	75.42	LIQ	2	0.459	0.538	0.001
50.00	75.42	LIQ	2	0.466	0.532	0.000

(continued on next page)

Table C.10 (continued)

T °C	P bar	phase	M	mole fractions† X_1	X_2	water
50.00	87.61	LIQ	2	0.660	0.337	0.001
50.00	87.65	LIQ	2	0.662	0.336	0.000
50.04	87.66	SCF	2	0.974	0.025	0.000
50.02	87.69	SCF	2	0.974	0.025	0.000
50.00	87.69	SCF	2	0.973	0.026	0.000
50.01	90.21	SCF	2	0.965	0.035	0.000
50.01	90.26	SCF	2	0.948	0.052	0.000
50.03	90.28	SCF	2	0.961	0.038	0.000
50.02	90.36	LIQ	2	0.750	0.248	0.000
50.04	90.41	LIQ	2	0.752	0.246	0.001
50.00	91.71	SCF	2	0.870	0.129	0.000
50.00	91.71	SCF	2	0.906	0.094	0.000
50.00	91.71	LIQ	2	0.815	0.183	0.000
50.00	91.71	SCF	2	0.871	0.128	0.000
50.00	91.73	LIQ	2	0.815	0.183	0.000
64.60	12.31	LIQ	2	0.051	0.948	0.001
64.63	12.31	LIQ	2	0.050	0.949	0.001
64.66	26.88	LIQ	2	0.113	0.885	0.001
64.62	27.09	LIQ	2	0.113	0.886	0.001
64.68	44.71	SCF	2	0.971	0.019	0.007
64.68	44.74	SCF	2	0.973	0.025	0.000
64.70	44.87	LIQ	2	0.196	0.803	0.001
64.70	45.19	LIQ	2	0.195	0.805	0.000
64.56	63.41	LIQ	2	0.292	0.707	0.001
64.60	63.55	LIQ	2	0.292	0.708	0.000
64.60	63.63	SCF	2	0.973	0.022	0.004
64.60	63.70	SCF	2	0.970	0.023	0.005
64.60	63.71	SCF	2	0.971	0.025	0.002
64.60	85.70	SCF	2	0.972	0.027	0.000
64.60	85.70	SCF	2	0.972	0.028	0.000
64.49	85.71	LIQ	2	0.431	0.568	0.001
64.60	85.71	SCF	2	0.973	0.027	0.000
64.60	100.76	SCF	2	0.959	0.040	0.000
64.60	100.82	SCF	2	0.959	0.040	0.000
64.60	100.98	LIQ	2	0.571	0.429	0.000
64.55	101.05	LIQ	2	0.575	0.425	0.000
64.60	109.21	SCF	2	0.882	0.117	0.000
64.60	109.25	SCF	2	0.852	0.148	0.000
64.60	109.38	LIQ	2	0.708	0.291	0.000
64.60	109.50	LIQ	2	0.710	0.290	0.000

† See footnote 1 to Table C.3

APPENDIX D: CORRELATION PARAMETERS

In Table D.1, the pure component parameters used for the correlation with the Peng-Robinson (1976) equation of state (u=2 and w=-1 in Eq. 2.7). The pure component parameters for the subcritical components were determined as described in Appendix A. The table lists the data for liquid volume and vapor pressure as a function of temperature that were used as input for the expressions given in Table A.2, as well the resulting values for the pure component parameters a and b. For the supercritical component (carbon dioxide) the normal acentric factor correlation was used.

Table D.1 Pure component parameters for the Peng-Robinson equation of state

Component	T °C	T K	ρ kg m^{-3}	P_{VP} bar	a Jm^3mol^{-2}	b m^3mol^{-2} $\times10^{-6}$
ethanol	30.0	303.2	787.8	0.1043	2.138	50.48
	35.0	308.2	782.5	0.1372	2.116	50.55
	40.0	313.2	777.2	0.1787	2.094	50.62
	45.0	318.2	771.8	0.2305	2.072	50.68
	50.0	323.2	766.3	0.2946	2.050	50.75
	55.0	328.2	760.8	0.3731	2.029	50.81
	60.0	333.2	755.2	0.4687	2.007	50.87
	65.0	338.2	749.5	0.5841	1.985	50.92
	70.0	343.2	743.8	0.7225	1.963	50.96
	75.0	348.2	737.9	0.8871	1.941	51.00
	90.0	363.2	724.0	1.5790	1.865	50.75
acetone	30.0	303.2	776.8	0.3804	2.208	62.17
	35.0	308.2	770.9	0.4660	2.192	62.27
	40.0	313.2	765.0	0.5664	2.177	62.35
	45.0	318.2	759.0	0.6837	2.162	62.44
	50.0	323.2	753.0	0.8196	2.147	62.52
	55.0	328.2	747.0	0.9764	2.132	62.59
	60.0	333.2	741.0	1.1562	2.117	62.65

(continued on next page)

Table D.1 (concluded)

Component	T °C	T K	ρ kg m^{-3}	P_{VP} bar	a Jm^3mol^{-2}	b m^3mol^{-2} $\times10^{-6}$
water	25.0	298.2	997.3	0.0317	0.8362	16.13
	30.0	303.2	996.0	0.0424	0.8293	16.11
	31.0	304.2	995.8	0.0450	0.8276	16.10
	35.0	308.2	994.0	0.0562	0.8226	16.08
	40.0	313.2	992.1	0.0738	0.8162	16.07
	50.0	323.2	988.1	0.1234	0.8032	16.02
	60.0	333.2	983.3	0.1992	0.7912	15.98
	70.0	343.2	977.5	0.3116	0.7799	15.96
	75.0	348.2	974.6	0.3855	0.7742	15.95
	80.0	353.2	971.8	0.4736	0.7688	15.94
	90.0	363.2	965.2	0.7011	0.7580	15.91
	100.0	373.2	957.9	1.0130	0.7483	15.91
n-butanol	30.0	303.2	806.1	0.0124	4.053	81.50
	40.0	313.2	796.1	0.0238	3.969	81.80
	50.0	323.2	785.9	0.0436	3.883	82.08
	60.0	333.2	775.6	0.0768	3.796	82.34
acetic acid	40.0	313.2	1028.4	0.0469	2.431	51.13
	50.0	323.2	1017.5	0.0766	2.403	51.28
	60.0	333.2	1006.0	0.1209	2.376	51.45
propionic acid	40.0	313.2	967.8	0.0134	3.534	67.95
	50.0	323.2	956.5	0.0237	3.488	68.26
	60.0	333.2	945.2	0.0402	3.441	68.54
butyric acid	40.0	313.2	938.0	0.0039	4.778	84.36
	50.0	323.2	928.2	0.0073	4.714	84.70
	60.0	333.2	918.5	0.0131	4.648	85.02
carbon dioxide		303.2			0.3970	26.65
		308.2			0.3923	26.65
		313.2			0.3876	26.65
		323.2			0.3785	26.65
		333.2			0.3696	26.65
		348.2			0.3610	26.65

Table D.2 lists the interaction parameters for the density-dependent model (Eq. 3.6 and the Peng-Robinson form of a cubic equation of state). The parameters were obtained from regression of binary data and were used for the predictions of the ternary behavior (except for the parameters for CO_2 - *n*-butanol parameters that were slightly modified to obtain a better description of the three-phase equilibrium behavior of the ternary system).

As can be seen in Table D.2, in several instances the parameters were found to be temperature independent, although a separate parameter regression at each temperature was performed. In other cases, the parameters were found to be weak functions of temperature.

Table D.2 Interaction parameters

Binary system	T (K)	$k_{12} = k_{21}$	$\lambda_{12} = -\lambda_{21}$ (J^2m^3/mol^2)
CO_2(1) - water(2)	298.2	0.012	-1710
	304.2	0.021	-1750
	313.2	0.024	-1740
	323.2	0.027	-1740
	333.2	0.028	-1710
	348.2	0.029	-1680
CO_2(1) - acetone(2)	all	0.00	0
CO_2(1) - *n*-butanol(2)	all	0.125	1310
CO_2(1) - acetic acid(2)	all	0.005	530
CO_2(1) - *n*-butyric acid(2)	313.2	0.023	527
water(1) - acetone(2)	313.2	-0.229	1305
	333.2	-0.213	1432
water(1) - *n*-butanol(2)	all	-0.164	1595
water(1) - acetic acid(2)	313.2	-0.147	410
	333.2	-0.142	580
water(1) - *n*-butyric acid(2)	313.2	-0.135	1686

APPENDIX E. DERIVATION OF FLUCTUATION EXPRESSIONS

In classical thermodynamics, a system at equilibrium is characterized by the minimization of a state function that depends upon the constraints placed on the system. For example, in an isolated system the total energy U is minimized. The conditions for the minimization of the appropriate state function result in a set of equilibrium conditions for the system. For a homogeneous system with no internal barriers to energy or mass transfer, the conditions for equilibrium would be that temperature, pressure and the chemical potential of all components be the same throughout the system. In statistical thermodynamics, the same conditions would apply, but are strictly valid only in an average sense; the exact values of the local density or energy in a small part of a system fluctuate around a mean value predicted by classical thermodynamics. The mean-squared deviation of any given quantity from the average is termed the principal fluctuation of that quantity. Also important is the correlation between fluctuations of two different properties, defined as :

$$\langle \delta X_i \, \delta X_j \rangle = \langle X_i X_j \rangle - \langle X_i \rangle \langle X_j \rangle \qquad [E.1]$$

which we term a pair-wise fluctuation. Clearly, if i=j this definition would include the principal fluctuations.

The fluctuations of thermodynamic properties, although very small for macroscopic systems under normal conditions, become important in the vicinity of phase transitions and critical points. Moreover, fluctuations are particularly significant when microscopic systems are investigated, as in light-scattering experiments, Brownian motion, or in molecular simulation. The derivation of the relationships governing the fluctuations of thermodynamic quantities also serves the purpose of elucidating the molecular mechanisms for the change of macroscopic properties when external conditions change (for example the response of the system volume to changes in total pressure).

Several relationships between pair-wise fluctuations and thermodynamic derivatives have been derived using different routes (Hill, 1956; Schofield, 1966) , but a general method for obtaining the fluctuations of any given pair of thermodynamic quantities under an arbitrary constraint has not, to our knowledge, been developed. In a recent paper Debenedetti (1986) presented relationships between the principal fluctuations and thermodynamic stability coefficients. Here, we derive general expressions for the pair-wise fluctuations of thermodynamic properties.

In the following, we consider a small (but still macroscopic) part of a larger system that is in thermodynamic equilibrium. The large system serves as an energy and mass reservoir. The small system (called simply system from now on) is defined by its extent. This definition can be operationally realized as follows : Suppose we select a fixed point in space as the origin. We would then imagine spheres (or another geometric shape) with progressively increasing diameters centered at that point. We consider as our system the one that satisfies a single extensive constraint that we have specified, e.g. a given total volume, total number of molecules of a species, or total energy. Exactly one extensive constraint is required for the definition of the system.

We will only be dealing with systems in which the fluctuations have a purely classical character and quantum effects are unimportant. A discussion of the conditions required for negligible quantum effects on the fluctuations is given elsewhere (Landau and Lifshitz, 1980).

According to classical thermodynamics, the energy of an n-component system can be written as a function of n+2 independent extensive variables (Modell and Reid, 1983):

$$U = U (X_1, X_2, \ldots X_n, X_{n+1}, X_{n+2}) \qquad [E.2]$$

The natural set of extensive variables for U comprise the total entropy S, total volume V, and N_i (i=1,n) , the number of molecules of each chemical species present. Note that the variables S, V, N_i may be ordered in an arbitrary way.

To derive the general relationship between fluctuations and the derivatives of U and its transformed functions, we start from the standard expression for the Gaussian distribution applicable for cases with more than one independent variable (Landau and Lifshitz, 1980) and obtain (Debenedetti, 1986) :

$$\begin{aligned} \langle \delta X_i \delta X_j \rangle_{X_{n+2}} &= kT_0 \, D^{-1}_{ij} && i,j \le n+1 \\ \langle \delta \xi_i \delta X_j \rangle_{X_{n+2}} &= kT_0 \, \delta_{ij} && i,j \le n+1 \\ \langle \delta \xi_i \delta \xi_j \rangle_{X_{n+2}} &= kT_0 \, D_{ij} && i,j \le n+2 \end{aligned} \qquad [E.3]$$

where $\xi_i = (\partial U/\partial X_i)_{X_{[i]}}$. The symbol $X_{[i]}$ means differentiation with all X's except X_i kept constant. T_0 is the equilibrium temperature of the system, k is Boltzmann's constant and δ_{ij} is Kronecker's delta. $\underline{D}$ is the matrix :

$$\underline{D} = \begin{bmatrix} \left.\frac{\partial \xi_1}{\partial X_1}\right|_{X_{[1]}} & \left.\frac{\partial \xi_2}{\partial X_1}\right|_{X_{[1]}} & \cdots & \left.\frac{\partial \xi_{n+1}}{\partial X_1}\right|_{X_{[1]}} \\ \left.\frac{\partial \xi_1}{\partial X_2}\right|_{X_{[2]}} & \cdots & \cdots & \cdots \\ \vdots & & & \vdots \\ \left.\frac{\partial \xi_1}{\partial X_{n+1}}\right|_{X_{[n+1]}} & \cdots & & \left.\frac{\partial \xi_{n+1}}{\partial X_{n+1}}\right|_{X_{[n+1]}} \end{bmatrix} \qquad [E.4]$$

D_{ij} and D^{-1}_{ij} are, respectively, the (ij)th element of the matrices $\underline{D}$ and $\underline{D}^{-1}$. Note the $\underline{D}$ is a real, symmetric matrix.

The variables ξ_i, can be identified as follows:

X_i	S	V	N_1	N_2	. . .	N_n
ξ_i	T	-P	μ_1	μ_2	. . .	μ_n

where P is the pressure and μ_i the chemical potential of component i. This is only one of (n+2)! possible and equally valid orderings of the variables.

We can write $\underline{D}$ in a more compact form (Kumar and Reid, 1986) :

$$\underline{D} = \frac{\partial(\xi_1,\xi_2,\xi_3,\ldots,\xi_{n+1})}{\partial(X_1,X_2,X_3,\ldots,X_{n+1})} = \begin{bmatrix} U_{11} & U_{12} & \cdots & U_{1,n+1} \\ U_{21} & U_{22} & \cdots & U_{2,n+1} \\ \cdot & & & \cdot \\ \cdot & & & \cdot \\ \cdot & & & \cdot \\ U_{n+1,1} & U_{n+1,2} & \cdot\cdot & U_{n+1,n+1} \end{bmatrix} \qquad [E.5]$$

where U_{ij} is the partial derivative $\partial^2 U/\partial X_i \partial X_j$.

Now, let us prove an important new relationship, namely that the inverse of $\underline{D}$ can be directly related to the derivatives of a transformed function of U. We will show that :

$$\underline{D}^{-1} = \frac{\partial(X_1,X_2,X_3,\ldots,X_{n+1})}{\partial(\xi_1,\xi_2,\xi_3,\ldots,\xi_{n+1})} = \begin{bmatrix} \left.\frac{\partial X_1}{\partial \xi_1}\right|_{\xi_{[1]}} & \left.\frac{\partial X_2}{\partial \xi_1}\right|_{\xi_{[1]}} & \cdots & \left.\frac{\partial X_{n+1}}{\partial \xi_1}\right|_{\xi_{[1]}} \\ \left.\frac{\partial X_1}{\partial \xi_2}\right|_{\xi_{[2]}} & & & \\ \cdot & & & \cdot \\ \cdot & & & \cdot \\ \cdot & & & \cdot \\ \left.\frac{\partial X_1}{\partial \xi_{n+1}}\right|_{\xi_{[n+1]}} & & \cdots & \left.\frac{\partial X_{n+1}}{\partial \xi_{n+1}}\right|_{\xi_{[n+1]}} \end{bmatrix} \qquad [E.6]$$

$\xi_{[i]}$ in Eq. E.6 indicates that differentiation is to be carried out at constant $\xi_1, \xi_2, \ldots \xi_{i-1}, \xi_{i+1}, \ldots \xi_{n+1}, X_{n+2}$.

The function

$$y^{(n+1)} = U - \sum_{i=1}^{n+1} X_i \xi_i \qquad [E.7]$$

is known as the n+1 Legendre transform of U. Using the properties of Legendre transforms (Callen, 1960; Beegle et al., 1974), we can identify the elements of $\underline{D}^{-1}$ in Eq. E.6 as:

$$\left.\frac{\partial X_i}{\partial \xi_j}\right|_{\xi_{[j]}} = -y_{ij}^{(n+1)} \qquad [E.8]$$

In order to prove Eq. E.6, it suffices to show that :

$$\frac{\partial(\xi_1, \xi_2, \xi_3, \ldots, \xi_{n+1})}{\partial(X_1, X_2, X_3, \ldots, X_{n+1})} \cdot \frac{\partial(X_1, X_2, X_3, \ldots, X_{n+1})}{\partial(\xi_1, \xi_2, \xi_3, \ldots, \xi_{n+1})} = \underline{I} \qquad [E.9]$$

Where $\underline{I}$ is the unit matrix. We write ξ_i as a function of the n+2 variables $X_1 \ldots X_{n+2}$:

$$d\xi_i = \left.\frac{\partial \xi_i}{\partial X_1}\right|_{X_{[1]}} dX_1 + \left.\frac{\partial \xi_i}{\partial X_2}\right|_{X_{[2]}} dX_2 + \ldots + \left.\frac{\partial \xi_i}{\partial X_{n+1}}\right|_{X_{[n+1]}} dX_{n+1} + \left.\frac{\partial \xi_i}{\partial X_{n+2}}\right|_{X_{[n+2]}} dX_{n+2} \qquad [E.10]$$

Differentiating with respect to ξ_j, keeping all ξ's (except ξ_j) and X_{n+2} constant, we obtain:

$$\frac{d\xi_i}{d\xi_j} = \delta_{ij} = \left.\frac{\partial \xi_i}{\partial X_1}\right|_{X_{[1]}} \left.\frac{\partial X_1}{\partial \xi_j}\right|_{\xi_{[j]}} + \left.\frac{\partial \xi_i}{\partial X_2}\right|_{X_{[2]}} \left.\frac{\partial X_2}{\partial \xi_j}\right|_{\xi_{[j]}} + \ldots + \left.\frac{\partial \xi_i}{\partial X_{n+1}}\right|_{X_{[n+1]}} \left.\frac{\partial X_{n+1}}{\partial \xi_j}\right|_{\xi_{[j]}} \qquad [E.11]$$

This completes the proof of Eq. E.6. Note that the treatment is general and is not restricted to the (n+1)-order matrix.

Now Eq. 3.6 can be rewritten:

$$\langle \delta X_i \delta X_j \rangle_{X_{n+2}} = kT_0 \, D_{ij}^{-1} = kT_0 \left. \frac{\partial X_i}{\partial \xi_j} \right|_{\xi_{[j]}} = - kT_0 \, y_{ij}^{(n+1)} \qquad [E.12]$$

There is only one additional derivative, namely $\langle \delta \xi_{n+2} \delta X_j \rangle$, that cannot be calculated directly from Eq. E.3. Expanding $\delta \xi_{n+2}$ in the manner of Eq. E.10, we have :

$$\langle \delta \xi_{n+2} \delta X_j \rangle_{X_{n+2}} = \left. \frac{\partial \xi_{n+2}}{\partial X_1} \right|_{X_{[1]}} \langle \delta X_1 \delta X_j \rangle_{X_{n+2}} + \left. \frac{\partial \xi_{n+2}}{\partial X_2} \right|_{X_{[2]}} \langle \delta X_2 \delta X_j \rangle_{X_{n+2}} + \ldots +$$

$$+ \left. \frac{\partial \xi_{n+2}}{\partial X_{n+1}} \right|_{X_{[n+1]}} \langle \delta X_{n+1} \delta X_j \rangle_{X_{n+2}} \qquad [E.13]$$

Now, using Eq. E.12 and the chain rule for partial differentiation,

$$\langle \delta \xi_{n+2} \delta X_j \rangle_{X_{n+2}} = kT_0 \left[\left. \frac{\partial \xi_{n+2}}{\partial X_1} \right|_{X_{[1]}} \left. \frac{\partial X_1}{\partial \xi_j} \right|_{\xi_{[j]}} + \left. \frac{\partial \xi_{n+2}}{\partial X_2} \right|_{X_{[2]}} \left. \frac{\partial X_2}{\partial \xi_j} \right|_{\xi_{[j]}} + \ldots + \right.$$

$$\left. + \left. \frac{\partial \xi_{n+2}}{\partial X_{n+1}} \right|_{X_{[n+1]}} \left. \frac{\partial X_{n+1}}{\partial \xi_j} \right|_{\xi_{[j]}} \right] = kT_0 \left. \frac{\partial \xi_{n+2}}{\partial \xi_j} \right|_{\xi_{[j]}, X_{n+2}} \qquad [E.14]$$

To summarize, we have obtained the following relationships between the fluctuations of any pair of thermodynamic variables under an arbitrary extensive constraint :

$$
\begin{aligned}
\langle \delta\xi_i \delta\xi_j \rangle_{X_{n+2}} &= -kT_0 \left.\frac{\partial \xi_i}{\partial X_j}\right|_{X_{[j]}} && i \le n+2 \ , \ j \le n+2 \\
\langle \delta\xi_i \delta X_j \rangle_{X_{n+2}} &= -kT_0 \left.\frac{\partial \xi_i}{\partial \xi_j}\right|_{\xi_{[j]}, X_{n+2}} && i \le n+2 \ , \ j \le n+1 \\
\langle \delta X_i \delta X_j \rangle_{X_{n+2}} &= -kT_0 \left.\frac{\partial X_i}{\partial \xi_j}\right|_{\xi_{[j]}, X_{n+2}} && i \le n+1 \ , \ j \le n+1
\end{aligned}
\qquad [E.15]
$$

We can write Eq. E.15 as a general expression for all cases, by using the convention :

if $\lambda_i = \xi_i$ or X_i then $\bar{\lambda}_i = X_i$ or ξ_i

Now Eq. E.15 becomes :

$$
\langle \delta\lambda_i \delta\lambda_j \rangle_{X_{n+2}} = -kT_0 \left.\frac{\partial \lambda_i}{\partial \bar{\lambda}_j}\right|_{\bar{\lambda}_{[j]}, X_{n+2}} \qquad [E.16]
$$

where it is understood that in case of conflict, the first constraint takes precedence over the second (this would be the case for the calculation of $\langle \delta\xi_i \delta\xi_{n+2} \rangle_{X_{n+2}}$).

We started from the U representation of the Fundamental Equation (Eq. E.2), and obtained expressions for the fluctuations of S, V, and N_i, as well as their conjugate variables. If we are interested in fluctuations involving U itself, we need to start from a slightly different formalism, in the S- representation of the Fundamental Equation. Writing :

$$
S = S (X_1, X_2, \ldots, X_n, X_{n+1}, X_{n+2}) \qquad [E.17]
$$

The correspondence between the X's and the ξ's in this case will be :

X_i	U	V	N_1	N_2 . . .	N_n
ξ_i	1/T	P/T	$-\mu_1/T$	$-\mu_2/T$	$-\mu_n/T$

Now the X_i variables are U,V and N_i, ordered in an arbitrary way. Following the exact same formalism as developed above (actually in[4] this is the framework for the development of Eq. E.3), we can obtain :

$$\langle \delta\lambda_i \delta\lambda_j \rangle_{X_{n+2}} = - k \left. \frac{\partial \lambda_i}{\partial \bar{\lambda}_j} \right|_{\bar{\lambda}_{[j]}} \qquad [E.18]$$

which is very similar to Eq. [E.16].

This completes our development of the general relationship between fluctuations and thermodynamic derivatives. An additional discussion of this methodology, with application examples, is given in Panagiotopoulos and Reid, 1986a.

APPENDIX F. PROGRAM LISTINGS : MONTE CARLO SIMULATION

The program to perform the Monte Carlo simulations for binary mixtures in the canonical NVT ensemble, according to the methods described in Chapter 4, was developed for execution on a CYBER 205 supercomputer. The programming language was a special version of the FORTRAN programming language (CDC FTN200) that has special extensions to take advantage of the vector processor that is primarily responsible for the high performance of the CYBER 205. All internal loops (that is, loops at the deepest level of iteration for the main program) were explicitly vectorized for maximum computational efficiency.

In addition to the part of the program executed on the supercomputer, a program was written (in normal FORTRAN 77) to generate the average thermodynamic properties of the fluid after applying the long-range corrections, from the detailed history of a simulation run produced by the simulation program. The averaging program also determines the fluctuations in the number density, energy and virial of the pressure for each subcell of the basic simulation cell.

Table F.1 presents a summary of the calling programs and subroutines, with a brief description of their function. Complete listings of the programs are given in the pages that follow, in the same order as presented in Table F.1.

Table F.1 Summary of programs and subroutines for Monte Carlo simulation

Name	Function
NVT2	Main program. After an initialization step, the basic Monte Carlo step with particle interchange is performed (as described in Section 5.6) to generate the desired number of configurations.
INP	Input subroutine. Reads the simulation parameters from appropriate input files
OUTP	Output subroutine. Generates the detailed output files with the simulation history
LJPOTEN	This subroutine is called once, at the beginning of each run, to initialize the tables containing the force and energy as a function of distance
PUTFCC	This subroutine initializes the position and type of the particles inside the simulation cell to positions corresponding to a face-centered cubic lattice.
AVG	This is the post-run averaging program that calculates the average properties of a fluid from the detailed record of the simulation history produced by the Monte Carlo simulation program.

```
C-----------------------------------------------------------------------

      PROGRAM NVT2

C-----------------------------------------------------------------------

C----   Parameter definitions

      parameter (pi=3.1415926536, twopi=6.2831853072)
      parameter (ncells=4, ntotal=4*ncells**3 ,nlf=ntotal/2)
      parameter (ncomp=2,
     1           ncross=ncomp*(ncomp+1)/2, ndiscr=7500,maxhist=10000)
      parameter (efgmin=-20.,efgmax=+20.,nefg=200)

C----   Common Blocks

      common/uparam/ulj(ndiscr,ncross), estar(ncross), sigmas(ncross)
     1              ,flj(ndiscr,ncross)
      common/initial/seed,accmax,accmin,redfact
      common/thermo/tstar, rhostar, pstar, nl
      common/techn/nconf, nsample1, nsample2, icont, maxconf
      common/distance/rcutoff, vstep(Ncomp), thstep(Ncomp),
     1                phstep(Ncomp), rstep, L, L2
      common/position/xyz(3*ntotal), Lrij(ntotal,ntotal)
      common/energy/eij(ntotal,ntotal),etotal
      common/rdfp/irdf(Ndiscr,Ncross),iconc(8,0:NCOMP)
     1 ,crdf(ncross)
      common/bft/xyztp(3*ntotal),ef(ntotal),eg(ntotal),
     1           efhist(nefg,ncomp),eghist(nefg,ncomp)

C----   Array and variable declarations

      dimension ehist(0:maxhist),movhist(0:maxhist),
     1          phist(0:maxhist),Lr(Ntotal)
      dimension dum(3*Ntotal), rmove(Ntotal), emove(ntotal),
     1          jcount(ntotal)
      dimension dum2(3*ntotal),eold(ntotal),idum(ntotal),idum1(ntotal)
      dimension e1move(ntotal),e2move(ntotal),pmove(ntotal),
     1          pij(ntotal,ntotal),p1move(ntotal),p2move(ntotal)
     1          ,ipos(ntotal),pcmol(ntotal)
     1          ,esubcell(ntotal),psubcell(ntotal)

      bit bcount(3*ntotal)
      integer seed
      real L, L2
      half precision ulj,flj,xyz,eij,ehist,phist,dum,rmove,emove
     1              ,xyztp,ef,eg,efhist,eghist
     2              ,dum2,eold,e1move,e2move,pmove,pij,p1move,p2move
     3              ,xmoved,ymoved,zmoved,pcmol,esubcell,psubcell
```

```
C-----------------------------------------------------------------------
C
C       EXECUTABLE PART
C
C-----------------------------------------------------------------------

C----   Open I/O files; read data

        call INP

C----   Initialize ulj and flj arrays

        call LJPOTEN

C----   Initialize other variables

        L = (ntotal/rhostar)**(1./3.)
        L2 = L/2.
        tstari = 1./tstar
        tstarim = -tstari
        nsucc = 0
        nsucci = 0
        do 90 j = 1,ncross
        do 90 jj = 1,ndiscr
90      irdf(jj,j) = 0
        do 91 j = 1,8
        do 91 jj=0,ncomp
91      iconc(j,jj) = 0
        do 92 j = 1,nefg
        do 92 jj = 1,ncomp
        efhist(j,jj) = 0.
92      eghist(j,jj) = 0.
        crdf(1) = rhostar*4*pi*(n1-1)/ntotal*rstep**3
        crdf(2) = rhostar*4*pi*n1*(ntotal-n1)/ntotal*rstep**3
        crdf(3) = rhostar*4*pi*(ntotal-n1-1)/ntotal*rstep**3

C-----------------------------------------------------------------------

C------ If this is not a continuation, initialize positions and vsteps

        if (icont.NE.0) then
        nconf = 0
        do 110 j = 1,ncomp
110     vstep(j) = 1./(16.*rhostar)**(1./3.)/sigmas(j)
        call PUTFCC
        endif

        maxconf = nconf + maxconf
        etotal = 0
        pstar = 0
```

```
C-----------------------------------------------------------------------
C
C       Initialize energies and distances for all particles

        do 190 kmoved = 1,ntotal


        if (Kmoved.LE.N1) then
        Ktype = 1
        else
        Ktype = 2
        endif

C----   Minimum image convention

        do 120 j=1,ntotal
        dum(j          ) = abs (xyz(kmoved          ) - xyz(j          ))
        dum(j+  ntotal) = abs (xyz(kmoved +  ntotal) - xyz(j+  Ntotal))
120     dum(j+2*ntotal) = abs (xyz(kmoved +2*ntotal) - xyz(j+2*Ntotal))

        do 130 j=1,3*Ntotal
        if (dum(j).GT.L2) dum(j) = L-dum(j)
130     dum(j) = dum(j)*dum(j)

        do 150 j=1,Ntotal
150     rmove(j) = SQRT ( dum(j)   dum(j+Ntotal) + dum(j+2*Ntotal) )

C----   Energy interaction calculation

        NLJ1 = Ktype
        NLJ2 = (MIN(2,ktype)-1)*(2*ncomp-MIN(2,ktype)+2)/2 + 1
     1         + ABS(2-ktype)


        do 200 j=1,Ntotal
200     Lr(j) = MIN(INT(rmove(j)/rstep)+1,Ndiscr)

        do 210 j = 1,nl
        pmove(j) = flj(Lr(j),nlj1)
210     emove(j) = ulj(Lr(j),nlj1)
        do 220 j = nl+1,ntotal
        pmove(j) = flj(Lr(j),nlj2)
220     emove(j) = ulj(Lr(j),nlj2)

        emove(kmoved) = 0
        pmove(kmoved) = 0

        do 240 j = kmoved+1,ntotal
        pstar = pstar + pmove(j)
240     etotal = etotal + emove(j)
```

```
        do 260 j = 1,ntotal
        pij(j,kmoved) = pmove(j)
        Eij(j,kmoved) = emove(j)
260     Lrij(j,kmoved) = lr(j)


        do 291 j = 1,nl
291     irdf(Lrij(j,kmoved),NLJ1) = irdf(Lrij(j,kmoved),NLJ1) + 1
        do 292 j = nl+1, ntotal
292     irdf(Lrij(j,kmoved),NLJ2) = irdf(Lrij(j,kmoved),NLJ2) + 1
        jc = 1
        if(xyz(kmoved).GE.L2) jc = 2
        if(xyz(kmoved+ntotal).GE.L2) jc = jc + 2
        if(xyz(kmoved+2*ntotal).GE.L2) jc = jc + 4
        ipos(kmoved) = jc


190     continue

C       End of loop for initial configuration over all particles
C-------------------------------------------------------------------

C----   Write initial configuration and energy in OUTP

        call OUTP1
        ehist(0) = etotal
        movhist(0) = 0
        phist(0) = pstar

C-------------------------------------------------------------------
C
C       MAIN LOOP
C
C-------------------------------------------------------------------


1000    continue

C----   Determine which particle moves

        Kmoved = INT(ranf()*Ntotal) + 1

        if (Kmoved.LE.N1) then
        Ktype = 1
        else
        Ktype = 2
        endif
```

```
C----   Find new particle position

        deltar = ranf()*vstep(ktype)
        w1 = ranf()*twopi - pi
        w2 = ranf()*twopi
        xmoved = xyz(Kmoved         ) + deltaR*COS(w1)*COS(w2)
        ymoved = xyz(Kmoved+  Ntotal) + deltaR*COS(w1)*SIN(w2)
        zmoved = xyz(Kmoved+2*Ntotal) + deltaR*SIN(w1)

C----   Test if particle has moved out of the box and correct

        if (xmoved.GT.L) xmoved = xmoved - L
        if (ymoved.GT.L) ymoved = ymoved - L
        if (zmoved.GT.L) zmoved = zmoved - L

        if (xmoved.LE.0) xmoved = xmoved + L
        if (ymoved.LE.0) ymoved = ymoved + L
        if (zmoved.LE.0) zmoved = zmoved + L

C----   Calculate minimum image convention distances

        dum(1;ntotal) = vabs(xmoved-xyz(1;ntotal);dum(1;ntotal))
        dum(1+ntotal;ntotal) = vabs(ymoved-xyz(1+ntotal;ntotal);
     1                              dum(1+ntotal;ntotal))
        dum(1+2*ntotal;ntotal) = vabs(zmoved-xyz(1+2*ntotal;ntotal);
     1                              dum(1+2*ntotal;ntotal))
        dum(kmoved           ) = 0.0
        dum(kmoved +   ntotal) = 0.0
        dum(kmoved + 2*ntotal) = 0.0

        where(dum(1;3*ntotal).gt.L2)
     1             dum(1;3*ntotal) = L-dum(1;3*ntotal)
        dum(1;3*ntotal) = dum(1;3*ntotal) * dum(1;3*ntotal)

        do 450 j=1,Ntotal
450     rmove(j) = SQRT ( dum(j) + dum(j+Ntotal) + dum(j+2*Ntotal) )

C----   Energy interaction update

        nlj1 = ktype
        nlj2 = (min(2,ktype)-1)*(2*ncomp-min(2,ktype)+2)/2 + 1
     1        + abs(2-ktype)

        rstepin = 1./rstep
        lr(1;ntotal) = vifix(rmove(1;ntotal)*rstepin+1;lr(1;ntotal))
        where (lr(1;ntotal).gt.ndiscr) lr(1;ntotal) = ndiscr

        lr(kmoved) = 1
```

```
      emove(1;nl) = q8vgathr(ulj(1,nlj1;ndiscr),lr(1;nl);
     1              emove(1;nl))
      emove(nl+1;ntotal-nl) = q8vgathr(ulj(1,nlj2;ndiscr),
     1          lr(nl+1;ntotal-nl);emove(nl+1;ntotal-nl))

C---- Energy update; Add new interactions

      detotal = q8ssum(emove(1;ntotal))

C---- Subtract old interactions

      deold = q8ssum(eij(1,kmoved;ntotal))
      detotal = detotal - deold

C-----------------------------------------------------------------------
C     Reject/Accept new configuration based on Metropolis scheme
C-----------------------------------------------------------------------

      pacc = 1.
      if (detotal.gt.0) pacc = exp (-detotal/tstar)

      if (ranf().lt.pacc) then

C---- Accept new configuration

C---- Calculate position of particle after the move

      jc = 1
      if(xmoved.GE.L2) jc = 2
      if(ymoved.GE.L2) jc = jc + 2
      if(zmoved.GE.L2) jc = jc + 4
      ipos(kmoved) = jc

C---- Update position

      xyz(kmoved         ) = xmoved
      xyz(kmoved+  ntotal) = ymoved
      xyz(kmoved+2*Ntotal) = zmoved

      Etotal = Etotal + DEtotal

C---- Calculate old contribution to pressure

      pold = q8ssum(pij(1,kmoved;ntotal))

C---- Calculate new contribution to pressure

      pmove(1;nl) = q8vgathr(flj(1,nlj1;ndiscr),lr(1;nl);
     1              pmove(1;nl))
      pmove(nl+1;ntotal-nl) = q8vgathr(flj(1,nlj2;ndiscr),
     1          lr(nl+1;ntotal-nl);pmove(nl+1;ntotal-nl))
```

```
C----   Update pressure

        pstar = pstar - pold + q8ssum(pmove(1;ntotal))

C----   Update interaction matrices

        eij(1,kmoved;ntotal) = emove(1;ntotal)
        pij(1,kmoved;ntotal) = pmove(1;ntotal)
        lrij(1,kmoved;ntotal) = lr(1;ntotal)
        eij(kmoved,1;1) = q8vscatp(emove(1;ntotal),ntotal,ntotal;
     1       eij(kmoved,1;1))
        pij(kmoved,1;1) = q8vscatp(pmove(1;ntotal),ntotal,ntotal;
     1       pij(kmoved,1;1))
        lrij(kmoved,1;1) = q8vscatp(lr(1;ntotal),ntotal,ntotal;
     1            lrij(kmoved,1;1))

        nsucc = nsucc + 1
        endif

C----   End of updates for succesful move

C-----------------------------------------------------------------------

C----   Update RDF information (assuming all lrij's different)

        iduml(1;nl) = q8vgathr(irdf(1,nlj1;ndiscr),lrij(1,kmoved;nl);
     1                  iduml(1;nl))
        iduml(1+nl;ntotal-nl) = q8vgathr(irdf(1,nlj2;ndiscr),
     1    lrij(1+nl,kmoved;ntotal-nl);iduml(1+nl;ntotal-nl))
        iduml(1;ntotal) = iduml(1;ntotal) + 1
        irdf(1,nlj1;ndiscr) = q8vscatr(iduml(1;nl),lrij(1,kmoved;nl);
     1                        irdf(1,nlj1;ndiscr))
        irdf(1,nlj2;ndiscr) = q8vscatr(iduml(1+nl;ntotal-nl),
     1     lrij(1+nl,kmoved;ntotal-nl);irdf(1,nlj2;ndiscr))

C----   Bookkeeping

        nconf = nconf + 1
        ehist(mod(nconf,nsample1)) = etotal
        movhist(mod(nconf,nsample1)) = kmoved
        phist(mod(nconf,nsample1)) = pstar
        if(nconf.gt.maxconf) goto 9999

C       if(nconf.ge.0) goto 2222
C-----------------------------------------------------------------------
C     Interchange Step
C-----------------------------------------------------------------------


        k1moved = int(ranf()*N1) + 1
        k2moved = int(ranf()*(Ntotal-N1)) + N1 + 1
```

```
C----   Interchange role of klmoved and k2moved in lrij (tentative)

        ill = lrij(klmoved,k2moved)
        lrij(klmoved,klmoved) = ill
        lrij(klmoved,k2moved) = 1
        lrij(k2moved,k2moved) = ill
        lrij(k2moved,klmoved) = 1

C----   Calculate new Energies

        elmove(1;nl) = q8vgathr(ulj(1,1;ndiscr),lrij(1,k2moved;nl);
     1                  elmove(1;nl))
        elmove(nl+1;ntotal-nl) = q8vgathr(ulj(1,2;ndiscr),
     1          lrij(nl+1,k2moved;ntotal-nl);elmove(nl+1;ntotal-nl))

        e2move(1;nl) = q8vgathr(ulj(1,2;ndiscr),lrij(1,klmoved;nl);
     1                  e2move(1;nl))
        e2move(nl+1;ntotal-nl) = q8vgathr(ulj(1,3;ndiscr),
     1          lrij(nl+1,klmoved;ntotal-nl);e2move(nl+1;ntotal-nl))

C----   Calculate old contribution to energy

        deold = q8ssum(eij(1,klmoved;ntotal)) + q8ssum(eij(1,k2moved;
     1          ntotal))

C----   Energy update; Add new interactions

        detotal = q8ssum(elmove(1;ntotal)) + q8ssum(e2move(1;ntotal))
        detotal = detotal - deold

C-----------------------------------------------------------------------
C       Reject/Accept new configuration based on Metropolis scheme
C-----------------------------------------------------------------------

        pacc = 1.
        if (detotal.gt.0) pacc = exp (-detotal/tstar)

        if (ranf().lt.pacc) then

C----   Accept new configuration

C----   Interchange position of particles before and after the move

        idump = ipos(klmoved)
        ipos(klmoved) = ipos(k2moved)
        ipos(k2moved) = idump
```

```
C----   Update position

        xmoved = xyz(klmoved          )
        ymoved = xyz(klmoved+  ntotal)
        zmoved = xyz(klmoved+2*ntotal)
        xyz(klmoved          ) = xyz(k2moved          )
        xyz(klmoved+  ntotal) = xyz(k2moved+  ntotal)
        xyz(klmoved+2*ntotal) = xyz(k2moved+2*ntotal)
        xyz(k2moved          ) = xmoved
        xyz(k2moved+  ntotal) = ymoved
        xyz(k2moved+2*Ntotal) = zmoved

C----   Update Energy and Pressure

        Etotal = Etotal + DEtotal

        p1move(1;n1) = q8vgathr(flj(1,1;ndiscr),lrij(1,k2moved;n1);
     1                  p1move(1;n1))
        p1move(n1+1;ntotal-n1) = q8vgathr(flj(1,2;ndiscr),
     1          lrij(n1+1,k2moved;ntotal-n1);p1move(n1+1;ntotal-n1))

        p2move(1;n1) = q8vgathr(flj(1,2;ndiscr),lrij(1,klmoved;n1);
     1                  p2move(1;n1))
        p2move(n1+1;ntotal-n1) = q8vgathr(flj(1,3;ndiscr),
     1          lrij(n1+1,klmoved;ntotal-n1);p2move(n1+1;ntotal-n1))

         pstar = pstar - q8ssum(pij(1,klmoved;ntotal)) -
     1                   q8ssum(pij(1,k2moved;ntotal)) +
     2           q8ssum(p1move(1;ntotal)) + q8ssum(p2move(1;ntotal))

C----   Update interaction matrices

        eij(1,klmoved;ntotal) = e1move(1;ntotal)
        eij(1,k2moved;ntotal) = e2move(1;ntotal)
        pij(1,klmoved;ntotal) = p1move(1;ntotal)
        pij(1,k2moved;ntotal) = p2move(1;ntotal)
        idum(1;ntotal) = lrij(1,klmoved;ntotal)
        idum1(1;ntotal) = lrij(1,k2moved;ntotal)
        lrij(1,klmoved;ntotal) = idum1(1;ntotal)
        lrij(1,k2moved;ntotal) = idum(1;ntotal)
        eij(klmoved,1;1) = q8vscatp(e1move(1;ntotal),ntotal,ntotal;
     1       eij(klmoved,1;1))
        eij(k2moved,1;1) = q8vscatp(e2move(1;ntotal),ntotal,ntotal;
     1       eij(k2moved,1;1))
        pij(klmoved,1;1) = q8vscatp(p1move(1;ntotal),ntotal,ntotal;
     1       pij(klmoved,1;1))
        pij(k2moved,1;1) = q8vscatp(p2move(1;ntotal),ntotal,ntotal;
     1       pij(k2moved,1;1))
        lrij(klmoved,1;1) = q8vscatp(idum1(1;ntotal),ntotal,ntotal;
     1            lrij(klmoved,1;1))
        lrij(k2moved,1;1) = q8vscatp(idum(1;ntotal),ntotal,ntotal;
     1            lrij(k2moved,1;1))
```

```
        nsucci = nsucci + 1

        else

C----   Return Lrij to its original state

        lrij(k1moved,k2moved) = ill
        lrij(k1moved,k1moved) = 1
        lrij(k2moved,k1moved) = ill
        lrij(k2moved,k2moved) = 1

        endif

C       End of updates for succesful interchange step
C-------------------------------------------------------------------
2222    continue

C----   Test if it is time to do book-keeping; do it or goto to 1000

        if (mod(Nconf,Nsample1).EQ.nsample1-1) then

C----   Calculate energy and pressure block averages

        ebavg = q8ssum(ehist(0;nsample1))
        pbavg = q8ssum(phist(0;nsample1))

        ebavg = ebavg/nsample1/ntotal
        pbavg = pbavg/(3*ntotal*estar(1))*rhostar/nsample1
        psucc = float(nsucc)/float(nsample1)
        psucci = float(nsucci)/float(nsample1)

        do 660 j = 1,ntotal
        eg(j) = q8ssum(eij(1,j;ntotal))
660     pcmol(j) = q8ssum(pij(1,j;ntotal))

C----   Calculate energies, virials and numbers in subcells

        do 650 j = 1,8
        bcount(1;ntotal) = ipos(1;ntotal).eq.j
        bcount(1+ntotal;n1) = ipos(1;n1).eq.j
        bcount(1+ntotal+n1;ntotal-n1) = ipos(1+n1;ntotal-n1).eq.j
        esubcell(j) = 0.5*q8ssum(eg(1;ntotal),bcount(1;ntotal))
        psubcell(j) = 0.5*q8ssum(pcmol(1;ntotal),bcount(1;ntotal))
        iconc(j,0) = q8scnt(bcount(1;ntotal))
        iconc(j,1) = q8scnt(bcount(1;n1))
650     iconc(j,2) = q8scnt(bcount(1+n1;ntotal-n1))
```

```
C----   Calculate BFT and histograms for f and g

        do 800 kmoved = 1,ntotal

        dum(1;ntotal) = vabs(xyztp(kmoved)-xyz(1;ntotal);dum(1;ntotal))
        dum(1+ntotal;ntotal) = vabs(xyztp(kmoved+ntotal)
     1                              -xyz(1+ntotal;ntotal);
     1                              dum(1+ntotal;ntotal))
        dum(1+2*ntotal;ntotal) = vabs(xyztp(kmoved+2*ntotal)
     1                              -xyz(1+2*ntotal;ntotal);
     1                              dum(1+2*ntotal;ntotal))

        where(dum(1;3*ntotal).gt.L2)
     1             dum(1;3*ntotal) = L-dum(1;3*ntotal)
        dum(1;3*ntotal) = dum(1;3*ntotal) * dum(1;3*ntotal)

        do 850 j=1,Ntotal
850     rmove(j) = SQRT ( dum(j) + dum(j+Ntotal) + dum(j+2*Ntotal) )

        ktype = 1
        if (kmoved.gt.nlf) ktype = 2
        nlj1 = ktype
        nlj2 = (min(2,ktype)-1)*(2*ncomp-min(2,ktype)+2)/2 + 1
     1        + abs(2-ktype)

        rstepin = 1./rstep
        lr(1;ntotal) = vifix(rmove(1;ntotal)*rstepin+1;lr(1;ntotal))
        where (lr(1;ntotal).gt.ndiscr) lr(1;ntotal) = ndiscr

        emove(1;nl) = q8vgathr(ulj(1,nlj1;ndiscr),lr(1;nl);
     1                emove(1;nl))
        emove(nl+1;ntotal-nl) = q8vgathr(ulj(1,nlj2;ndiscr),
     1           lr(nl+1;ntotal-nl);emove(nl+1;ntotal-nl))

        ef(kmoved) = q8ssum(emove(1;ntotal))
        ef(kmoved) = min(ef(kmoved),half(efgmax))
        ncountf = int((ef(kmoved)-efgmin)/(efgmax-efgmin)*nefg) + 1
        ncountf = max(1,ncountf)
        ncountf = min(nefg,ncountf)
        efhist(ncountf,ktype) = efhist(ncountf,ktype) + 1
        ncountg = int((eg(kmoved)-efgmin)/(efgmax-efgmin)*nefg) + 1
        ncountg = max(1,ncountg)
        ncountg = min(nefg,ncountg)
        ktype = 1
        if (kmoved.gt.nl) ktype = 2
        eghist(ncountg,ktype) = eghist(ncountg,ktype) + 1

800     continue

        ef(1;ntotal) = vexp(ef(1;ntotal)*half(tstarim);ef(1;ntotal))
        eg(1;ntotal) = vexp(eg(1;ntotal)*half(tstari);eg(1;ntotal))
```

```
      bftf1 = q8ssum(ef(1;nlf))/nlf
      bftf2= q8ssum(ef(nlf+1;ntotal-nlf))/(ntotal-nlf)
      bftg1 = q8ssum(eg(1;nl))/nl
      bftg2= q8ssum(eg(nl+1;ntotal-nl))/(ntotal-nl)

C---- Write results in OUT

      write(10,611)  Nconf,psucc,psucci,ebavg,pbavg,
     1   ehist(nsample1-1)/ntotal,phist(nsample1-1)/ntotal,
     1   bftf1,bftf2,bftg1,bftg2,
     1  ((iconc(j,jj),j=1,8),jj=0,ncomp)
     2  ,(esubcell(j),j=1,8),(psubcell(j),j=1,8)
611   format(i7,2f6.3,4f9.4/4g10.3/24i3/8f9.2/8f9.2)

C---- Adjust step size to keep acceptance ratios within bounds

      if (psucc.LT.accmin) then
      do 640 j = 1,ncomp
640   vstep(j) = vstep(j)/redfact
      else if(psucc.GT.accmax) then
      do 641 j = 1,ncomp
641   if(vstep(j).lt.12) vstep(j) = vstep(j)*redfact
      endif
      nsucc = 0
      nsucci = 0
      endif

      if (mod(nconf,nsample2).eq.nsample2-1) then
      call outp1
      endif


      goto 1000

9999  stop
      end
```

```
C-----------------------------------------------------------------------

      subroutine INP

C-----------------------------------------------------------------------

C----   Parameter definitions

      parameter (ncells=4, ntotal=4*ncells**3,nlf=ntotal/2)
      parameter (ncomp=2,
     1           ncross=ncomp*(ncomp+1)/2, ndiscr=7500,maxhist=10000)
      parameter (efgmin=-20.,efgmax=+20.,nefg=200)

C----   Common Blocks

      common/uparam/ulj(ndiscr,ncross), estar(ncross), sigmas(ncross)
     1             ,flj(ndiscr,ncross)
      common/initial/seed,accmax,accmin,redfact
      common/position/xyz(3*ntotal), Lrij(ntotal,ntotal)
      common/thermo/tstar, rhostar, pstar, nl
      common/techn/nconf, nsample1, nsample2, icont, maxconf
      common/distance/rcutoff, vstep(Ncomp), thstep(Ncomp),
     1                phstep(Ncomp), rstep, L, L2
      common/bft/xyztp(3*ntotal),ef(ntotal),eg(ntotal),
     1          efhist(nefg,ncomp),eghist(nefg,ncomp)

C----   Array and variable declarations

      integer seed
      real L,L2
      half precision ulj,flj,xyz,eij,ehist,phist,dum,rmove,emove
     1              ,xyztp,ef,eg,efhist,eghist

      icont = 0
      open (1,file='COMPDATA')
      open (2,file='INDATA')
      open (10,file='OUT')
      open (11,file='OUT1')
      open (12,file='OUT2')
      open (20,file='XYZ',err=10, iostat = icont)

10    read (1,*) nl,tstar,rhostar
      read (1,*) estar,sigmas
      read (2,*) seed,accmax,accmin,redfact,
     1           maxconf,nsample1,nsample2
      rcutoff = (ntotal/rhostar)**(1./3.)/2.
      if (rcutoff.gt.4.) rcutoff = 4.
      call ranset(seed)
      call ranget(seed)
      write (10,'(i10,2f10.5)') nl,tstar,rhostar
      write (10,'(10f8.4)') estar,sigmas
      write (10,'(i20,3f8.3,3i10)') seed,accmax,accmin,redfact,
```

```
     1            maxconf,nsample1,nsample2
          write (10,'(f10.5)') rcutoff
          read(20,*,err=40,end=40,iostat=icont) nconf,
     1                       seed,(vstep(j),j=1,ncomp)
          call ranset(seed)
          do 30 j = 1,ntotal
          read (20,*,err=40,end=40,iostat=icont) jj,xyz(j),
     1       xyz(j+ntotal),xyz(j+2*ntotal),xyztp(j),xyztp(j+ntotal),
     2       xyztp(j+2*ntotal)
          if (j.NE.jj) then
          icont = 9999
          goto 40
          endif
30        continue

40        return
          end




C-----------------------------------------------------------------------

          subroutine OUTP1

C-----------------------------------------------------------------------

          parameter (pi=3.1415926536, twopi=6.2831853072)
          parameter (ncells=4, ntotal=4*ncells**3,nlf=ntotal/2)
          parameter (ncomp=2,
     1             ncross=ncomp*(ncomp+1)/2, ndiscr=7500,maxhist=10000)
          parameter (efgmin=-20.,efgmax=+20.,nefg=200)

          common/techn/nconf, nsample1, nsample2, icont, maxconf
          common/position/xyz(3*ntotal), Lrij(ntotal,ntotal)
          common/distance/rcutoff, vstep(Ncomp), thstep(Ncomp),
     1                  phstep(Ncomp), rstep, L, L2
          common/thermo/tstar, rhostar, pstar, nl
          common/energy/eij(ntotal,ntotal),etotal
          common/rdfp/irdf(Ndiscr,Ncross),iconc(8,0:NCOMP)
     1    ,crdf(ncross)
          common/cputime/cputim
          common/initial/seed,accmax,accmin,redfact
          common/bft/xyztp(3*ntotal),ef(ntotal),eg(ntotal),
     1           efhist(nefg,ncomp),eghist(nefg,ncomp)

          real L,L2
          half precision ulj,flj,xyz,eij,ehist,phist,dum,rmove,emove
     1               ,xyztp,ef,eg,efhist,eghist
          dimension rrdf(ncross),fnorm(ncomp),gnorm(ncomp),
     1           efnorm(nefg,ncomp),egnorm(nefg,ncomp)
```

```
      integer seed

      write(*,5) nconf, (second(0)-cputim)/nsample2*1000
5     format('  Nconf = ',i8,' CPU time = ',f10.4,' ms/conf')
      cputim = second(0)

      rewind(20)
      call ranget(seed)
      write (11,'(i10,i20,3g15.4)' ) nconf,seed,(vstep(j),j=1,ncomp)
      write (20,'(i10,i20,3g15.4)' ) nconf,seed,(vstep(j),j=1,ncomp)
      do 21 j=1,ntotal
      write (11,'(i10,3f10.6)') j,xyz(j),xyz(j+ntotal),xyz(j+2*ntotal)
21    write (20,'(i10,6f10.6)') j,xyz(j),xyz(j+ntotal),xyz(j+2*ntotal)
     1         ,xyztp(j),xyztp(j+ntotal),xyztp(j+2*ntotal)
      ncount = 1
      rrdf(1) = 0.
      rrdf(2) = 0.
      rrdf(3) = 0.
      write(11,40) (irdf(1,j),j=1,ncross)
40    format(/' RDFs    ',3I9)
      do 30 j = 2, ndiscr
      rrdf(1) = rrdf(1) + irdf(j,1)/crdf(1)/j/j/irdf(1,1)
      rrdf(2) = rrdf(2) + irdf(j,2)/crdf(2)/j/j/(irdf(1,1)/float(n1)+
     1       irdf(1,3)/(float(ntotal-n1)))
      rrdf(3) = rrdf(3) + irdf(j,3)/crdf(3)/j/j/irdf(1,3)
      ncount = ncount + 1
      if (mod(ncount,50).eq.0) then
      write (11,36) rstep*j,(rrdf(jj)/50,jj=1,ncross)
36    format(f9.4,9f9.4)
      ncount = 0
      rrdf(1) = 0.
      rrdf(2) = 0.
      rrdf(3) = 0.
      endif
30    continue
      write(11,*)

      if(q8ssum(efhist(1,1;ncomp*nefg)).lt.1) goto 61
      do 60 j = 1,ncomp
      fnorm(j) = 1./q8ssum(efhist(1,j;nefg))
      gnorm(j) = 1./q8ssum(eghist(1,j;nefg))
      efnorm(1,j;nefg) = efhist(1,j;nefg)*fnorm(j)
60    egnorm(1,j;nefg) = eghist(1,j;nefg)*gnorm(j)
      write(12,'(i7,6g10.3,i6)') nconf,(1./fnorm(j)
     1   ,1./gnorm(j),j=1,ncomp),efgmin,efgmax,nefg
      write(12,'(4g10.3)') ((efnorm(j,jj),egnorm(j,jj),jj=1,ncomp),
     1                       j=1,nefg)
      write(12,*)
61    continue

      return
      end
```

```
C-----------------------------------------------------------------------

      subroutine LJpoten

C-----------------------------------------------------------------------

C----   Parameter definitions

      parameter (ncomp=2,
     1           Ncross=Ncomp*(Ncomp+1)/2, Ndiscr=7500,maxhist=10000)

C----   Common Blocks

      common/Uparam/ULJ(Ndiscr,Ncross), estar(Ncross), sigmas(Ncross)
     1             ,FLJ(Ndiscr,Ncross)
      common/distance/rcutoff, vstep(Ncomp), thstep(Ncomp),
     1              phstep(Ncomp), rstep, L, L2
      half precision ulj,flj,xyz,eij,ehist,phist,dum,rmove,emove
     1             ,xyztp,ef,eg,efhist,eghist


      rstep = rcutoff*sigmas(1)/Ndiscr
      do 100 j = 1,Ncross
C----   I had to skip the first two values of r because of numerical
C----   limitations of the half precision variables.  They are set
C----   to zero with negligible error on the properties of the fluid
      rdum = rstep*2.5
      do 150 jj = 3,Ndiscr-1
           sl=(sigmas(j)/rdum)**12
           ULJ(jj,j) = 4*estar(j)*(sl-(sigmas(j)/rdum)**6)
           FLJ(jj,j) = (4*estar(j)*sl+ULJ(jj,j))*6
150        rdum = rdum+rstep
      ulj(1,j) = 0.
      flj(1,j) = 0.
      ulj(2,j) = 0.
      flj(2,j) = 0.
      ULJ(Ndiscr,j) = 0
100   FLJ(Ndiscr,j) = 0

      return
      end
```

```
C-----------------------------------------------------------------------

      subroutine PUTFCC

C-----------------------------------------------------------------------

C----   Parameter definitions

      parameter (ncells=4, ntotal=4*ncells**3,nlf=ntotal/2)
      parameter (ncomp=2,
     1           ncross=ncomp*(ncomp+1)/2, ndiscr=7500,maxhist=10000)
      parameter (efgmin=-20.,efgmax=+20.,nefg=200)

C----   Common Blocks

      common/position/xyz(3*ntotal), Lrij(ntotal,ntotal)
      common/thermo/tstar, rhostar, pstar, nl
      common/initial/seed,accmax,accmin,redfact
      common/distance/rcutoff, vstep(Ncomp), thstep(Ncomp),
     1                 phstep(Ncomp), rstep, L, L2
      common/bft/xyztp(3*ntotal),ef(ntotal),eg(ntotal),
     1           efhist(nefg,ncomp),eghist(nefg,ncomp)

      half precision ulj,flj,xyz,eij,ehist,phist,dum,rmove,emove
     1               ,xyztp,ef,eg,efhist,eghist

      integer seed
      dimension nrandom(ntotal)
      logical isocc(ntotal)


C-----------------------------------------------------------------------

      do 10 j = 1,ntotal
10    isocc(j) = .false.
      j=1
20    imolec= INT(ranf()*ntotal)+1
      if (.NOT.isocc(imolec)) then
      nrandom(j) = imolec
      isocc(imolec) = .true.
      j = j+1
      endif

      if (j.LE.ntotal) goto 20

C-----------------------------------------------------------------------

      rcell = (4./rhostar)**(1./3.)
      ncount = 0
      do 200   j = 1,Ncells
      rx =   j*rcell
      do 200  jj = 1,Ncells
```

```
      ry =  jj*rcell
      do 200 jjj = 1,Ncells
      rz = jjj*rcell
      Ncount = Nrandom(((j-1)*Ncells*Ncells+(jj-1)*Ncells+JJJ-1)*4+1)
      Nfcount =        ((j-1)*Ncells*Ncells+(jj-1)*Ncells+JJJ-1)*2+1
      xyz(Ncount           ) = rx - rcell
      xyz(Ncount  +  Ntotal) = ry - rcell
      xyz(Ncount  +2*Ntotal) = rz
      xyztp(Nfcount           ) = rx - rcell
      xyztp(Nfcount  +  Ntotal) = ry - rcell
      xyztp(Nfcount  +2*Ntotal) = rz
      Ncount = Nrandom(((j-1)*Ncells*Ncells+(jj-1)*Ncells+JJJ-1)*4+2)
      Nfcount =        ((j-1)*Ncells*Ncells+(jj-1)*Ncells+JJJ-1)*2+1+
     1                 nlf
      xyz(Ncount           ) = rx - rcell/2
      xyz(Ncount  +  Ntotal) = ry - rcell/2
      xyz(Ncount  +2*Ntotal) = rz
      xyztp(Nfcount           ) = rx - rcell/2
      xyztp(Nfcount  +  Ntotal) = ry - rcell/2
      xyztp(Nfcount  +2*Ntotal) = rz
      Ncount = Nrandom(((j-1)*Ncells*Ncells+(jj-1)*Ncells+JJJ-1)*4+3)
      Nfcount =        ((j-1)*Ncells*Ncells+(jj-1)*Ncells+JJJ-1)*2+2
      xyz(Ncount           ) = rx
      xyz(Ncount  +  Ntotal) = ry - rcell/2
      xyz(Ncount  +2*Ntotal) = rz - rcell/2
      xyztp(Nfcount           ) = rx
      xyztp(Nfcount  +  Ntotal) = ry - rcell/2
      xyztp(Nfcount  +2*Ntotal) = rz - rcell/2
      Ncount = Nrandom(((j-1)*Ncells*Ncells+(jj-1)*Ncells+JJJ-1)*4+4)
      Nfcount =        ((j-1)*Ncells*Ncells+(jj-1)*Ncells+JJJ-1)*2+2+
     1                 nlf
      xyz(Ncount           ) = rx - rcell/2
      xyz(Ncount  +  Ntotal) = ry
      xyz(Ncount  +2*Ntotal) = rz - rcell/2
      xyztp(Nfcount           ) = rx - rcell/2
      xyztp(Nfcount  +  Ntotal) = ry
      xyztp(Nfcount  +2*Ntotal) = rz - rcell/2
  200 continue

      return
      end
```

```
      program avgiii

      parameter(pi=3.141592654,ncomp=2,maxpts=2500,ninter=ncomp*
     1 (ncomp+1)/2,ntotal=256)
      common/c1/ nconf(maxpts),psucc(maxpts),psucci(maxpts),
     1         ebavg(maxpts),pbavg(maxpts),iconc(8,0:ncomp,maxpts)
     2         ,esubcell(8,maxpts),psubcell(8,maxpts),
     3         esavg(8),psavg(8),e2savg(8),p2savg(8),
     4         ficavg(8,0:ncomp),fic2avg(8,0:ncomp),avgf(0:ncomp)
     5         ,enavg(8),pnavg(8),epavg(8),bftf(ncomp,maxpts)
     6         ,bftg(ncomp,maxpts),bftfavg(ncomp),bftgavg(ncomp)
     7           ,fmuc(ncomp),fmue(ncomp)

      character*20 file1,file2
      dimension sigmas(ninter),estar(ninter),nm(ncomp)
      double precision seed
      real nnf1,nln2gavg,nln2f1,nm

      write (*,*) ' Enter filename for input : '
      read(*,'(a)') file1
      write (*,*) ' Enter filename for output : '
      read(*,'(a)') file2
      if (file1.eq.file2) goto 99
      open(1,file=file1,err=99,form='formatted',access='sequential')
      open(2,file=file2,form='formatted',access='sequential')
      write (*,*) ' Enter starting and ending configuration : '
      read(*,*) nstart,nend
      nc=1
      read (1,*) n1,tstar,rhostar
      read (1,*) estar,sigmas
      read (1,'(f20.0,3f8.3,3i10)') seed,accmax,accmin,redfact,
     1          maxconf,nsample1,nsample2
C      read (1,*) seed,accmax,accmin,redfact,
C     1         maxconf,nsample1,nsample2
      read (1,*) rcutoff

20    read(1,611,err=30,end=30) nconf(nc),psucc(nc),psucci(nc)
     1 ,ebavg(nc),pbavg(nc),bftf(1,nc),bftf(2,nc),
     1 bftg(1,nc),bftg(2,nc),((iconc(j,jj,nc),j=1,8),jj=0,ncomp),
     2 (esubcell(j,nc),j=1,8),(psubcell(j,nc),j=1,8)
611   format(i7,2f6.3,2f9.4/4g10.3/24i3/8f9.2/8f9.2)
      nc = nc + 1
      goto 20
30    nc = nc - 1

      psuavg = 0.
      psuiavg = 0.
      eavg = 0.
      e2avg = 0.
      pavg = 0.
      p2avg = 0.
      egavg = 0.
```

```
      pgavg = 0.
      e2gavg = 0.
      p2gavg = 0.
      pngavg = 0.
      engavg = 0.
      epgavg = 0.
      n1n2gavg = 0.
      do 394 j = 1,8
      esavg(j) = 0.
      e2savg(j) = 0.
      psavg(j) = 0.
      p2savg(j) = 0.
      enavg(j) = 0.
      pnavg(j) = 0.
      epavg(j) = 0.
      do 394 jj = 0,ncomp
      avgf(jj) = 0.
      ficavg(j,jj) = 0.
394   fic2avg(j,jj) = 0.
      do 395 j = 1,ncomp
      bftfavg(j) = 0.
395   bftgavg(j) = 0.
      ncact = 0

      do 400 i = 1,n2
      if (nconf(i).lt.nstart) then
      nstarta = nconf(i)
      goto 400
      endif
      if (nconf(i).gt.nend) goto 438
      nenda = nconf(i)
      ncact = ncact + 1
      psuavg = psuavg + psucc(i)
      psuiavg = psuiavg + psucci(i)
      eavg = eavg + ebavg(i)
      e2avg = e2avg + ebavg(i)*ebavg(i)
      pavg = pavg + pbavg(i)
      p2avg = p2avg + pbavg(i)*pbavg(i)
      do 401 j = 1,8
      esavg(j) = esavg(j) + esubcell(j,i)
      e2savg(j) = e2savg(j) + esubcell(j,i)*esubcell(j,i)
      psavg(j) = psavg(j) + psubcell(j,i)
      p2savg(j) = p2savg(j) + psubcell(j,i)*psubcell(j,i)
      enavg(j) = enavg(j) + esubcell(j,i)*iconc(j,0,i)
      pnavg(j) = pnavg(j) + psubcell(j,i)*iconc(j,0,i)
      epavg(j) = epavg(j) + esubcell(j,i)*psubcell(j,i)
      egavg = egavg + esubcell(j,i)
      pgavg = pgavg + psubcell(j,i)
      e2gavg = e2gavg + esubcell(j,i) * esubcell(j,i)
      p2gavg = p2gavg + psubcell(j,i) * psubcell(j,i)
      engavg = engavg + esubcell(j,i) * iconc(j,0,i)
      pngavg = pngavg + psubcell(j,i) * iconc(j,0,i)
```

```
      epgavg = epgavg + esubcell(j,i) * psubcell(j,i)
      nln2gavg = nln2gavg + iconc(j,1,i)*iconc(j,2,i)
      do 401 jj = 0,ncomp
      avgf(jj) = avgf(jj) + iconc(j,jj,i)*iconc(j,jj,i)
      ficavg(j,jj) = ficavg(j,jj) + iconc(j jj,i)
401   fic2avg(j,jj) = fic2avg(j,jj) + iconc(j,jj,i)*iconc(j,jj,i)
      do 402 jj = 1,ncomp
      bftfavg(jj) = bftfavg(jj) + bftf(jj,i)
402   bftgavg(jj) = bftgavg(jj) + bftg(jj,i)
400   continue
438   continue

      psuavg = psuavg/ncact
      psuiavg = psuiavg/ncact
      eavg = eavg/ncact
      e2avg = e2avg/ncact
      pavg = pavg/ncact
      p2avg = p2avg/ncact
      egavg = egavg/ncact/8
      pgavg = pgavg/ncact/8
      e2gavg = e2gavg/ncact/8
      p2gavg = p2gavg/ncact/8
      engavg = engavg/ncact/8
      pngavg = pngavg/ncact/8
      epgavg = epgavg/ncact/8
      nln2gavg = nln2gavg/ncact/8
      do 410 j = 1,8
      esavg(j) = esavg(j)/ncact
      e2savg(j) = e2savg(j)/ncact
      psavg(j) = psavg(j)/ncact
      p2savg(j) = p2savg(j)/ncact
      enavg(j) = enavg(j)/ncact
      pnavg(j) = pnavg(j)/ncact
      epavg(j) = epavg(j)/ncact
      do 410 jj =0,ncomp
      ficavg(j,jj) = ficavg(j,jj)/ncact
410   fic2avg(j,jj) = fic2avg(j,jj)/ncact
      do 418 jj = 0,ncomp
      if(jj.eq.0) goto 417
      bftfavg(jj) = bftfavg(jj)/ncact
      bftgavg(jj) = bftgavg(jj)/ncact
417   continue
418   avgf(jj) = avgf(jj)/ncact/8

      write(2,'(a,i3,a,i3,3(a,f8.4))')
     1 'Ntotal =',ntotal,'  N1 =',n1,'   Tstar = ',tstar,
     1 ' Rhostar = ',rhostar,' Rcutoff = ',rcutoff
      write(2,'(6f8.3,f19.0/3f8.3,3i10)')
     1 estar,sigmas,seed,accmax,accmin,redfact,
     1 maxconf,nsample1,nsample2
      write(2,'(a,i7,a,i7,a,i7)') ' Ncount = ',ncact,
     1     '  from Conf. # ',nstarta,'  to ',nenda
```

```
      write(2,'(a,6f9.4)') 'A ',psuavg,psuiavg,eavg,e2avg-eavg**2,
     1  pavg,p2avg-pavg**2
      write(2,'(a,8f9.2/2x,8f9.2)') 'E ',(esavg(j),j=1,8),
     1  (e2savg(j)-esavg(j)**2,j=1,8)
      write(2,'(a,8f9.2/2x,8f9.2)') 'P ',(psavg(j),j=1,8),
     1  (p2savg(j)-psavg(j)**2,j=1,8)
      write(2,'(a,8f9.2/a,8f9.2)') 'EN'
     1  ,(enavg(j)-esavg(j)*ficavg(j,0),j=1,8),
     1  'PN',(pnavg(j)-psavg(j)*ficavg(j,0),j=1,8)
      do 420 jj = 0,ncomp
420   write(2,'(a,i1,8f9.2/2x,8f9.2)') 'I',jj,(ficavg(j,jj),j=1,8),
     1  (fic2avg(j,jj)-ficavg(j,jj)**2,j=1,8)

      ecorr = eavg
      pcorr = pavg + rhostar*tstar
      fmuc(1) = -tstar*log(bftfavg(1)) + tstar*log(rhostar)
      fmuc(2) = -tstar*log(bftfavg(2)) + tstar*log(rhostar)
      nm(1) = float(n1)/float(ntotal)
      nm(2) = 1 - nm(1)
      do 510 j = 1,ncomp
      do 510 jj =1,ncomp
      NLJ = (MIN(j,jj)-1)*(2*ncomp-MIN(j,jj)+2)/2 + 1
     1      + ABS(j-jj)
      ecorr = ecorr + 8.*pi*rhostar*
     1          estar(nlj)/estar(1)*nm(j)*nm(jj)
     1  *((sigmas(nlj)/sigmas(1))**12/9./rcutoff**9 -
     2  (sigmas(nlj)/sigmas(1))**6/3./rcutoff**3)
      fmuc(j) = fmuc(j) + 16.*pi*rhostar*
     1          estar(nlj)/estar(1)*nm(jj)
     1  *((sigmas(nlj)/sigmas(1))**12/9./rcutoff**9 -
     2  (sigmas(nlj)/sigmas(1))**6/3./rcutoff**3)
      pcorr = pcorr + 8.*pi/3.*rhostar**2*
     1          estar(nlj)/estar(1)*nm(j)*nm(jj)
     1  *(4.*(sigmas(nlj)/sigmas(1))**12/3./rcutoff**9 -
     2  2.*(sigmas(nlj)/sigmas(1))**6/rcutoff**3)
510   continue

      fmue(1) = fmuc(1) + tstar*log(nm(1))
      fmue(2) = fmuc(2) + tstar*log(nm(2))
      eefl = e2gavg - egavg**2
      enfl = engavg - egavg*ntotal/8
      pnfl = pngavg - pgavg*ntotal/8
      nnfl = avgf(0) - ntotal**2/8.**2
      epfl = epgavg - egavg*pgavg
      nln2fl = nln2gavg -float(n1)*(ntotal-n1)/8.**2
      write(2,'(2(a,f8.4,2x)/4(a,f8.4,2x)/4(a,f8.4,2x)
     1  /4(a,f8.3,2x)/2(a,f8.3,2x)/4(a,f6.2,2x))')
     1  'Ecorr =',ecorr,'Pcorr =',pcorr,
     1  'uc 1=',fmuc(1),'uc 2=',fmuc(2),'ue 1=',fmue(1),
     1  'ue 2=',fmue(2),'F1 =',bftfavg(1),
     1  'F2 =',bftfavg(2),'G1 =',bftgavg(1),'G2 =',bftgavg(2),
     2  '<U>1/8= ',egavg,'<U,U>= ',eefl,
```

```
     3  '<F>1/8= ',pgavg,'<U,N>= ',enfl,
     4  '<F,N>= ',pnfl,'<U,F>= ',epfl,
     5  '<N,N>= ',nnfl,'<N1,N1>= ',
     6  avgf(1)-n1**2/8**2,'<N2,N2> = ',avgf(2)-(ntotal-n1)**2/8**2,
     7  '<N1,N2>= ',n1n2fl
        cratio = (nnfl + pnfl/3./tstar)/ntotal*8
        beta = nnfl/rhostar/tstar/ntotal*8
        alfa = pcorr*beta/tstar - (enfl-ecorr*nnfl)/ntotal*8/
     1  tstar**2
        gamma = rhostar + (enfl*(1-ntotal/8/nnfl)+epfl/3/tstar)*rhostar
     1  /ntotal*8/tstar
        cv = (eefl - enfl**2/nnfl)/ntotal*8/tstar**2
        write(2,'(6(a,f7.4,1x))') 'cratio=',cratio,'beta=',beta,
     1  'alfa=',alfa,'gamma=',gamma,'bg/a=',beta*gamma/alfa
     1  ,'cv=',cv
99      stop
        end
```

APPENDIX G. MONTE CARLO SIMULATION RESULTS

G.1 Pure Lennard-Jones (6,12) fluid

The results of the simulation runs for the pure Lennard Jones fluid are presented in Table G.1. The chemical potentials listed in the table, as well as in the tables that follow, were calculated using Eq. 5.7 rather than 5.12, since this calculation could be performed immediately, whereas application of Eq. 5.12 required plotting the function $L(u^*)$ versus u^*. Eq. 5.12 is preferred, however, because it is generally more reliable at high densities and provides estimates of the errors for the calculation of the chemical potential. The results for the chemical potential from the two methods (Eq. 5.7 and Eq. 5.12) were found to agree within our estimated accuracy for all runs at densities up to $\rho^*=0.700$. Two values for each state condition are listed in the table for the reduced chemical potential μ^* (defined by Eq. 5.8b), for the following reason: Since the simulation programs are written for a binary mixtures, simulations for the pure Lennard Jones fluid were performed by using identical sets of parameters for the two components. The deviation between the two estimates of the chemical potential illustrate the typical accuracy of our calculations.

The last column of the table lists the average fluctuations of the number of molecules in each subcell of the basic simulation cell. This number was determined by determining the standard deviation of the number of molecules in each subcell for the entire simulation and then averaging for all the subcells. In general, the results for the fluctuation in the number of molecules for each subcell were quite close for all subcells (as shown in Table 6.3 for a mixture simulation), except in a materially unstable region where the fluctuations were large.

Table G.1 Monte Carlo simulation results for the pure Lennard - Jones (6,12) fluid

T^*	ρ^*	R_c	M $\times 10^5$	AR†	$-E^*$	P^*	$-\mu^*$	$-\mu^*$	$\langle \delta N \delta N \rangle$
0.928	0.010	4.00	3	0.87	0.088	0.0088	4.37	4.37	30.2
0.928	0.025	4.00	3	0.73	0.224	0.0201	3.67	3.67	36.0
0.928	0.050	4.00	3	0.58	0.460	0.0334	3.29	3.28	51.1
0.928	0.700	3.57	8	0.50	4.939	-0.250	4.00	4.02	6.6
0.928	0.750	3.49	8	0.50	5.288	0.046	3.31	4.14	6.6
0.928	0.775	3.46	20	0.49	5.445	0.307	3.50	3.70	5.3
0.928	0.800	3.42	8	0.50	5.602	0.626	3.92	1.93	5.2
1.150	0.050	2.50	10	0.63	0.427	0.0461			38.3
1.150	0.050	4.00	6	0.63	0.431	0.0461	3.92	3.92	38.4
1.150	0.075	4.00	5	0.53	0.650	0.0613	3.67	3.66	45.0
1.150	0.075	4.00	6	0.53	0.638	0.0612	3.67	3.67	42.6
1.150	0.100	2.50	10	0.50	0.853	0.0721			45.6
1.150	0.100	4.00	6	0.50	0.873	0.0699	3.55	3.55	56.2
1.150	0.125	4.00	6	0.50	1.081	0.0777	3.50	3.51	61.3
1.150	0.150	4.00	8	0.50	1.302	0.0787	3.50	3.49	59.2
1.150	0.300	2.50	10	0.50	2.324	0.046			60.7
1.150	0.400	0.40	10	0.50	2.919	-0.011			38.7
1.150	0.500	2.50	5	0.50	3.487	-0.061			12.0
1.150	0.500	2.50	10	0.50	3.505	-0.055			17.4
1.150	0.550	2.50	10	0.51	3.790	-0.055			10.8
1.150	0.600	2.50	5	0.50	4.130	0.040			10.5
1.150	0.600	2.50	10	0.50	4.130	0.034			9.8
1.150	0.600	3.75	5	0.50	4.133	-0.002			0.0
1.150	0.600	3.75	5	0.50	4.133	-0.002			0.0
1.150	0.600	3.76	6	0.50	4.118	0.000	3.79	3.58	8.4
1.150	0.625	3.71	6	0.50	4.291	0.110	3.61	3.62	7.9
1.150	0.636	2.50	6	0.49	4.375	0.153			8.2
1.150	0.636	3.69	5	0.50	4.360	0.159			0.0
1.150	0.650	3.67	6	0.50	4.467	0.160	3.67	3.48	7.7
1.150	0.700	2.50	6	0.49	4.813	0.417			7.1
1.150	0.700	3.57	6	0.50	4.792	0.480	2.13	2.91	6.2
1.150	0.750	2.50	10	0.50	5.121	0.947			6.2
1.150	0.800	2.50	10	0.50	5.424	1.642			5.3
1.150	0.800	3.42	6	0.50	5.406	1.709	0.39	0.86	5.7
1.150	0.835	2.50	5	0.49	5.603	2.406			6.6
1.556	0.050	4.00	6	0.69	0.367	0.0691	5.00	5.01	30.4
1.556	0.050	4.00	6	0.69	0.367	0.0691	5.00	5.01	0.0
1.556	0.050	4.00	6	0.69	0.367	0.0691	5.00	5.01	30.4
1.556	0.113	4.00	8	0.50	0.819	0.1354	4.14	4.13	37.0
1.556	0.181	4.00	8	0.50	1.284	0.1870	3.78	3.79	40.6

(continued on next page)

Table G.1 (concluded)

T^*	ρ^*	R_c	M $\times 10^5$	AR†	$-E^*$	P^*	$-\mu^*$	$-\mu^*$	$\langle \delta N \delta N \rangle$
1.556	0.226	4.00	8	0.50	1.562	0.214	3.66	3.64	29.9
1.556	0.317	4.00	8	0.50	2.161	0.266	3.48	3.42	24.1
1.556	0.362	4.00	8	0.50	2.424	0.282	3.37	3.36	23.0
1.556	0.400	4.00	6	0.50	2.682	0.344	3.25	3.32	20.5
1.556	0.452	4.00	8	0.50	2.979	0.385	3.14	3.19	13.4
1.556	0.600	3.76	6	0.50	3.932	0.893	2.11	2.19	9.1
1.556	0.800	3.42	8	0.50	5.093	3.448	1.47	1.41	5.4

† Acceptance ratio (fraction of successful displacement steps)

G.2 Test results for comparison with literature

The results for the mixture described in Section 6.2 are presented in Table G.2. Results for the chemical potential of the same mixture have been presented ny Shing and Gubbins, 1983. The comments made in the previous section concerning the method of calculation of the chemical potentials are also valid for this table. The fluctuation of the number of molecules in each subcell now is composed of four distinct entries: the fluctuations in the total number of molecules, regardless of species, and the cross fluctuations of the three possible pairs of molecules, of type 1-1, 2-2 and 1-2 respectively. Note that the last fluctuation ($\delta N_1 \delta N_2$) is usually negative at high densities, which implies that there is a negative correlation between the presence of the two types of molecules.

One additional column in this table, labeled IE, gives the "interchange efficiency", defined as the fraction of successful interchange steps. The same organization of the tables for the Monte Carlo simulation results applies for the other mixtures studied (Tables G.3 - G.5). For the lower density runs in Tables G.3 - G.5 no interchange was attempted, since the normal displacement step is sufficient to rapidly equilibrate the distribution of molecules. For these cases, the interchange efficiency is listed as 0.

Table G.2 Monte Carlo simulation results for a mixture with $\epsilon^*_{12}=1.41, \epsilon^*_{22}=2, \sigma^*_{12}=\sigma^*_{22}=1$ at $T^*=1.2$

N_1	ρ^*	M $\times 10^5$	AR†	IE‡	$-E^*$	P^*	$-\mu^*_{1,c}$	$-\mu^*_{2,c}$	$-\mu^*_1$	$-\mu^*_2$	total	$\langle\delta N_i \delta N_j\rangle$ 1-1	2-2	1-2
71	0.700	6	0.50	0.63	8.771	-1.521	5.81	9.94	7.35	10.33	12.1	8.1	21.8	-8.2
128	0.700	6	0.50	0.65	7.417	-0.795	4.21	9.73	5.04	10.56	7.5	9.8	14.8	-8.6
171	0.700	6	0.50	0.69	6.449	-0.310	3.84	8.63	4.32	9.96	7.5	10.4	11.8	-6.5
218	0.700	6	0.50	0.72	5.495	0.186	3.34	7.08	3.54	9.37	6.5	8.2	5.1	-2.8
251	0.700	6	0.50	0.75	4.855	0.561	2.69	7.10	2.71	11.83	6.3	6.9	0.9	-0.4

† Acceptance ratio (fraction of successful displacement steps)
‡ Interchange efficiency (fraction of successful interchange steps); see also comments in Section G.2.

G.3 Mixture I

Table G.3 Monte Carlo simulation results for Mixture I at $T^*=1.15$

N_1	ρ^*	M $\times 10^5$	AR†	IE‡	$-E^*$	P^*	$-\mu^*_{1,c}$	$-\mu^*_{2,c}$	$-\mu^*_1$	$-\mu^*_2$	total	$\langle\delta N_i \delta N_j\rangle$ 1-1	2-2	1-2
8	0.050	6	0.63	0	0.422	0.0462	3.71	3.91	7.70	3.94	38.7	0.9	37.4	0.2
16	0.050	6	0.63	0	0.410	0.0465	3.72	3.90	6.91	3.97	36.4	1.8	34.2	0.2
32	0.050	6	0.64	0	0.398	0.0470	3.73	3.89	6.12	4.04	37.2	3.7	32.6	0.5
64	0.050	6	0.65	0	0.372	0.0480	3.76	3.86	5.35	4.19	35.7	7.8	26.3	0.8
96	0.050	6	0.66	0	0.355	0.0483	3.79	3.84	4.92	4.38	34.3	11.2	20.8	1.2
128	0.050	6	0.66	0	0.351	0.0486	3.81	3.81	4.61	4.61	35.6	16.3	16.3	1.5
8	0.075	6	0.53	0	0.627	0.0616	3.37	3.65	7.36	3.69	43.1	0.9	41.8	0.2
16	0.075	6	0.53	0	0.623	0.0617	3.39	3.65	6.57	3.72	44.2	1.8	41.1	0.7
32	0.075	6	0.54	0	0.592	0.0632	3.40	3.63	5.79	3.79	42.3	3.9	36.7	0.8
64	0.075	6	0.56	0	0.551	0.0656	3.44	3.59	5.04	3.92	37.9	7.9	27.7	1.1
96	0.075	6	0.56	0	0.532	0.0659	3.48	3.56	4.60	4.10	38.1	12.4	22.2	1.8
128	0.075	6	0.57	0	0.524	0.0667	3.52	3.52	4.32	4.32	39.8	18.2	16.8	2.3
8	0.100	6	0.50	0	0.853	0.0719	3.17	3.55	7.15	3.59	65.3	0.9	62.8	0.8
16	0.100	6	0.50	0	0.837	0.0735	3.18	3.53	6.37	3.60	52.0	1.8	48.0	1.1
32	0.100	6	0.50	0	0.786	0.0743	3.20	3.49	5.59	3.64	45.0	3.7	40.1	0.6
64	0.100	6	0.50	0	0.747	0.0779	3.25	3.45	4.84	3.78	44.2	7.4	32.7	2.1
96	0.100	6	0.50	0	0.710	0.0809	3.31	3.40	4.44	3.94	45.8	13.6	27.0	2.6

(continued on next page)

Table G.3 (continued)

N_1	ρ^*	M $\times 10^5$	AR†	IE‡	$-E^*$	P^*	$-\mu^*_{1,c}$	$-\mu^*_{2,c}$	$-\mu^*_1$	$-\mu^*_2$	total	$\langle \delta N_i \delta N_j \rangle$ 1-1	2-2	1-2
128	0.100	6	0.50	0	0.704	0.0802	3.35	3.35	4.15	4.15	41.8	17.4	20.0	2.2
8	0.125	6	0.50	0	1.065	0.0781	3.02	3.48	7.01	3.52	70.7	1.0	69.0	0.4
16	0.125	6	0.50	0	1.008	0.0810	3.03	3.47	6.22	3.54	50.7	2.0	46.6	1.1
32	0.125	6	0.50	0	0.995	0.0854	3.07	3.45	5.46	3.60	64.9	4.3	54.0	3.3
64	0.125	6	0.50	0	0.907	0.0873	3.14	3.39	4.73	3.72	42.4	8.1	31.4	1.5
96	0.125	6	0.50	0	0.873	0.0907	3.20	3.32	4.33	3.86	47.8	12.5	28.2	3.6
128	0.125	6	0.50	0	0.872	0.0905	3.27	3.26	4.07	4.05	44.1	18.6	19.3	3.1
64	0.150	6	0.50	0	1.096	0.0957	3.04	3.32	3.84	4.12	58.1	7.6	42.5	4.0
96	0.150	6	0.50	0	1.067	0.0989	3.09	3.27	4.22	3.81	46.0	13.3	26.3	3.3
128	0.150	6	0.50	0	1.038	0.1002	3.19	3.20	3.99	4.00	41.2	18.5	19.2	1.8
64	0.175	6	0.50	0	1.288	0.0993	2.99	3.30	4.59	3.63	89.2	10.6	60.3	9.2
96	0.175	6	0.50	0	1.197	0.1025	3.08	3.23	4.21	3.77	44.3	14.4	26.8	1.5
128	0.175	6	0.50	0	1.220	0.1034	3.16	3.17	3.95	3.97	50.2	18.3	23.2	4.4
32	0.500	6	0.50	0.77	3.285	0.052	2.49	3.61	4.88	3.77	16.4	3.7	18.3	-2.8
64	0.500	6	0.50	0.75	3.124	0.077	2.63	3.50	4.23	3.83	17.0	7.8	19.4	-5.1
96	0.500	6	0.50	0.73	3.029	0.133	2.87	3.34	4.00	3.88	11.9	11.5	15.2	-7.4
128	0.500	6	0.50	0.72	3.016	0.138	3.03	3.05	3.82	3.85	16.1	15.5	15.2	-7.3
32	0.525	6	0.50	0.77	3.410	0.011	2.36	3.76	4.75	3.91	10.8	3.8	13.2	-3.1
64	0.525	6	0.50	0.74	3.264	0.113	2.67	3.51	4.27	3.85	12.0	7.8	16.0	-5.9
96	0.525	6	0.50	0.72	3.165	0.150	2.77	3.23	3.89	3.77	11.6	11.7	15.6	-7.8
128	0.525	6	0.50	0.72	3.136	0.171	3.07	3.07	3.87	3.87	12.9	14.8	15.1	-8.5
16	0.550	6	0.50	0.79	3.683	0.019	2.08	3.78	5.27	3.85	16.3	1.8	17.5	-1.5
32	0.550	6	0.50	0.77	3.575	0.070	2.25	3.47	4.64	3.63	11.8	3.8	14.0	-3.0
64	0.550	6	0.50	0.73	3.409	0.156	2.56	3.43	4.15	3.77	11.9	8.0	16.3	-6.2
96	0.550	6	0.50	0.71	3.315	0.155	2.75	3.18	3.87	3.72	10.5	11.7	15.9	-8.6
128	0.550	6	0.50	0.70	3.308	0.224	2.90	2.92	3.70	3.72	12.3	14.7	14.7	-8.6
16	0.575	6	0.50	0.79	3.839	0.075	1.89	3.81	5.08	3.88	11.3	1.9	12.6	-1.6
32	0.575	6	0.50	0.76	3.732	0.128	2.28	3.63	4.67	3.79	10.9	3.8	13.3	-3.1
64	0.575	6	0.50	0.73	3.569	0.168	2.36	3.36	3.95	3.69	9.0	8.0	14.0	-6.5
96	0.575	6	0.50	0.71	3.469	0.185	2.80	3.09	3.93	3.63	10.3	11.9	15.5	-8.5
128	0.575	6	0.50	0.70	3.429	0.225	2.86	2.95	3.66	3.74	9.6	14.3	14.2	-9.4
16	0.600	6	0.50	0.79	3.994	0.095	1.89	3.77	5.07	3.85	9.8	1.8	11.0	-1.5
32	0.600	6	0.50	0.76	3.893	0.140	1.90	3.41	4.29	3.57	10.3	3.9	12.9	-3.3
64	0.600	6	0.50	0.72	3.707	0.282	1.90	3.35	3.49	3.68	9.9	8.2	14.7	-6.5
96	0.600	6	0.50	0.70	3.607	0.284	2.38	3.11	3.51	3.65	10.2	11.9	15.5	-8.6
128	0.600	6	0.50	0.69	3.583	0.315	2.97	2.65	3.77	3.45	9.9	15.0	15.2	-10.1

(continued on next page)

Table G.3 (concluded)

N_1	ρ^*	M $\times 10^5$	AR†	IE‡	$-E^*$	P^*	$-\mu^*_{1,c}$	$-\mu^*_{2,c}$	$-\mu^*_1$	$-\mu^*_2$ total	$\langle\delta N_1, \delta N_j\rangle$ 1-1	2-2	1-2
32	0.625	6	0.50	0.76	4.027	0.257	1.64	3.66	4.04	3.81	8.0	3.9	10.7	-3.3
64	0.625	6	0.50	0.72	3.853	0.347	2.17	3.09	3.77	3.42	7.2	8.2	12.7	-6.9
96	0.625	6	0.50	0.69	3.768	0.401	2.22	2.84	3.35	3.38	10.6	12.2	16.2	-8.9
128	0.625	6	0.50	0.68	3.733	0.421	2.53	2.61	3.33	3.41	9.1	14.6	14.9	-10.2
16	0.650	6	0.50	0.79	4.309	0.294	1.35	3.29	4.54	3.36	7.1	1.8	8.4	-1.6
32	0.650	6	0.50	0.76	4.196	0.351	1.57	3.20	3.96	3.35	9.6	3.8	11.9	-3.0
32	0.650	5	0.50	0.75	4.196	0.388	1.27	3.38	3.66	3.53	7.8	3.9	10.2	-3.1
64	0.650	6	0.50	0.71	4.014	0.444	1.77	2.76	3.36	3.09	7.8	8.3	13.2	-6.9
64	0.650	5	0.50	0.71	4.004	0.511	1.97	2.97	3.56	3.30	7.6	8.2	13.2	-6.9
96	0.650	5	0.50	0.68	3.900	0.529	2.27	2.82	3.40	3.36	7.9	12.5	15.4	-10.0
96	0.650	6	0.50	0.68	3.903	0.551	2.09	2.62	3.22	3.16	7.5	12.3	14.9	-9.8
128	0.650	6	0.50	0.67	3.872	0.528	2.61	2.40	3.41	3.20	7.4	14.6	14.6	-10.9
128	0.650	5	0.50	0.67	3.868	0.519	2.55	2.47	3.35	3.27	7.8	14.5	14.9	-10.8
32	0.750	8	0.50	0.73	4.796	1.138	0.14	1.75	2.54	1.90	6.2	4.0	9.1	-3.4
64	0.750	8	0.50	0.68	4.596	1.244	0.10	1.41	1.69	1.74	6.5	8.8	12.7	-7.5
96	0.750	8	0.50	0.64	4.472	1.337	0.83	1.19	1.96	1.73	6.4	13.3	15.4	-11.2
128	0.750	8	0.50	0.63	4.429	1.381	1.07	1.09	1.87	1.89	5.9	15.7	15.5	-12.7

† Acceptance ratio (fraction of successful displacement steps)
‡ Interchange efficiency (fraction of successful interchange steps)

G.4 Mixture II

Table G.4 Monte Carlo simulation results for Mixture II at $T^*=1.15$

N_1	ρ^*	M $\times 10^5$	AR†	IE‡	$-E^*$	P^*	$-\mu^*_{1,c}$	$-\mu^*_{2,c}$	$-\mu^*_1$	$-\mu^*_2$ total	$\langle\delta N_1 \delta N_j\rangle$ 1-1	2-2	1-2
8	0.050	6	0.77	0	0.201	0.0520	3.78	3.66	7.76	3.70	32.3	0.9	31.0	0.2
16	0.050	6	0.77	0	0.207	0.0518	3.78	3.66	6.97	3.74	31.7	1.7	29.2	0.4
32	0.050	6	0.76	0	0.220	0.0515	3.78	3.67	6.17	3.83	33.5	3.6	27.7	1.1
8	0.063	6	0.74	0	0.250	0.0634	3.60	3.47	7.59	3.50	33.4	0.9	32.1	0.2
16	0.063	6	0.73	0	0.259	0.0631	3.61	3.47	6.80	3.54	33.8	1.8	31.1	0.4

(continued on next page)

Table G.4 (continued)

N_1	ρ^*	M $\times 10^5$	AR†	IE‡	$-E^*$	P^*	$-\mu^*_{1,c}$	$-\mu^*_{2,c}$	$-\mu^*_1$	$-\mu^*_2$ total	$\langle \delta N_1 \delta N_j \rangle$ 1-1	2-2	1-2
32	0.063	6	0.72	0	0.277	0.0628	3.62	3.47	6.01	3.63 34.2	3.7	29.1	0.7
8	0.075	6	0.70	0	0.303	0.0738	3.47	3.30	7.46	3.34 34.5	0.9	33.1	0.3
16	0.075	6	0.70	0	0.311	0.0735	3.48	3.31	6.67	3.38 35.9	1.8	33.0	0.5
32	0.075	6	0.68	0	0.330	0.0729	3.49	3.33	5.88	3.48 35.1	3.6	29.3	1.1
64	0.075	6	0.66	0	0.372	0.0707	3.52	3.34	5.11	3.67 36.0	7.9	24.5	1.8
32	0.088	6	0.65	0	0.385	0.0823	3.40	3.19	5.79	3.35 38.0	3.6	31.7	1.3
64	0.088	6	0.63	0	0.436	0.0803	3.41	3.22	5.01	3.55 37.6	8.1	25.3	2.1
96	0.088	6	0.60	0	0.483	0.0777	3.46	3.25	4.58	3.79 41.2	13.3	21.8	3.1
128	0.088	6	0.58	0	0.537	0.0752	3.50	3.28	4.29	4.07 44.4	20.0	16.7	3.8
96	0.100	6	0.57	0	0.552	0.0865	3.40	3.15	4.53	3.69 43.4	13.5	22.5	3.7
128	0.100	6	0.54	0	0.614	0.0827	3.43	3.18	4.22	3.98 45.5	19.9	16.6	4.5
160	0.100	6	0.52	0	0.679	0.0795	3.46	3.20	4.00	4.33 46.9	27.0	12.4	3.7
192	0.100	6	0.50	0	0.732	0.0766	3.49	3.23	3.82	4.82 47.3	33.8	7.8	2.8
224	0.100	6	0.50	0	0.803	0.0732	3.53	3.25	3.68	5.65 56.4	48.0	3.8	2.3
160	0.125	6	0.50	0	0.845	0.0896	3.39	3.08	3.93	4.21 50.1	28.9	11.7	4.7
192	0.125	6	0.50	0	0.915	0.0849	3.42	3.11	3.75	4.70 55.0	39.7	7.7	3.8
224	0.125	6	0.50	0	0.993	0.0808	3.48	3.15	3.63	5.54 55.3	45.3	3.8	3.2
240	0.125	6	0.50	0	1.071	0.0778	3.50	3.17	3.58	6.36 68.0	62.7	1.8	1.8
248	0.125	6	0.50	0	1.048	0.0784	3.49	3.15	3.52	7.14 57.5	55.8	0.9	0.4
224	0.150	6	0.50	0	1.202	0.0856	3.44	3.07	3.60	5.46 71.6	59.7	3.7	4.1
240	0.150	6	0.50	0	1.227	0.0828	3.48	3.09	3.56	6.28 63.4	58.4	1.8	1.6
248	0.150	6	0.50	0	1.268	0.0811	3.46	3.11	3.49	7.10 62.5	60.0	0.8	0.8
224	0.625	6	0.50	0.15	3.988	-0.002	3.85	3.06	4.00	5.45 11.3	9.6	3.6	-0.9
248	0.625	6	0.50	0.14	4.230	0.073	3.53	2.90	3.56	6.88 11.5	11.0	0.9	-0.2
16	0.650	6	0.50	0.20	2.431	0.068	3.83	2.83	7.02	2.90 34.6	1.8	32.5	0.1
96	0.650	6	0.50	0.19	3.016	-0.046	3.98	2.97	5.11	3.51 25.1	8.8	17.8	-0.7
160	0.650	6	0.50	0.16	3.565	-0.069	4.00	3.06	4.54	4.18 20.3	10.2	11.6	-0.8
240	0.650	6	0.50	0.13	4.300	0.127	3.57	2.96	3.64	6.15 9.8	8.9	1.8	-0.5
32	0.700	6	0.50	0.19	2.622	0.005	4.14	2.93	6.53	3.08 36.1	3.4	32.6	0.1
128	0.700	6	0.50	0.16	3.481	-0.102	4.08	3.04	4.88	3.84 17.5	8.2	14.0	-2.4
224	0.700	6	0.50	0.11	4.447	2.848	3.08	2.85	3.23	5.24 7.7	6.9	3.4	-1.3
64	0.800	6	0.50	0.14	3.307	0.060	4.03	2.91	5.62	3.24 30.5	5.6	26.4	-0.8
96	0.800	6	0.50	0.13	3.610	-0.069	4.04	2.98	5.16	3.52 14.9	6.5	14.4	-3.0
128	0.800	6	0.50	0.12	3.932	-0.016	3.95	3.07	4.75	3.87 10.3	6.7	11.4	-3.9

(continued on next page)

Table G.4 (concluded)

N_1	ρ^*	M $\times 10^5$	AR†	IE‡	$-E^*$	P^*	$-\mu^*_{1,c}$	$-\mu^*_{2,c}$	$-\mu^*_1$	$-\mu^*_2$	total	$\langle\delta N_1 \delta N_j\rangle$ 1-1	2-2	1-2
160	0.800	6	0.50	0.10	4.308	0.148	3.61	2.85	4.15	3.98	10.4	7.2	9.9	-3.4
192	0.800	6	0.50	0.08	4.688	0.462	3.24	2.60	3.58	4.19	8.9	6.5	6.5	-2.2
96	0.900	6	0.50	0.10	4.022	0.007	3.81	2.86	4.94	3.41	10.7	5.6	12.8	-3.9
128	0.900	6	0.50	0.08	4.429	0.237	3.63	2.69	4.43	3.48	10.3	6.1	12.8	-4.3
160	0.900	6	0.50	0.06	4.830	0.754	2.96	2.57	3.50	3.70	9.2	5.7	9.9	-3.2
64	0.950	6	0.50	0.10	3.816	-0.068	4.03	2.97	5.62	3.30	12.7	4.6	16.1	-4.0
96	0.950	6	0.50	0.08	4.234	0.153	3.59	2.79	4.72	3.33	11.1	5.6	15.4	-5.0
128	0.950	6	0.50	0.06	4.656	0.538	2.56	2.50	3.36	3.29	9.1	5.5	10.9	-3.7
32	1.050	6	0.50	0.09	3.763	-0.160	4.03	2.81	6.42	2.96	14.6	2.9	17.5	-2.9
64	1.050	6	0.50	0.07	4.207	0.138	3.61	2.91	5.20	3.24	11.6	4.3	16.0	-4.4
96	1.050	6	0.50	0.05	4.673	0.529	3.33	2.47	4.46	3.01	10.0	5.5	15.6	-5.6
160	1.050	6	0.50	0.02	5.539	2.826	-2.83	1.16	-2.28	2.29	5.8	6.2	9.3	-4.8
32	1.150	6	0.50	0.06	4.107	0.093	3.81	2.90	6.20	3.05	10.2	2.8	13.6	-3.1
64	1.150	6	0.50	0.05	4.589	0.507	2.32	2.54	3.92	2.87	8.8	3.9	14.1	-4.6
32	1.200	6	0.50	0.06	4.272	0.191	3.29	2.60	5.68	2.76	9.5	2.8	13.2	-3.3
16	1.250	6	0.50	0.05	4.175	0.080	3.32	2.76	6.51	2.83	10.7	1.6	13.4	-2.1
8	1.300	6	0.50	0.05	4.217	0.049	3.92	2.67	7.91	2.71	9.7	0.8	10.8	-1.0

† Acceptance ratio (fraction of successful displacement steps)
‡ Interchange efficiency (fraction of successful interchange steps); see also comments in Section G.2.

G.5 Mixture III

Table G.5 Monte Carlo simulation results for Mixture III

N_1	ρ^*	M $\times 10^5$	AR†	IE‡	$-E^*$	P^*	$-\mu^*_{1,c}$	$-\mu^*_{2,c}$	$-\mu^*_1$	$-\mu^*_2$	total	$\langle\delta N_1 \delta N_j\rangle$ 1-1	2-2	1-2
$T^* = 0.928$														
64	0.010	3	0.94	0	0.030	0.0091	4.33	4.30	5.62	4.57	38.6	7.3	21.1	0.2
128	0.010	3	0.92	0	0.045	0.0090	4.35	4.30	4.99	4.95	29.5	15.4	14.0	-0.0

(continued on next page)

Table G.5 (continued)

N_1	ρ^*	M $\times 10^5$	AR†	IE‡	$-E^*$	P^*	$-\mu^*_{1,c}$	$-\mu^*_{2,c}$	$-\mu^*_1$	$-\mu^*_2$	total	$\langle\delta N_1 \delta N_j\rangle$ 1-1	2-2	1-2
$T^* = 0.928$														
192	0.010	3	0.89	0	0.065	0.0089	4.36	4.31	4.62	5.60	29.4	23.1	6.6	-0.2
128	0.025	3	0.83	0	0.115	0.0215	3.60	3.50	4.24	4.15	30.9	15.1	14.1	0.9
192	0.025	3	0.78	0	0.162	0.0210	3.64	3.51	3.90	4.80	33.5	25.6	7.2	0.3
64	0.050	3	0.78	0	0.153	0.0422	3.06	2.90	4.35	3.17	32.1	8.0	21.8	1.1
128	0.050	3	0.72	0	0.234	0.0400	3.12	2.92	3.77	3.57	35.6	17.5	14.6	1.8
192	0.050	3	0.66	0	0.331	0.0373	3.20	2.96	3.47	4.24	38.8	29.2	7.1	1.2
8	0.100	8	0.70	0	0.215	0.0827	2.64	2.34	5.85	2.37	32.7	0.9	30.8	0.5
16	0.100	8	0.69	0	0.231	0.0812	2.65	2.35	5.23	2.41	32.4	1.[illegible]	29.4	0.6
32	0.100	8	0.67	0	0.265	0.0796	2.69	2.36	4.62	2.48	33.3	3.8	27.2	1.1
64	0.100	10	0.63	0	0.342	0.0757	2.77	2.39	4.06	2.66	37.8	8.6	24.0	2.6
96	0.100	10	0.58	0	0.427	0.0709	2.85	2.43	3.76	2.86	42.0	15.7	19.6	3.4
240	0.125	8	0.50	0	1.864	0.0284	3.28	2.47	3.34	5.04	518.9	499.9	2.3	8.3
240	0.125	10	0.50	0.38	1.668	0.0339	3.26	2.48	3.32	5.05	235.7	226.0	1.8	3.9
8	0.150	8	0.62	0	0.321	0.1164	2.49	2.05	5.70	2.08	34.4	0.9	32.5	0.5
16	0.150	8	0.60	0	0.344	0.1143	2.53	2.06	5.10	2.12	34.5	1.9	31.2	0.7
32	0.150	10	0.58	0	0.395	0.1103	2.58	2.09	4.51	2.22	37.3	4.2	29.8	1.7
64	0.150	10	0.53	0	0.515	0.1010	2.70	2.14	3.98	2.40	41.0	9.5	25.2	3.2
96	0.150	10	0.50	0	0.645	0.0914	2.81	2.20	3.72	2.63	49.8	17.1	21.8	5.5
8	0.200	8	0.55	0	0.423	0.1463	2.46	1.87	5.67	1.90	36.0	0.9	33.8	0.6
16	0.200	8	0.53	0	0.456	0.1441	2.48	1.89	5.06	1.95	37.2	1.9	33.1	1.1
16	0.200	10	0.53	0.53	0.456	0.1449	2.50	1.88	5.07	1.94	38.5	1.9	34.2	1.2
32	0.200	10	0.51	0	0.523	0.1371	2.56	1.92	4.49	2.05	39.7	4.5	30.2	2.5
64	0.200	10	0.50	0	0.684	0.1204	2.70	1.98	3.99	2.25	45.1	10.4	26.0	4.4
96	0.200	10	0.50	0	0.856	0.1026	2.87	2.05	3.78	2.48	57.4	19.7	23.3	7.2
8	0.250	8	0.50	0	0.529	0.1729	2.46	1.75	5.68	1.78	35.4	0.9	33.3	0.6
16	0.250	8	0.50	0.47	0.565	0.1676	2.52	1.76	5.10	1.82	36.7	1.9	32.4	1.2
32	0.250	10	0.50	0.45	0.654	0.1573	2.59	1.81	4.52	1.93	44.1	4.7	33.1	3.2
64	0.250	10	0.50	0.42	0.838	0.1332	2.77	1.90	4.06	2.16	50.3	11.5	27.5	5.7
96	0.250	10	0.50	0	1.131	0.1050	3.00	1.97	3.91	2.41	135.4	49.8	34.0	5.8
8	0.400	8	0.50	0	0.830	0.2366	0.64	1.54	3.86	1.57	35.3	0.8	33.7	0.4
16	0.400	10	0.50	0.35	0.882	0.2250	2.69	1.58	5.26	1.64	37.9	1.9	33.1	1.4
32	0.400	10	0.50	0.33	1.003	0.2004	2.83	1.63	4.76	1.75	44.7	4.6	33.5	3.3

(continued on next page)

Table G.5 (continued)

N_1	ρ^*	M $\times 10^5$	AR†	IE‡	$-E^*$	P^*	$-\mu^*_{1,c}$	$-\mu^*_{2,c}$	$-\mu^*_1$	$-\mu^*_2$	total	$\langle\delta N_1 \delta N_1\rangle$ 1-1	$\langle\delta N_1 \delta N_1\rangle$ 2-2	$\langle\delta N_1 \delta N_1\rangle$ 1-2
T* = 0.928														
64	0.400	10	0.50	0	1.330	0.1508	3.02	1.71	4.31	1.98	59.3	13.7	30.5	7.6
96	0.400	10	0.50	0	1.595	0.1043	3.19	1.84	4.10	2.28	58.3	16.7	24.2	8.7
16	0.500	10	0.50	0.29	1.078	0.2519	2.83	1.49	5.41	1.55	36.8	1.9	32.4	1.2
32	0.500	10	0.50	0.27	1.237	0.2142	2.91	1.56	4.84	1.69	43.9	4.7	32.8	3.2
64	0.500	10	0.50	0.24	1.570	0.1542	3.15	1.67	4.44	1.94	34.3	9.0	21.8	1.8
96	0.500	10	0.50	0.21	1.924	0.0873	3.48	1.77	4.39	2.20	59.9	22.4	22.2	7.6
16	0.600	6	0.50	0.24	1.272	0.2785	3.02	1.47	5.59	1.53	29.7	1.9	26.7	0.6
32	0.600	6	0.50	0.22	1.458	0.2365	3.11	1.53	5.04	1.65	41.2	4.4	31.3	2.7
64	0.600	6	0.50	0.20	1.811	0.1444	3.40	1.63	4.68	1.90	42.0	10.3	23.9	3.9
96	0.600	6	0.50	0.19	2.144	0.0412	3.70	1.77	4.61	2.21	32.6	14.5	16.5	0.8
16	0.700	6	0.50	0.20	1.465	0.2923	3.15	1.42	5.73	1.48	28.9	1.9	26.0	0.5
32	0.700	6	0.50	0.19	1.657	0.2480	3.25	1.48	5.18	1.61	29.4	3.8	24.6	0.5
64	0.700	6	0.50	0.17	2.047	0.1338	3.52	1.60	4.80	1.87	28.5	7.4	20.3	0.4
96	0.700	6	0.50	0.15	2.463	0.0256	3.73	1.71	4.64	2.15	22.7	10.7	15.2	-1.6
16	0.750	6	0.50	0.19	1.547	0.3020	3.17	1.39	5.75	1.45	20.1	1.8	18.8	-0.2
32	0.750	6	0.50	0.17	1.749	0.2462	3.35	1.43	5.28	1.55	23.9	3.8	20.5	-0.2
64	0.750	6	0.50	0.16	2.151	0.1242	3.63	1.56	4.91	1.83	18.3	6.6	15.5	-1.9
96	0.750	6	0.50	0.14	2.593	0.0189	3.76	1.72	4.67	2.15	18.5	8.7	13.9	-2.1
224	0.750	6	0.50	0.06	4.665	-0.1243	4.38	1.77	4.51	3.70	7.3	7.0	3.2	-1.5
240	0.750	6	0.50	0.05	4.973	0.0532	4.44	1.69	4.49	4.26	6.1	6.1	1.7	-0.8
224	0.775	6	0.50	0.05	4.827	-0.0108	4.09	1.65	4.22	3.58	7.2	6.6	3.4	-1.4
240	0.775	6	0.50	0.05	5.131	0.1104	2.98	1.67	3.04	4.24	6.0	6.2	1.6	-0.9
224	0.785	6	0.50	0.05	4.886	0.0727	3.97	1.39	4.09	3.32	7.5	6.6	3.3	-1.2
16	0.800	6	0.50	0.16	1.654	0.3318	3.16	1.37	5.74	1.43	24.5	1.8	22.7	-0.0
16	0.800	6	0.50	0.16	1.654	0.3318	3.16	1.37	5.74	1.43	24.5	1.8	22.7	0.0
32	0.800	6	0.50	0.16	1.851	0.2653	3.44	1.43	5.37	1.55	18.0	3.4	16.8	-1.1
64	0.800	6	0.50	0.14	2.279	0.1540	3.69	1.51	4.98	1.77	16.3	6.2	14.8	-2.3
96	0.800	6	0.50	0.12	2.759	0.0469	3.79	1.61	4.70	2.05	15.9	8.5	13.1	-2.8
128	0.800	6	0.50	0.10	3.233	-0.0703	3.94	1.74	4.58	2.38	11.8	8.8	10.8	-3.9
192	0.800	6	0.50	0.06	4.354	-0.0039	3.65	1.65	3.91	2.94	8.5	7.0	7.0	-2.8
224	0.800	6	0.50	0.04	4.966	0.1917	3.69	1.44	3.81	3.37	5.7	5.6	3.3	-1.6
240	0.800	6	0.50	0.04	5.284	0.3771	2.70	1.45	2.76	4.02	5.3	5.4	1.7	-0.9
32	0.825	6	0.50	0.15	1.906	0.2763	3.44	1.41	5.37	1.53	20.3	3.4	18.1	-0.6
64	0.825	6	0.50	0.13	2.348	0.1599	3.67	1.51	4.95	1.78	15.4	5.8	14.9	-2.6
96	0.825	6	0.50	0.11	2.823	0.0444	3.79	1.64	4.70	2.07	14.9	7.4	14.1	-3.3

(continued on next page)

Table G.5 (continued)

N_1	ρ^*	M $\times 10^5$	AR†	IE‡	$-E^*$	P^*	$-\mu^*_{1,c}$	$-\mu^*_{2,c}$	$-\mu^*_1$	$-\mu^*_2$	total	$<\delta N_1 \delta N_j>$ 1-1	2-2	1-2
T* = 0.928														
128	0.825	6	0.50	0.09	3.336	-0.0091	3.90	1.67	4.54	2.31	10.0	7.4	10.4	-3.9
160	0.825	6	0.50	0.07	3.898	0.0446	3.84	1.75	4.28	2.66	7.5	7.0	8.4	-4.0
192	0.825	6	0.50	0.05	4.492	0.1054	3.70	1.47	3.97	2.75	8.1	6.7	6.7	-2.7
224	0.825	6	0.50	0.04	5.120	0.4016	3.55	1.25	3.68	3.18	7.1	6.5	3.8	-1.6
32	0.850	6	0.50	0.14	1.964	0.2754	3.39	1.37	5.32	1.49	18.2	3.3	17.1	-1.1
64	0.850	6	0.50	0.12	2.406	0.1519	3.63	1.54	4.92	1.81	16.2	5.9	15.3	-2.5
96	0.850	6	0.50	0.10	2.906	0.0486	4.00	1.48	4.91	1.92	13.6	7.2	13.7	-3.7
128	0.850	6	0.50	0.08	3.433	0.0259	4.04	1.67	4.68	2.31	10.5	7.7	11.6	-4.4
160	0.850	6	0.50	0.06	4.009	0.0475	3.83	1.60	4.26	2.51	7.9	6.8	8.6	-3.8
192	0.850	6	0.50	0.04	4.614	0.3141	3.30	1.49	3.56	2.77	7.2	6.6	6.7	-3.1
32	0.875	6	0.50	0.13	2.014	0.3024	3.44	1.36	5.37	1.49	16.0	3.2	15.9	-1.6
64	0.875	6	0.50	0.11	2.476	0.1976	3.68	1.49	4.96	1.75	16.6	5.7	15.7	-2.4
96	0.875	6	0.50	0.09	2.980	0.0641	3.86	1.54	4.77	1.98	10.8	6.8	12.6	-4.3
128	0.875	6	0.50	0.07	3.536	0.0411	4.04	1.49	4.69	2.14	9.3	7.1	10.0	-3.9
160	0.875	6	0.50	0.05	4.126	0.1374	3.81	1.50	4.24	2.41	8.9	6.1	9.4	-3.3
32	0.900	6	0.50	0.13	2.056	0.2906	3.42	1.33	5.35	1.46	11.7	3.1	12.6	-2.0
64	0.900	6	0.50	0.11	2.540	0.1746	3.63	1.52	4.92	1.78	14.6	5.6	15.2	-3.1
96	0.900	6	0.50	0.08	3.065	0.1222	3.80	1.47	4.71	1.91	10.7	6.5	12.9	-4.3
128	0.900	6	0.50	0.06	3.630	0.1302	3.44	1.46	4.08	2.10	7.7	6.7	10.1	-4.6
160	0.900	6	0.50	0.04	4.235	0.3258	3.49	1.34	3.93	2.25	7.5	6.5	8.4	-3.7
32	0.950	6	0.50	0.11	2.181	0.3566	3.32	1.31	5.25	1.43	15.2	3.0	15.1	-1.5
64	0.950	6	0.50	0.09	2.677	0.2613	3.53	1.39	4.82	1.65	12.1	5.1	13.6	-3.3
96	0.950	6	0.50	0.07	3.228	0.1988	3.98	1.34	4.89	1.78	9.1	6.0	11.9	-4.4
128	0.950	6	0.50	0.05	3.826	0.3551	3.42	1.32	4.06	1.96	8.5	6.2	11.5	-4.6
32	1.000	6	0.50	0.10	2.274	0.4031	3.45	1.27	5.38	1.40	11.1	3.1	12.7	-2.3
64	1.000	6	0.50	0.08	2.810	0.3425	3.62	1.35	4.91	1.61	10.1	4.9	12.4	-3.6
96	1.000	6	0.50	0.05	3.397	0.3861	3.23	1.28	4.14	1.72	8.9	5.6	12.4	-4.5
128	1.000	6	0.50	0.03	4.018	0.6622	4.38	0.96	5.03	1.61	6.9	6.3	9.9	-4.7
T* = 1.061														
32	0.400	6	0.50	0.38	0.958	0.2770	2.70	1.62	4.90	1.76	38.4	4.2	30.3	2.0
32	0.400	6	0.50	0.38	0.958	0.2770	2.70	1.62	4.90	1.76	38.4	4.2	30.3	2.0
32	0.400	6	0.50	0	0.961	0.2816	2.71	1.61	4.92	1.75	35.3	4.5	27.4	1.7
32	0.400	6	0.50	0	0.961	0.2816	2.71	1.61	4.92	1.75	35.3	4.5	27.4	1.0
64	0.400	6	0.50	0	1.206	0.2333	2.90	1.71	4.38	2.02	52.7	11.6	28.9	6.1
96	0.400	6	0.50	0	1.454	0.1836	3.09	1.81	4.13	2.31	43.0	16.7	20.1	3.1

(continued on next page)

Table G.5 (continued)

N_1	ρ^*	M $\times 10^5$	AR†	IE‡	$-E^*$	P^*	$-\mu^*_{1,c}$	$-\mu^*_{2,c}$	$-\mu^*_1$	$-\mu^*_2$	$\langle \delta N_1 \delta N_j \rangle$ total	1-1	2-2	1-2
	T* = 1.061													
128	0.400	6	0.50	0.31	1.738	0.1383	3.28	1.87	4.02	2.61	37.0	21.4	12.9	1.4
32	0.500	6	0.50	0	1.177	0.3251	2.78	1.48	4.98	1.62	39.7	3.3	32.7	1.8
64	0.500	6	0.50	0	1.468	0.2650	3.00	1.61	4.47	1.91	32.3	9.5	18.8	2.0
96	0.500	6	0.50	0	1.785	0.1990	3.18	1.71	4.22	2.21	30.6	14.6	15.7	0.2
128	0.500	6	0.50	0.25	2.105	0.1263	3.41	1.77	4.14	2.51	24.7	15.2	12.1	-1.3
128	0.500	6	0.50	0.25	2.093	0.1243	3.43	1.79	4.16	2.52	24.6	14.8	12.3	-1.2
32	0.600	6	0.50	0.26	1.381	0.3747	2.85	1.42	5.06	1.56	24.5	3.6	21.2	-0.2
32	0.600	6	0.50	0	1.398	0.3764	2.88	1.37	5.08	1.51	26.5	4.7	20.3	0.8
64	0.600	6	0.50	0.24	1.716	0.2895	3.14	1.50	4.61	1.81	23.3	7.6	17.1	-0.7
64	0.600	6	0.50	0	1.738	0.3098	3.09	1.50	4.56	1.80	21.7	6.8	17.1	-1.1
96	0.600	6	0.50	0.23	2.051	0.1992	3.34	1.62	4.38	2.12	23.6	11.0	15.2	-1.3
96	0.600	6	0.50	0	2.080	0.2157	3.36	1.55	4.40	2.05	26.9	9.9	15.2	0.9
128	0.600	6	0.50	0.21	2.441	0.1219	3.61	1.69	4.34	2.42	17.4	11.7	11.5	-2.9
32	0.700	6	0.50	0	1.597	0.4281	2.89	1.28	5.09	1.42	20.1	4.2	18.4	-1.2
32	0.700	6	0.50	0.22	1.581	0.4188	2.91	1.27	5.12	1.41	18.1	3.4	17.0	-1.1
64	0.700	6	0.50	0.20	1.974	0.3407	3.12	1.38	4.59	1.68	21.9	6.9	16.8	-0.9
64	0.700	6	0.50	0	1.956	0.3203	3.22	1.43	4.69	1.74	18.4	5.5	15.5	-1.3
96	0.700	6	0.50	0.18	2.379	0.2412	3.28	1.47	4.32	1.97	18.0	9.0	14.2	-2.6
96	0.700	6	0.50	0	2.382	0.2624	3.33	1.45	4.37	1.95	18.4	11.9	14.2	-3.8
128	0.700	6	0.50	0.16	2.799	0.1668	3.50	1.57	4.23	2.31	15.4	9.5	12.0	-3.1
32	0.750	6	0.50	0	1.689	0.4405	2.93	1.25	5.14	1.39	15.3	2.8	15.8	-1.7
32	0.750	6	0.50	0.20	1.697	0.4592	2.89	1.23	5.09	1.37	23.1	3.6	20.6	-0.6
64	0.750	6	0.50	0	2.102	0.3615	3.09	1.34	4.56	1.64	19.5	7.5	16.6	-2.3
64	0.750	6	0.50	0.18	2.094	0.3526	3.13	1.35	4.60	1.65	16.4	6.2	15.3	-2.5
96	0.750	6	0.50	0.16	2.520	0.2724	3.30	1.40	4.34	1.90	14.6	7.9	13.5	-3.4
96	0.750	6	0.50	0	2.535	0.2644	3.26	1.40	4.31	1.90	15.1	8.9	13.7	-3.8
128	0.750	6	0.50	0.14	2.982	0.2027	3.48	1.44	4.22	2.18	10.5	8.3	11.0	-4.4
32	0.800	6	0.50	0	1.810	0.5033	2.89	1.17	5.09	1.31	17.7	3.7	16.4	-1.2
32	0.800	6	0.50	0.18	1.797	0.4961	2.96	1.19	5.17	1.33	17.4	3.4	16.5	-1.2
64	0.800	6	0.50	0	2.231	0.4445	3.16	1.23	4.63	1.54	15.0	7.9	13.9	-3.4
64	0.800	6	0.50	0.16	2.236	0.4075	3.09	1.29	4.56	1.60	15.2	5.8	14.0	-2.3
96	0.800	6	0.50	0.14	2.680	0.3410	3.33	1.33	4.37	1.83	12.6	7.4	12.9	-3.8
96	0.800	6	0.50	0	2.684	0.2953	3.28	1.30	4.32	1.80	12.1	8.4	14.7	-5.5
128	0.800	6	0.50	0.11	3.175	0.2780	3.56	1.33	4.29	2.07	11.7	7.8	11.1	-3.6
32	0.850	6	0.50	0.16	1.906	0.5467	2.91	1.14	5.11	1.28	18.1	3.2	17.7	-1.4

(continued on next page)

Table G.5 (concluded)

N_1	ρ^*	M $\times 10^5$	AR†	IE‡	$-E^*$	P^*	$-\mu^*_{1,c}$	$-\mu^*_{2,c}$	$-\mu^*_1$	$-\mu^*_2$	$\langle \delta N_1 \delta N_j \rangle$ total	1-1	2-2	1-2
T* = 1.061														
32	0.850	6	0.50	0	1.912	0.5765	2.95	1.10	5.16	1.24	15.8	3.1	15.5	-1.4
64	0.850	6	0.50	0	2.370	0.4778	2.99	1.14	4.46	1.44	12.9	6.6	11.6	-2.6
64	0.850	6	0.50	0.14	2.353	0.4479	3.11	1.17	4.58	1.47	12.5	5.7	14.0	-3.6
96	0.850	6	0.50	0	2.844	0.4201	3.41	1.20	4.45	1.69	12.3	7.9	11.8	-3.7
96	0.850	6	0.50	0.12	2.837	0.4124	3.26	1.15	4.30	1.65	10.3	6.7	11.5	-3.9
128	0.850	6	0.50	0.09	3.369	0.4142	3.17	1.22	3.91	1.95	10.9	7.2	11.9	-4.1
32	0.900	6	0.50	0.14	2.009	0.6142	2.90	1.00	5.10	1.14	12.1	3.1	13.3	-2.2
64	0.900	6	0.50	0.12	2.483	0.5306	3.03	1.03	4.50	1.34	11.8	5.1	13.9	-3.6
96	0.900	6	0.50	0.10	3.004	0.5115	3.08	1.20	4.12	1.70	9.8	6.2	11.9	-4.2
128	0.900	6	0.50	0.07	3.559	0.6081	3.20	0.96	3.94	1.69	8.7	6.8	10.8	-4.5
T* = 1.194														
96	0.300	6	0.50	0.45	1.076	0.2275	2.95	2.01	4.12	2.57	39.0	14.7	18.8	2.8
128	0.300	6	0.50	0.43	1.286	0.2006	3.07	2.08	3.90	2.91	36.3	19.6	14.1	1.4
160	0.300	6	0.50	0.41	1.513	0.1671	3.25	2.15	3.81	3.32	36.0	25.1	10.3	0.3
192	0.300	6	0.50	0.38	1.788	0.1381	3.34	2.20	3.68	3.85	59.6	45.9	7.4	3.1
64	0.400	6	0.50	0.39	1.155	0.3198	2.78	1.71	4.44	2.05	36.8	8.7	23.6	2.3
96	0.400	6	0.50	0.37	1.386	0.2731	2.95	1.81	4.12	2.37	27.3	12.0	15.7	-0.2
128	0.400	6	0.50	0.35	1.649	0.2283	3.13	1.89	3.96	2.72	32.6	17.6	13.9	0.5
160	0.400	6	0.50	0.33	1.950	0.1852	3.32	1.94	3.88	3.11	36.2	24.0	10.4	0.9
192	0.400	6	0.50	0.31	2.252	0.1379	3.41	1.99	3.75	3.64	43.6	34.9	6.9	0.9
96	0.500	6	0.50	0.31	1.695	0.3075	3.00	1.60	4.17	2.16	27.4	11.9	16.4	-0.4
128	0.500	6	0.50	0.29	1.997	0.2504	3.20	1.71	4.03	2.54	20.6	13.0	11.4	-1.9
160	0.500	6	0.50	0.27	2.360	0.2079	3.30	1.75	3.86	2.92	24.8	17.9	9.5	-1.3
192	0.500	6	0.50	0.26	2.690	0.1141	3.53	1.82	3.87	3.47	18.9	16.2	6.3	-1.8
96	0.600	6	0.50	0.25	2.007	0.3611	3.04	1.44	4.21	2.00	21.9	9.7	15.3	-1.5
128	0.600	6	0.50	0.23	2.371	0.2966	3.07	1.55	3.90	2.38	14.9	10.5	11.1	-3.3
160	0.600	6	0.50	0.21	2.759	0.2448	3.37	1.61	3.93	2.78	19.1	13.9	9.6	-2.2
192	0.600	6	0.50	0.20	3.173	0.1744	3.50	1.64	3.84	3.30	11.[illegible]	[illegible]	.1	-2.6
96	0.700	6	0.50	0.20	2.308	0.4577	3.04	1.26	4.21	1.82	14.	.6	13.5	-3.4
128	0.700	6	0.50	0.18	2.741	0.4003	3.03	1.31	3.85	2.14	12.8	8.7	11.1	-3.5
160	0.700	6	0.50	0.15	3.200	0.3446	3.27	1.28	3.83	2.45	11.2	8.4	9.6	-3.4
192	0.700	6	0.50	0.13	3.693	0.3587	3.04	1.28	3.38	2.94	10.0	8.5	6.4	-2.5

† Acceptance ratio (fraction of successful displacement steps)

‡ Interchange efficiency (fraction of successful interchange steps); see also comments in Section G.2.